Technische Universität München
TUM School of Engineering and Design

Seismic performance assessment of an innovative type of buckling restrained brace containing tire-derived lightweight aggregate concrete

Ali Naghshineh

Vollständiger Abdruck der von der TUM School of Engineering and Design der Technischen Universität München zur Erlangung eines

Doktors der Ingenieurwissenschaften (Dr.-Ing.)

genehmigten Dissertation.

Vorsitz: Prof. Dr.-Ing. Martin Mensinger

Prüfer*innen der Dissertation:

1. Prof. Dr.-Ing. Oliver Fischer
2. Prof. Dr. Fariborz M Tehrani, Ph.D., California State University, Fresno, USA

Die Dissertation wurde am 30.05.2022 bei der Technischen Universität München eingereicht und durch die TUM School of Engineering and Design am 07.11.2022 angenommen.

ABSTRACT

Seismic performance assessment of an innovative type of buckling restrained brace containing tire-derived lightweight aggregate concrete

Ali Naghshineh

Technical University of Munich, 2022

Predicting structural behaviour subjected to dynamic excitations is a complex problem, when a structure dissipates considerable amount of kinetic energy produced by an earthquake, the damage level can be predicted. In conventional design these damages allow to occur in “structural fuses” which are formed due to the yielding of the structure in certain elements using reduction factors. This reduction of forces which are allowed in conventional seismic design procedures occurred as an inelastic action in specially detailed critical regions of the structure such as beams or adjacent to the beam-column joints. To avoid structural damage in the primary members of the system a number of innovative control systems have been created. Among them passive energy dissipation devices are distinguished by a capability to improve energy dissipation in the structural system either by transferring the kinetic energy to heat such as frictional sliding, yielding of metals, and viscoelastic solids or fluids, or among vibrating modes including supplemental oscillators (Soong & Dargush, 1999). Conventional braces buckle in compression which leads to progressive degrading behavior and loss of stiffness. To resolve this issue, the unbounded brace, which provides unbounding layer between surrounding concrete and the steel core, was developed by Professor Wada, so that the steel core can take all axial loads. A buckling restrained brace consisting of a ductile steel core in a concrete or mortar encased steel tube, the steel core provides the yielding mechanism, and the tube prevents buckling of the core, in which scrap-tire rubber can be used as an alternative material of mortal steel tube. Another aspect of this thesis is the application for the use of recycled scrap tire aggregates to decrease waste and contribute to sustainability.

It is very crucial to develop a system focused on sustainability to allow us to transition from curbside recycling to a broader perspective of employing different types of waste. Because aggregates account for a considerable amount of concrete mixtures, using waste aggregate materials such as tire-derived aggregate has a considerable influence on resource conservation. Tire-derived aggregate (TDA) is derived from waste tires in a standard range of practical sizes. Adding rubber to a concrete mixture provides some advantages in its characteristics including higher toughness and impact, increased ductility, lower density, and sound isolation (Siddique and Naik, 2004). The application of ductile materials with improved damping properties, such as tire-derived lightweight aggregate concrete, further enhances the overall performance of the system.

In ASCE 7-22, the minimum earthquake lateral force is divided by Seismic Force Resisting System(s) (SFRS) reduction factor known as the response modification factor. This factor is regardless of span length, bracing configuration, the building height, and the period of the structure Most of the research carried out in the past focused on the behaviour of buckling restrained braced frames in steel structures, and various approaches have also been proposed to capture their seismic evaluation. Further studies are required to characterize the capacities of the overall brace frame system in concrete moment resisting frames (CMRFs) using buckling restrained brace encased steel with tire-derived aggregate filling as well as an experimental study to examine the actual behavior of buckling restrained braces as new design approaches of other types of bracings. The purpose of this thesis is to investigate the influence and reliability of the application of ductile materials with improved damping properties on the seismic design factors as well as the overall earthquake performance of the system.

Therefore, the objectives of this thesis are to (i) evaluate seismic force reduction factors of CMRFs employing BRB, (ii) investigate, numerically, the effectiveness of BRB on the seismic performance of concrete moment resisting frames, (iii) examine, experimentally (collaborate experimental test) and numerically the seismic response of BRB with TDA and with concrete filling subjected to artificial and real earthquakes, (iv) develop a design guideline for buckling restrained braced frames with TDA filling.

To achieve the first and second objectives, the mechanical properties of tire-derived lightweight aggregate concrete (TDLWAC), as an alternative damping property conducted by Tehrani et al. 2020, were used to model the innovative BRB with encased steel composite containing TDA

filling. Seismic design factors of four-, eight-, and 14-story special concrete moment resisting frames (CMRFs) equipped with BRBF, designed on the basis of the current edition of ASCE/SEI 7-22, and a comparison between the BRB encased steel with TDA infill as new damping properties as well as the BRB encased steel with concrete infill were discussed. In addition, the effects of building height, and span length for four different bracing configurations such as Single-Leg Braces (SLB), Chevron Inverted V Braces (CIVB), Chevron V Braces (CVB), and Split X braces (SXB), were investigated. Moreover, nonlinear response history analyses using twenty-one scaled ground motions based on ASCE 7 and the fundamental period of each structure were performed to demonstrate the efficiency of these bracing systems on the seismic response of special concrete moment resisting frames (SCMRFs). To achieve the third objective, the collaborating experimental test was performed on a shake table with a one-story steel frame equipped with three BRBs with TDA filling and three BRB with concrete filling subjected to various ground motions as well as artificial loadings, and their application for a Single Leg Brace (SLB) was verified at the Structures Laboratory of California State University (CSU), Fresno (Pathan et al. 2021). Then four models are created based on the experimental tests using ETABS as well as OpenSees software. The results cover comparison for acceleration, displacement, stiffness, hysteretic behviour, damping ratios, as well as the ductility of BRB with TDA and concrete fillings. The results suggest that such an application could be advantageous for integrating the BRBTDAs into the structural system, improving seismic safety, enhancing the damping properties of the system, and contribute to sustainability. The approaches involved in the second and third objectives are the basis for the fourth objective.

Acknowledgments

First and foremost, I would like to thank my supervisor, Professor Dr.-Ing. Oliver Fischer for his encouragement, assistance, and advice throughout this research study. His continual encouragement and support have given me the confidence to focus and progress. In addition, I greatly appreciate my co-supervisor Professor Dr. Fariborz M. Tehrani for his constant support and insightful remarks and hints throughout this research.

Also, our collaborators at the Department of Civil & Geomatics Engineering at California State University of Fresno (USA), Professor Dr. Fariborz M. Tehrani, Mr. Logan Couch, and Ms. Nasreen B. Pathan for their collaborations throughout the experimental part of the thesis. Besides, I would like to thank Dr. Farbod Khoshnoud for his support during my study.

Finally, I would like to express my gratitude to my wife Dr. Leila Farkhondeh Kish (OB/GYN) whose love, consistent inspiration, encouragement, advice, support, and patience have encouraged me to accomplish this academic journey.

Dedication

To my wife: Leila Farkhondeh Kish

Table of Contents

List of Figures

List of Tables

CHAPTER 1
Introduction

1.1 Background and Problem Definition

Conventional bracing systems dissipate energy by buckling in compression and yielding in tension, their lack of ductility, nonsymmetric behaviour, and connection fracture caused considerable damage during previous earthquakes (Tremblay et al. 1966). The Buckling Restrained Brace Frame (BRBF), consisting of a ductile steel core in concrete or encased concrete with steel tube, attempts to avoid such brittle modes of failure. The steel core provides the required yielding mechanism while the tube prevents buckling of the core, hence, increasing the ductility of the system. The application of ductile materials with improved damping properties, such as tire-derived light-weight aggregate concrete, further enhances the overall performance of the system. The purpose of this study is to investigate the influence of such an application on the response modification, overstrength, and ductility factors as well as the general earthquake performance of the system. In addition, the use of waste tiers in buckling restrained brace frame contribute to sustainability by reducing waste.

1.2 Research Significance and Motivation

When a structure dissipates kinetic energy as a result of a strong ground motion, the damage levels can be identified, the structural codes allow the kinetic energy to be dissipated by yielding in specific regions, resulting in structural damages (Ko & Field, 2003); therefore, a number of control systems have been studied in order to avoid these damages. There are three major control systems classes: passive, active, and semi-active (Tehrani, Nazari & Naghshineh, 2022). Among them, passive energy dissipation devices are designated by a capability to improve energy dissipation in the structural system either by transferring the kinetic energy to heat such as frictional sliding, yielding of metals and viscoelastic solids or fluids or among vibrating modes including supplemental oscillators (Soong & Dargush, 1999). Conventional braces buckle in compression, which leads to progressive degrading behavior and loss of stiffness. To resolve this issue, the unbounded brace, which provides an unbounded layer between surrounding concrete

and the steel core, was developed by Professor Wada to take all axial loads. Unbonded braces can provide both stiffness and a stable energy absorption capability, the brace forces are reduced, and they do not need to be designed for buckling (Ko & Field, 2003). It results in lower costs of new construction or retrofitting existing buildings, with lower forces in the superstructure and foundation. These bracing systems have symmetric hysteresis curves, high ductility, and large drift capacity (Asgarian et al. 2009).

Tire-derived aggregate is derived from waste tires in a standard range of practical sizes. Besides the environmental benefits of TDA, it can be used as an engineering application that is lightweight, durable with the engineering properties that make TDA appropriate for a variety of civil engineering applications, it has also significant cost advantages. Compared to concrete, rubber is a significantly softer material that can tolerate far more deformation before failing. Crumb rubber is composed of smaller particles, whereas tire chips are made up of larger rubber particles used to replace fine and coarse aggregate in concrete (Tehrani et al. 2019). The rubber stress-strain curve is nonlinear with lowering stiffness at first and then rising, while cement past/mortals have a brittle behavior and higher compressive strength than tensile/flexural strength, with the linear stress-strain curve. Moreover, the mechanical parameters such as compressive strength, tensile strength, flexural strength, and modulus of elasticity were reduced with rubber-based aggregate being used. Therefore, concrete containing a substantial portion of rubber aggregate was more ductile than conventional concrete (Tehrani et al. 2019; Treloar 1994; Wood 1977; Hertz 1991; Yang et al. 2013; Toutanji et al. 1996; Humphrey et al. 2010; Aslani 2016; Tehrani et al. 2018).

In ASCE 7-22, the minimum earthquake lateral force is divided by Seismic Force Resisting System(s) (SFRS) reduction factor known as the response modification factor. This factor is regardless of span length, bracing configuration, the period of the structure, and the building height. Several studies have been conducted to study the seismic design factors and performance of conventional BRBFs (Moni et al. 2016; Mahmoudi and Zaree, 2013; Asgarian and Shokrgozar, 2009). Most of the research carried out in the past focused on the behaviour of buckling restrained braced frames in steel structures, and various approaches have also been proposed to capture their seismic evaluation (Hosseienzadeh et al. 2016; Bai and Ou 2016; Corte et al., 2014; Mahmoudi et al. 2013; Nguyen et al. 2010; Balling et al. 2009; Asgarian et al. 2009; Kumar et al. 2005; Kim et al. 2004; Sabelli et al. 2003). Further studies are required to characterize the capacities of the

overall brace frame system to examine the actual behaviour of buckling restrained braces encased steel with TDA/Concrete fillings as new design approaches of other types of bracings. Furthermore, the application of BRB with TDA and with concrete infill must be experimentally and numerically validated.

In summary, the seismic design components of different concrete structures equipped with buckling restrained braces encased steel with TDA and with concrete filling should be investigated. Moreover, the application of buckling restrained brace with TDA and concrete fillings needs to be verified against the experimental tests. The current study aims to address the aforementioned research significance by using numerical analyses as well as by simulation of experimental tests.

1.3 Objectives and Scope of Work

The objectives of this thesis are to: (i) evaluate seismic force reduction factors of CMRFs employing BRB, (ii) investigate, numerically, the effectiveness of BRB on the seismic performance of concrete moment resisting frames, (iii) examine, experimentally (collaborate experimental test) and numerically the seismic response of BRB with TDA and with concrete filling subjected to artificial and real earthquakes, (iv) develop a design guideline for buckling restrained braced frames with TDA filling. The scope of this research is as follows:

- Extracting the mechanical properties of tire-derived lightweight aggregate concrete (Tehrani et al. 2020) to model BRB with encased steel composite containing TDA and concrete filling.
- Conducting push-over analysis to calculate overstrength, ductility, and response modification factors for different CMRFs equipped buckling restrained braces considering different heights, span lengths, and bracing configurations as well as the evaluation of structures using nonlinear response history analysis.
- Performing a full-scale experimental test (This collaborative experimental test was performed by an MSc student at CSU, 2020) to investigate the application of buckling restrained brace with TDA and with concrete filling for a Single Leg Brace (SLB) and to evaluate their dynamic performance.

- Comparative study of experimental with the numerical investigation of BRB with TDA and with concrete infill to assess their acceleration, displacement, stiffness, damping ratios, and ductility.

1.4 Thesis Layout

The thesis is divided into five chapters as followings:

- Chapter 1 consists of an introduction; research significance and motivation; objectives and scope of work; including a brief literature review.
- Chapter 2 includes the literature review including the concept of energy dissipation applications, control systems, buckling restrained brace frames, and the mechanical properties of tire-derived light weight aggregate.
- Chapter 3 includes an introduction to seismic hazards, ground motions parameters, different types of analysis procedures, seismic assessment and retrofitting techniques, as well as the methodology.
- Chapter 4 consists of the seismic design parameters and performance evaluation of different CMRFs equipped with an innovative type of buckling restrained brace using tire-derived lightweight aggregate concrete infill and conventional BRB using concrete infill. Following that, a comparison between experimental and analytical works for BRB with TDA infill and with conventional concrete infill is discussed.
- Chapter 5 includes the summary of the research project, the main contributions and conclusions, and recommendations for future work.

CHAPTER 2
Literature Review

2.1 Background

In recent years, the perception of “energy dissipation” or “supplemental damping” has been developed into a proven technology, and some of these devices have become popular throughout the world. The notion of control theory is to comprehend the dynamic characteristics and stability of the system. In general, the damage energy can be reduced by supplemental damping, which can be added by incorporating passive/active/semi-active energy dissipaters. Moreover, dampers have been used to improve the dynamic characteristics and stability of structures. In this regard, a passive control system is more reliable than an active system as it does not require external power or complex sensing equipment. Tuned mass dampers, base isolation, friction dampers, viscous dampers, viscoelastic dampers, and hysteretic dampers shall be categorized as this group. In addition, while the majority of buildings in the southern European nations were constructed and designed in compliance with previous codes, their seismic performance needs improvement.

2.2 Seismic Resilience

In conventional design, engineers tend to enhance the ductility of structural components which causes damage to nonstructural elements. Seismic isolation systems improve the resilience and performance of structures by limiting damage and economic losses caused by earthquakes utilizing flexible isolation devices (Tehrani 1992, Tehrani et al. 2020).

Smart dampers and materials are one type of seismic isolation control system, which can be classified into three major types: passive control system, active control system, and semi-active control system as well as the hybrid system as shown in Figure 2-1. These control systems can be combined to form a hybrid control system, which is composed of passive and active devices or passive and semi-active devices (Tehrani et al. 2020).

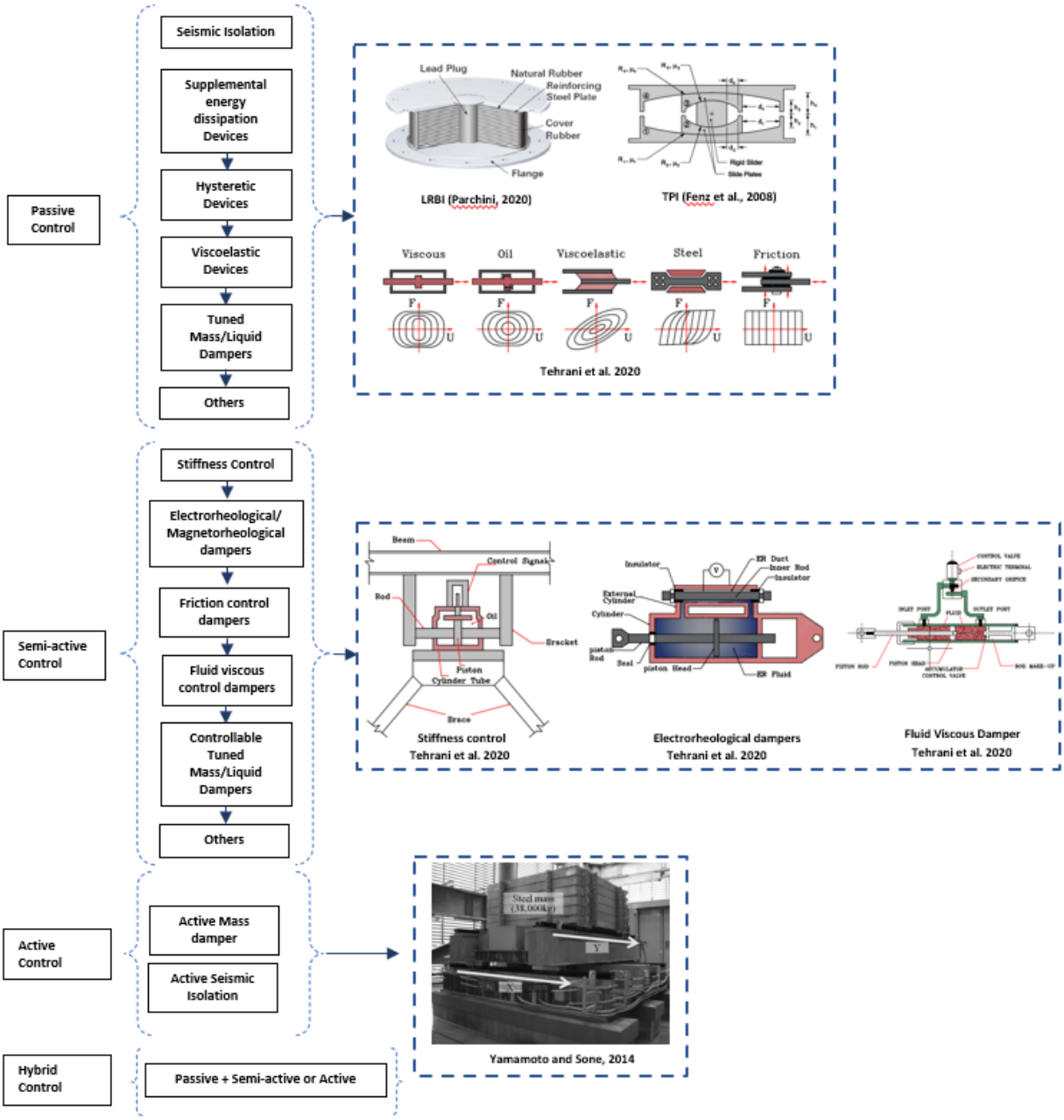

Figure 2-1. Different types of control systems

2.2.1 Active control systems

A large amount of energy is needed in order to run Active control systems. Electrohydraulic or electromechanical actuators generate control forces based on data from sensors which determine the structural response or external excitation locally or remotely, as demonstrated in Figure 2-2.

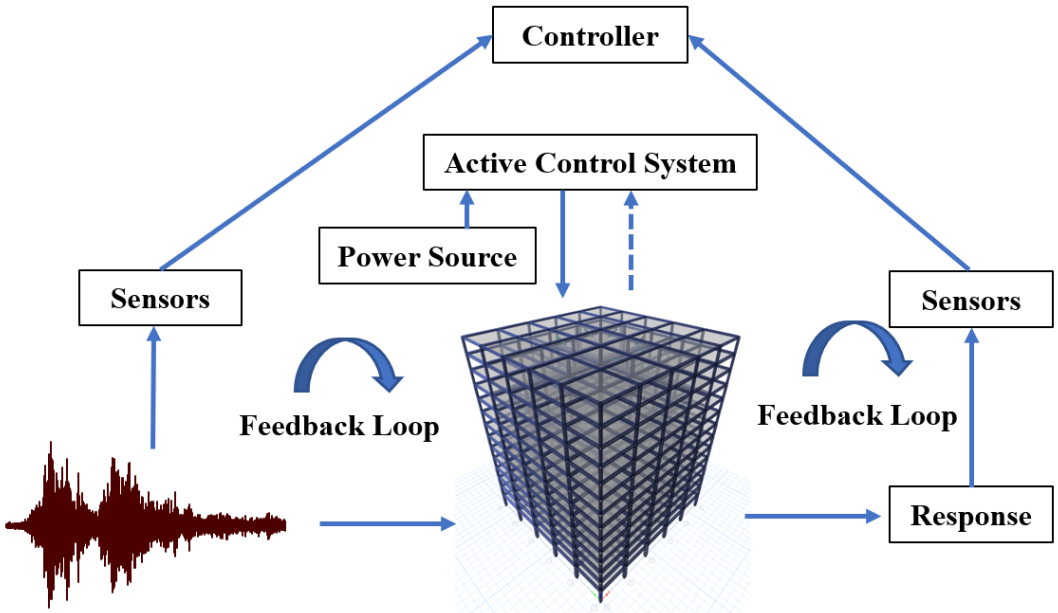

Figure 2-2. Active control system (based on Symans et al. 1997)

2.2.2 Passive Energy Dissipation Devices

Unlike active control systems, passive control systems do not require external power sources to operate, they can be used to reduce the demand of the system by altering the dynamic properties of a structure. Figure 2-3 shows the passive control system, in which the response of the structure in terms of a function can be used to develop control forces at the location of interest. Passive control systems are also known as supplemental energy dissipation systems can enhance the energy dissipation capacity of a structure. They can dissipate energy in different mechanisms including yielding (i.e., BRB), friction, viscous fluid (i.e., shearing), and viscoelastic action (i.e., rubber materials) (Tehrani et al. 2020; Soong and Constantinou 1994; Constantinou et al. 1996; Constantinou et al. 1993).

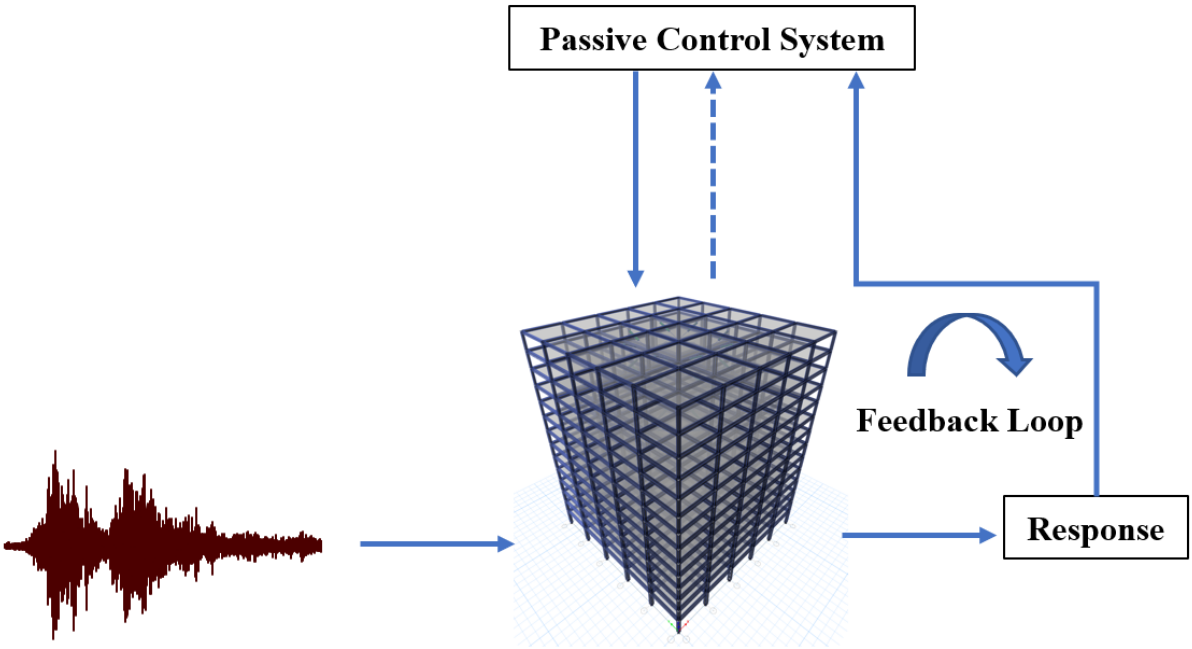

Figure 2-3. Passive control system (based on Symans et al. 1997)

2.2.3 Semi-active control systems

Semi-active control systems are modified passive control system that allows mechanical properties to be adjustable. A small amount of external power and a controller are required for a semi-active control system, the control forces are generated by the motion of the structure in conjunction with a controller that monitors feedback and generates appropriate command signals, which is shown in Figure 2-4. Magnetorheological and electrorheological dampers, stiffness and natural period controller, friction devices, fluid viscous dampers, tuned mass, and liquid dampers are some examples of semi-active control systems (Symans et al. 1997).

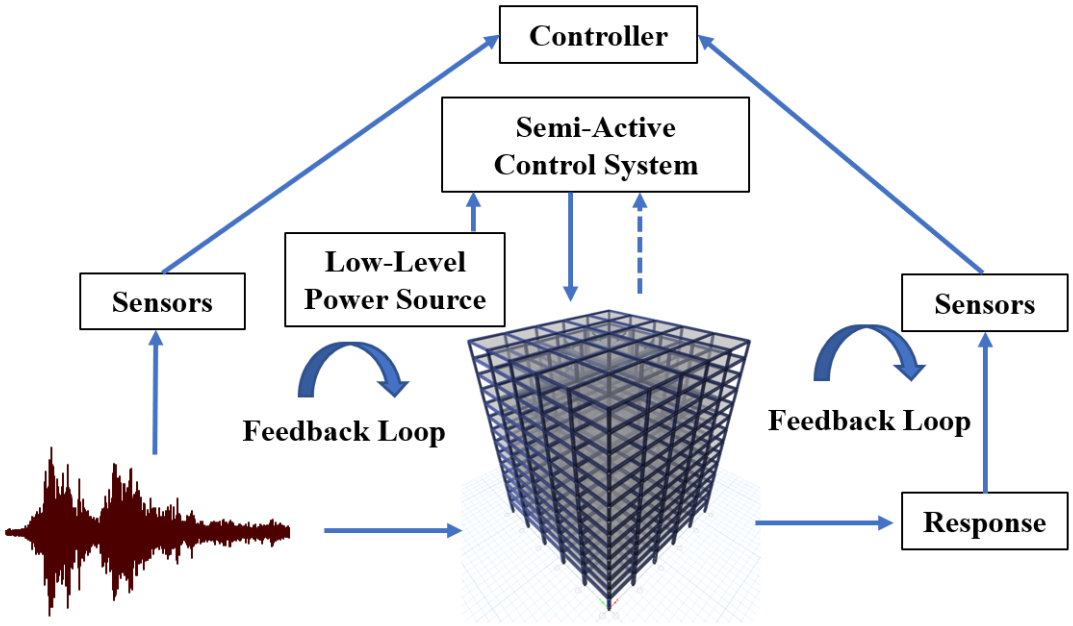

Figure 2-4. Semi-Active control system (based on Symans et al. 1997)

This section presents some works of literature on control systems. European passive control systems for seismic protection of new and existing buildings were examined in order to improve their passive control technologies (Mazzolani, 2001). The southern European parts around the Mediterranean Sea are generally affected by seismic prone. The lessons learned during severe earthquakes from 1976 to 1999 showed many reinforced concrete structures collapsed due to bad quality of materials, untrained workmanship, inappropriate design, and code provisions, in contrast, most of the performance of steel structures was satisfactory, thus more advanced technologies for seismic protection began to produce. In 1998 the ministry of public works in Italy categorized passive protection techniques into seismic isolation, energy dissipation, and mix techniques. The isolation systems were classified into three main groups based on the isolator types including elastomeric and steel, elastoplastic, and sliding or rolling isolators. The energy dissipation systems are classified into three groups based on the dissipating effect involving viscoelastic, elastoplastic, and friction dissipators. The main conclusions of the research projects include BRITE 2 (rubber bearing, rolling ball rubber bearing for base isolation), ISTECH (shape memory alloy on seismic protection of heritage buildings), REEDS (viscoelastic, elastoplastic,

shock transmitters, and viscous dampers), MANSIDE (seismic isolation using shape memory alloy), HARIS (elastomeric isolation bearing systems), ECOEST 2 (RC structures utilizing dissipative bracings), SPACE (semi-active and passive control systems) presented a scientific basis of new technologies for seismic protection of buildings.

Dallard et al. (2001) described the structure and retrofitting techniques to control the vibration of the London Millennium footbridge. During the opening day, unexpected vibration was occurred by the pedestrians crossed the bridge. The results showed this phenomenon could occur to those bridges having a frequency below 1.3Hz. Therefore, a retrofitting technique using fluid viscous and tuned mass dampers were developed to control the vibration with an excess of 20% damping level as presented in Figure 2-5.

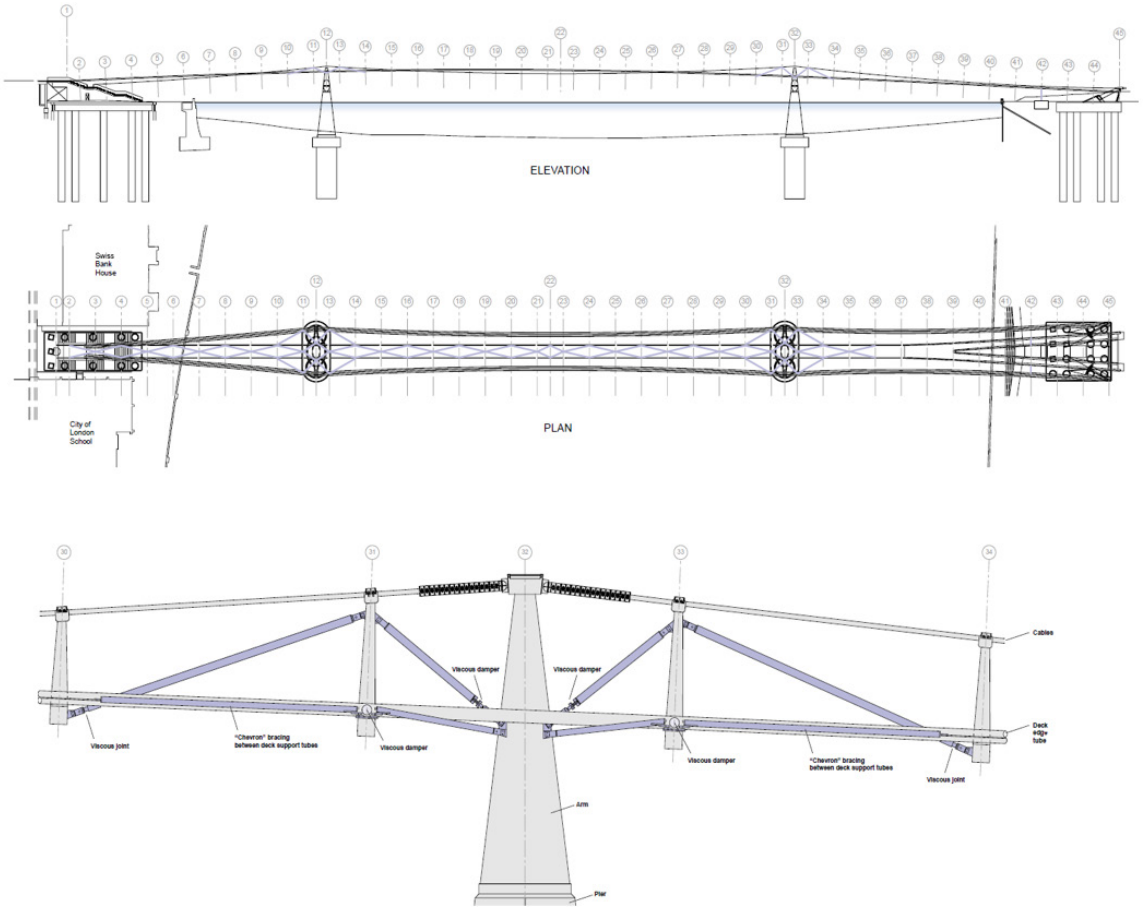

Figure 2-5. Arrangement of dampers in plan and elevation of the bridge (Dallard, et al. 2001)

The minimum target of natural frequency was set to 1.5Hz, to avoid resonant in structural response. In order to verify the proposed scheme, two viscous dampers connected with two chevron braces, and double pendulum tuned mass dampers were installed at midspan. The tests were performed using different configurations of viscous dampers including two viscous dampers fitted, one viscous damper at the northern end of the centre span fitted, and no viscous dampers fitted. The recorded acceleration time histories subjected to resonance induced by humans were used to determine TMD frequencies and damping. The different configurations of dampers were used to measure the frequency response function (FRF), then to calculate the modal properties. The results showed the response of the bridge was substantially reduced by just two dampers, also the vertical and lateral tuned mass dampers were in agreement with analytical predictions.

Part 1 of the numerical modeling and control algorithm of the footbridge to control its vibration using MR dampers in TMD was investigated by Occhiuzzi et al. (2002). Due to footbridges' light design loads as well as their aesthetic reasons, they are usually designed as slender structures. This slenderness causes vibration issues. To overcome these issues supplementary damping devices including Tuned Mass Damper were used as the most common technique. TMD devices reduce the response of the structure by transferring part of the structural vibration to the auxiliary mass, which strongly depends on a proper tuning of the auxiliary mass based on the expected natural mode of structure. Vibration induced by pedestrian loads in footbridges might differ from the expected one, therefore magnetorheological fluids were adopted as a semi-active TMDs to achieve desire tuning, in which the yielding threshold is dependent on the intensity of the magnetic field and by changing the current in the coils the desire dynamic properties can be obtained. A 50 kN semi-active MR damper is shown in Figure 2-6 (EU-funded space project).

Figure 2-6. MR damper (Occhiuzzi et al. 2002)

Adjusting on-line tuning of TMD was performed by two different approaches the first path was the feedback from vibration frequencies of structure and TMD, consequently, the tuning error was modified by the current input. The second path was using a control algorithm to derive the current inside the coils to minimize the selected parameters.

Part 2 of this study was conducted by Seiler et al. (2002), which focused on numerical and practical perception for vibration control of footbridge utilizing MR dampers in TMD. The additional mass in tuned mass dampers vibrates with the same frequency and opposite direction of the structure, therefore reducing maximum displacements and accelerations. In general, natural frequencies of a structure are about 10% to 20% higher than the real ones which reduced the effectiveness of passive TMD. To avoid this phenomenon a semi-active MR damper in a TMD was developed instead of a passive device, thus the mechanical properties of the damper can be modified by a magnetic field based on the feedback from the structure, during a dynamic excitation an optimal force was evaluated by the algorithm in order to minimize the bridge displacement. In this study, a footbridge in Forchheim, Germany, was equipped with TMD. The properties of TMD were tuned based on the Den Hartog criteria, and a comparison between semi-active and passive TMD was carried out using a two-degree of freedom structural model. Stationary load with different harmonic components and frequency of bridge was assumed as dynamic loading induced by pedestrians. Based on the numerical results in Figure 2-7, there was no improvement in the bridge response between semi-active TMD and optimal passive TMD. However, the displacements were reduced by a semi-active TMD in comparison with optimal passive configuration, thus semi-

active TMD was able to adapt to different system properties as well as control a wider range of frequencies.

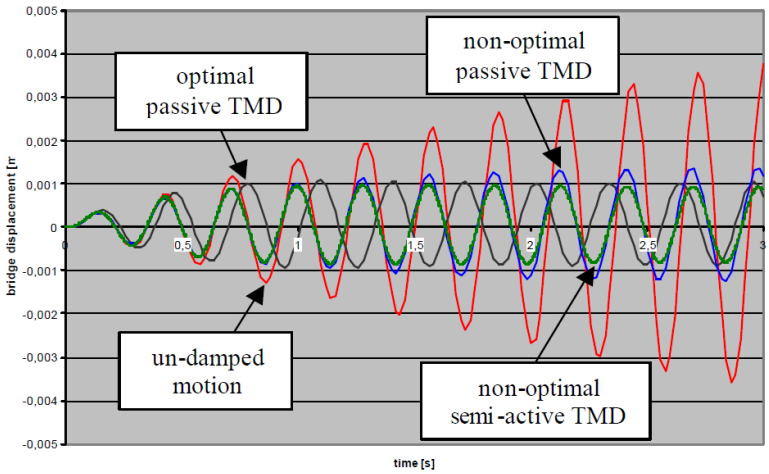

Figure 2-7. Bridge responses with optimal and non-optimal TMD properties (Seiler et al. 2002)

Tuned masse dampers were used in practical applications in the 1970s, such as John Hancock tower and Citicorp center in the USA to mitigate the structural response subject to wind load. Ricciardelli et al. (2000) presented an empirical algorithm to optimize the performance of Tuned Mass Dampers (TMD) based on the feedback of structure. A 64-story building subjected to turbulence was considered to verify this algorithm. A numerical example showed the effectiveness of this procedure without any knowledge of natural frequencies. Future studies are required to optimize the structure and TMD responses.

Seiler et al. (2003) presented the development and application of new technology for semi-active vibration damper “Semi-aktive Schwingungsdämpfer Entwicklung und Anwendung einer neuen Technologie”. In order to reduce the dynamic structural response of very slender structures including slender footbridges and filigree roof structures or general construction members in high seismic zones, special strategies need to be considered. More economical solutions were provided using new semi-active dampers compared to conventional design.

Spizzuoco et al. (2004) described the performance and the implementation of a semi-active magnetorheological (MR) control system. This paper investigated the efficiency of MR dampers for a 4-story steel structure on the multi-axis shaking table and covered the fundamental questions

in the literature including the type and complexity of the equipment to be examined in the real-life application. The effectiveness to reduce the structural dynamic response subjected to different excitation was proved, in which the control algorithm was used to minimize the structural energy and reduce the maximum displacements without increasing the accelerations. Moreover, MR dampers had a larger reduction in displacements compared with optimally designed passive devices.

The approaches and regulations for passive energy dissipation systems and seismic isolations of bridges and buildings in Europe and Italy were discussed by Dolce and Santarsiero, 2004. A comparison between European codes (EC8-2002) and US codes (IBC-2000) was conducted. Moreover, isolated and fixed structural forces based on Italian code were compared. Design and construction of buildings using passive control systems in terms of performance levels, seismic actions, and analysis methods were evaluated. In terms of performance level Italian code along with EC8 defined two main limit states, the ultimate limit state (ULS) referred to seismic action with a return period of 475 years and the service or damage limit state (DSL) referred to limits of interstorey drift in both sub-and superstructures with a return period of 95 years. Damage limit state (DSL) defined these limits to 0.005h and 0.0075h (h is the story height) for attached and non-contact structural elements. Additionally, EC8 and IC2003 had an additional check for isolation devices by factor 1.2, thus the return period increased to 750 years. Performance levels in IBC-2000 (US code) were classified into design basis earthquake (DBE) for safety checks of the isolations units and maximum credible earthquake (MCE) for the design displacements of the structure with a return period of 475 and 2500 years respectively. In terms of seismic actions, both EC8 and IC2003 had the same procedure for the calculation of isolated and fixed structures by considering a 5% damped elastic response spectrum. U.S. Code (IBC-2000) had a similar approach, if the building is located in the zone where S_1 is greater than 0.6g, site-specific spectra are required. A simplified analysis is required for the U.S. code for a preliminary design of the isolation system and to check the displacement and base shear calculated from the sophisticated analysis. In terms of the analysis method, the most unfavorable mechanical and physical values of the isolation system were considered. It was concluded there was considerable consistency in the

different codes. A comparison between design seismic forces on a fixed base and base-isolated structures showed that typical Italian buildings have a fundamental period of 0.5 seconds, thus, to reduce the design forces an isolation period of 2.0 seconds was recommended. The Italian codes allowed general analysis methods for the design of energy dissipation systems such as dissipating braces. Occhiuzzi, 2009 proposed a methodology to calculate the modal damping ratios of non-proportional damping schemes based on the state-space representation of dynamic systems. This methodology was adopted and used to calculate different results of modal damping ratios in the literature. Similar results were suggested an optimal first modal damping of 20%. It was also shown the higher mode effects can be neglected in designing a supplemental damping system.

Experimental investigations of MR dampers in passive and active control systems were performed using two prototype MR semi-active dampers manufactured in Germany (Caterino et al., 2013). A large range of frequencies, different currents, and displacement amplitudes was performed to show the dissipative capacity of the devices. The passive system was created by constant current feeding and the semi-active system was driven by an energy-based control algorithm. It was observed the effectiveness of semi-active MR dampers depended on the electric part of the control system to operate in real-time, the response time of SM MR damper can be limited to 8-10-ms. Based on the recorded values of dissipated energy and maximum control force an equivalent linear viscous damping coefficient was proposed for the preliminary design of semi-active MR dampers. Moreover, the properties of semi-active MR dampers were compared with passive ones, and it was confirmed the energy dissipation in SA MR dampers was higher even for different input motions.

2.3 Buckling Restrained Braced Frames

Steel concentrically braced frames have been used to protect the building against lateral loads as they are simple in design and fabrication. They dissipate energy by buckling in compression and yielding in tension. However, their poor performance during past earthquakes caused

extensive damage (Tremblay et al.1966), which was caused by several factors including limited ductility, fracture of connection, and their unsymmetrical behaviour in tension and compression.

The Buckling Restrained Braces (BRBs) on the other hand consist of a ductile steel core in a concrete or mortar encased steel tube. The steel core provides the yielding mechanism, and the tube prevents the buckling of the core, which can be an alternative to conventional braces. The buckling restrained bracing element as well as hysteretic Behavior of Both Conventional and buckling restrained bracing members are presented in Figure 2-8 (Moni et al. 2016).

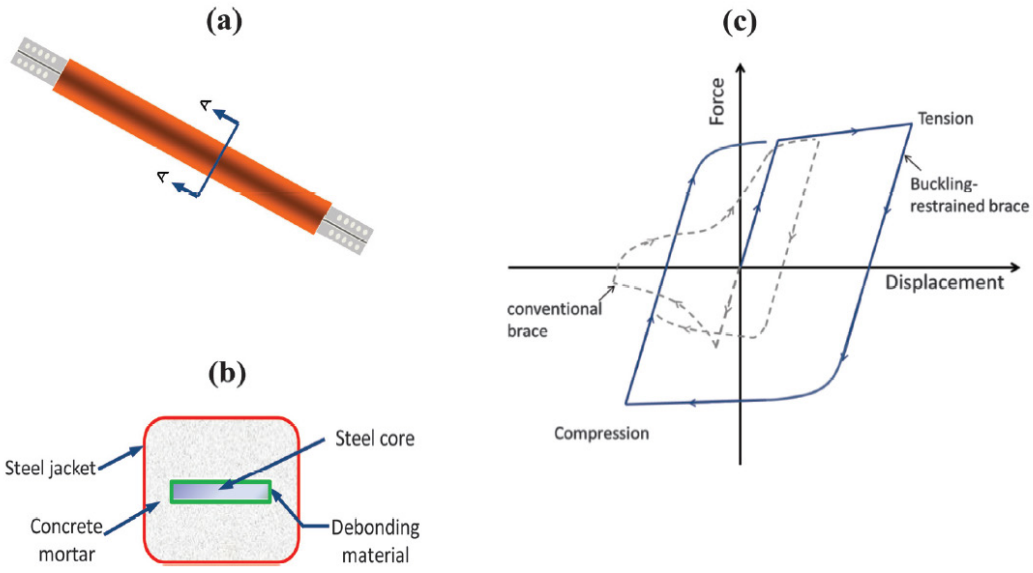

Figure 2-8. (a) Typical BRC, (b) cross section, and (c) Lateral load-roof displacement relationship (Moni et al. 2016)

Since the 2010 NBCC prescribed the over strength and ductility factor for BRBFs independent of span length, buildings height, and bracing positions, this paper investigated the seismic design factors including the effects of building height and span length. The study parameters were including over strength, ductility, response modification factor for low to midrise Buckling Restrained Braced Frames (BRBFs), moreover, nonlinear static push over analysis and dynamic time history analysis were conducted to assess the dynamic response of the four, six and eight-story frames with different span length.

In addition, the configuration of inverted-V chevron and split-X were used in the frames. With these configurations, twelve frames were designed according to NBCC 2010 and CSA 2009. All

the frames have three bays (3@ 6m,8m) in each direction and a story height of 4m, and a maximum allowable total height of 40m according to CSA 2009.

The story shear of the bracing due to lateral loading was almost similar for frames with different bracing positions. However, the axial forces in Split-X braces (BRX) with the same span length were larger than in Chevron Braces (BRC). BRX connects two levels between two columns nodes, therefore attracting more gravity forces and experiencing more forces. Eigenvalue analyses were performed and compared with the period obtained by NBCC 2019 which underestimated the period of the BRBFs as presented in Table 2-1. The overstrength and ductility of BRBFs were evaluated by static nonlinear pushover analysis which was limited to the design drift limit of 2.5% as demonstrated in Figure 2-9.

Table 2-1. Fundamental period of the structure (Moni et al. 2016)

Span length (m)	6		8		
Bracing	BRC	BRX	BRC	BRX	Empirical equation
# Story					
4	0.57	0.57	0.57	0.57	0.4
6	0.72	0.72	0.72	0.72	0.6
8	0.92	0.92	0.92	0.92	0.8

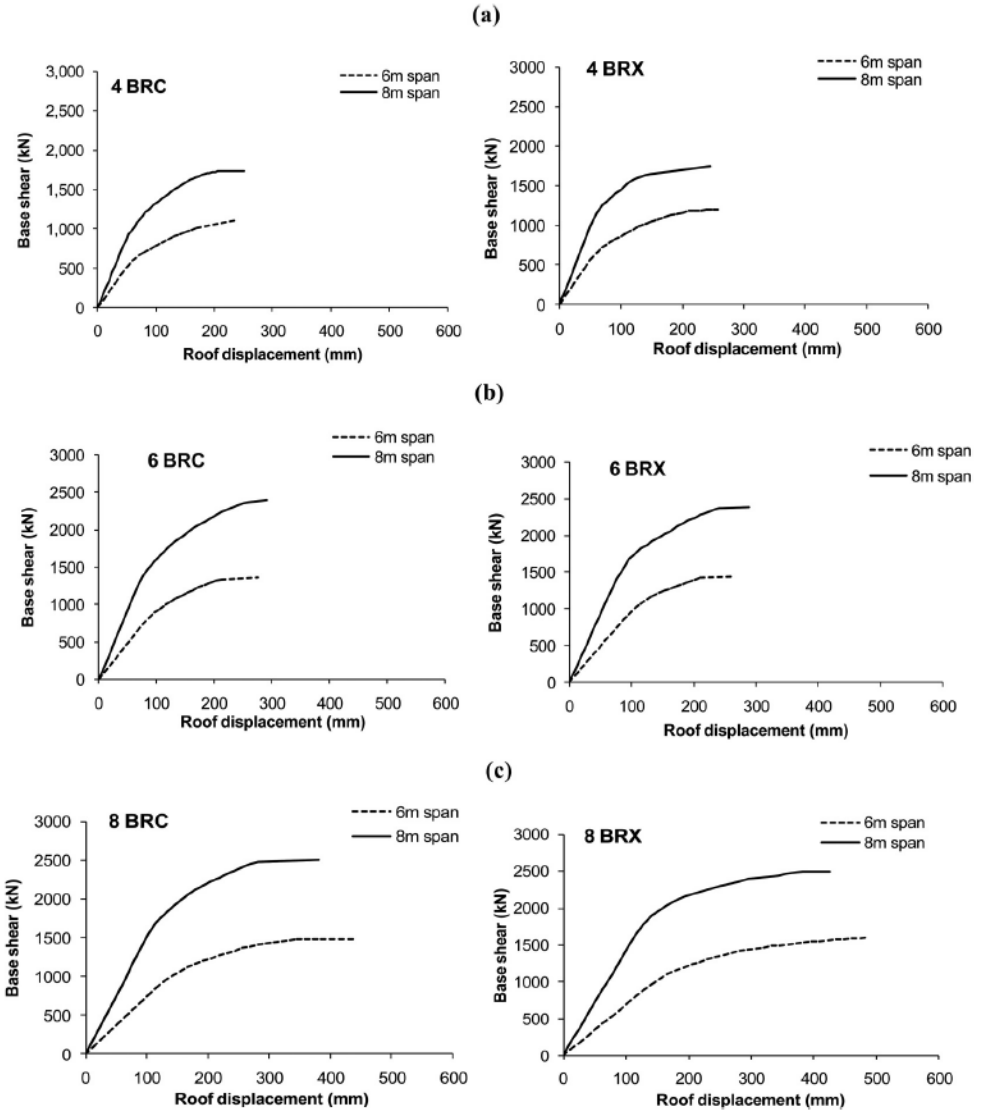

Figure 2-9. Pushover response curve for (a) Four-story, (b) six-story, and (c) eight-story (Moni et al. 2016)

It was observed that when the span length increased, elastic stiffness and ultimate strength increased. Figure 2-10 showed the overstrength and ductility factors for the BRBFs with chevron inverted-V and X-braces. It was also observed the overstrength factor decreased when the bay length increased and the BRFs with longer spans resulted in a higher ductility factor. Since there were 5% differences in ductility for BRBFs of the same height with different bracing positions, the bracing positions had no effect on the ductility factor.

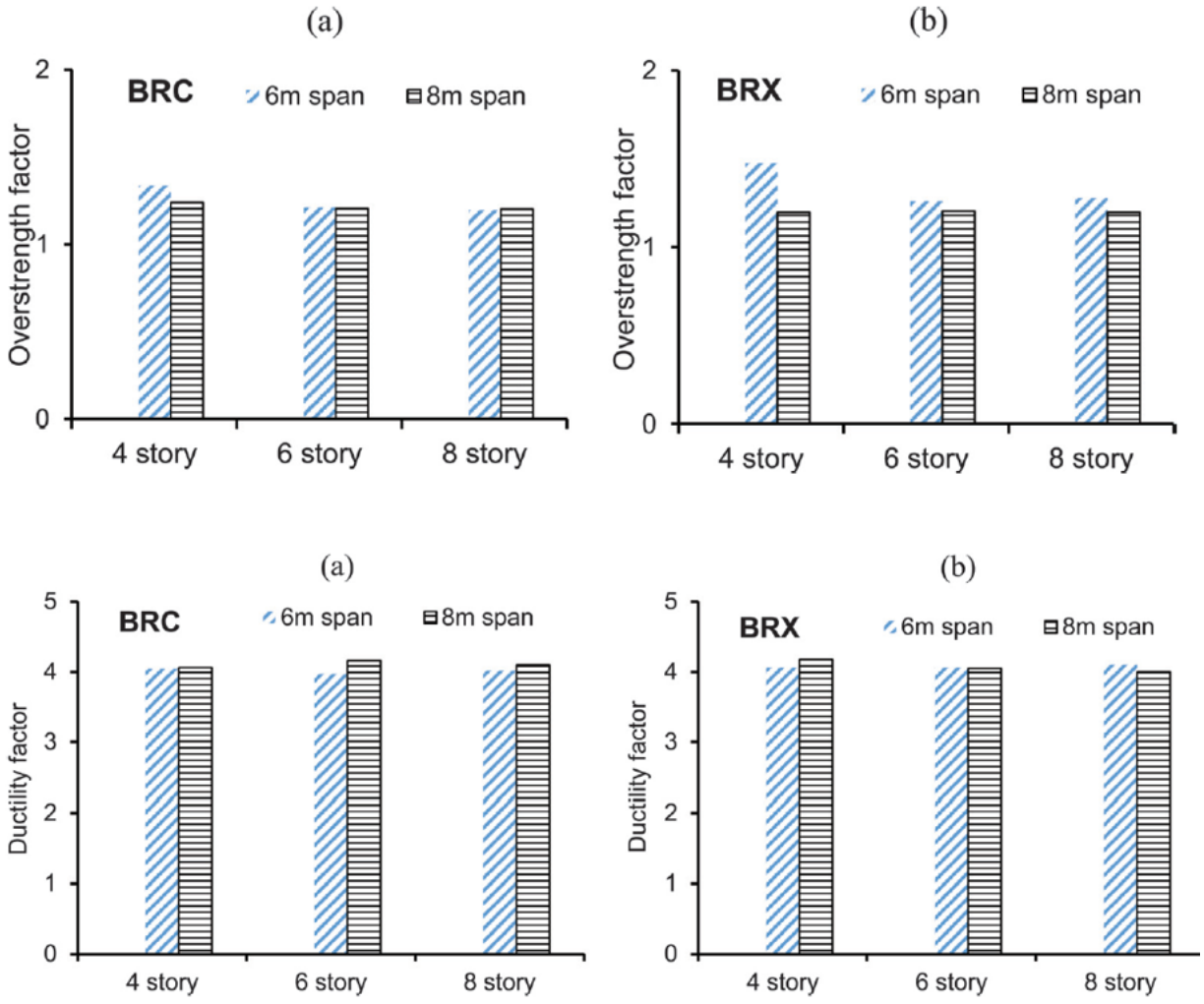

Figure 2-10. Overstrength and ductility factor (a) Chevron bracing and (b) X-bracing (Moni et al. 2016)

Response modification factors were calculated by multiplying the ductility factor with the overstrength factor. It was shown that the response modification factor reduced with the increase of the story height and the increase of the span length. The response modification factors were affected by the bracing configuration due to their difference of 11%.

Moreover, a nonlinear dynamic time history analysis was performed to assess the seismic performance of the BRBFs by using ten ground motions for Vancouver. It can be observed from Figure 2-11 that the maximum interstory drift demand was generated at the first-floor level, and there was no difference between the bracing configurations. Generally, it was observed that BRBF

height shifted the interstory drift demand to a higher level, while for the BRBFs with the same height the drift demand shifted to a lower story or remained unchanged when length increased.

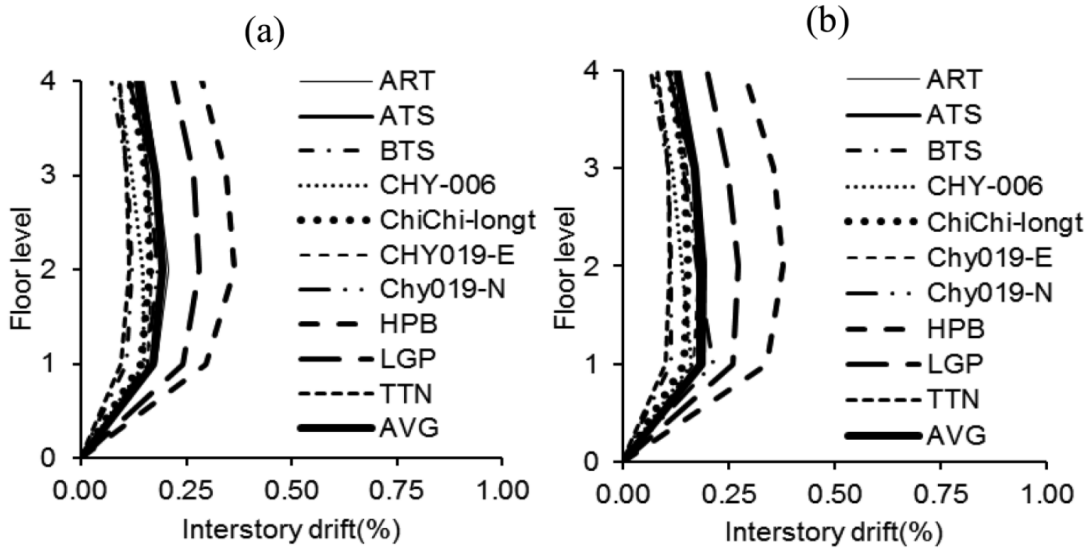

Figure 2-11. Interstory drift demand for 4-story chevron braced (a) 6m span and (b) 8 m spans (Moni et al. 2016)

The base shear demands were calculated based on nonlinear time history analysis, it was seen that the average base shear demands for frames with larger spans were experienced higher base shear demands. Moreover, the demand increased when the number of stories increased, and bracing configuration had a small effect on the base shear demand. The base shear capacity/demand ratios decreased when the height increased for chevron braced frames, but it remained the same for X-braced frames.

Two different span lengths of 6m and 8m for four-, six, and eight-story buildings including chevron inverted-V and split X-braces were designed and analyzed. Nonlinear static/pushover analysis was performed to assess the over strength, ductility, and response modification factors. Moreover, a nonlinear response history analysis was performed to evaluate the seismic performance of the designed BRBFs.

The empirical equation proposed by NBCC 2010 underestimated the natural period of BRBFs. The span length had a direct effect on the base shear capacity of BRBFs. The overstrength factor decreased when the height and span length increased. It was noted the BRBFs with longer span

length had a higher ductility factor and lower response modification factor, also the bracing configuration may affect the ductility and response modification factors. Nonlinear time history analysis showed that the interstory drift demand concentration shifted to a higher story level as the height increased. However, when span length increased with the same height, the drift demand remained constant or moved to lower heights. As the building height and span length increased, the base shear demand increased. Capacity over demand ratios demonstrated higher roof drift and base shear capacities for all the frames, in comparison to the demand values. The response modification factors for BRBFs need more assessment using different design details including floor height and more sophisticated modeling detail coupled with the buckling restrained braces. This study was limited to modeling the steel core of BRB, and the effects of concrete and debonding materials were neglected.

Bracings have been used as the most common lateral load resisting system; however, they don't perform well in the nonlinear range of deformation such as low ductility, nonsymmetrical hysteresis curve (tension and compression), and stiffness degradation caused by buckling in cyclic loading. Therefore, the new generation of the bracing system "Buckling Restrained Braced Frames (BRBF)" have being investigated. These bracing systems have symmetric hysteresis curves, high ductility, and large drift capacity (Asgarian et al. 2009).

The design codes are based on linear methods by considering nonlinear behaviour. and since the structures possess reverse strength (over-strength) and capacity to dissipate energy, design loads are reduced by force reduction factor or response modification factor in design codes. The response modification factor for buckling restrained braced frame requires more investigation, therefore this paper focused on the evaluation of overstrength force reduction caused by ductility and response modification factors of twenty-four BRBFs. To obtain these factors nonlinear static pushover analysis, nonlinear incremental dynamic analysis, and linear dynamic analysis were performed.

The calculation of base shear and stress based on structural elastic analysis is bigger than the structural response, hence these forces are reduced in seismic design codes. The response

modification factor involves the inelastic behaviour of a structure and highlights over strength and ductility of the structure in an elastic stage. Therefore, the response modification factor accounts for the structure's ductility and overstrength, as well as the change in the degree of stresses considered in its design. Bilinear elasto perfectly plastic relation is a way to idealize real nonlinear behaviour as shown in Figure 2-12.

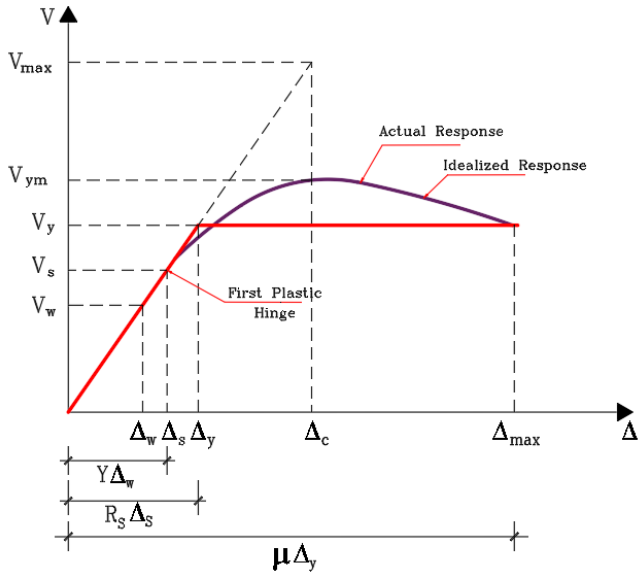

Figure 2-12. General structure response (based on Uang et al. 1991)

In this figure, V_y represents the yield force, Δ_y is the yield displacement, V_e (V_{max}) is the elastic response strength of the structure. The maximum base shear, V_e, to the maximum base shear in elasto perfectly behaviour, V_y, is the ratio of force reduction factor ($R_m = V_e / V_y$). The overstrength factor on the other hand is defined by the ratio of maximum base shear, V_y, to the first yield strength, V_s, ($R_s = V_y / V_s$).

In this study, the overstrength, ductility, and the response modification factors of buckling restrained braced frames, 4, 6, 8, 10, 12, and 14 story buildings having a bay length of 6m and four different bracing configurations such as split X, chevron V, chevron –inverted V and diagonal were designed based on IERD. The OpenSees software was used for computational modeling. To calculate the overstrength factor, R_s, the incremental nonlinear dynamic analysis of the models was performed and the PGA's of the selected ground motion had changed by several tries and errors in order to meet the failure criteria for the followings: the inelastic base shear is

the maximum nonlinear base shear, push over analysis was performed to obtain the base shear associated with the initial plastic hinge by increasing lateral force proportionate to fundamental mode shape. It means the linear ultimate limit nonlinear dynamic analysis was considered in nonlinear static analysis. To calculate R_m, first V_y was calculated based on nonlinear dynamic analysis, and the maximum linear base shear, V_e, was obtained by linear dynamic analysis and then, the ductility reduction factor was calculated. It was observed that overstrength, ductility, and response modification factors decreased as the height of the building increased. In addition, the response modification factor is affected by the type of bracing arrangement and tentative values of 8.35 and 12 were suggested for the ultimate limit state and allowable stress design methods.

Due to complexity in brace hysteretic behaviour such as unsymmetrical properties in compression and tension which results in the different distribution of internal forces and predicted deformation by conventional design methods, the capacities of selected braces in certain stories are greater than required, whereas the capacities of selected braces in other stories are close to design requirement. Also, the distribution of design forces in beams and columns differs from what is predicted in an earthquake. Hence this paper focused on the performance of the concentrically braced building under seismic loads. Nonlinear dynamic analysis was performed for high-performance hysteretic braces, concentrically braced frames with conventional braces, and viscoelastic dampers (Sabelli et al. 2003). Results were shown buckling restrained braces were very effective and were able to overcome many of the issues related to concentric braced frames. It was also observed the response was not to R. This study was limited to CBF and only examined the seismic demands. Further studies are required to characterize the capacities of the overall brace frame system. Moreover, experimental studies to examine the actual behaviour of buckling restrained braces as well as new design approaches of other types of bracings are required.

2.4 Application of Sustainable Concrete

The United Nations word commission on environment and development described sustainable development as “development that meets the needs of the present without compromising the ability of future generations to meet their own needs.” Sustainability is a long-term goal and to achieve

sustainable development numerous steps should be followed including the understanding of the environment, society, economy, and culture and the connection between them (UNESCO 2022). Figure 2-13 demonstrates the sustainable construction concept, which shall evolve over time, and requires immediate action of all parties such as politicians, the global community, decision-makers, and leaders to guarantee that the built environment of the future is safe, robust, durable, and has a sustainable environment, society, and economy (GLOB 2022).

Figure 2-13. Sustainability in the Built Environment (GLOBE 2022)

Cement paste and aggregate are the two main components of conventional concrete, crushed stone or natural sand and gravel bond together and form artificial stone because of the chemical reaction between cement and water (Brzev and Pao 2016). Green concrete is defined as concrete that has a minimal environmental impact during manufacturing, or has life cycle sustainability with excellent performance, or uses at least one waste component (Suhendro 2014).

Concrete sustainability has evolved by using alternative fuels and raw materials in cement production, as well as utilizing reclaimed water and reused materials. The selection of materials in the concrete mixture such as cementitious materials, aggregates, admixtures, and water have a direct effect on sustainable concrete. Cement production is an “energy-intensive process”, improving cement productions have the potential to improve the environmental impacts which are based on the concrete performance such as using dry klins, preheater/precalciner technology to

collect waste heat, improved grinding process, and considering alternative fuels such as bio-fuel. Aggregates occupy more space in concrete mixtures and they may require less energy to produce than cement, they minimize embodied energy and CO2 emissions, benefiting towards sustainability (ACI 130, 2019). Crushed stone and natural sand and gravel aggregates have been widely used in the concrete mixture; however, the use of natural aggregates production is declining due to the reduction of their sources compared with crushed aggregate (USGS 2011). Non-conventional aggregates such as lightweight aggregate, recycled/reused aggregates, recycled concrete, screening, crushed glass aggregate, waste plastic aggregate, recycled scrap tire aggregate, and recycled asphalt pavement aggregate are becoming more popular. They reduce waste materials, CO_2 emissions, and embodied energy, therefore their use contribute to sustainability. In addition, sustainable admixtures can reduce the cementitious material content, lowering the demand for potable water in the concrete mixture, and improving concrete durability (ACI 130, 2019).

Waste tires are a major global problem, they consist of complex materials, and they are not biodegradable, decompose slowly, and some are dumped in landfills that release toxins into water and soil. They often catch fires and might burn for up to nine months and emit carcinogenic and mutagenic toxins into the atmosphere (Williams 2017; AZOCleantech 2021). Therefore, the waste recycling is becoming more viable, European tire industries have improved significantly in their manufacturing processes by using sustainable raw materials, replacing new recyclable materials, and at the end of tires life cycle, they are treated through the ELT management companies, in addition, the secondary raw materials are increasing to be used in industry such as construction (ETRMA 2022). In Germany half of the used tires are used as a substitute fuel. A.T.U-Tochterunternehmen ESTATO Umweltservice GmbH is one of the leading recycling companies in Europe (almost 600 branches) which processes around 8 million used tires per year. According to European guidelines, about 30% of tiers can be used globally, while the rest disassemble into original components including 60% rubber, and 40% textile fibers and metal wires, which are available based on individual requirements (WDK 2022). The focus of this study is the application for the use of recycled scrap tire aggregates in order to reduce waste and contribute to sustainability.

2.5 Review of Tire-Derived Light Weight Aggregate's mechanical properties

Tire-derived aggregate is derived from waste tires in a standard range of practical sizes. TDA is described as pieces of scrap tires with a basic geometrical shape with two practical types, Type A ranging from 75 to 100mm, and Type B ranging from 150 to 300 mm (ASTM D6270-08). A summary of the shear stress-displacement relationship is presented in Table 2-2 (Ghaaowd et al. 2017).

Table 2-2. TDA Internal Shear strength (Ghaaowd et al., 2017)

Test parameters and results	Humphrey and Sandford (1993) and Humphrey et al. (1993)	Foose et al. (1996)	Bernal et al. (1997)	Gebhardt (1997)	Yang et al. (2002)	Xiao et al. (2013)	This study
Box shape	Square	Circular	Square	Square	Not recorded	Rectangle	Rectangle
Shear box areal dimensions (mm)	286×286 and 387×387	279 (diameter)	300×300	910×910	Not recorded	790×800	3,048× 1,219
Shear box height (mm)	228	314	225	810	Not recorded	1,219	1,830
Box width to maximum particle size ratio	3.8–5.0	2.1	6	2.1	Not recorded	10.5	4
Maximum shear box displacement (mm)	35	90	60	230	25	180	690
Shearing rate (mm=min)	7.6	1.3	1	1	1	22	1–100
Maximum TDA size (mm)	76	150	50	432	10	75	320
Average unit weight (kN/m^3)	5.5	5.9	5.9	5.6	5.73	7.91–13.2	5.04–8.04
Normal stress range (kPa)	17–68	9–50	7–54	5.5–28	—	24–96	19.5–76.7
Maximum normal stress (kPa)	68	80	54	28	83	96	88.4
Internal friction angle (degrees)	19–26	30	35[a]	38	32	36.1	30.2–41.1
Apparent cohesion (kPa)	4.3–11.5	3	0	0	0	14.3	0

Besides the environmental benefits of TDA, it can be used as an engineering application that is lightweight, durable and has significant cost advantages. The following literature is a brief explanation of the mechanical properties of TDA as well as the experimental results of rubberized lightweight aggregate concrete that can be used as an alternative material to model and evaluate the performance of Buckling Restrained Brace.

2.5.1 Mechanical properties

In this part mechanical properties of TDLWA including compressive strength, split tensile strength, flexural strength, toughness, modulus of elasticity acoustic, thermal conductivity, and electrical resistivity are discussed.

The properties of rubberized concrete were investigated by (Locher, 1994) by changing the size and quantity of discarded tires in the form of rubber chips. Stress-strain diagram as well as splitting tensile tests were performed at the end of 7, 28-day, and six months based on the

specimens by adding rubbers with different volume ratios of 15, 30, and 45% into C20. Adding rubber chips decreased the elastic energy capacity of normal concrete and increased its plastic energy capacity. Similar findings were obtained by (Toutanji, 1996), the specimens showed a reduction in compressive and flexural strength and high toughness of flexural specimens, more investigation to improve the concrete strength by adding rubber tire chips as an alternative aggregate is required.

Concrete mixtures with normal aggregates can be designed with existing methods. However, special provisions are required, when normal aggregates are replaced with unconventional components. This study is focused on rubberized concrete mixtures and their mechanical properties (Khatib and Bayomy, 1999). Fine crumb rubber and coarse tire chips were used in Portland cement concrete. Three groups of eight designated rubberized mixes developed including group A containing crumb rubber and replaced the fine aggregate from 5-100%, in group B coarse aggregate was replaced by tire chips in the range of 5-100%, group C rubber content wad divided equally between crump and chips and replaced the coarse by chips and sand by crumb in the range of 5-100%. The experimental tests were performed based on ASTM standards using compressive and flexural strength tests. The compressive and flexural strengths reduced as the rubber content increased, when the rubber content reached 60% the samples showed remarkable elastic deformation. To avoid strength reduction, it was recommended rubber contents shall not be greater than 20% of the total aggregate volume. Durability, fire resistance as well as the life cycle cost of rubber Portland cement concrete need more investigation.

Modified concrete using waste tire chip has low strength and stiffness and high toughness. When its strength is too low, it is impossible to use waste tire rubber-filled concrete for construction purposes. This study investigated the possible increase in strength and stiffness with a reduced cost by using waste tires in the shape of fibers (Li et al. 2004). Split tensile strength, compressive strength, and modulus of elasticity tests were conducted on 42 cylinders, among them, twelve cylinders were used without and with waste tire chips, and 30 specimens were made using waste tire fibers including different lengths and stiffness. The results indicated using waste tire fibers in modified concrete has higher stiffness and strength compared with waste tire chips,

moreover, the analytical study proved that waste tire fibers can reduce stress concentrations. Further studies such as beam fatigue tests are required to assess the practical use of rubberized concrete in construction.

An experimental study was performed using silica fume to improve the mechanical properties of rubberized concrete, crumb rubber as fine aggregate, and tire chips as coarse aggregate were employed. The range of the rubber contents was from 2.5% to 50% by the aggregate volume, and 5%, 10%, and 20% of silica fume were added as an equal replacement of cement. The study parameters were including the compressive and splitting tensile strengths, and modulus of elasticity on 70 concrete mixtures using water-cementitious material ratios of 0.60 and 0.40 with the initial compressive strengths of 54 and 86 MPa to control the mixtures (Güneyisi et al. 2004). With the rubber content increased from 0% to 50%, the compressive and splitting tensile strengths, as well as modulus of elasticity decreased. These parameter reductions were increased by using silica fume, which resulted in a 43%, 27%, and 15% increase in compressive, splitting tensile strengths, and modulus of elasticity respectively. However, rubber content should be limited to 25% of the total aggregate volume. The rubberized concrete duarability under different weathering conditions needs more investigation.

Material has high toughness when the entire energy is created due to fracture in plastic, while when this energy is generated due to fracture in elastic, the material is brittle. This study focused on replacing a portion of aggregate with rubber to enhance the ductility of concrete. The objectives of this research were including the effects of rubber content and rubber types on compressive strength (cylinder and cube), static and dynamic modulus of elasticity and the brittle index of rubberized concrete (Zheng et al. 2008). Property of cement past, aggregates' stiffness, and calculation methods are the main criteria related to the elastic modulus of concrete. The static modulus is calculated based on the slope of a stress-strain curve, and the dynamic modulus is determined from ultrasonic, longitudinal, and transverse waves in rubberized concrete specimens. The brittle index was calculated based on energy from the area under stress-strain curves as presented in Figure 2-14. A1 is the non-recovered area of plastic energy capacity and A2 is the recovered area of elastic energy capacity. The ratio of A2/A1 is the brittle index. When this ratio

is zero all energies are irreversible. while when it is infinity, all energies are reversible. The brittle index is higher in brittle material and is lower in ductile material.

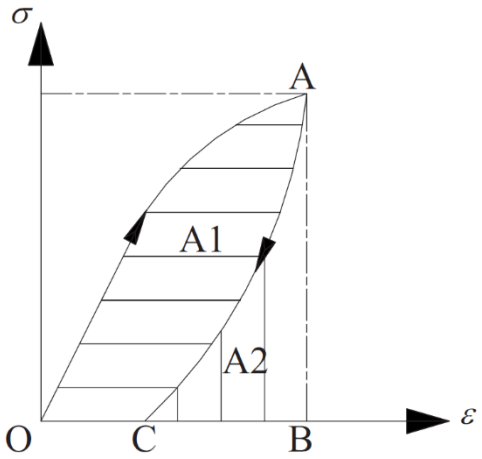

Figure 2-14. Brittle index (Zheng et al. 2008)

Two types of rubber were used in the experimental tests ground rubber and crushed rubber as shown in Figure 2-15. The target compressive strength of 40 MPa was selected. Cylinder and cube specimens were used for the static and dynamic modulus of elasticities respectively, compressive strength was measured for both.

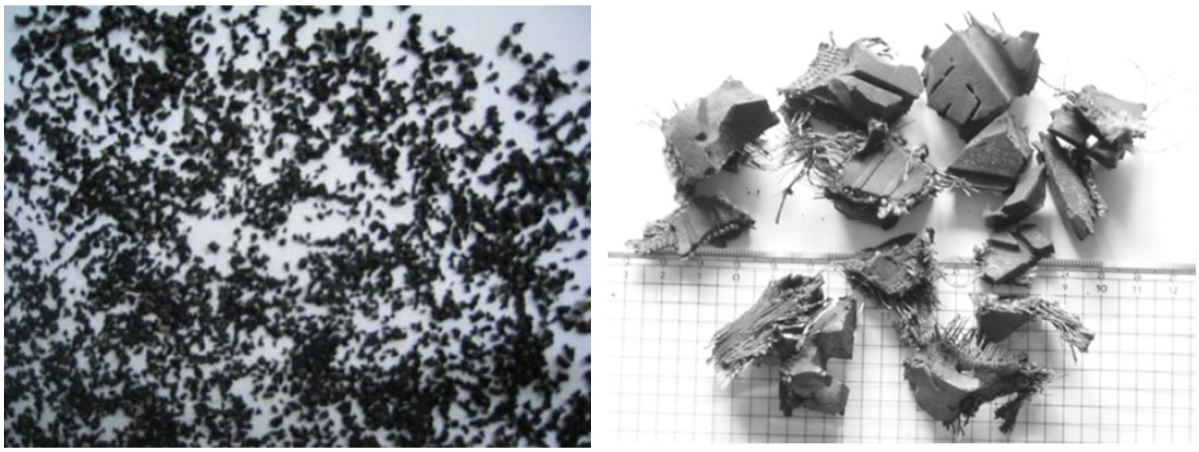

Figure 2-15. GR-8 (ground rubber), and CR-40 (Crushed rubber), (Zheng et al., 2008)

When the rubber content increased unit weight and compression decreased as presented in Figure 2-16. The average compressive strength of normal concrete at 28 days was 38 MPa. The

strength of crushed rubber using the content of 15, 30, and 45% decreased to 30.1, 21, and 18.1 MPa, while the compressive strength of ground rubber was 33.5, 25.8, and 19.6 MPa.

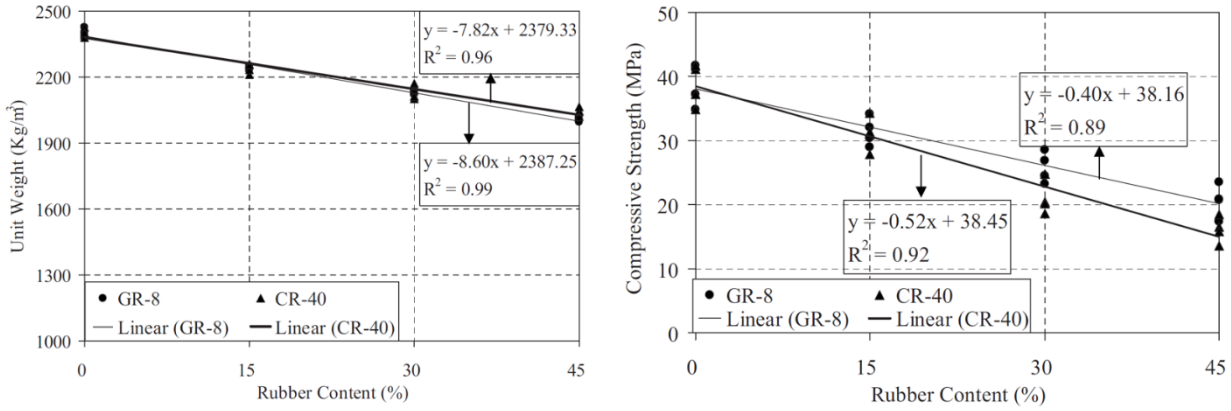

Figure 2-16. Unit weight and compressive strength of rubber content (Zheng et al. 2008)

The ACI equation to calculate the static modulus of elasticity was in the range of 15.8 to 31.5 GPa which unpredicted the modulus of elasticity of rubberized concrete. A similar trend of modulus of elasticity was observed for both GR-8 and CR-40. The dynamic modulus of elasticity was tested using pulse velocity, it was observed when the in-rubber content increased the dynamic modulus reduced. In general, an increasing amount of rubber content reduced the compressive strength, static, and dynamic modulus of elasticity. Brittle index values of normal concrete were higher than rubberized concrete, which showed the ductility of the material. The optimal content of 30% for crushed rubber was recommended for strength and deformation properties, decreasing brittleness index was reached by using ground rubber. More parametric studies are required to define a framework for construction projects. Similar results were obtained by (Issa and Salem, 2013), and the behavior of recycled crumbed rubber as a replacing material for fine aggregate in mixed concrete design ranging from 0% to 100% was investigated. The rubber content of crumbed rubber is suggested to be below 25% for compressive strength. Lower density, higher ductility, insulation, and damping were the advantages of using crumbed rubber in mix design concrete, however, a significant reduction in compressive strength when the rubber content was above 25%, unpredicted failure mode, and economical aspects were the disadvantages.

Mechanical properties of Tire-Derived Light Weight Aggregate Concrete (TDLWAC) were conducted using 38 cylindrical and 36 beam specimens (Miller and Tehrani, 2017). Since a few

studies were found to work on the rubber aggregate as a replacement for light weight aggregate, this study was investigated the splitting tensile, compressive strength, flexural toughness, flexural strength, and an impact flexure test of rubberized lightweight aggregate. The target strength was 21 MPa, Cylinder and beam specimens were contained shale light weight coarse aggregate, natural sand fine aggregate, cement, and water, then the TDA was added to cylinder and beam specimens by replacement ratios of 0% to 100% as shown in Figure 2-17, and 20% increments were used for both specimens. Compressive strength, static modulus of elasticity, and splitting tensile strength were tested on 38 cylinders specimens, and flexural strength, toughness, and impact flexure were tested on 36 beams specimens per ASTM C39 and C78. The compression test was carried out using a 500 kN testing machine which was applied 0.24 MPa per second in order to capture the strain gauge report. ASTM C469 was used to determine the static modulus of elasticity, and the stress-strain relationship was determined by the load-deflection data obtained during each test.

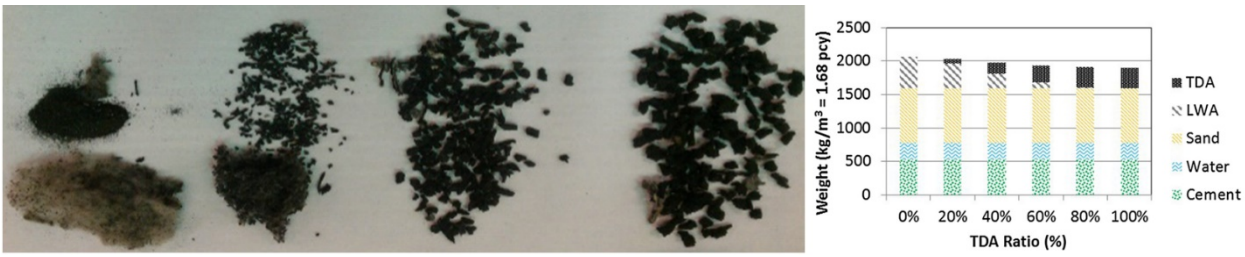

Figure 2-17. The crumb rubber and six mix designs (Miller and Tehrani, 2017)

Splitting tensile strength was determined by the load-deflection relationship and in accordance with ASTM C496. Static flexure test was carried out according to ASTM C78, the load was applied at two points with a rate of 1mm per minute, and the obtained data from the strain gages was used to determine the modulus of rupture using ASTM C78, and the flexural toughness in line with ASTM C1018-97. The last test was the impact flexure test, the 1110N falling weight was applied at three different drop heights, and the impulse force was calculated based on the acceleration time history data for the impact which was recorded by the accelerometer. The drop height calculation for the impact flexure test was presented in Table 2-3 and different tests setup are presented in Figure 2-18.

Table 2-3. Calculated the drop heights (Miller and Tehrani, 2017)

Rubber Content %	Static Load kN (lbf)	Deflection at Static Load mm (in.)	Equivalent Drop Height mm (in.)
0%	27.71 (6229)	1.9 (0.0762)	48 (1.899)
20%	24.12 (5422)	2.3 (0.0915)	50 (1.984)
40%	20.00 (4496)	1.9 (0.0753)	34 (1.354)
60%	19.78 (4446)	1.7 (0.0653)	29 (1.161)
80%	14.56 (3273)	1.9 (0.0727)	24 (0.952)
100%	13.55 (3046)	2.1 (0.0810)	25 (0.987)

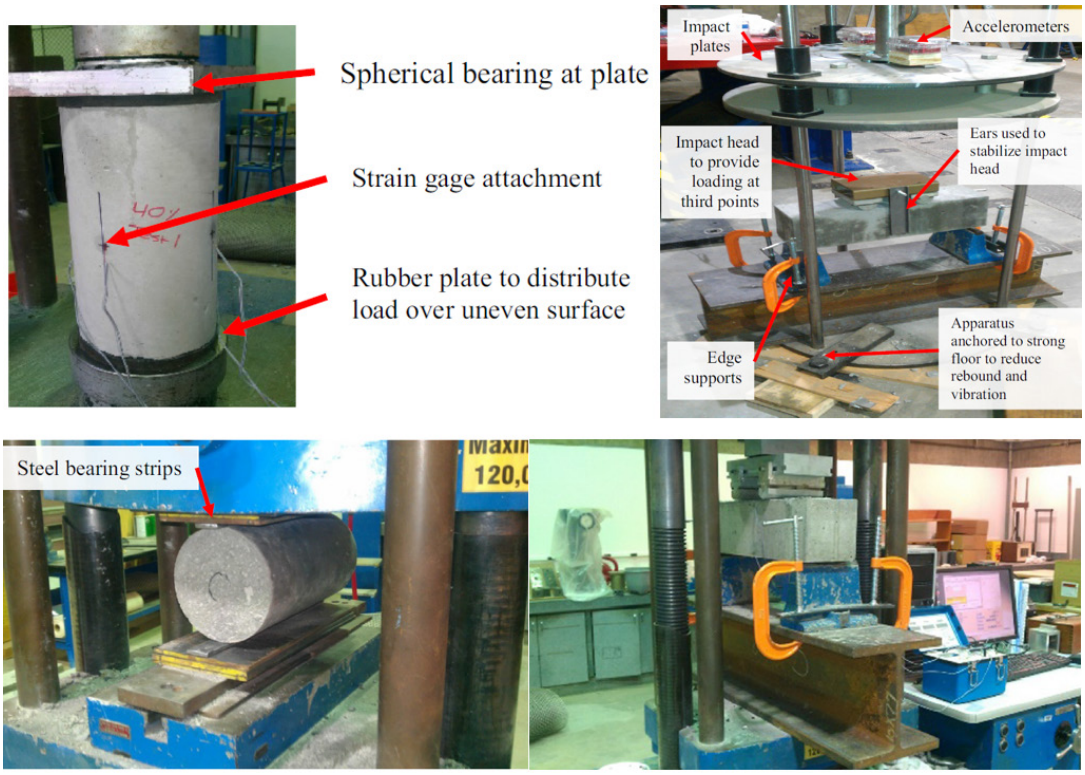

Figure 2-18. Four different tests set up (Miller and Tehrani, 2017)

The compression strength was decreased when the rubber increased and there was more transverse deformation before failure. The compression strength was reached 23.4 M as shown in Figure 2-19, and the failure mode was type 3 as specified by ASTM C39. Since the stress-strain relationship did not fit the ASTM standard, the initial linear elastic relationship was used for calculation.

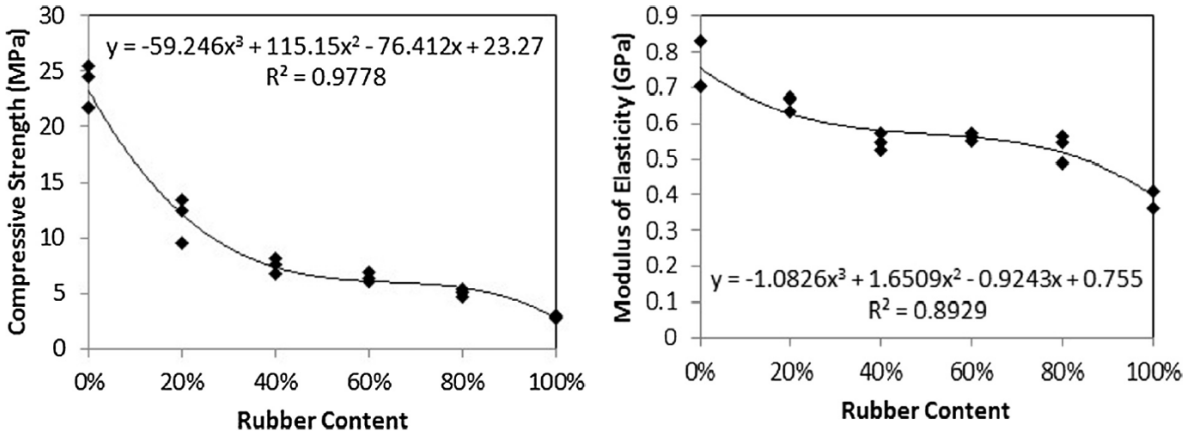

Figure 2-19. Compressive strength and modulus of elasticity to rubber content (Miller and Tehrani, 2017)

The failure during the splitting tensile test developed by a single crack down the center of the cylinder, it was observed the relationship between the splitting tensile test and rubber was more linear (Figure 2-20).

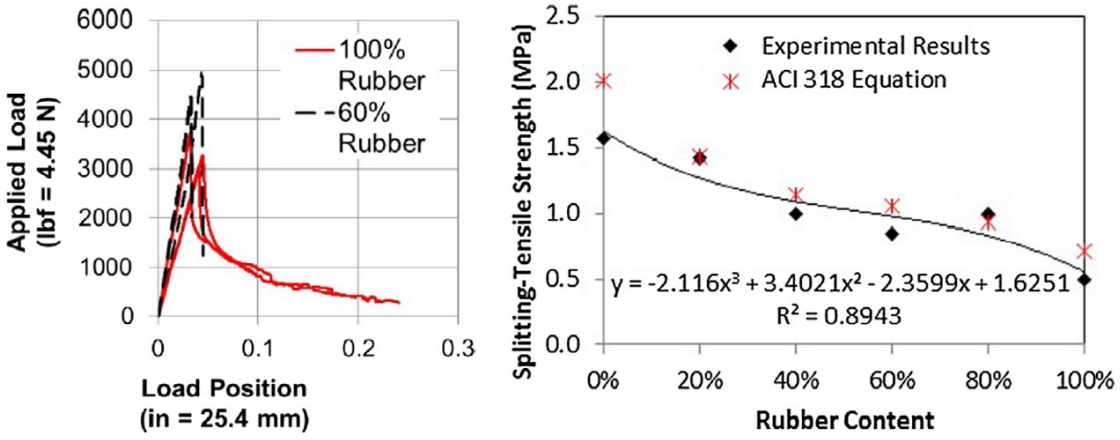

Figure 2-20. Splitting-tensile load-deformation curves and Splitting-tensile strength to rubber content (Miller and Tehrani, 2017)

The flexure strength was obtained by the modulus of rupture, and its value decreased when the rubber increased. The flexural toughness on the other hand was increased when the rubber replacement values were 80% and 100% (Figure 2-21).

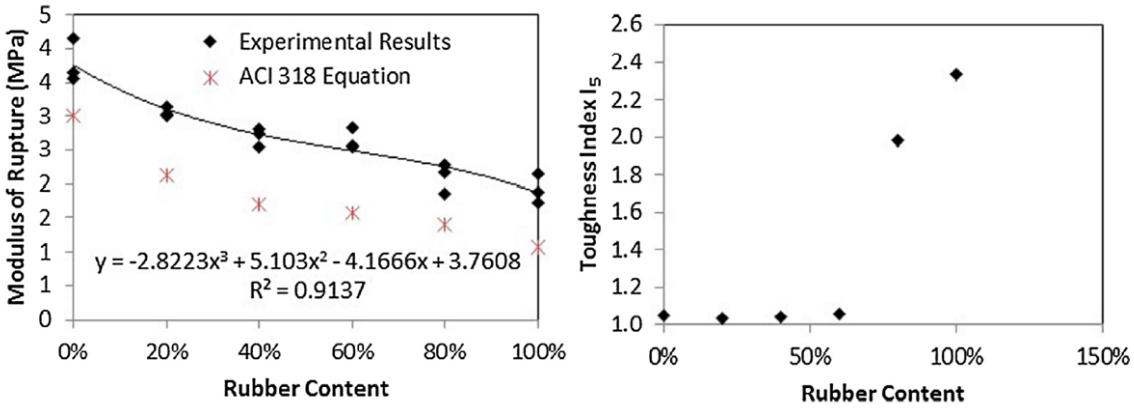

Figure 2-21. Modulus of rupture and flexural toughness to rubber content (Miller and Tehrani, 2017)

There was no correlation between rubber content and the maximum calculated impulse as shown in Table 2-4.

Table 2-4. Impact flexure test results (Miller and Tehrani, 2017)

Rubber Content (%)	Max. Net Impulse N-sec (lbf-sec)
0	536 (121)
20	442 (99)
40	441 (99)
60	486 (109)
80	494 (111)
100	482 (108)

It was concluded that the static mechanical strength decreased when the rubber content increased, but ductility and toughness increased these materials were found to be useful where energy absorption was considered to be an important aspect. Dynamic testing was limited and both full and small-scale tests shall be performed for more practical data.

Heat transfer and sound absorption properties of rubberized concrete were found to be higher and lower respectively compared with normal concrete (Sukontasukkul, 2009). The properties of crumb rubber including compressive, tensile strengths, acoustic, thermal conductivity, and electrical resistivity in a hollow concrete block were investigated using sixty-four specimens containing crumb rubber ranging from 0%, 10%, 25%, and 50% as a replacement to fine aggregate (Mohammed et al. 2012). The conclusions were including a reduction in both compressive and

tensile strength of crumb rubber, lower thermal conductibility, improved sound absorption, and greater electrical resistance as compared to conventional hollow concrete blocks.

The effects of rubber types and their content were investigated by Aslani (2016). The study parameters were tensile strength, flexural and compressive strengths, modulus of elasticity, strain, and stress-strain curves. The proposed compressive stress-strain relationship was in good agreement with experimental test results. The material properties of large-size TDA were studied (Ahn et.al. 2014). It was shown that the unit weight of TDA depends on placement and compaction, a whole yield, and the secant friction angles of 24 and 60 were set as upper bound and lower bound respectively. It was also seen that the low unit weight of these materials can be used for landslide repair as well as weak foundation soils. The shear behaviour tests of the TDA with large particles were performed and related properties and interface shear strength against concrete were measured (Ghaaowd et.al., 2017). The internal failure was found to be nonlinear with a decrease of peak secant friction angle from 39.6 to 30.2. The TDA-concrete interface failure was linear, and the preliminary shear stiffness of the TDA-concrete interface was higher than the TDA internal shear test.

2.5.2 Impact resistance and ductility

Apart from the mechanical properties of TDLWA some related references regarding dynamic properties as well as its damping properties are discussed.

The impact resistance of rubberized concrete was examined (Topçu and Avcular, 1997), it was observed using rubberized concrete in concrete barriers is more economical, and more reliable for their elasticity compared to normal concrete. Dynamic parameters of concrete and rubberized concrete including dynamic modulus of elasticity, natural frequency, and damping were compared together (Zheng et al. 2008). Beams specimens were used to test the natural frequency and damping ratio by free vibration method, and the dynamic modulus of elasticity was established using cubic specimens by beam element and elastic wave methods. It was observed the dynamic modulus elasticity of plain concrete was higher than rubberized concrete, however, the damping ratios of rubberized concrete increased significantly, especially in rubberized coarse aggregate

(CR-40). The 30% of rubber content was suggested to obtain better static and dynamic properties. Compressive strength tests of 24 cylindrical specimens and dynamic impact tests of 6 concrete barrier were examined using shredded waste tire chips contained concrete specimens (Atahan and Sevim, 2008). Increasing the shredded tire chips in the specimens decreased the compressive strength and modulus of elasticity. Kinetic energy absorption was about 180% when shredded tire chips content increased from 0 to 100%, therefore concrete safety barriers containing STC can be used for energy absorption. To examine the safety of these barriers further investigations are required. Similar results were obtained by (Aiello and Leuzzi, 2010; Atahan and Yücel, 2012). Performance of the rubberized, plain concrete and hybrid rubberized with the combination of rubberized at top and plain at bottom of the double layer beam were investigated (Al-Tayeb et al. 2013). Rubberized concrete was prepared by adding the rubber content of 5%, 10%, and 20%. Six specimens were used in this experimental study and their fracture energy, and the load-displacement were studied, three specimens were loaded under an impact load of 20 N from a height of 0.30 m, and the rest were used for the static load test. Moreover, dynamic behaviors of the specimens were simulated using the finite element method by LUSAS V.14 software. The increased amount of rubber improved the impact behavior of rubberized concrete but reduced the compressive stress by 5-20% and tensile stress by 11-17% as well as the modulus of elasticity by 8-22%. The hybrid structure had a maximum peak tub and bending loads compared with plain and rubberized concrete, due to its capability of absorbed impact energy by being rubberized at the top and resisting the tensile stress of plain concrete at the bottom. The area under impact bending versus displacement curve is known as fracture energy was higher in dynamic than the static fracture energy. As the crumb rubber content added to concrete mixture, the fracture energy under impact load for rubberized concrete increased by 85-279%, this was 141-464% in hybrid system. There was a good match between predicted impact load versus displacement behavior by finite element method compared with the experimental results, failure mode was bending, and it was consistence in all the beams. Further investigations including utilizing steel fiber reinforcement in hybrid rubberized system to improve their tensile strength are required.

The impact resistance of rubber and steel fiber reinforced concrete using different rubber particle sizes of 0.178 mm, 1.11 mm, and 2 mm and steel fiber size of 30 mm was reported by (Liu et al. 2012). The compressive strength of normal concrete with 40 MPa was used as a reference, and rubber content ratios increased from 5% to 20%, the pressure loads of 0.2 MPa, 0.3 MPa, 0.4 MPa, and 0.5 MPa were used for the impact test by using Split-Hopkinson Pressure Bar. Three concrete mixes of normal concrete, reinforced rubber concrete, and steel fiber reinforced concrete were used in this investigation. Steel fiber improved the compressive strength of rubber concrete to some extent. Normal concrete and rubber reinforced concrete (RRC) had a similar strain rate under the same impact load. The rubber reinforced concrete had increased the energy absorbing capacity when the rubber contents were below 10%. In general, the deformation and energy absorbing capacity of RRC and SRRC were higher compared with that of normal concrete.

Damping ratio and seismic behavior of rubberized concrete by replacing coarse aggregate at different ratios on small scale columns specimens were studied utilizing shake table and free vibration tests (Xue and Shinozuka, 2013). The study parameters were involved in evaluating the modulus of elasticity and compressive strength using compression tests on standard concrete cylinders as well as strength failure mechanism and the effectiveness of silica fume for increasing compressive strength. For this purpose, 6 columns with a lumped mass on top, a foundation at the bottom for their seismic behavior, and 27 cylinders for the compression tests were prepared as shown in Figure 2-22.

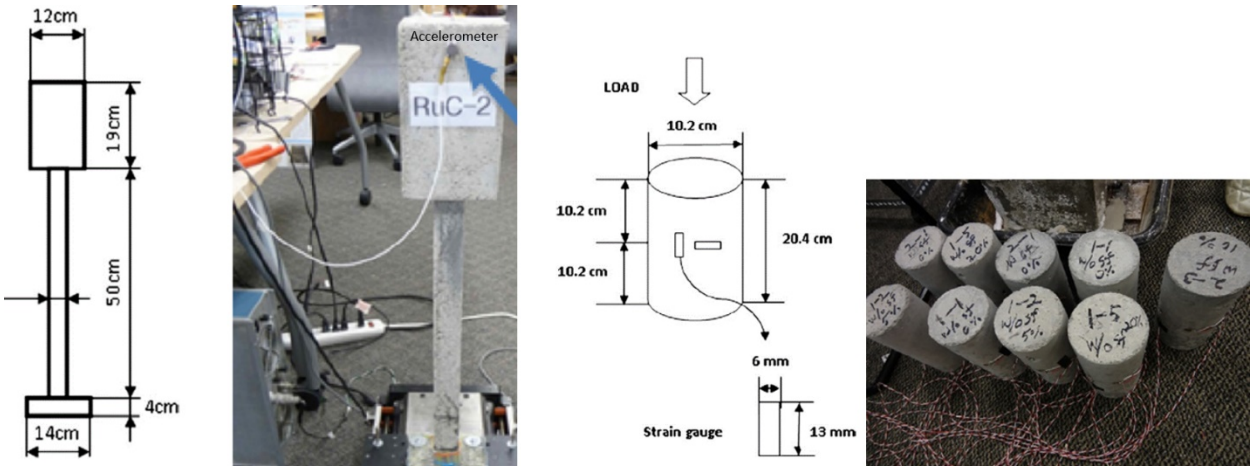

Figure 2-22. Free vibration and compressive strength tests (Xue and Shinozuka, 2013)

The energy dissipation capacity of normal and rubberized concrete was determined using free vibration tests, an accelerometer was installed on the lumped mass and the impact load including free vibration was applied by a hammer. Figure 2-23 presented the power spectrum distribution for normal and rubberized concrete columns, due to different impact intensities, different magnitudes of power spectrum density were computed. However, their peak frequencies were identical, with a lower natural frequency of 5.65 HZ for rubberized concrete compared with 7.85 HZ for normal concrete, the difference was caused by the decrease in the rubberized concrete's modulus of elasticity. The rubberized concrete columns experienced greater damping ratios compared to normal concrete.

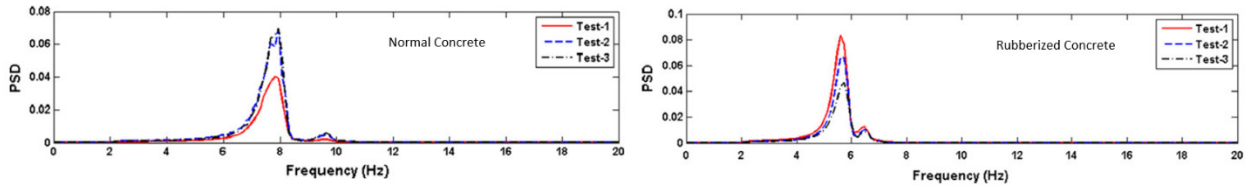

Figure 2-23.Frequency Vs. Power spectrum distribution for normal and rubberized concrete (Xue and Shinozuka, 2013)

Shake table tests were performed by El Centro ground motion, in which its frequency was doubled to a higher range, which was closer to the specimens' natural frequencies with the amplitude of 1.0g. Seismic response acceleration was reduced approximately to 27% by adding a rubber crumb into the concrete mixture. The difference between the seismic response spectrum of

rubberized concrete columns (8.1% damping) and normal concrete damping (4.8% damping) is presented in Figure 2-24, which is due to the damping and natural frequencies.

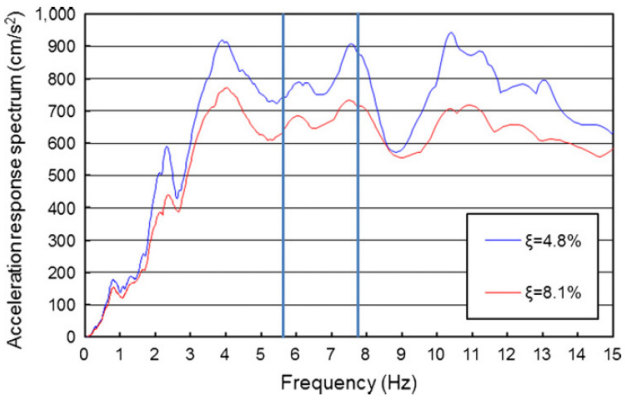

Figure 2-24. Seismic response spectrum (Xue and Shinozuka, 2013)

Free vibration and shake table tests were conducted by adding a 15% rubber content ratio. Cylindrical tests were used for modulus of elasticity and compressive strength with rubber ratios ranging from 5% to 20%. It was concluded adding a rubber crumb increased the damping ratio to 62% and reduced the peak response acceleration to 27% compared with normal concrete. The compressive strength of rubberized concrete with 20% rubber content was reduced to 46.68%, and the modulus of elasticity reduced with the addition of rubber crump content. The bonding of cement paste and rubber was improved by adding silica fume to the cement paste, which resulted in a compressive strength increase. In order to provide a good compressive strength for a practical approach further study of the rubber, a concrete bonding mechanism is required.

The mechanical behavior and self-compacting characteristics of three different concrete mixes containing 0%, 22.2%, and 33.3% of grinded tire rubber with the same water-cement and water-cement-fine filler ratios were investigated (Bignozzi and Sandrolini, 2006). Self-compacting is suitable for concrete using tire rubber wastes in concrete mix design, however, the amount of superplasticizer in self-compacting rubberized concrete is higher compared to self-compacting concrete. The stiffness and compressive strength of concrete decreased with increasing rubber in its mix. Significant ductility and capability to resist post-failure were observed by self-compacting rubberized concrete. This study was limited to three concrete mixes, further formulations and

parametric are required to investigate the size, amount, and origin of tire rubber particles in the mix design.

The effect of crumb rubber concrete on toping the profiled steel sheeting in composite slabs as more ductile material was investigated (Mohammed, 2010). The shear bond between profiled steel as a ductile material and concrete as a brittle material depends on geometry and flexibility. Therefore, composite action between the crumb rubber concrete and profiled steel sheeting was investigated and compared with conventional concrete and profiled steel sheeting using eight slabs specimens. The slabs are divided into two sets with different shear spans of 900mm and 450mm. The profiles sheet's shear transferring capacity known as the m-k value was evaluated using the BS 5950 method, where m and k are the empirical values of mechanical interlocking and friction between rubberized concrete and profiled steel sheeting. Rubberized concrete slabs with a shorter shear span had a similar ultimate failure load to the conventional slab, however, the conventional span experienced a higher failure load for a longer shear span. The ductility requirement was achieved using rubberized concrete, and the m-k value had a higher bond shear capacity compared to the Eurocode 4 method.

The ductility and energy absorption capacity of RC columns utilizing concrete waste tire rubber with different compressive strengths, tire rubber size, and content were investigated (Son et al. 2011). Two types of concrete with compressive strength of 24 and 28 MPa and two different crumb rubber particles sizes of 0.6 and 1 mm were used in twelve column specimens. It was noticed, that there was a reduction in modulus of elasticity, compressive strength, and compressive load capacity of column specimens using waste tire rubber in concrete. Moreover, lateral deformations and energy dissipation capacity of concert column specimens utilizing waste tire rubber concrete were twice compared to normal concrete column specimens, and ductility was increased to 45-90% using 0.5-1% waste tire particles in concrete mixtures.

Experimental and analytical were conducted to study the impact of tire-derived aggregates on ductility and toughness of lightweight aggregate concrete, then to demonstrate the performance of tire-derived lightweight aggregate under impact load, concrete dynamic destructive tests were conducted (Tehrani et al. 2019). Six distinct concrete mixes were studied with various amounts of

TDA. The mechanical properties including tensile and flexural strength, and the elastic module were tested to determine the TDA to LWA ratio. The fracture mechanism is used to model the flexural behaviour of TDA. The TDA concrete was modeled with the four-stage model as shown in Figure 2-25.

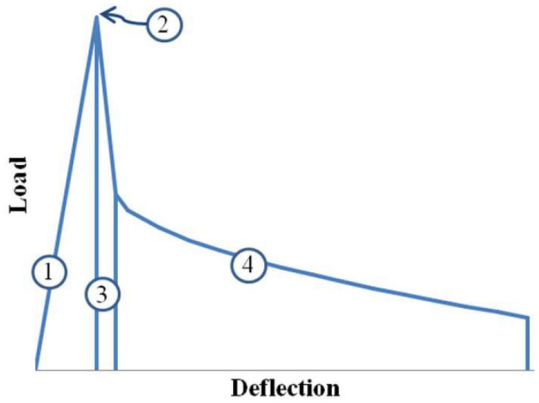

Figure 2-25. Four stage fracture model (Tehrani et al., 2019)

Stage one is the linear elastic behaviour, because the cement mortal has a far higher stiffness than tire chips, the behaviour is considered to be solely determined by cement mortar. Stage two is the pre-critical crack growth, in this stage micro-cracks appear, therefore stress-strain curve is nonlinear. However, when the cement mortal cracks are subjected to flexural load, there is no transition between the first and third stages. Stage three is the critical crack growth based on the fracture mechanism. In light of cement mortal brittle behaviour, the first crack is assumed to be the critical crack, and the fracture grows when the stress at the crack mouth is greater than the modulus of rupture. When the critical stress is greater than the fracture toughness of the cement mortal, linear elastic fracture mechanics will be dominating as cracks widen. The rubber's stiffness is lower compared to cement mortal, and it is anticipated to take a very small load. Stage four is crack bridging when fibers bridge the cracks in the concrete. It is evident that a fourth stage exists in comparing the four-stage fracture model to the load-deflection curve as presented in Figure 2-26. As a result of a similar response of the rubber aggregate to fiber reinforcement, the rubber behaviour shall be accounted for in this stage. The results indicated the rubber aggregate reduced the strength and stiffness and increased the flexural toughness of concrete. The load-deflection

curves indicated that high quantities of rubber aggregates improve concrete's post-peak behavior, this behaviour is a brittle decrease in flexural strength caused by Cement mortar cracking. Moreover, the aspect ratio plays an important role in improving post-cracking behaviour. When the stress in the aggregate is less than the ultimate strength of the material, a larger aspect ratio enhances the capacity of the TDA. More study on the pull-out strength of aggregate including the effects of shape and types of aggregate is required to provide in-depth details of TDA behaviour. In addition, considering the random distribution of aggregate in improving load to crack opening provides the interplay between a number of neighboring aggregates inside the matrix.

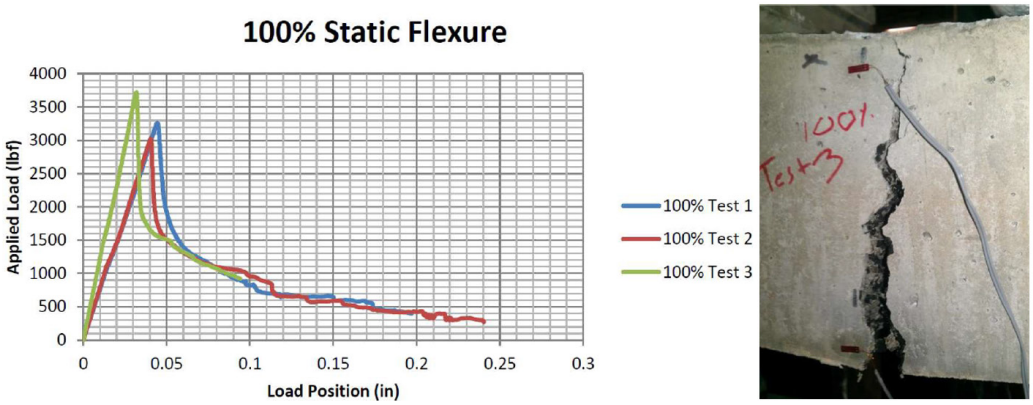

Figure 2-26. Load position against applied load and pre-failure cracking (Kurtis, 2007; Tehrani et al. 2019)

2.5.3 An overview of TDLWA

An overview of the use of scrap-tire rubber in some of the published research showed some characteristics of adding rubber to a concrete mixture including reduced compressive strength, lower density, higher impact and toughness, increased ductility, and sound isolation. Moreover, adding magnesium oxychloride cement to rubber concrete produced better bonding characteristics and therefore their strength can be improved. However the particle size, rubber content, type of cement as well as mineral and chemical use of admixtures need more investigation (Siddique and Naik, 2004).

Assessment of the mechanical properties of rubberized concrete including compressive, tensile, and flexural strengths is the overall goal of research on this topic (Tehrani and Miller, 2018). With increasing the rubber content flexural and compression strengths decrease, but the damping capacities increase. The mechanical properties of TDA make them suitable for some applications such as sound and safety barriers. The toughness and ductility characteristics of TDA are desirable for their application under dynamic loads. However, a large-scale experimental test is required to verify their feasibility. Further studies are required to investigate their environmental effect, long performance, bonding between rubber and cement paste, as well as design guidelines and specifications.

2.6 Literature Summary

Structural protective systems can be categorized into three major groups including seismic isolation, passive energy dissipations, semi-active and active control systems as well as hybrid control systems. Passive energy dissipation devices, for example, are distinguished by their capability to improve energy dissipation by transferring kinetic energy to heat via frictional sliding, yielding metals and viscoelastic solids or fluids, or among vibrating modes such as supplemental oscillators (Soong & Dargush, 1999).

Some European control systems for seismic protection of new and existing buildings as well as bridges are explained. The performance of Buckling Restrained Braces (BRBs), their hysteresis behavior, and response modification factors are discussed, these bracing systems have symmetric hysteresis curves, high ductility, and large drift capacity which results in lower costs of new or existing structures as well as lower force in the superstructure and foundation (Asgarian et.al. 2009).

Rubber is a considerably softer material than concrete and can withstand substantially more deformation before collapsing. Crumb rubber contains smaller particles, while tire chips consist of larger rubber particles that are used to substitute fine and coarse aggregate in concrete (Tehrani et al. 2019). An overview of the published research projects on the properties of rubberized concrete as a replacement for fine and coarse aggregate showed the compressive and flexural strength of rubberized concrete decreased as the rubber percentage in concrete increased. However, these

research projects indicated that rubberized concrete has a lower unit weight, increases the effect of damping and absorbs more energy, and has better toughness compared to normal concrete. Cement past/mortals stress-strain curve is linear and has a brittle behaviour with greater compressive strength than tensile/flexural strength, while the stress-strain curve of rubber is nonlinear with lower stiffness at first and then rising. In addition, rubber-based aggregate reduced mechanical characteristics such as compressive strength, flexural strength, tensile strength, and modulus of elasticity. As a result, concrete containing a significant amount of rubber aggregate was more ductile than normal concrete (Tehrani et al. 2019; Treloar 1994; Wood 1977; Hertz 1991; Yang et al. 2013; Toutanji et al. 1996; Humphrey et al. 2010; Aslani 2016; Tehrani et al. 2018).

Most of the research carried out in the past focused on the behaviour of buckling restrained braced frames in steel structures, and various approaches have also been proposed to capture the seismic evaluation and the response modification factors (Sabelli et al. 2003; Kim et al. 2004; Kumar et al. 2005; Asgarian et al. 2009; Nguyen et al. 2010; Balling et al. 2009; Mahmoudi et al. 2013; Corte et al. 2015; Hosseinzadeh et al. 2016; Moni et al., 2016; Bai and Ou 2016).

Further studies are required to characterize the capacities of the overall brace frame system as well as experimental studies to examine the actual behaviour of buckling restrained braces encased steel with TDA/Concrete fillings as new design approaches of other types of bracings. Therefore, the influence of ductile materials with improved damping properties, such as tire-derived lightweight aggregate concrete of the available experimental results (Tehrani et al. 2020) should be evaluated as an alternative material in the Buckling Restrained Brace frames. Moreover, a comparison between experimental and analytical works for BRB with TDA infill and with concrete infill should be validated to verify the reliability of this application.

CHAPTER 3
Earthquake background and Methodology

3.1 Executive Summary

The first section introduces the concept of tectonic plates, fault types, seismic waves, measuring the seismic ground motions, attenuation relationships, seismic hazard analysis, and ground motions characteristics.

The advantages, disadvantages, and limitations of linear and nonlinear procedures are explained in the next section. A detailed methodology for the nonlinear static procedure and the nonlinear dynamic procedure is described, including the effects of stiffness with an example, different types of target displacement methods, selection of ground motions, and scaling. In this section, nine different ground motions are selected based on the target response spectrum, and the ground motions parameters are determined. In addition, methods regarding the seismic performance assessment and the strengthening of Reinforced concrete (RC) buildings are presented. The acceptance criteria for linear and nonlinear procedures, as well as deformation and force control action, are discussed.

Subsequently, the history and methodology of seismic design factors are presented, followed by an explanation of the methods involved in the design of a buckling restrained braced frame.

3.2 Seismic Hazards

"These signs of the Second Coming are all around us and seem to be increasing in frequency and intensity. For example, the list of major earthquakes in The World Almanac and Book of Facts, 2004 shows twice as many earthquakes in the decades of the 1980s and 1990s as in the two preceding decades (pp. 189–90). Increases by comparison with 50 years ago can be dismissed as changes in reporting criteria, but the accelerating pattern of natural disasters in the last few decades is ominous (Oaks, 2004)".

3.2.1 Plates Tectonic Theory

The earthquake energy has variety of sources including crust dislocations, volcanic activities, or artificial earthquakes such as mining activities, and explosions. The theory of tectonic "plate tectonics" which is derived from seafloor spreading and continental drift theories, may be explained by the earthquake occurrence. Rigid rock slabs with a 100km thickness from the lithosphere or crust as well as a portion of the upper mantle, the outer rock layer (crust) has a non-uniform thickness of roughly 25-60 km below the continent and a non-uniform thickness of about 4-6 km under oceans. The mantle consists of dense silicate rocks starting from the depth of 30km to about 2900km. The outer core and inner cores are about 2200km and 1278km the lithosphere which has brittle behaviour and strength, therefore most earthquakes occur in this layer (Elnashai and Di Sarno, 2015). Seismic belts are where earthquake more occurs (Kanai, 1983). Plate boundaries are classified into three groups including transform faults, spreading zones, and subduction zones (USGS, 2016).

Divergent or Spreading zones: As molten rock expands and moves two plates against each other, new materials can be added, and divergent zones are found. These phenomena occur mostly in oceans within 30km of the surface at shallow depths, the North American and Eurasian plates are an example of spreading zones that move against one another along the mid-Atlantic ridge.

Transform faults: When the plates move past one another, transform faults are found. Earthquakes at this boundary occur at shallow depth and have a linear pattern. The San Andreas fault, along the coast of California and northern Mexico, is an example of a transform fault.

Convergent or Subduction zones: When one plate subduct or push another plate downward into the mantle, subduction zones are formed. Shallow to deep earthquakes, deep ocean trenches, and mountain ranges with active volcanoes are described as the distinctive nature of subduction zones. Along the northwest coast of the United States, southern Alaska, western Canada, and the Aleutian Islands, this boundary can be found.

3.2.2 Fault Types

Ground motions which are manifested by releasing energy in the earth's crust are among the primary natural hazards which can result in loss of life. When two ground masses move through

each other, the tectonic process's accumulated energy is released through interface zone rupture, the distorted blocks snap back into harmony, and earthquake ground motion is created. This procedure is "elastic rebound", and the fault is a fracture in the crust. Seismic waves are then created during the rapid rupture of "crustal rock". Once these waves are traveling from the source through the earth's layers their velocity determined by the characteristic of the earth's layers. The parameters to define a fault motion are presented in Figure 3-1. Where Azimuth (φ) is the angle of the fault trace ($0° \leq \varphi \leq 360°$), δ is the angle between fault plane and horizontal plane, λ (slip or rake) is the angle of horizontal direction and relative displacement ($-180° \leq \lambda \leq 180°$), Δu is the relative displacement, and the surface area of S is a highly stressed region.

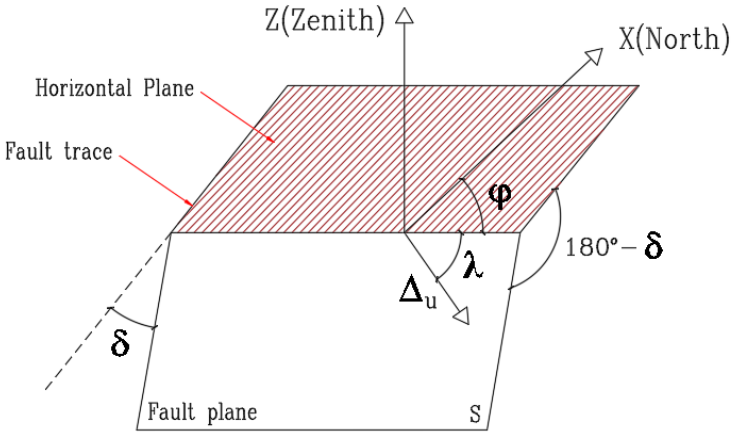

Figure 3-1. Fault motion parameters (based on Elnashai and Di Sarno, 2015)

The most common fault mechanisms are shown in Figure 3-2. Dip slip faults and strike-slip faults are the most prevalent processes of earthquake sources.

Dip slip faults: One block slide vertically in opposition to the other, this phenomenon creates normal, reverse, and thrust faults. Normal fault can be created when the block under the fault plane (footwall) rises and away from the overhanging fault plane (hanging walls), shear failure is due to tensile forces. Reversed fault can be created when the hanging walls move up with respect to the footwall, failure is due to compressive forces. Thrust faults are the reverse fault with a very small dip.

Strike-slip faults: The side blocks slide horizontally which creates strike-slip. Right or left strike-slip faults can be created when the blocks slip along a vertical fault plane which causes either compression or tension.

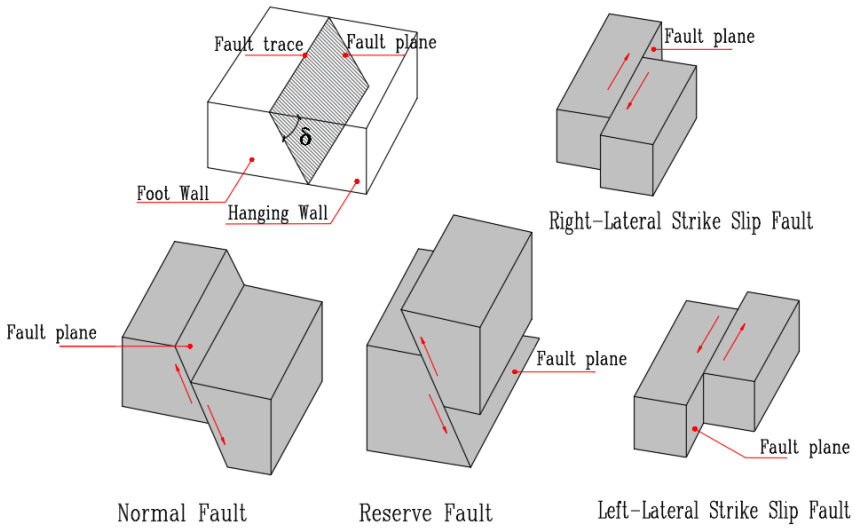

Figure 3-2. Fault mechanisms (based on Elnashai and Di Sarno, 2008, Housner, 1973)

Hypocenter or focus is the point under the surface, and where the rupture occurred, the epicenter is the projection of the focus, and the focal depth is the distance between focus and epicenter as presented in Figure 3-3. Shallow, intermediate and deep focus are the three types of earthquakes which have a focal depth of 5-15km, 20-50km, and 300-700km respectively (Elnashai and Di Sarno, 2008).

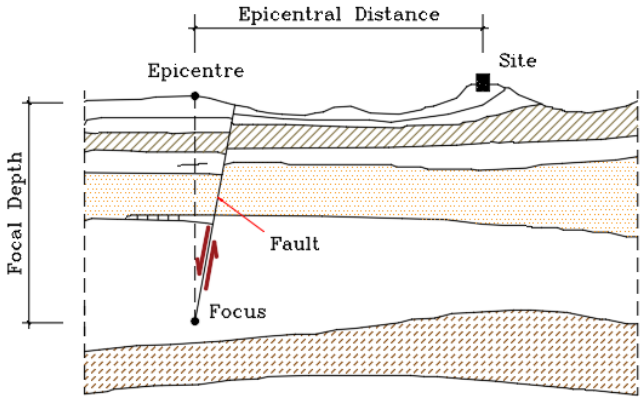

Figure 3-3. Source parameters (based on Elnashai and Di Sarno 2008, Mallet 1862)

3.2.3 Seismic Waves

Seismic waves are 10% of the tectonic energy due to brittle fractures of the earth's crust. Body and surface waves are the two forms of seismic waves.

Body waves: They move through the interior layers of the earth's crust, which include P-waves or longitudinal or primary waves, which cause compression and tension in the rock with relatively little damage as displayed in Figure 3-4a, these are similar to sound waves and can travel through fluids and solids. S-waves or transverse or secondary waves due to side to side vertical and horizontal movements, which cause shear stress in the rock, their motions can be categorized into vertical (SV) and horizontal (SH) components with significant damage as presented in Figure 3-4b. Shear waves show large amplitude with a long period and can only travel through solids. The speed of primary waves is between 1.5 to 8 km/sec, and shear waves travel at 50% to 60% of the speed of primary waves.

Surface waves: They travel through the crust's outer layers, which include L- or LQ-waves (Love waves), their motion is horizontal with large amplitudes and long periods (60-300 seconds) with a velocity of around 4.0 km/sec, are also called G-waves as shown in Figure 3-4c (Richter, 1958), S-waves are faster than R-waves (Rayleigh waves) with large amplitudes as indicated in Figure 3-4d. LQ-waves can not travel through fluid as they are generated by the constructive interface of S-waves motion in horizontal body waves.

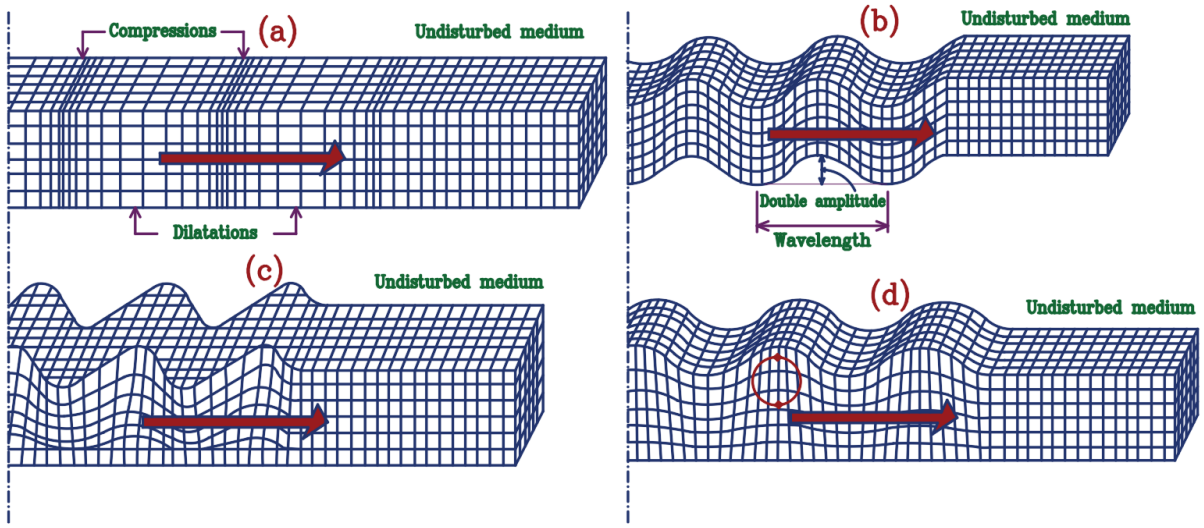

Figure 3-4. (a) Primary body waives, (b) secondary body waves, (c) primary surface waves, and (d) secondary surface waves (based on Bolt, 2003)

3.2.4 Locating the epicentre

Figure 3-5 shows the P and S shadow zones. P-Waves have a higher speed than S-Waves, therefore the location of an earthquake and distance from the source can be measured. In the S shadow zone, only p-waves can travel, because S-waves can't move through the liquid, and in the P and S shadow zones only reflected waves and body waves can't pass through.

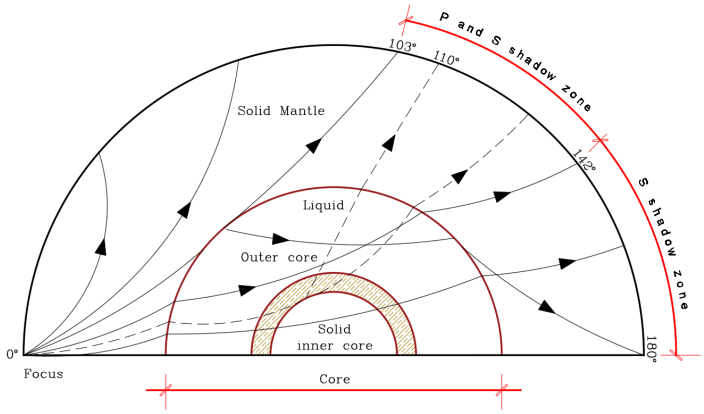

Figure 3-5. Selected ray paths (Kennett, 1982)

The distance between epicenter and recording station can be calculated from Equation 3.1, where t_s (s) and t_p (s) are the arriving time of S and P waves, v_s (km/sec) and v_p (km/sec) are the velocities of S and P waves.

$$d = \frac{t_s - t_p}{\frac{1}{v_s} - \frac{1}{v_p}} \tag{3.1}$$

For this purpose, at least three stations are required, and by overlapping, the circles' epicenter can be found as shown in Figure 3-6.

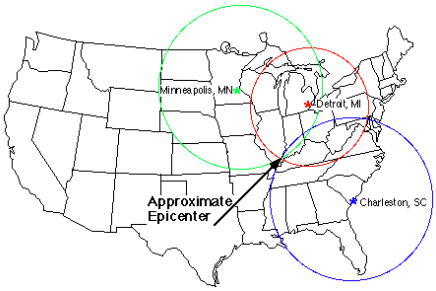

Figure 3-6. The intersection of three circles (UPSeis)

3.2.5 Measuring the earthquake

There are two types of measuring the earthquake qualitative and quantitative namely intensity and magnitude.

Intensity is a non-instrumental method to measure the structural damage, and human reaction to the earthquake, "Mercalli Cancani Seiberg (MCS)", "Modified Mercalli (MM)", "Medvedev Sponheuer Karnik (MSK)", "European Macroseismic Scale (EMS)", and "Japanese Meteorological Agency (JMA)" are some of the most important intensity scale (Elnashai and Di Sarno, 2008). Table 3-1 is the modified Mercalli which is the most common intensity scale.

Table 3-1. Modified Mercalli (MM) Intensity Scale -Giuseppe Mercalli (1902) (USGS, 2022)

Intensity	Shaking	Damage Description
I	Not felt	Not felt or felt by a very few people.
II	Week	Felt by very few people, especially on higher stories.
III	Week	Felt by persons indoors.
IV	Light	Felt by persons indoors and by many outdoors.
V	Moderate	Felt by everyone, unstable objects overturned.
VI	Strong	Felt by all, slight damage.
VII	Very Strong	Negligible damage to well-designed and constructed buildings, slight to moderate damage to the ordinary structure, and considerable damage to poorly built structures.
VIII	Severe	Slight damage to specially designed structures, considerable damage and partial collapse to ordinary structures, and great damage to poorly built structures.
IX	Violent	Significant damage in specially designed structures, severe damage in substantial buildings with partial collapse. Buildings shifted off foundations.
X	Extreme	Most frame structures including foundations destroyed as well as some well-built wooden structures.

Magnitude is based on the body or surface waves' maximum amplitude. The most common magnitude is described below (Elnashai and Di Sarno, 2008).

In the standard "Wood- Anderson seismographs" at 100km from the epicenter with the maximum seismic wave amplitude (A, in microns), Richter or local magnitude (M_L) can be calculated from equation 3.2.

$$M_L = \log(A) - \log(A_o) \tag{3.2}$$

Where A_o is a calibrated factor related to distance (Richter, 1961). It was assumed that magnitude 3 has a distance of 100km to an earthquake with a maximum amplitude of one.

Body waves magnitude (m_b) estimate the P-Waves amplitude with a period of about one second, which is suitable for deep earthquakes can be measured by m_b from equation 3.3. Where A is amplitude, T is period, and $\sigma(\Delta)$ is a function of epicenter distance in degrees.

$$m_b = log\left(\frac{A}{T}\right) + \sigma(\Delta) \tag{3.3}$$

Surface wave magnitude (M_s) measures the LR-waves' amplitude having a period of about twenty seconds, for a very distant earthquake, can be measured by M_s and with equation 3.4. Where A is amplitude, T is period, and Δ is distance and in degrees.

$$M_S = log\ (A/T) + 1.66\ log(\Delta) + 3.30 \tag{3.4}$$

The moment magnitude (M_w) can be used for the shear mechanism as well as the measurement of the entire range of ground motions, which is characterized as a function of M_o, and can be calculated from Equations 3.5 and 3.6. Where shear modulus, G, related to the material on all sides of the fault, this value in the crust is expected to be 32,000 MPa, and 75,000 MPa, A is the area of the fault rupture, and Δu is the average slip between faults.

$$M_o = \mathrm{GA}\Delta u \tag{3.5}$$

$$M_w = 0.67 log\ M_0 - 10.70 \tag{3.6}$$

Richter magnitude (M_L) has some limitations and applies to small and shallow earthquakes with an epicenter of less than 600 km, therefore for worldwide scales m_b, M_S, and M_W can be used, these parameters are presented in Table 3-2, the relation between magnitude and energy release is presented in Figure 3-7.

Table 3-2. Major magnitude scales properties (Elnashai and Di Sarno, 2008)

Scale type	Author	Earthquake size	Earthquake depth	Epicentre distance (km)	Reference parameter	Applicability	Saturation
M_L	Richter (1935)	Small	Shallow	<600	Wave amplitude	Regional (California)	✓
m_b	Gutenberg and Richter (1956)	Small-to-medium	Deep	>1,000	Wave amplitude (P-waves)	Worldwide	✓
M_S	Richter and Gutenberg (1936)	Large	Shallow	>2,000	Wave amplitude (LR-waves)	Worldwide	✓
M_w	Kanamori (1977)	All	All	All	Seismic moment	Worldwide	n.a.

Key: n.a. = not applicable; ✓ = saturation occurs.

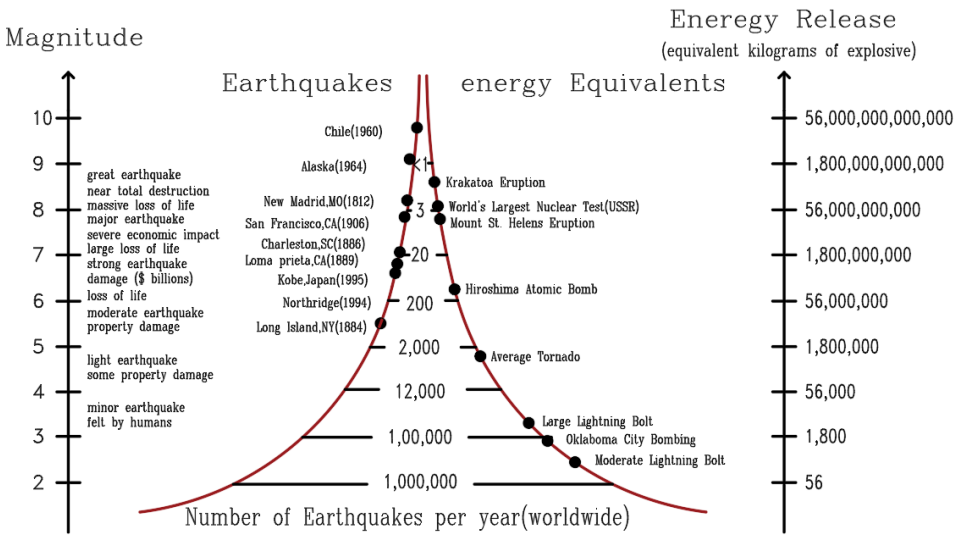

Figure 3-7. Magnitude Vs. energy release (Bolt, 2003)

3.2.6 Significant Historical Earthquakes

3.2.6.1 Attenuation Relationships

They are equations for determining and predicting the ground motion parameters, these data can be used for assessment and design purposes. These relationships provide a function between ground motion properties such as acceleration, velocity, and displacement. There are many studies on attenuation (Atkinson and Adams, 2013; Boore and Atkinson, 2008; Douglas, 2006; Trifunac and Brady, 1976, Campbell, 1985, Idriss, 1978, Green and Hall, 1994).

In the empirical approach, the data matched a function developed from the theory. Theoretical methods collect the empirical data to calculate the values of parameters. Y, the strong ground motion can be derived from regression analysis, log-normal distribution "Y" can be predicted with Equation 3.7 (Campbell, 1985).

$$\log(Y) = \log(b_1) + log[f_1(M)] + log[f_2(R)] + log[f_3(M,R)] + log[f_4(E_i)] + \log(\varepsilon) \quad (3.7)$$

Where b_1 is a scaling factor, f_i is the function of magnitude M, R is source to site distance, and geotechnical structure effects, E_i, ε is a parameter for errors. Peak ground acceleration with focal depth and magnitude is presented in Figure 3-8.

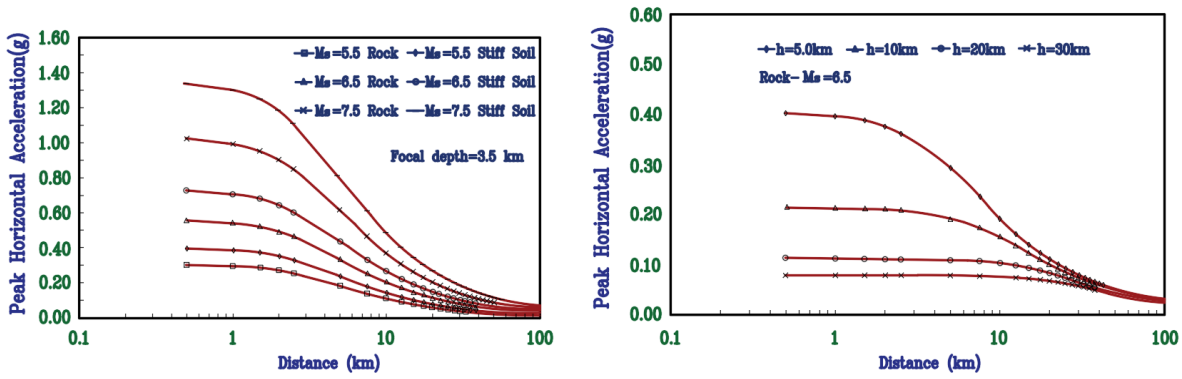

Figure 3-8. Attenuation of PGHA (based on Elnashai and Di Sarno, 2008)

The "site-to-source" distances that are typically employed in attenuation relationships are presented in Figure 3-9.

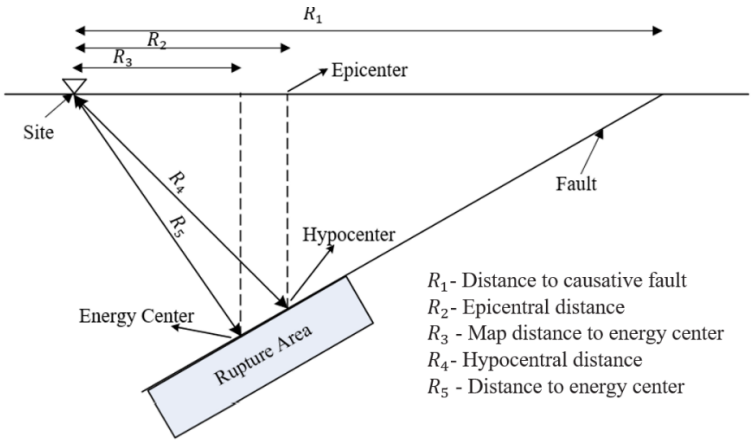

Figure 3-9. Site to source definition (TM, 1986)

Equation 3.8 was proposed by Boore, Joyner, and Fumal (1993). This relationship is for horizontal earthquakes for shallow earthquakes ($5.0 \ll M \leq 7.7, D \leq 100Km$) in the western part of North America.

$$log_{10}(y) = b_1 + b_2(M-6) + b_3(M-6)^2 + b_4 r + b_5 log_{10}(r) + b_6 G_B + b_7 G_c + \sigma_{\log(y)} \quad (3.8)$$

Depending on the shear wave velocities, the site is categorized into four classes A, B, C, and D. Equation 3.8 can be reduced to equation 3.9 by substituting the constants.

$$log_{10}(y) = -0.038 + 0.216(M - 6) - 0.777log_{10}(R^2 + h)^{1/2} + 0.158G_B + 0.25G_C \quad (3.9)$$

Where Y is the ground motion, $r = \sqrt{R^2 + h^2}$, M is the moment magnitude, and R is the shortest distance directly over the fault rupture from the site to the earth's surface. GB and GC are the site coefficient and $\sigma_{\log(y)}$ is the combined standard error of Y for each record of ground motions, "$b_1 = -0.105$, $b_2 = 0.229$, $b_3 = 0$, $b_4 = 0$, $b_5 = -0.778$, $b_6 = 0.162$, $b_7 = 0.251$, h = 5.57 and σ = 0.230 (for geometrical mean σ = 0.208) and for larger horizontal component $b_1 = -0.038$, $b_2 = 0.216$, $b_3 = 0$, $b_4 = 0$, $b_5 = -0.777$, $b_6 = 0.158$, $b_7 = 0.254$, h = 5.48 and σ = 0.205".

Next Generation Attenuation Relationship (NGAs, 2008) was a joint program by the Pacific Earthquake Engineering Research Center (PEER), the U.S. Geological Survey, and the Southern California Earthquake Center with a focus on the prediction and development of new ground motions. In this program, five attenuation relationships developed independently but interacted with one another. Subsequently, NGA East and NGA West 2 have begun in 2010 for the prediction of ground motions for the central, eastern, and western united states (PEER, 2019).

3.2.7 Seismic Hazard Analysis

For earthquake-resistant design, it is imperative to have a very reliable estimate of site-specific design motion, which can be conducted by a seismic hazard analysis (SHA). There are two basic philosophies in defining design motions: deterministic and probabilistic. A rational objective way to account for the uncertainties due to lack of knowledge and poor quality of data is to describe the various quantities by suitable statistical distributions and obtain the resulting distributions for the ground motion parameters and structural response. Additionally, in earthquake engineering, it has been conventional to distinguish between earthquake hazard and earthquake risk. Earthquake hazard is used to indicate the intensity of ground motion at a location, despite the consequences while earthquake risk is determined by the consequences. A high hazard for example, may not reflect a high risk. In conventional probabilistic method the structure is designed for the ground motion that will be exceeded with a specified probability level at least once throughout its lifetime. A lower or higher probability level is chosen depending on the importance of the structure, Gupta (1990).

Depending on the technique used, SHA can be categorized as either deterministic or probabilistic, deterministic seismic hazard analyses (DSHA) involve four basic steps including source identification, earthquake determination for each source, ground motion relationship selection, and calculation of the design ground motion parameter(s), regardless of the kikelihood of an event, DSHA caused by a single magnitude earthquake from a single source at a single distance from the location. Figure 3-10 presents an example of DSHA, with three different earthquake sources away from the site, and the results are presented in Table 3-3, therefore the peak ground acceleration is 0.16g.

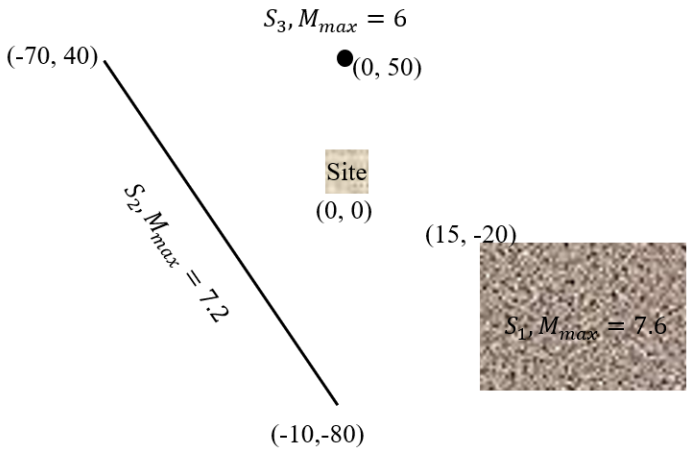

Figure 3-10. An example of DSHA

Table 3-3. Calculation Results

Source	M_{max}	R(Km)	PGA
1	7.6	25	0.16g
2	7.2	44.7	0.08g
3	6	50	0.04g

Probabilistic seismic hazard analysis (PSHA), on the other hand, includes all possible magnitude earthquakes on all sources as well as distances from the site, considering the likelihood of each combination. Therefore, a specific probability of exceedance for a ground motion is feasible using PSHA. Overall, PSHA involves four basic steps such as source identification, recurrence connections including “magnitude distribution and average rate of occurrence for each source”, estimation of ground motion, and developing the site hazard curve (Green and Hall, 1994).

3.2.7.1 Recurrence law Terminology

The frequency of occurrence of an earthquake that is more likely to occur is very important to estimate, specially in a region that may have an impact on the construction site during the facility's lifetime, which can be modeled by Poisson's distribution in equation 3.10. Where n is the number of earthquakes, m is the magnitude, t_r is the reference time period, and N expected the number of earthquakes.

$$P[m > M, t_r] = \frac{(Nt_r)^n \, e^{-Nt_r}}{n!} \tag{3.10}$$

The probability that the specific level of an earthquake will be exceeded in a region during a specified time is exceedance probability, and the average time interval in years or the number of years on average which can be expected between repeat occurrence of similar events such as earthquakes, floods, snow and ice accumulation is time period or recurrence (FEMA P-749, 2010). The expected number of earthquakes N can be calculated from equation 3.11, in which a and b are constants and can be determined from seismological data.

$$lnN = a - bM \tag{3.11}$$

Because this equation is a basic mathematical formula for defining earthquake recurrence, it may overpredicts the earthquake occurrence at the large magnitude, with poor agreement between predicted and measured values for small magnitudes, which is due to envisages continuous slips. Therefore, accurate models were introduced (Elnashai and Di Sarno, 2008, Coppersmith and Youngs, 1990). The likelihood of an earthquake event can be calculated from equation 3.12 by combining equations 3.10 and 3.11.

$$P[m > M, t_r] = 1 - e^{-e^{(a-bM)t_r}} \tag{3.12}$$

The return period T_R can be calculated from equation 3.13.

$$T_R = \frac{1}{N} = -\frac{t_r}{\ln(1-p)} = e^{(bM-a)} \tag{3.13}$$

The ground motions desired probability of exceedance is used for earthquake design, their relationship with return period TR is presented in Figure 3-11.

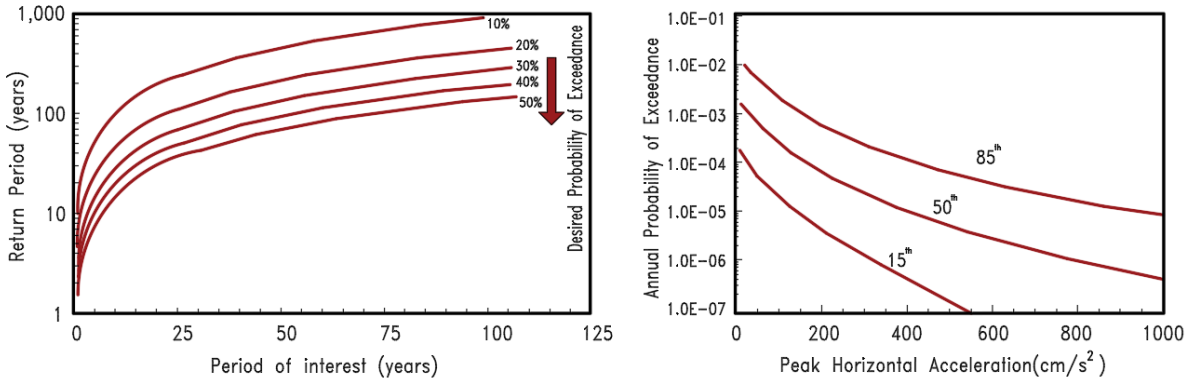

Figure 3-11. Left is the period of interest Vs. return period and right is the hazard curves (based on Elnashai and Di Sarno, 2008)

3.2.8 Ground motions parameters

Earthquake ground motions resemble wave signals, accelerographs are used to record the ground motions, there are three major aspects of ground motions namely amplitude, frequency content, and duration, the ground motion characteristics are presented in Table 3-6 (Kramer, 1996).

3.2.8.1 Amplitude parameters

The amplitude parameters deal with the peak of time history. The motion parameters including acceleration, velocity, and displacement are presented for the Chi-Chi earthquake in Figure 3-12.

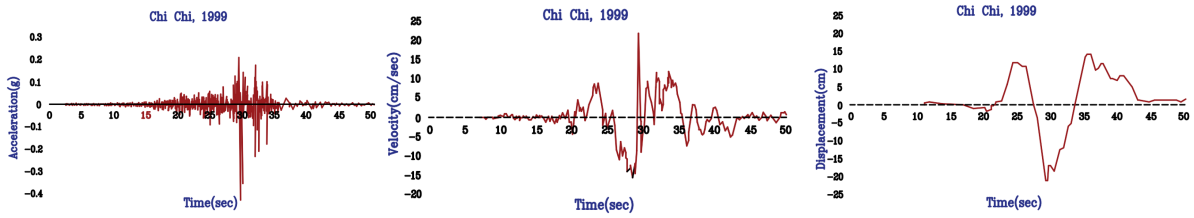

Figure 3-12. Acceleration, velocity, and displacement of Chi-Chi earthquake in 1999

Peak acceleration also called peak ground accelerations (PGA), or peak horizontal acceleration (PHA), is the maximum absolute value of horizontal acceleration from the accelerogram governed by high frequency. The Peak vertical acceleration (PVA) is considered to be two-thirds of PHA (Newmark and Hall, 1982). Usually, ground motions having high peak accelerations are more destructive compared with lower accelerations.

Peak velocity also called peak ground velocity (PGV), or peak horizontal velocity (PHV), is controlled by ground motions of intermediate frequency. PHV may provide a more precise indication of damage than PHA, for structures which are in intermediate frequency range and sensitive to loading.

Peak Displacement also called peak ground displacement (PGD) governed by low-frequency ground motions appropriate for long period structures. However, they are less commonly used than PHA and PHV, because of "signal processing errors" and "long period noise" (Kramer, 1996).

Newmark and Hall (1982), have developed a theory, in which acceleration is associated to structural response and potential damage of an earthquake. This can be described as a function of the size which depends on the site distance to the source of an earthquake, embedment, weight, characteristics of damping, and stiffness. An example of the single-cycle pick amplitude as well as the number of peaks of similar amplitude is shown in Figure 3-13. It was seen the single-cycle often occurred at high frequencies, therefore has less damage in lower frequencies. Whereas the plot on the right might have more damage to the structure.

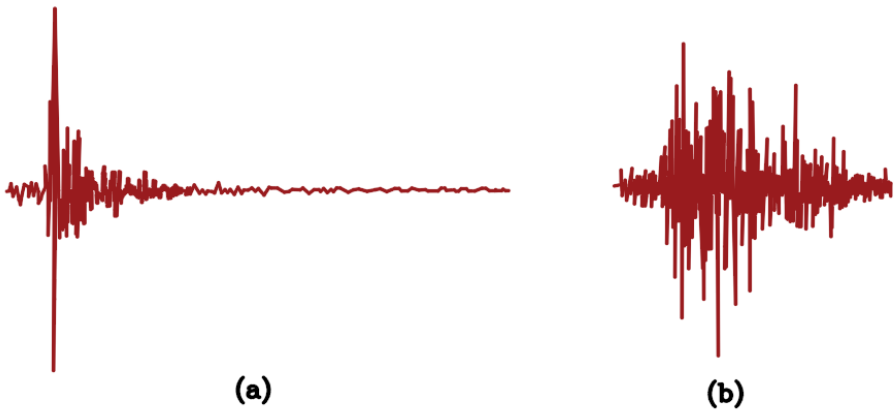

Figure 3-13. (a) N29W Melendy Ranch record, 1972, (b) Longitudinal record from Koyna, 1967 (Kramer, 1996, Hudson, 1979).

3.2.8.2 Frequency content parameters

It defines the "distribution of the amplitude of ground motion among different frequencies". Frequency content has significant effects on ground motions, and their characteristics cannot be completed without frequency content (Kramer, 1996).

3.2.8.2.1 Fourier spectra

The periodic function in Figure 3-14 can be extended to harmonic function using Fourier transform techniques. The Fourier series can provide a comprehensive description of the ground motion and the inverse Fourier transform can recover it (Kramer, 1996).

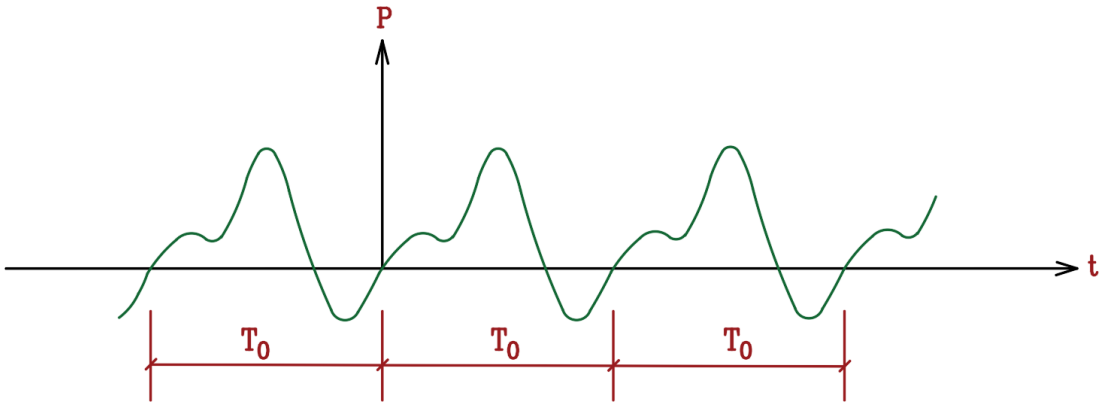

Figure 3-14. Periodic excitation (Chopra, 2012)

A Fourier series is harmonic functions summation, which can be stated in either "trigonometric notation" or "complex notation" as presented in equations 3.14 to 3.17. Where the frequency, $\omega_n = \frac{2\pi}{T_f}$ (Kramer, 1996).

$$x(t) = a_0 + \sum_{n=1}^{\infty}(a_n cos\omega_n t + b_n sin\omega_n t) \quad (3.14)$$

$$a_0 = \frac{1}{T_f}\int_0^{T_f} x(t)dt \quad (3.15)$$

$$a_n = \frac{1}{T_f}\int_0^{T_f} x(t)cos\omega_n t dt \quad (3.16)$$

$$b_n = \frac{1}{T_f}\int_0^{T_f} x(t)sin\omega_n t dt \quad (3.17)$$

Figure 3-15 represented transferring of a ground motion into the sum of a series of simple harmonic functions, these functions are used to calculate the total response.

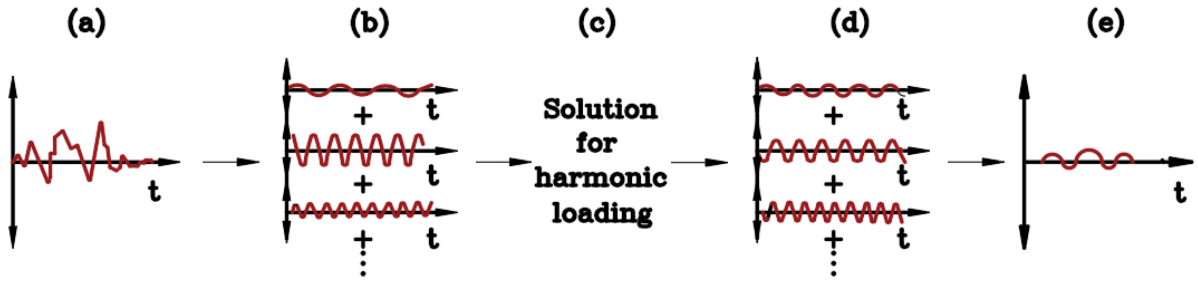

Figure 3-15. Fourier Series representation: (a) time history of an earthquake, (b) sum of series of harmonic loads which represent the time history, (c) response calculation for each harmonic load, (d) sum of series of harmonic responses, (e) time history response (Kramer, 1996)

Fourier amplitude spectrum is a plot of Fourier amplitude versus period, which shows the distribution of the amplitude of ground motions with frequency.

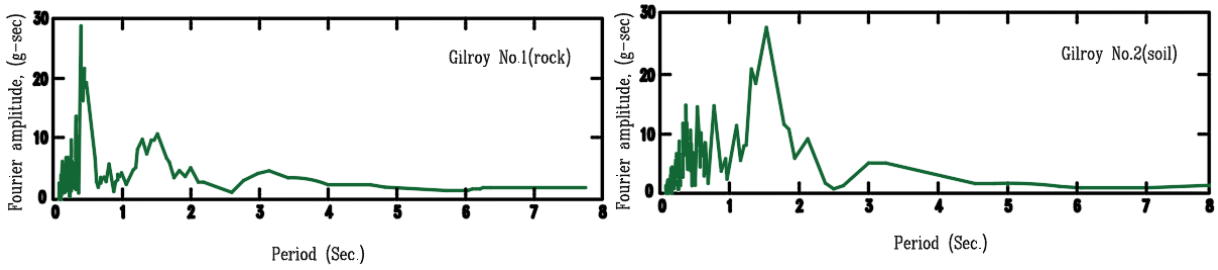

Figure 3-16. Fourier amplitude spectra versus period (Kramer, 1996)

Rock has a higher amplitude for short period, while soil has a higher amplitude over a long period as presented in Figure 3-16.

3.2.8.2.2 Response Spectrum:

It does not define the ground motion, but it provides the effects of ground motions on structures. The response spectrum is “the maximum response of a single degree of freedom system” concerning frequency and damping ratio as presented in Figure 3-17.

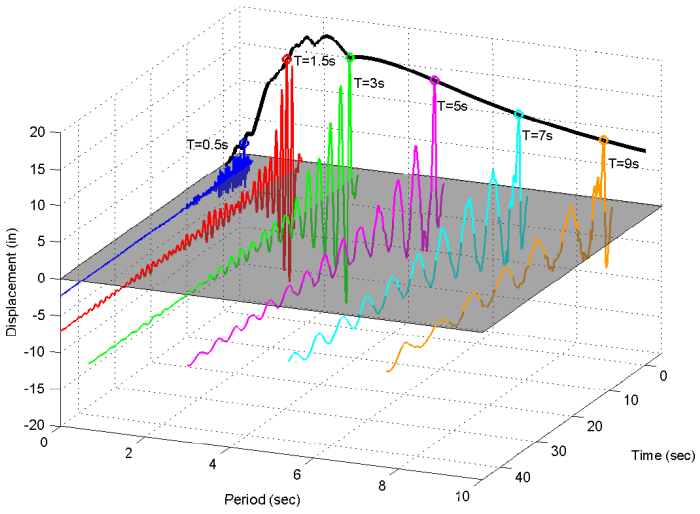

Figure 3-17. Linear displacement spectra (Hachem, 2004).

3.2.8.2.3 Predominant period

The predominant period, T_p, is the period of vibration at which the maximum value of the Fourier amplitude spectrum occurs. Figure 3-18 represents two Fourier amplitude spectra with the same predominant period, T_p, but different frequency contents.

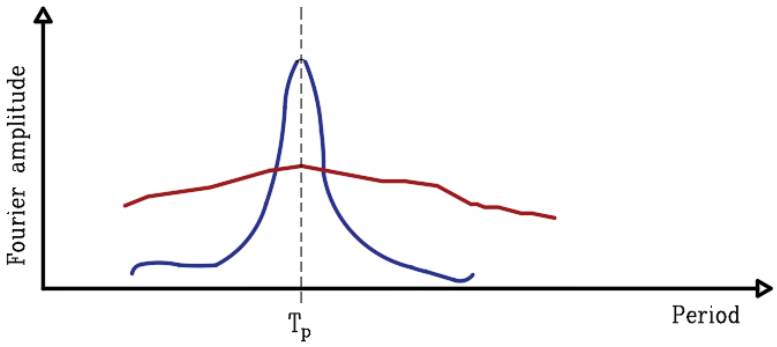

Figure 3-18. Two Fourier amplitude Spectra (based on Kramer, 1996)

3.2.8.2.4 Bandwidth

The bandwidth is the frequency range in which certain level of Fourier amplitude is surpassed. For smoothed spectra, it can be calculated by the maximum amplitude times $1/\sqrt{2}$.

3.2.8.2.5 v_{max}/a_{max}

It is a maximum velocity over maximum acceleration, which gives the period (Sec) as demonstrated in Table 3-4. For a simple harmonic motion $v_{max}/a_{max}= T/2\pi$, and high-frequency earthquake T can indicate which periods are more significant.

Table 3-4. v_{max}/a_{max} (Seed and Idriss, 1982).

Site Condition	v_{max}/a_{max}
Rock	55 cm/sec/g = 0.056 sec
Stiff soils (<200 ft)	110 cm/sec/g = 0.112 sec
Deep stiff soils (>200 ft)	135 cm/sec/g = 0.138 sec

3.2.8.3 Duration

The duration deals with the damage caused by an earthquake. A motion of a short period with a high amplitude may not damage the structure, while a motion of a long period with moderate amplitude can cause substantial damage to a structure. Bracketed duration (Bolt, 1973, Chang and Franklin, 1987; Kramer, 1996) is a measure of ground motion duration above a certain threshold acceleration value (i.e. 0.05g), the duration of ground motion also can be expressed in terms of equivalent cycles of ground motions as presented in Table 3-5.

Table 3-5. Equivalent number of cycles (Kramer, 1996).

Earthquake Magnitude	Number of Significant Stress Cycles
$5\frac{1}{4}$	2–3
6	5
$6\frac{3}{4}$	10
$7\frac{1}{2}$	15
$8\frac{1}{2}$	26

Figure 3-19 is an example of the Chi-Chi (Taiwan) earthquake in 1999, the duration between first and last exceedance is the bracketed duration, Table 3-6 represents the ground characteristics based on amplitude, frequency and duration.

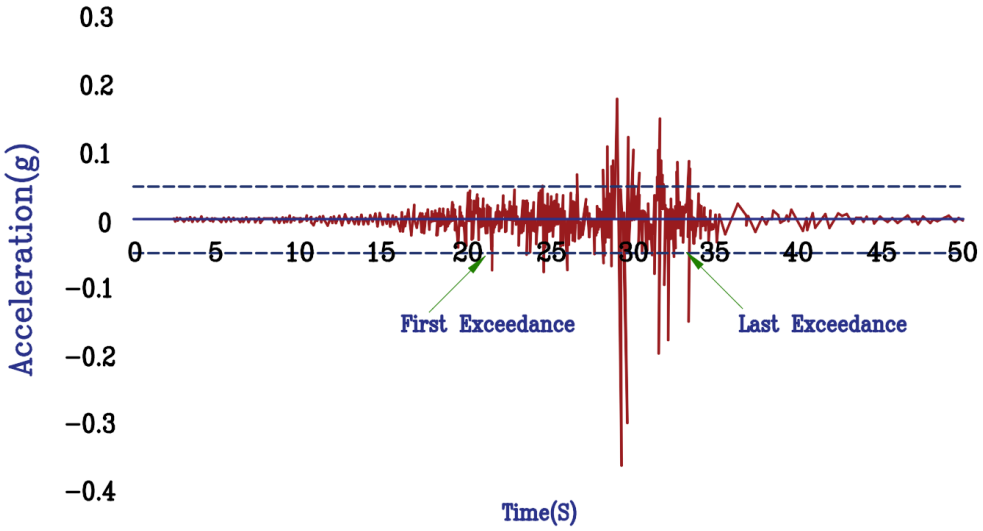

Figure 3-19. Bracketed duration

Table 3-6.Ground motion characteristics (Kramer, 1996).

	Ground motion characteristic		
Ground motion parameter	**Amplitude**	**Frequency Content**	**Duration**
Peak acceleration, PHA and PHV	×		
Peak velocity, PHV	×		
Sustained maximum acceleration, SMA	×		
Effective design acceleration, EDA	×		
Predominant period, T_p		×	
Bandwidth		×	
Central frequency, Ω		×	
Shape factor, δ		×	
Power spectrum intensity, G_0	×	×	×
Ground frequency, ω_g		×	
Ground damping, ζ_g		×	
υ_{max}/a_{max}		×	
Duration, T_d			×
rms acceleration, a_{rms}	×	×	
Characteristic intensity, I_c	×	×	×
Arias intensity, I_a	×	×	×
Cumulative absolute velocity, CAV	×	×	×
Response spectrum intensity, SI(ζ)	×	×	
Velocity spectrum intensity, VSI	×	×	
Acceleration spectrum intensity, ASI	×	×	
Effective peak acceleration, EPA	×	×	
Effective peak velocity, EPV	×	×	

3.2.8.4 Arias of intensity and cumulative absolute velocity

It is a measure of the strength of ground motion, this accumulation of energy can be determined by the integral of the square of the ground acceleration, velocity, or displacement with equation 3.18 (Arias, 1970, Elnashai and Di Sarno, 2008).

$$AI = \frac{\pi}{2g}\int_0^{t_r} a^2(t)dt \tag{3.18}$$

Where a(t) is the time-acceleration history, Tr is the accelerogram total duration, and g is the gravity acceleration.

Cumulative Absolute Velocity (CAV) is the area under the absolute accelerogram and can be computed from equation 3.19, where T_d is the duration of ground motion (Kramer, 1996).

$$CAV = \frac{\pi}{2g}\int_0^{T_d} |a(t)|dt \tag{3.19}$$

3.3 Analysis Procedures

The component forces and deformation shall be determined using appropriate Linear and/or nonlinear analysis procedures.

3.3.1 Linear procedures

3.3.1.1 Linear Static Procedure (LSP)

The linear static approach shall be used to calculate the seismic forces, associated internal forces, and displacements. The ASCE 7-16 and its earlier versions have some limitations on the Equivalent lateral force procedure including height and structural irregularity; however, the revised version of ASCE 7-22 removed these restrictions in some cases. The equivalent lateral force procedure is based on several simple assumptions and involves calculating base shear and distributing it vertically and horizontally.

3.3.1.2 Linear Dynamic Procedure (LDP)

Modal Response Spectrum Analysis (MRSA) and Linear Response History Analysis (LRHA) are two commonly used methods for representing the linear dynamic response of structures, such as internal seismic forces and structure displacement. The MRSA method can be used to identify

the stiffness and mass distribution of a structure, whereas the LRHA method can be used to maintain the indications for example bending moments, both positive and negative, as well as compression and tension brace forces (ASCE 7-22).

3.3.2 Nonlinear procedures

3.3.2.1 Nonlinear Static Procedure (NSP)

The Nonlinear Static Procedure is based on the monotonically increasing different lateral load distributions a specified displacement is reached. A Nonlinear Static Procedure can consist of different load cases with different distributions of load on the structure including acceleration, a lateral force that is proportional to a specified mode shape, static load pattern, and any combination of acceleration, lateral force, and static load pattern. In this method, the structural and member stiffness are updated at every step and plastic hinges develop at a location of structural damage. The force and deformation curve or capacity curve is no longer linear and has a parabolic shape due to the degradation of the building. Figure 3-20 shows converting multiple degrees of freedom to a comparable single degree of freedom while being subjected to a response spectrum representing seismic ground motion, in this method global displacement, component actions, and story drifts can be determined (ASCE 41-17).

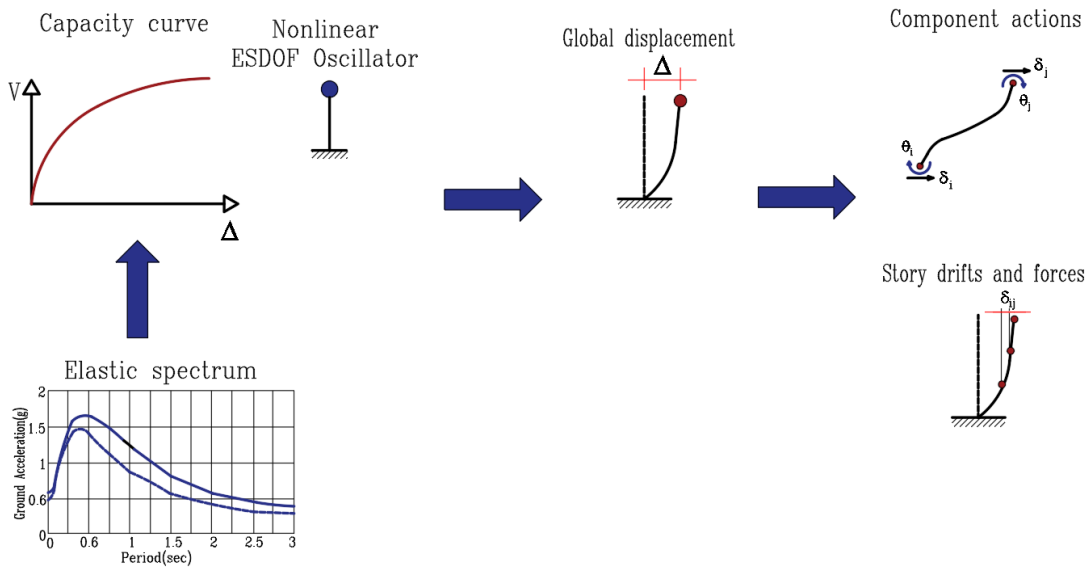

Figure 3-20. Nonlinear static assessment procedure (FEMA 273/274/356, ATC 58)

Nonlinear static analysis or nonlinear pushover analysis is to calculate structural strength capacities as well as the deformation demand, although it has no rigorous theoretical background. This procedure involves pushing the structure under a lateral load pattern to the level of deformation expected in a design earthquake. The main goal of pushover analysis is to assess deformation demands in critical sections with undesired properties such as strength, stiffness discontinuities, extra loads on brittle elements, structural overall stability, and regions exposed to large deformation demands which require special detailing (Lawson et al. 1994).

3.3.2.1.1 Background of Pushover analysis

The static pushover analysis is based on the assumption that the response of the multi-degree of freedom structure can be equivalent to a single degree of freedom system. This signifies that the response is under control by a single constant mode throughout the time history regardless of the level of deformation. Although these assumptions are incorrect, several investigations have investigated these assumptions can have a good prediction of the maximum seismic response of MDOF (Lawson et. al. 1994, Krawinkler and Seneviratna, 1998; Miranda and Bertero, 1994, Fajfar et. al. 1988, Sajidi et.al. 1981, Miranda, 1991). The equation of multi-degree of freedom can be written as equation 3.20 using this assumption (Krawinkler and Seneviratna, 1998). Where M is the mass matrices, C is the damping matrices, Q is the story force vector, $\ddot{x_g}$ is the ground acceleration, and X is relative displacement vector equal to shape vector, φ, by roof displacement, X_1.

$$M\{\varphi\}\ddot{x_1} + C\{\varphi\}\dot{x_1} + Q = -M\{1\}\ddot{x_g} \tag{3.20}$$

The reference single degree of freedom can be defined from equation 3.21.

$$x^* = \frac{\{\varphi\}^T[M]\{\varphi\}}{\{\varphi\}^T[M]\{1\}} x_t \tag{3.21}$$

The differential equation 3.22 is the equivalent single degree of freedom system and can be obtained by multiplying $\{\varphi\}^T$ in equation 3.20 and substituting x_t from equation 3.21.

$$M^*\ddot{x}^* + C^*\dot{x}^* + Q^* = -M^*\ddot{x_g} \tag{3.22}$$

Where M^*, C^*, and Q^* can be obtained from equations 3.23 to 3.25.

$$M^* = \{\varphi\}^T [M]\{1\} \tag{3.23}$$

$$C^* = \{\varphi\}^T C\{\varphi\} \frac{\{\varphi\}^T [M]\{1\}}{\{\varphi\}^T [M]\{\varphi\}} \tag{3.24}$$

$$Q^* = \{\varphi\}^T Q \tag{3.25}$$

Presuming the shape vector is known, From the results of the nonlinear pushover analysis of MDOF the force deformation characteristics of the ESDF can be determined. Figure 3-21 presents the base shear vs. roof displacement (a) and idealized bilinear of ESDF with effective stiffness K_e (b).

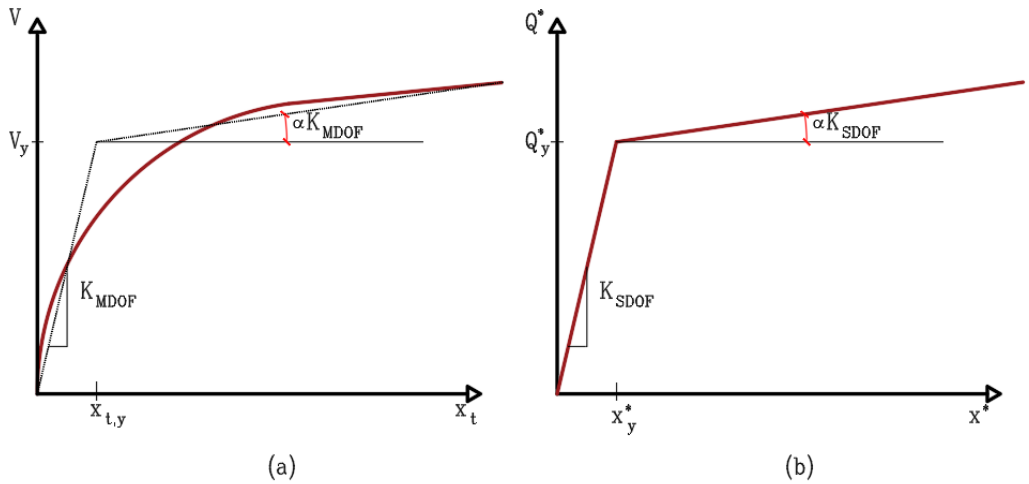

Figure 3-21. Force-displacement characteristics of MDOF structure and equivalent SDOF system (Krawinkler and Seneviratna, 1998)

The effective stiffness, $K_e=V_y/x_{t,y}$, and hardening stiffness, $K_s=\alpha K_e$. The force-displacement parameters of the ESDOF system can be obtained from equations 3.26 to 3.30. Where V_y is the base shear yield value, $x_{t,y}$ is the roof displacement, Q_y is the story yield vector at V_y, α is the strain hardening ratio, and T_{eq} is the initial period of the ESDOF.

$$Modifiction\ Factor = MF = \frac{\{\varphi\}^T [M]\{\varphi\}}{\{\varphi\}^T [M]\{1\}} \tag{3.26}$$

$$x_y^* = \frac{\{\varphi\}^T [M]\{\varphi\}}{\{\varphi\}^T [M]\{1\}} x_{1,y} \tag{3.27}$$

$$Q_y^* = \{\varphi\}^T Q_y \tag{3.28}$$

$$T_{eq} = 2\pi \left[\frac{M^* x_y^*}{Q_y^*}\right]^b \tag{3.29}$$

$$K_{SDOF} = \frac{Q_y^*}{x_y^*} \tag{3.30}$$

Sensitivity studies have shown that when the structural response is dominated by the fundamental mode, precise predictions can be reached, and the modification factor is steady for small to moderate variations in $\{\varphi\}$. It is also recommended by the National Hazard Reduction Program (FEMA 273, 1996), and seismic rehabilitation of existing buildings (FEMA 273, 1996; SEAOC, 2000), as well as various guidelines (Mwafy, 2001).

3.3.2.1.2 Lateral Load Distribution

The distribution of load applied to the structure can be a scaled combination of one or more of the load cases below (Gunay, 2011):

- Any static load cases.
- In a uniform acceleration in a global direction, the force and assigned mass at each joint are proportional and act in a specific direction.
- Any eigen or Ritz mode's modal load. The force at each joint acts in the modal displacement direction and is proportional to the eigenvector and the mass tributary to that joint.

The load combination for a static nonlinear case is incremental and operates in addition to the existing load on the structure when it uses a prior nonlinear case.

3.3.2.1.3 Nonlinear Model for structural components

Concentrated plasticity can be defined with moment rotation parameters and it can be categorized into the plastic hinge and nonlinear spring hinge as demonstrated in Figure 3-22a and Figure 3-22b. The finite length hinge, fiber section, and finite element depicted in Figure 3-22c to Figure 3-22e can represent distributed plasticity (Deierlein et al. 2010).

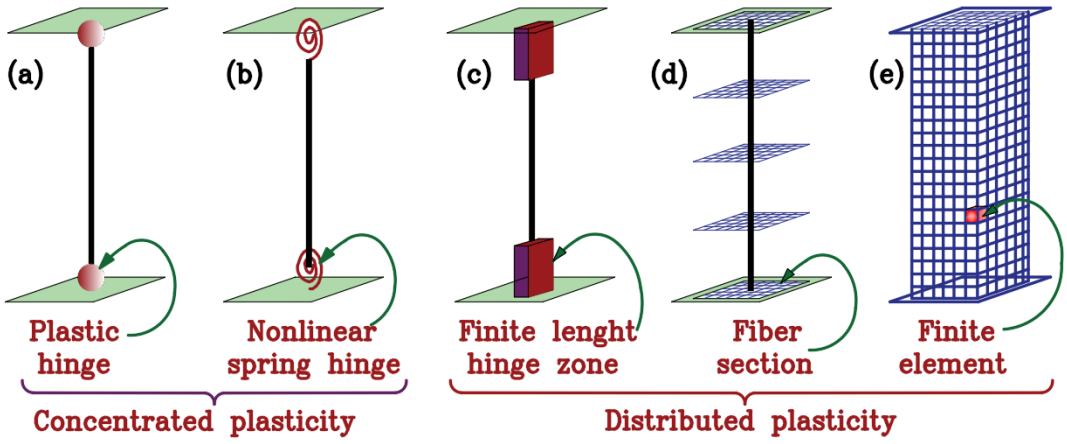

Figure 3-22. Beam-Column idealized elements (Based on Deierlein et al. 2010)

Figure 3-23 demonstrates the concentrated plasticity of the hinge model for a flexural component of reinforced concrete. The quasi-static term takes into consideration concrete cracking, bond-slip, and other criteria that represent the element's modified elastic characteristics. The chord rotation's backbone curve and cyclic response are used to calibrate the spring characteristics. The component parameters, which include post capping, θ_{pc}, pre-capping, θ_p, and cyclic deterioration, λ, can be determined using ATC 72 and FEMA 356 (Elwood et al. 2007; Elwood and Eberhard, 2006; Haselton et al. 2007).

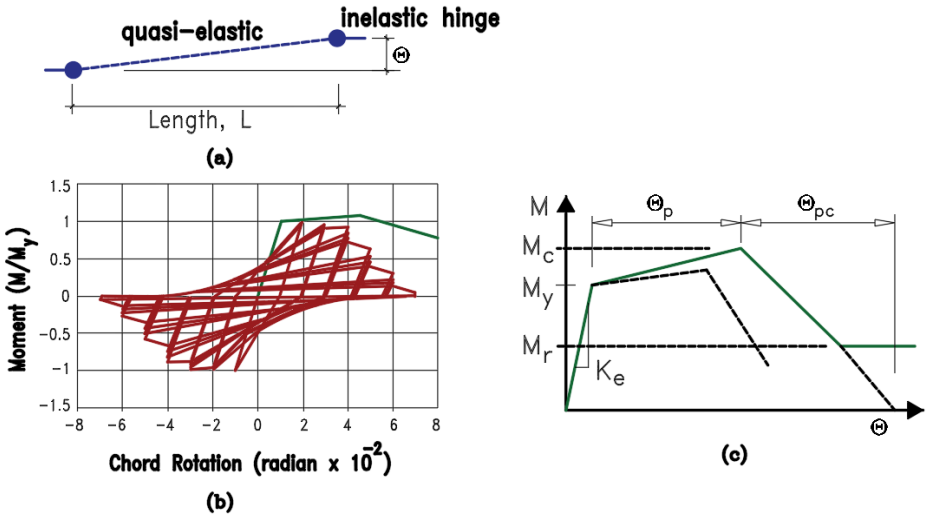

Figure 3-23. (a) Idealized flexural element (b) hysteretic response and monotonic backbone curve (c) monotonic backbone curves (PEER 2019; ATC 72-1)

Figure 3-24 is a simple example that shows how the pushover analysis was performed on a 2-D concrete reinforced frame with three columns and different stiffnesses (K_1, K_2, K_3). The concrete columns have heights of 4, 8, and 16 m, and the frame has two bays each at 8m, supported by a rigid beam. The plastic hinges are defined based on FEMA-356 at the top and bottom of each column. It can be observed when the base shear is about 750 kN with a displacement of 8cm K_1 is zero and when these values increased to 1700 kN and 25cm K_2 is zero. In other words, the stiffness of the structure changes by increasing the base shear. When the displacement reached 1m a mechanism is formed, and the structural system starts collapsing.

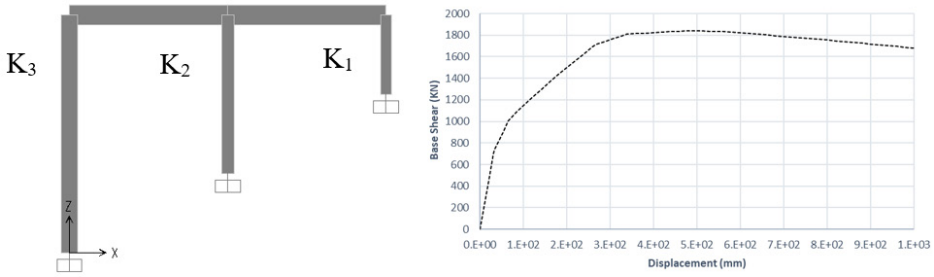

Figure 3-24. An example of pushover analysis

3.3.2.1.4 Target displacement

Target displacement is the maximum expected deformation for the design seismic. The two main methods namely as Capacity Spectrum Method and the Displacement Coefficient method. However, FEMA 274 (1997) and FEMA 440 (2005) present additional background information.

3.3.2.1.4.1 Capacity Spectrum Method

These methods are based on FEMA 274 (1997), in the first method data from equivalent single-degree of freedom (ESDOF) systems are used to calculate the target displacement of multi-degree of freedom (MDOF). The nonlinear force-deformation curve must be idealized as a bilinear response. Figure 3-25 presents the idealized bilinear response, V_y=180 kN.

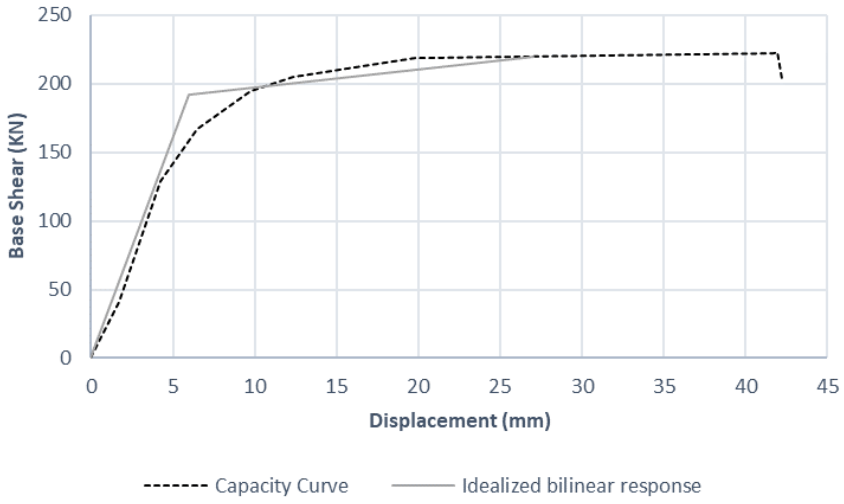

Figure 3-25. Pushover result and the Idealized lateral force-displacement

The difference between MDOF and ESDOF can be calculated by the coefficient C_o from equation 3.31. Where $\phi_{1,\gamma}$ is the ordinate of mode shape 1 at the roof, and Γ_1 is the first mode mass participation factor and can be calculated with equation 3.32.

$$C_o = \phi_{1,\gamma}\Gamma_1 \tag{3.31}$$

$$\Gamma_1 = \frac{\{\phi_1\}^T[M]\{1\}}{\{\phi_1\}^T[M]\{\phi_1\}} \tag{3.32}$$

[M] is a diagonal mass matrix, therefore equation 3.32 can be rewritten as equation 3.33.

$$\Gamma_1 = \frac{\sum_1^N m_i\phi_{i,n}}{\sum_1^N m_i\phi_{i,n}^2} \tag{3.33}$$

In contrary with the first method, in which initial effective stiffness is used to calculate the design displacement response, in the second method maximum response is determined by the crossing of the capacity curve and the spectral demand curve. This point of intersection is known as the performance point, and the displacement at the performance point is known as the displacement demand for the given level of seismic hazard (ATC 40). Different stiffnesses which are used by these two methods are presented in Figure 3-26.

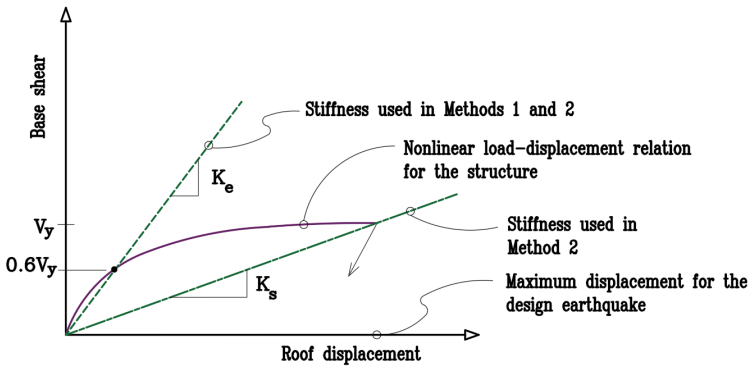

Figure 3-26. Different stiffnesses are used by two methods (FEMA 274, 1997)

The capacity curve can be obtained by transferring the capacity curve (shear vs. roof displacement) into spectral acceleration, Sa, versus spectral displacement, Sd. Figure 3-27 represents the capacity spectrum curve obtained from the capacity curve. Spectra plotted in this format is the Acceleration Displacement Response Spectra (ADRS), Mahaney et al. (1993).

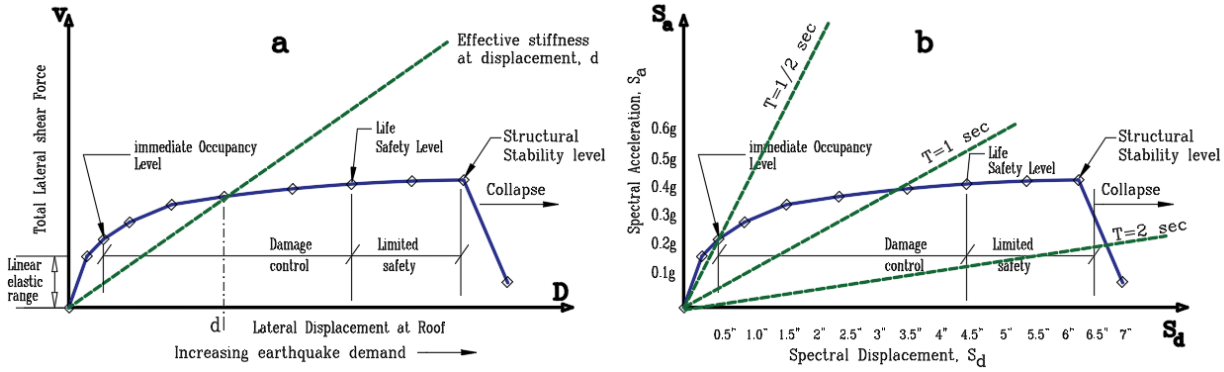

Figure 3-27. (a) Capacity Curve, (b) Capacity Spectrum (ATC 40)

To convert a standard spectrum into ADRS, the value of S_{di} shall be calculated for each point on the standard spectrum as presented in Figure 3-28 and equation 3.34. Where S_a and S_d are the Spectral acceleration and displacement and can be calculated from equations 3.35 and 3.36.

$$S_{di} = \frac{T_i^2}{4\pi^2} S_{ai} g \tag{3.34}$$

$$S_{ai} g = \frac{2\pi}{T_1} S_v \tag{3.35}$$

$$S_{di} = \frac{T_i}{2\pi} S_v \tag{3.36}$$

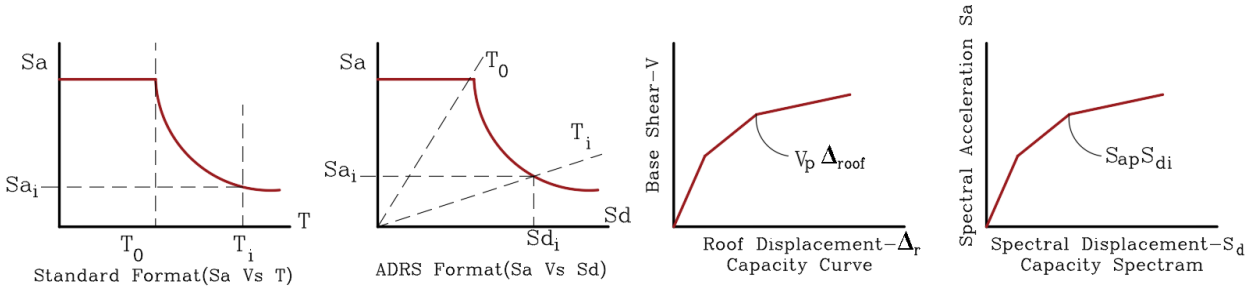

Figure 3-28. Response spectrum and capacity spectrum conversion (ATC 40)

In order to develop the capacity spectrum, the value of S_{ai} and S_{di} shall be calculated for each point on the capacity spectrum as presented in Figure 3-28 and equations 3.37, and 3.38. Where S_a is the modal mass coefficient, PF_1 is the modal participation factor for the first mode and relates to the roof amplitude of the first mode, which can be calculated from equation 3.26. Figure 3-29 and Figure 3-30 represent the capacity spectrum method.

$$S_{ai} = \frac{V_i/W}{\alpha_1} \tag{3.37}$$

$$S_{di} = \Delta_{roof} \Big/ (PF_1 \times \emptyset_{1,roof}) \tag{3.38}$$

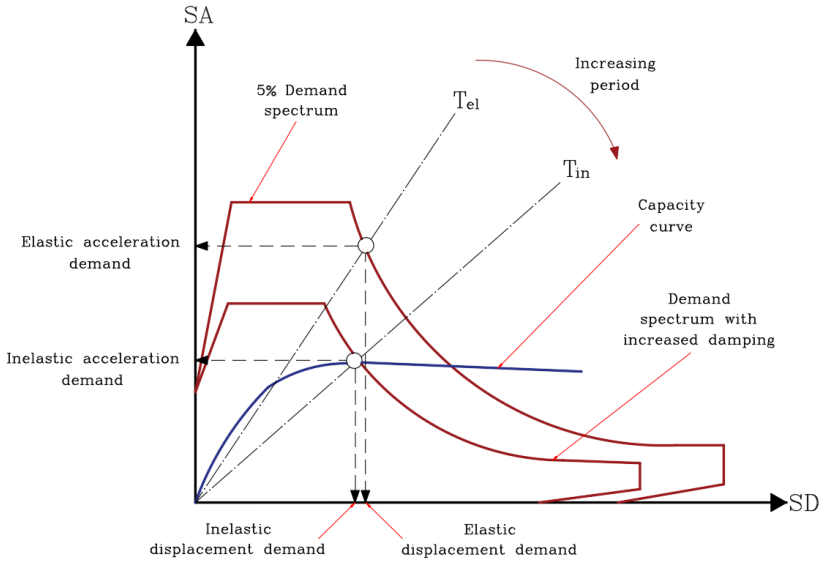

Figure 3-29. Capacity spectrum method (Mwafy, 2001)

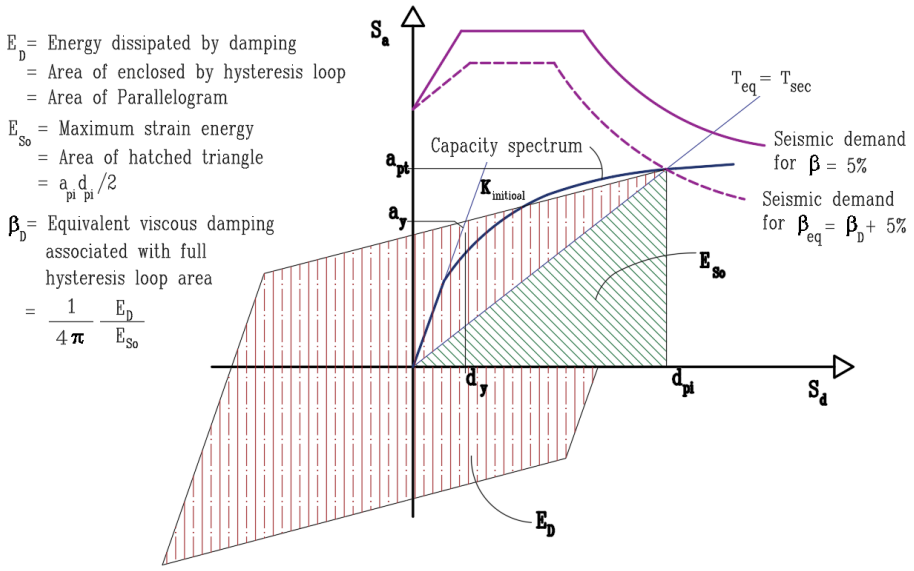

Figure 3-30. Graphical representation of the Capacity-Spectrum Method of equivalent linearization (based on ATC 40, FEMA 274)

Once the performance point has been identified the acceptance of the design can be judged, for example in Figure 3-27b and Figure 3-31, the performance point is located in the damage control range, which indicates less damage than limited for the life safety level.

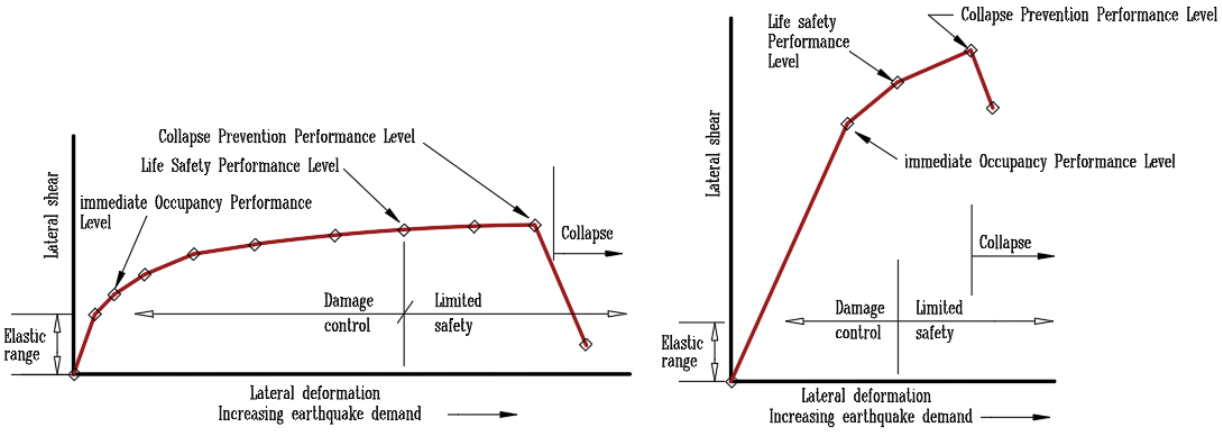

Figure 3-31. Forces versus displacement for ductile/nonductile structures (based on FEMA 274, 1997)

3.3.2.1.4.2 Displacement Coefficient method

An idealized bilinear displacement versus base shear with primary slope, K_i, and post-yield slope, α, shall be used to determine effective lateral stiffness, K_e, and the effective yield strength, V_y, as shown in Figure 3-32.

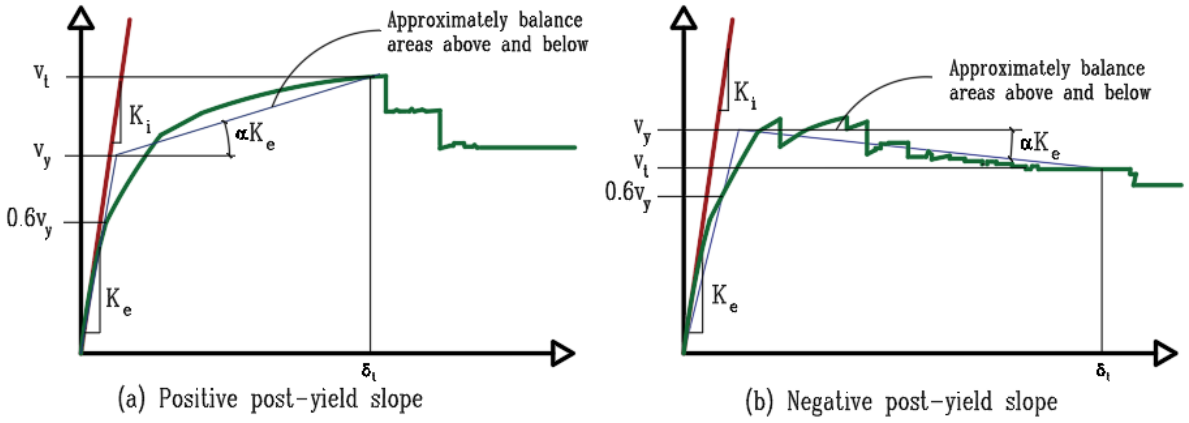

Figure 3-32. Idealized base shear-displacement curve (based on FEMA 356, 2000)

The target displacement is recommended by FEMA-356 & ASCE-41 using Equation 3.39 for rigid diaphragms at each level of buildings, as non-rigid diaphragms, and diaphragm flexibility might be explicitly incorporated in the model followed by procedures as suggested for rigid diaphragms. The idealized force-displacement graph shall be employed to evaluate the effective fundamental period, T_e, with Equation 3.40.

$$\delta_T = C_0 C_1 C_2 C_3 S_a \frac{T_e}{4\pi^2} \tag{3.39}$$

$$T_e = T_i \sqrt{\frac{K_i}{K_e}} \tag{3.40}$$

$$C_1 = 1 + \frac{R-1}{aT_e^2} \text{ for } T_e < T_S, C_1 = 1 \text{ for } T_e \geq T_S \tag{3.41}$$

$$R = \frac{S_a}{V_y/W} C_m \tag{3.42}$$

$$C_3 = 1 + \frac{|a|(R-1)^{3/2}}{T_e} \tag{3.43}$$

In which, C_0 is a modification factor to link the spectral displacement of SDOF to the roof displacement of MDOF. C_1 can be determined with Equation 3.41, which is a factor that relates to inelastic and elastic displacements, in this Equation "a" represents the site class factor; the strength ratio, R, shall be determined using Equation 3.42, which takes into account yield strength, V_y, effective seismic weight, W, effective mass factor, C_m, and response spectrum acceleration, S_a. C_2 considers stiffness and strength degradation as well as the pinching effect. C_3 reflects the P-Δ effects, which can be computed by Equation 3.43.

3.3.2.2 Nonlinear Dynamic Procedure (NDP)

The nonlinear dynamic procedure also known as nonlinear response history analysis is based on the mathematical integration of the equations of motions. In this method, a stiffness matrix is used to update element stiffness, which accounts for P-delta effects and hysteretic behaviour. Figure 3-33 presents the calculation of component deformations based on a model subjected to ground motion, from which global displacement, story drifts, and element distortion can be determined (ASCE 41-17).

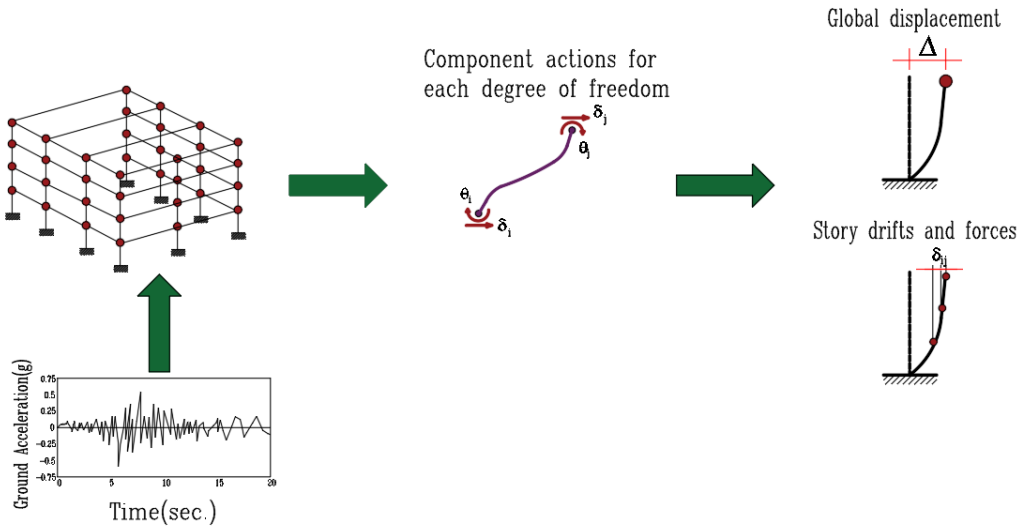

Figure 3-33. Nonlinear dynamic process (FEMA 440, 2005)

Nonlinear dynamic procedure or nonlinear response history analysis of a building is the nonlinear load deformation of individual components of the structure which incorporating directly by a mathematical model and subjected to ground motion acceleration histories (ASCE 41-17).

The nonlinear behaviour of the members shall be considered the same as the pushover analysis. To recognize the inelastic behavior of the building the equation of motion is modified to equation 3.44. Where u is the vector to lateral force-displacement, m is a diagonal matrix, c is the damping matrix, $f_s(u)$ is the inelastic force deformation relation, $\ddot{u}_g(t)$ is the ground acceleration, and ι is the influence vector. In this analysis the force deformation for each member is hysteretic and nonlinear, the unloading and reloading curves are differing from the initial loading curve, these force deformation relations are presented in Figure 3-34 for different materials. In this method, the stiffness matrix changes at each time step and must be formulated based on their element tangent stiffens matrices and deformation and its path dependence (Chopra, 2012).

$$m\ddot{u} + c\dot{u} + f_s(u) = -m\iota\ddot{u}_g(t) \tag{3.44}$$

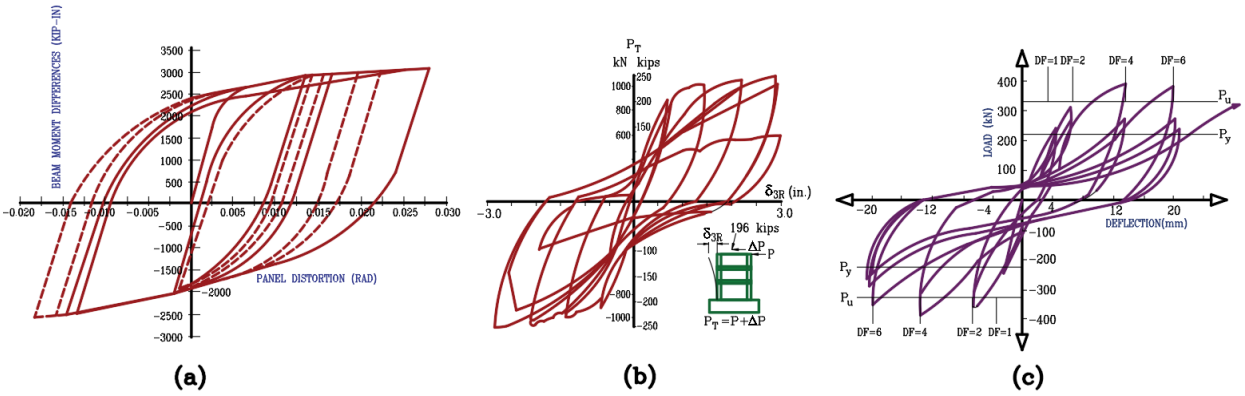

Figure 3-34. Force deformation relations for structural components, a-structural steel, b-reinforced concrete, and c- masonry (Based on Chopra, 2012)

P-Δ effects, structural modeling assumptions, and ground motion parameters are among the important factors which affect the results. The second-order or P-Δ effect is the gravity loads acting on the laterally deformed structure, these effects reduce the initial stiffness of the structure slightly when the structure is in the elastic part, however, when the structure is in inelastic part, it causes a rapid in lateral force resistance with negative stiffness.

3.3.2.2.1 Response history analysis and scaling

The connections between the response of the structure and ground-motion parameters have been explored through different strategies (Gavin et al. 2011, Cordova et al. 2000, Baker 2007). For the NDP, response history analysis shall be conducted by horizontal ground motion acceleration

histories. Scaling and spectral matching are two approaches for adjusting time series to comply with the design response spectrum. Scaling includes multiplying the initial time series by the scaling factor, then the matched spectrum is equal to or exceeds the design spectrum over a given period range, in another word this method is time history scaling which involves modifying a time history scale/steps since it is difficult to capture the tolerance over the entire spectrum, the idea is to focus on the period range of interest, usually 0.2T to 1.5T. Matching the time series frequency content to be in line with the design spectrum is Spectral matching (Gavin et al. 2011), this method is spectral matching based on Lihanand and Tseng (1988) and Tseng et al. (1991), which includes modifying an acceleration time history related to the time domain, to make it consistent with a target spectrum. In 1993 Abrahamson wrote the computer code for structural matching RSP match which is later updated by Hancock et al. (2006).

Selecting time histories play an important role in final results. Time histories shall be selected based on recorded earthquakes with a magnitude similar to the design earthquake magnitude usually (±1), distance (±10km), faulting mechanism (reverse/thrust, subduction zones), spectral acceleration within 20 to 30% of the target natural period, same site class and directivity effect. Comparison of pre- and post-matching of ground motions parameters which are explained in section 3.3.1.9, presented in Table 3-7 and Table 3-8.

Table 3-7. Calculated ground motions parameters pre-matching

		Selected Seismic motions							
ID	**Accelerogram**	**Imperial Valley-02**	**San Fernando**	**Imperial Valley-B**	**Imperial Valley-E**	**Irpinia_ Italy-01**	**Loma Prieta**	**Cape Mendocino**	**Tohoku**
1	PGA (g)	0.2808	0.2247	0.2195	0.4813	0.2266	0.1611	0.1136	0.4276
2	PGV (cm/sec)	3.9392	51.7184	40.9384	40.9442	36.9817	18.6620	20.7842	22.4456
3	PGD (cm)	8.6648	15.9156	16.2496	16.3747	13.1208	12.5708	12.3365	10.8011
4	v_{max}/a_{max} (sec)	0.1123	0.0985	0.1901	0.0867	0.1663	0.1180	0.1864	0.0535
5	Arias Intensity (cm/sec)	1.5561	0.67673	0.4488	2.1276	1.1837	0.4029	0.2390	12.0282
6	CAV (cm/sec)	1331.3816	768.3862	544.7995	1008.5533	1027.3880	739.7195	490.1371	5991.014
7	Housner Intensity (cm)	129.2311	79.2768	96.1341	188.5255	130.6848	83.1547	69.8461	81.7636
8	Predominant Period (sec)	0.46	0.24	0.3	0.4	0.38	0.00	0.00	0.26
9	Significant Duration (sec)	24.19	13.15	14.38	6.59	15.024	27.51	18.20	61.91

Table 3-8. Calculated ground motions parameters post-matching

		Selected Seismic motions							
ID	**Accelerogram**	**Imperial Valley-02**	**San Fernando**	**Imperial Valley-B**	**Imperial Valley-E**	**Irpinia_ Italy-01**	**Loma Prieta**	**Cape Mendocino**	**Tohoku**
1	PGA (g)	0.4531	0.5366	0.4034	0.5006	0.3852	0.4983	0.3751	0.4345
2	PGV (cm/sec)	46.4493	56.4436	79.6715	48.7033	49.3628	52.8166	47.5717	52.9828
3	PGD (cm)	374.3697	177.152	49.4271	92.1476	78.2575	27.5041	284.4909	35.1488
4	v_{max}/a_{max} (sec)	0.1044	0.10721	0.2012	0.0991	0.1306	0.1080	0.1291	0.1242
5	Arias Intensity (cm/sec)	5.4779	3.1985	2.3758	2.2797	4.0542	4.1441	4.1484	14.1395
6	CAV (cm/sec)	2949.6625	1947.6631	1556.6310	1356.5980	2160.9412	2616.8100	2364.2200	6945.4920
7	Housner Intensity (cm)	168.9188	173.9257	172.0642	174.724	172.7276	175.0499	170.2383	169.6044
8	Predominant Period (sec)	0.14	0.10	0.16	0.14	0.34	0.18	0.16	0.24
9	Significant Duration (sec)	28.71	20.31	22.05	13.25	21.89	35.64	26.04	67.14

Acceleration, velocity, and displacement for both pre- and post-matched time histories are presented in Appendix A.

3.3.3 Seismic Assessment and Retrofit of Existing Buildings

Seismic evaluation and retrofit are two important terms to predict building behavior. Seismic assessment can be defined as a methodology of evaluating a building's deficiencies that prevents the building to achieve its performance objectives. Seismic retrofit is identified as the design methodology to enhance the seismic performance level of structural or nonstructural elements, this can be achieved by correcting the deficiencies to a selected performance objective (ASCE 41-17). Rehabilitation, however, is an upgrade required to meet the present requirement.

3.3.3.1 General Definitions

Action is an internal moment, torque, shear, axial force, deformation, rotation, or displacement relating to a displacement produced by a structural degree of freedom; described as a force-controlled (non-ductile) or deformation-controlled (ductile). A component is section of an architectural, electrical, mechanical, or structural system of a building, which can be categorized into two main groups primary or secondary components.

Components that influence the lateral stiffness of the structure shall be classified as primary or secondary. The primary component is an element that resist the seismic forces and adapt seismic deformations for the structure in order to achieve a desired performance level. The secondary

component is an element that allows seismic deformations and is not necessary to resist the seismic forces to attain the desired performance goal. When the total initial horizontal stiffness of secondary components is greater than 25% of the total initial horizontal stiffness of primary components, some secondary components should be classified as primary components in order to limit secondary component total stiffness to below 25% of primary components. If the action of the secondary component improves the deformation demand or force on the primary component, the secondary component should be classified as the primary component (ASCE 41-17).

3.3.3.2 Deformation Control and force control actions

All action shall be grouped into the following categories (ASCE 41-17):

1. Deformation control (ductile failure mechanisms)
2. Force control (brittle failure mechanisms)

Figure 3-35 represents the component force versus deformation curve. In this figure types, one and two are deformation control which represent the ductile behavior, whereas type three is a force control which shows a brittle or non-ductile behavior. In this figure points 0 to 1 are in the elastic range and points 1 to 3 are in the plastic range, point 3 indicated the loss of seismic force-resisting capacity, followed by the point 4 which is due to the loss of gravity load resisting capacity, this plastic range can have a negative and positive "post-elastic slope" and a "strength-degraded" area with residual strength to withstand seismic forces and gravity loads in points 1 to 2 for both types 1 and 2. Type 3 curve has a brittle or non-ductile behavior, points 0 to 1 are in the elastic range, whereas point 3 experiences loss of seismic force-resisting capacity followed by loss of gravity at point 4 (ASCE 41-17).

The expected strength of the component (Q_{CE}), which represents the resistance of a component mean value corresponding at the deformation level shall be used for the deformation-controlled actions. The force-controlled actions shall be evaluated using component strength lower bond (Q_{CL}), which is described as the average minus one standard deviation of the yield strength, Q_y (ASCE 41-17).

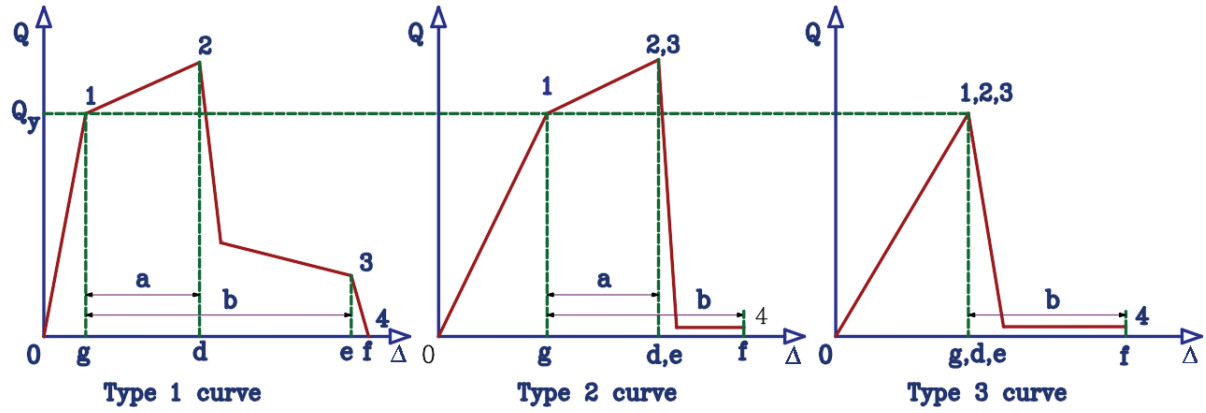

Figure 3-35. Component force versus deformation curves (based on ASCE 41-17, 2017)

Figure 3-36a and Figure 3-36b show normalized force versus deformation and the parameters a to e. The linear response is represented by line AB, while the effective yield is represented by point B. The strain hardening between point B and point C is 0-10% of the elastic slope. The strength component is represented by point C, and the strength degradation is shown by line CD. The reduced strength is represented by line DE, and the component strength is 0 beyond point E. Figure 3-36c represents the acceptance criteria for deformation versus the normalized force of primary and secondary elements associated with various performance levels including "Immediate Occupancy (IO), Life Safety (LS), and Collapse Prevention (CP)" (FEMA 356, 2000).

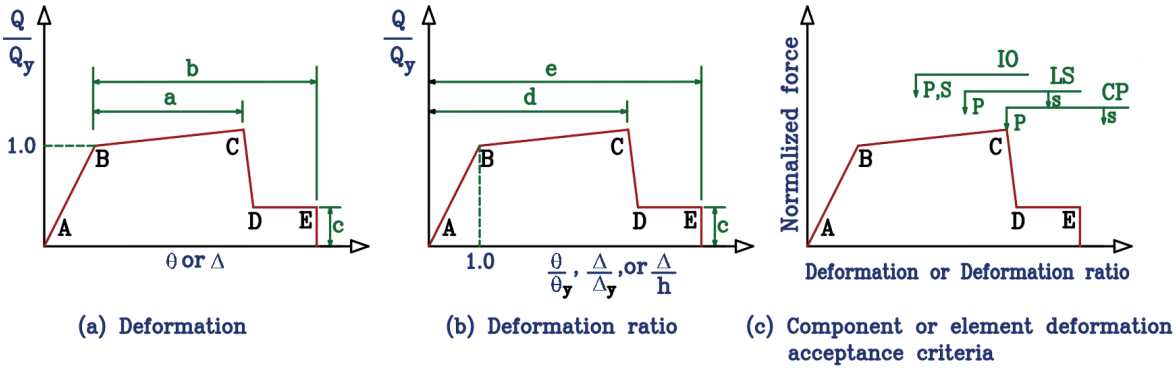

Figure 3-36. Generalized Component Force-Deformation Relations (FEMA 356, 2000)

Deformation and force control may be included as components, the deformation acceptance criteria can be defined as either deformation (e.g. Slender members) or deformation ratio (e.g. Shear walls).

Table 3-9 demonstrates the performance levels based on guidelines (1997), and Vision 2000. Performance levels are determined by the projected behaviour of the building or the amount of structural damage and its economic aspects for both structural and nonstructural elements.

Table 3-9. Structural performance level (Krawinkler, 1997)

Performance level		Description
NEHRP	**Vision 2000**	
Operational	Fully Functional	No significant damage has occurred to structural and non-structural components.
Immediate Occupancy	Operational	No significant damage has occurred to the structure, non-structural elements are secure, and most would function.
Life Safety	Life Safety	Significant damage to structural elements, non-structural elements are secure, but may not function.
Collapse Prevention	Near Collapse	Substantial damage to structural and non-structural elements. Little margin against collapse.

The specified or nominal properties shall be considered as lower bound and relating expected material properties shall be computed by multiplying the lower bound values by factors defined based on ASCE 14-17 in Table 3-10.

Table 3-10. Factors to translate Lower-Bound to expected material properties (ASCE 41-17, 2017)

Material property	**Factor**
Concrete compressive strength	1.5
Reinforcing steel tensile and yield strength	1.25
Concrete steel yield strength	1.50

For existing materials, the expected concrete strength shall not be greater than the mean value minus standard deviation. Also, the required level of information shall be based on the designated performance goal and in compliance with Table 3-11.

Table 3-11. Data collection requirement (ASE 41-17, 2017)

	Level of Knowledge					
Data	**Minimum**		**Usual**		**Comprehensive**	
Performance Level	Life Safety (S-3) or lower		Damage Control (S-2) or lower		Immediate Occupancy (S-1) or lower	
Analysis Procedures	LSP, LDP		All		All	
Testing	No tests[a]		Usual testing		Comprehensive testing	
Drawings	Design drawings	Field survey drawings prepared in absence of design drawings	Design drawings	Field survey drawings prepared in absence of design drawings	Design drawings	Field survey drawings prepared in absence of design drawings
Condition Assessment[b]	Visual	Comprehensive	Visual	Comprehensive	Visual	Comprehensive
Material Properties	From design drawings (or documents)[c]	From default values	From design drawings (or documents) and tests	From usual tests	From design drawings (or documents) and tests	From comprehensive tests
Knowledge Factor (κ)[d]	0.9[e,f]	0.75	1.00	1.00	1.00	1.00

Note: LSP, linear static procedure; LDP, linear dynamic procedure.
[a] Except where no default material properties are provided in this standard.
[b] In the absence of sufficient component detailing information from the design drawings, missing information shall be supplemented by a comprehensive condition assessment.
[c] Where material properties are missing from the design drawings (or documents), default values may be used in conjunction with $\kappa = 0.75$.
[d] Refer to Chapters 9 through 12 for additional material-specific requirements and limitations.
[e] If the building meets the benchmark requirements of Table 3-2, then $\kappa = 1.0$.
[f] If inspection or testing records are available to substantiate the design drawings, then $\kappa = 1.0$.

3.3.3.3 Acceptance criteria

3.3.3.3.1 Linear procedures

In the linear procedures, the acceptance criteria are always based on the force for both actions. Deformation control for Linear Static Procedure (LSD), and Linear Dynamic Procedure (LDP) are based on expected strength Q_{CE}. Component strength Q_c shall be greater than demand on the component Q_U as presented in equation 3.45. Where m is the component capacity modification factor, Q_{CE} is the expected strength, k is the knowledge factor and Q_{UD} is the deformation caused by earthquake and gravity loads, which can be calculated from the linear analysis.

$$mkQ_{CE} > Q_{UD} \tag{3.45}$$

Force control for Linear Static Procedure (LSD), and Linear Dynamic Procedure (LDP) are based on lower bound strength. Component strength Q_c shall be greater than demand on the component Q_U as presented in equation 3.46. Where Q_{CL} is the lower band strength and the component demand, Q_{UF}, can be calculated from capacity design.

$$kQ_{CL} > Q_{UF} \tag{3.46}$$

Capacity checks for linear methods are presented in Table 3-12.

Table 3-12. Component action capacity for Linear Procedure (ASE 41-17, 2017)

Parameters	**Deformation controlled**	**Force controlled**
Existing material strength	Expected mean value with allowance for strain hardening	Lower bound value
Existing action capacity	${}_kQ_{CE}$	${}_kQ_{CL}$
New material strength	Expected material strength	Specified material strength
New action capacity	Q_{CE}	Q_{CL}

3.3.3.3.2 Nonlinear procedures

In the Nonlinear procedures, the acceptance criteria are always based on deformation for deformation control. Expected deformation capacities shall be greater than maximum deformation demands for Deformation control in Nonlinear Static Procedure (NSD), and Nonlinear Dynamic Procedure (NDP). The component capacities can be obtained from inelastic deformation limits and the component demands from the nonlinear analysis.

Force control for Linear Static Procedure (LSD), and Linear Dynamic Procedure (LDP) are based on force control. The component capacities are based on a lower bound, which can determine from all coexisting forces and deformations at the target displacement. Capacity checks for nonlinear methods are presented in Table 3-13.

Table 3-13. Component action capacity for Nonlinear Procedure (ASE 41-17, 2017)

Parameters	**Deformation controlled**	**Force controlled**
Deformation capacity (E-C)	k × Deformation limit	N/A
Deformation capacity (N-C)	Deformation limit	N/A
Strength capacity (E-C)	N/A	k× Q_{CL}
Strength capacity (N-C)	N/A	Q_{CL}

Note: Existing Component (E-C), New Component (N-C)

3.3.3.4 Assessment procedure main checks

Due to the lack of transverse reinforcement in old concrete buildings, shear strength shall be determined based on ACI 318 chapter 11 for effective elastic response and chapter 21 for ductile components. Bending is the deformation control action and checks need to perform in terms of plastic hinge rotation as presented in Figure 3-36c and Table 3-14.

Table 3-14. Numerical acceptance for Nonlinear procedures, RC beams (ASCE 41-17, 2017)

			Modeling Parameters[a]			Acceptance Criteria[a]		
			Plastic Rotation Angle (radians)		Residual Strength Ratio	Plastic Rotation Angle (radians)		
						Performance Level		
Conditions			a	b	c	IO	LS	CP
Condition i. Beams controlled by flexure[b]								
$\frac{\rho - \rho'}{\rho_{bal}}$	Transverse reinforcement[c]	$\frac{V^{d}}{b_w d\sqrt{f'_{cE}}}$						
≤0.0	C	≤3 (0.25)	0.025	0.05	0.2	0.010	0.025	0.05
≤0.0	C	≥6 (0.5)	0.02	0.04	0.2	0.005	0.02	0.04
≥0.5	C	≤3 (0.25)	0.02	0.03	0.2	0.005	0.02	0.03
≥0.5	C	≥6 (0.5)	0.015	0.02	0.2	0.005	0.015	0.02
≤0.0	NC	≤3 (0.25)	0.02	0.03	0.2	0.005	0.02	0.03
≤0.0	NC	≥6 (0.5)	0.01	0.015	0.2	0.0015	0.01	0.015
≥0.5	NC	≤3 (0.25)	0.01	0.015	0.2	0.005	0.01	0.015
≥0.5	NC	≥6 (0.5)	0.005	0.01	0.2	0.0015	0.005	0.01
Condition ii. Beams controlled by shear[b]								
Stirrup spacing ≤ *d*/2			0.0030	0.02	0.2	0.0015	0.01	0.02
Stirrup spacing > *d*/2			0.0030	0.01	0.2	0.0015	0.005	0.01
Condition iii. Beams controlled by inadequate development or splicing along the span[b]								
Stirrup spacing ≤ *d*/2			0.0030	0.02	0.0	0.0015	0.01	0.02
Stirrup spacing > *d*/2			0.0030	0.01	0.0	0.0015	0.005	0.01
Condition iv. Beams controlled by inadequate embedment into beam–column joint[b]			0.015	0.03	0.2	0.01	0.02	0.03

Note: f'_{cE} in lb/in.^{2} (MPa) units.
[a] Values between those listed in the table should be determined by linear interpolation.
[b] Where more than one of conditions i, ii, iii, and iv occur for a given component, use the minimum appropriate numerical value from the table.
[c] "C" and "NC" are abbreviations for conforming and nonconforming transverse reinforcement, respectively. Transverse reinforcement is conforming if, within the flexural plastic hinge region, hoops are spaced at ≤ *d*/3, and if, for components of moderate and high ductility demand, the strength provided by the hoops (V_s) is at least 3/4 of the design shear. Otherwise, the transverse reinforcement is considered nonconforming.
[d] *V* is the design shear force from NSP or NDP.

Shear walls controlled by flexural deformation shall be controlled in terms of the plastic hinge rotation, and shear walls controlled by shear deformation shall be controlled in terms of the lateral drift ratio as presented in Figure 3-37. Beam column joints are a force-controlled action and shall be controlled in terms of joint shear strength.

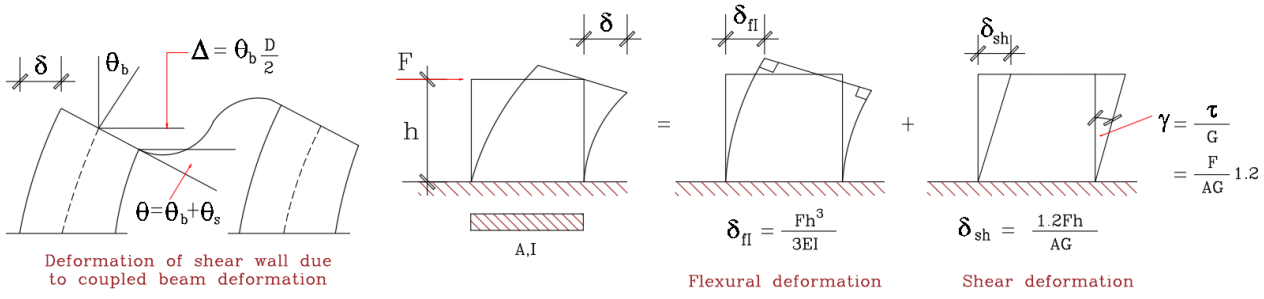

Figure 3-37. Structural wall mechanism (Lignos, 2015)

3.4 The seismic response modification factor

3.4.1 Introduction

Building seismic force values are determined by dividing forces correlated with the structural elastic response by a response modification factor, known as R factor. The ATC-06 in 1985 was proposed as the first report for response modification factor. In 1988 uniform building code (UBC) implemented comparable components to represent the allowable stress design approach. Based on this theory, a well-detailed seismic system can withstand substantial inelastic deformation without failing, this behavior is known as ductility, in which the system creates greater lateral strength than its intended design strength (ATC-06, 1982; ATC-19, 1995; UBC, 1988).

The lateral force was recommended by the structural engineering association of California (SEAOC) in 1959, by considering the minimum design base shear with equation 3.47.

$$V = K\frac{0.05}{\sqrt[3]{T}}W \tag{3.47}$$

In this equation "K" is a lateral force factor ranging from 0.67 to 1.33 for several lateral load resisting systems, "T" is the fundamental period of the building, and "W" represents the total dead load. Consequently, UBC (1961) was updated the base shear by adding a "Z" factor from equation 3.48, where Z is a factor varying from 0.25, 0.5, and 1 depending on the seismic zone.

$$V = ZK\frac{0.05}{\sqrt[3]{T}}W \tag{3.48}$$

Then in 1965 the ATC-06 (ATC-19, 1995) considered risk assessment, nonlinearity, and economical aspects of the base shear design and integrated them by considering the R factor. The base shear was modified to equation 3.49 regardless of the period of the structure and equation 3.50 considering the fundamental period and the soil profile, S.

$$V = \frac{2.5A_a}{R}W \tag{3.49}$$

$$V = \frac{1.2A_vS}{RT^{0.67}}W \tag{3.50}$$

In these equations, A_a and A_v are the peak acceleration and peak velocity. Figure 3-38 shows the use of the response modification factor, the elastic and reduced elastic response spectrum for the design purpose (ATC-06, 1982).

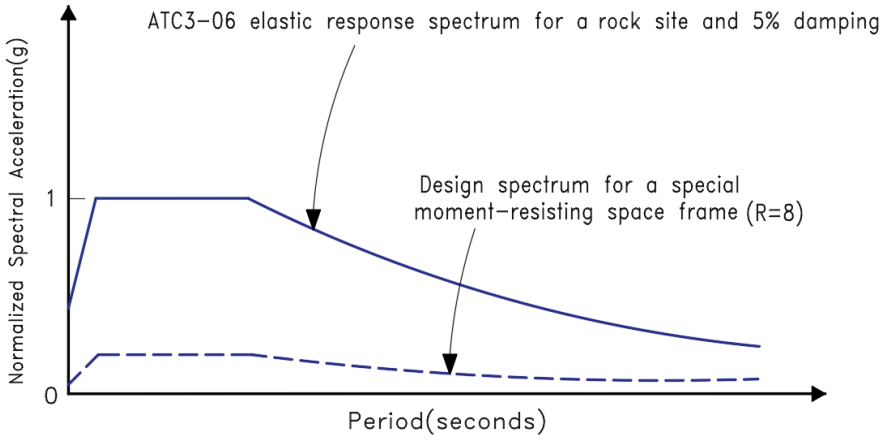

Figure 3-38. Elastic and design response spectrum (based on ATC-19, 1995; ATC-06, 1982)

The UBC (1985) modified the base shear to the equation 3.51, later in 1988 the structural engineering association of California (SEAOC) and UBC (1994) introduce an alternative equation for base shear as presented in equation 3.52.

$$V = \frac{1.25SZIKSW}{T^{0.67}} \tag{3.51}$$

$$V = \frac{1.25SZICW}{R_w T^{0.67}} W \tag{3.52}$$

Where "Z" is the seismic zone, "I" is the importance factor, "S" accounts for soil profile, "K" is the horizontal force factor, and "R_w" is the response modification factor for allowable stress design.

3.4.2 Parameters of response modification factors

The components of R factor depend on the performance level, in this research only life safety is considered. The response of a building subjected to monotonically increasing load results in a force-displacement relationship, which can be converted to an idealized bilinear curve. There are two methods to estimate yield forces and yield displacements namely Paulay & Priestly and the equal energy method as presented in Figure 3-39.

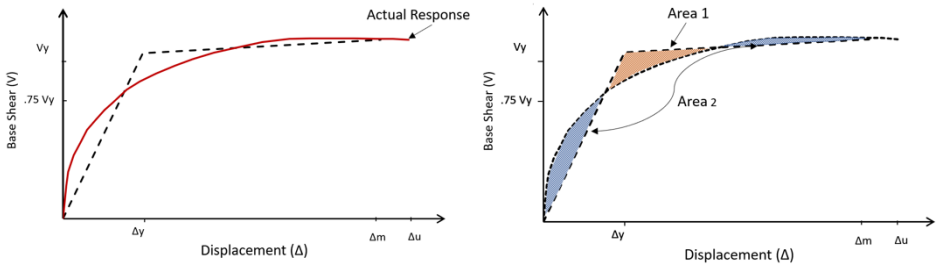

Figure 3-39. Correspondence bilinear transformation (ATC-19, 1995)

Paulay & Priestly in 1992, improved load-displacement approximation for reinforced concrete components. In this method yield strength, V_y, is assumed, then the force corresponding value of 0.75 V_y is considered at the force-displacement curve to determine the secant stiffness of the frame. The equal energy method is based on the assumption of the enclosed area of the curve above is equal to the enclosed area of the curve below the bilinear approximation. The elastic stiffness, as well as the ductility ratio, can be calculated with equations 3.53 and 3.54.

$$K_1 = \frac{V_m - V_y}{\Delta_m - \Delta_y} \tag{3.53}$$

$$\mu_\Delta = \frac{\Delta_m}{\Delta_y} \tag{3.54}$$

Herrin, K_1 is the elastic stiffness, V_m is the maximum force, and V_y is the yield force, μ_Δ is the ductility ratio, Δ_y is the yield displacement, Δ_u and Δ_m are the displacements associated with before failure and a limit state. The experimental evaluation of force-displacement relationships involves using an earthquake simulator test, which is very costly. In 1986 Uang and Bertero and in 1987 Whittaker established force-displacement relationships from the testing of concentrically steel braced frames and eccentrically steel braced frame. R was defined by the Berkeley research using three variables from equation 3.55.

$$R = R_s R_\mu R_\xi \tag{3.55}$$

Herein, R_s and R_μ, are reverse strength and ductility, and R_ζ accounts for damping. The strength factor was calculated by dividing maximum base shear over design base shear, and the ductility was determined by elastic base shear divided by the maximum base shear as presented in Figure 3-40.

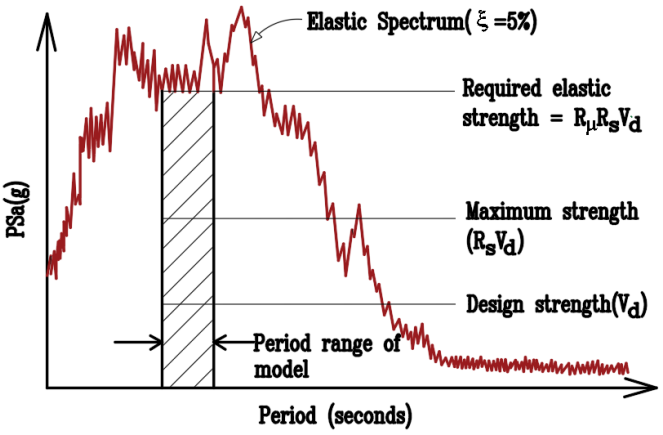

Figure 3-40. Ductility and strength factors (ATC-19, 1995)

Equation 3.55 was updated to equation 3.56 using the redundancy factor, R_R, that represents the quantifying of a building's seismic framing system, R_s and R_μ are period-dependent factors. (Freeman, 1990; ATC 34, 1995).

$$R = R_s R_\mu R_R \tag{3.56}$$

Reverse strength, R_S, has been investigated using nonlinear static analysis, which can be expressed from the ratio of the base shear force, V_o, to the design base shear, V_d, with equation 3.57 (Freeman, 1990; Osteras & Krawinkler, 1990; Uang and Maarouf, 1993; Huwang and Shinozuka, 1994; Asgarian et al. 2009 and Moni et al. 2016).

$$R_s = \frac{V_o}{V_d} \tag{3.57}$$

The displacement ductility ratio for a system or the strain, curvature, or rotation ductility ratio for an element level are two ways to express the ductility ratio. The focus of this research is on displacement ductility. In 1982, Newmark and Hall defined the ductility factor, R_μ, which depends on the frequency of the structure as expressed with equation 3.58.

$$\left\{\begin{array}{c} \mathrm{Ta} < 0.1 \rightarrow R_\mu = 1.0 \\ \hline 0.12 < \mathrm{Ta} < 0.5 \rightarrow R_\mu = \sqrt{2\mu - 1} \\ \hline \mathrm{Ta} > 1 \rightarrow R_\mu = \mu \end{array}\right\} \tag{3.58}$$

In 1994 Miranda and Bertero developed the work done by Krawinkler and Nassar in 1992 and established a relationship between ductility, ductility reduction factor, and the natural period of the structure. Therefore, the ductility factor, R_μ, can be determined with equations 3.59 to 3.61 depending on the soil types, where T is the period, μ is the ductility, and T_g is the predominant period.

$$R_\mu = \frac{\mu - 1}{1 + \frac{1}{10T - \mu T} - \frac{1}{2T} e^{-1.5|\ln(T) - 0.6|^2}} + 1 \geq 1 \quad for\ rock \tag{3.59}$$

$$R_\mu = \frac{\mu - 1}{1 + \frac{1}{12T - \mu T} - \frac{1}{5T} e^{-2|\ln(T) - 0.2|^2}} + 1 \geq 1 \quad for\ alluvium \tag{3.60}$$

$$R_\mu = \frac{\mu - 1}{1 + \frac{T_g}{3T} - \frac{3T_g}{4T} e^{-3|\ln(T/T_g) - 0.25|^2}} + 1 \geq 1 \quad for\ soft\ soil \tag{3.61}$$

3.5 Design of Buckling Restrained Braced Frame

A Buckling Restrained Brace (BRB), consisting of a ductile steel core in a concrete or mortar encased steel tube, can alternatively replace conventional braces. The steel core provides the yielding mechanism while the tube prevents buckling of the core. The buckling restrained bracing element and hysteretic behaviour of conventional and buckling restrained bracing members are presented in Figure 3-41(Alam et al. 2012, Moni et al. 2016).

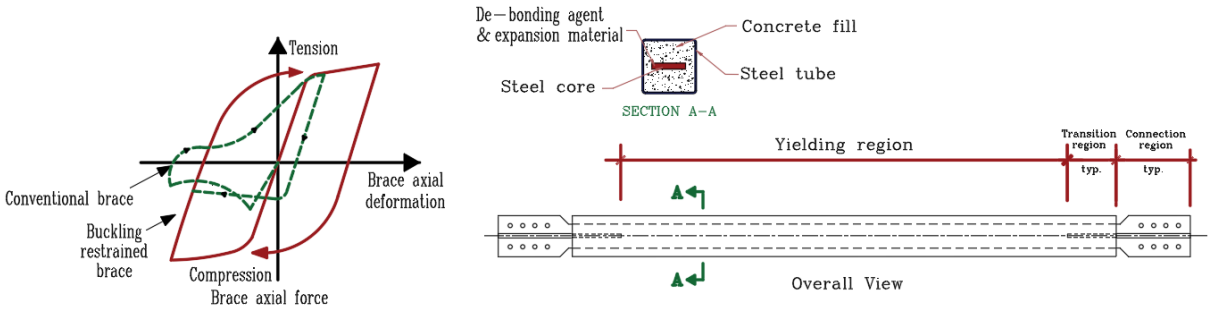

Figure 3-41. Lateral load-roof displacement relationship on the left and typical BRB on the right (Kersting et al. 2015)

The steel core is the primary source of energy dissipation and is expected to undergo inelastic deformation during a moderate to severe earthquake. The ductility of BRBF can be attained by limiting the buckling of the steel core (AISC 341, 2016). Apart from single diagonal bracing and inverted-V (chevron) bracing presented in Figure 3-42a, zig-zag diagonal bracing, V-bracing, and multistory X-bracing are other types of configurations. Figure 3-42b is the stiffness determination of a composite element, and Figure 3-42c shows the kinematic behavior of the buckling restrained brace frame, where Δ_{bx} is the axial deformation, Δ_x is the story drift, α is the inclination angle, h_{sx} is the story height, L_{wp} is the brace work point length, and θ_x is the drift story angle. Therefore, the yield length ratio (YLR) can be defined as the length of the yielding region, L_y, over L_{wp}.

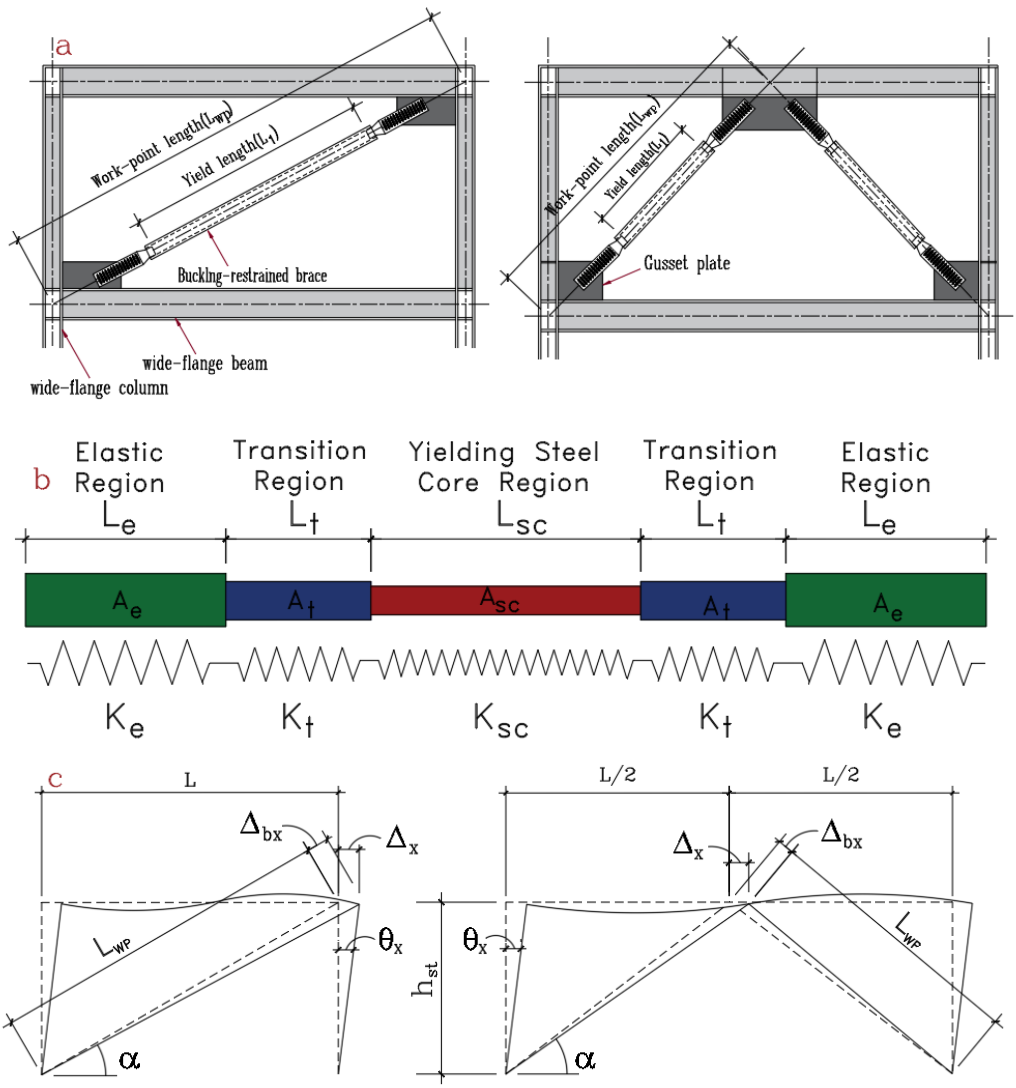

Figure 3-42. (a)Typical BRBF configuration, (b) *Stiffness, (c) kinematic behavior (Kersting et al. 2015, *CoreBrace)

Braces shall be designed based on an expected story drift of a greater value of 2% of the story height or two times of story drift $Max\,(0.02 \times h_{sx}\ or\ 2 \times \Delta_x)$, also brace connections and "adjoining members" shall be designed based on the adjusted brace strength, $\beta\omega R_y P_{ysc}$, and $\omega R_y P_{ysc}$ in compression and tension. Where P_{ysc} is the axial yield strength of the steel core, β and ω are the compression strengths and strain hardening adjustment factors from equations 3.62 and 3.63, F_{ysc} is the yield strength of the steel core, and A_{sc} is the cross-section area of the yielding segment of the steel core. R_y is equal to one, if the axial yield strength of the steel core is determined by a coupon test (AISC 341, 2016). The adjustment factors are presented in Figure 3-43, where P_{max} and T_{max} are the maximum compression force and the maximum tension force relating to 200% of the design story drift for linear methods. For nonlinear response history analysis, this value can be obtained from the analysis results.

$$\beta = \frac{\beta\omega P_{ysc} A_{sc}}{\omega P_{ysc} A_{sc}} = \frac{P_{max}}{T_{max}} \tag{3.62}$$

$$\omega = \frac{\omega P_{ysc} A_{sc}}{P_{ysc} A_{sc}} = \frac{T_{max}}{F_{ysc} A_{sc}} \tag{3.63}$$

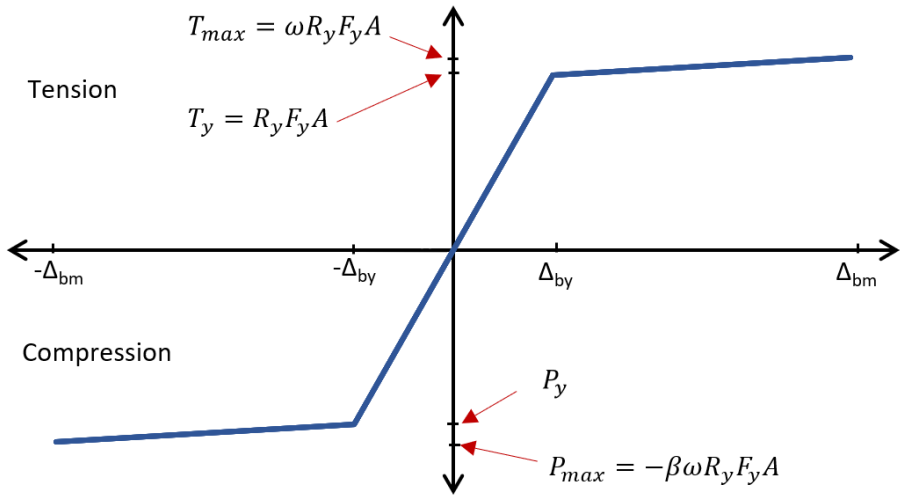

Figure 3-43. Brace force-displacement (AISC 341-16)

When the beam is assumed to be rigid with the small deformation in the BRB steel core, the strain, ε_{sc}, in the BRB core can be calculated from equation 3.64.

$$\varepsilon_{sc} = \frac{\theta_x sin2\alpha}{2YLR} \tag{3.64}$$

In Figure 3-42b, K_{sc} is the axial stiffness of the yielding core with equation 3.65, K_e is the effective stiffness of composite element, and K_F is the axial stiffness adjustment factor from equations 3.66 and 3.67.

$$k_{sc} = \frac{A_{sc}E}{L_{wp}} \tag{3.65}$$

$$k_{eff} = \frac{1}{\sum_{i=0}^{n} \frac{1}{k_i}} \tag{3.66}$$

$$KF = \frac{k_{eff}}{k_{sc}} \tag{3.67}$$

The steel core area, A_{sc}, of BRBFs was calculated from equation 3.68 (Kersting et al. 2015).

$$A_{sc} = \frac{P_u}{\emptyset F_{ysc}} \tag{3.68}$$

In this formula F_{ysc} is the yield stress of the steel core, P_u is the brace load, and $\emptyset$ is the strength reduction factor can be taken as 0.9 (Kersting et al. 2015).

3.6 Summary

The concept of seismic hazard and its parameters are explained in detail. Different analysis procedures for calculating component forces and deformation are described, including the Linear Static procedure (LSP), Linear Dynamic procedure (LDP), Nonlinear Static procedure (NSP), and Nonlinear Dynamic procedure (NDP). The seismic evaluation and retrofitting of existing buildings to predict structural behavior is presented. Furthermore, seismic response modification factors and its components are described, including the proposed methods by Newmark and Hall (1982) and 1994 Miranda and Bertero (1994), followed by the design methodology of buckling restrained braced frame.

CHAPTER 4

Seismic response of structures equipped with an Innovative Buckling Restrained Brace (IBRB)

4.1 Abstract

The dissipation energy in steel concentrically braced frames is by yielding in tension and by buckling in compression, they are easy to design and fabricate, therefore they have been frequently employed to safeguard structures from lateral loads. However, numerous issues have affected their performance in the recent earthquake, particularly poor connections, poor ductility, and their unsymmetrical hysteresis behaviour. The Buckling Restrained Braced Frame (BRBF), consisting of a ductile steel core in concrete or encased concrete with steel tube, attempts to avoid such brittle failure modes. The steel core provides the required yielding mechanism while the tube prevents buckling of the core, increasing the ductility of the system. The application of ductile materials with improved damping properties, such as tire-derived lightweight aggregate concrete, further enhances the system's overall performance.

The purpose of the first part of this chapter is to investigate the influence of such an application on the response modification, overstrength, and ductility factors as well as the general earthquake performance of four-, eight- and 14-story special reinforced concrete moment resisting frames equipped with BRBF. The current study compares 48 different BRBF models with TDA and concrete infills with different bracing configurations, including chevron (inverted-V and V), Split X, and single-leg BRBF with different span lengths of 6 m and 8 m. The evaluations include nonlinear response history analyses to provide insights on the performance of BRBF using available experimental stress-strain characteristics of tire-derived lightweight aggregate concrete as an alternative material. Furthermore, the effectiveness of tire-derived lightweight aggregate concrete as an alternative damping material in BRFB is examined by comparing BRBF with the new damping properties and concrete. Buildings equipped with BRB encased in TDA reduced the base shear demand by an average of 7% when compared to concrete infill, and the prescribed value for response modification factor for buildings of 50 meters or less provides an acceptable estimation of the lower bond factors in approximately 95% of the cases.

Subsequently, the second part of this chapter is the collaborated experimental test as well as the analytical study of Buckling Restrained Brace Frames. For this purpose, the effectiveness of tire-derived aggregate in buckling restrained braces as a ductile material with a higher damping ratio and lower density has been examined at California State University's Structures Laboratory (CSU). Based on experimental and theoretical investigations, this study compares the structural application of buckling restrained braces with TDA and with conventional concrete infill subjected to various ground motions as well as artificial excitations utilizing ETABS and OpenSees software. The evaluations include modeling a full-scale experimental setup equipped with a single-leg BRB. The effectiveness of the application is demonstrated by comparing accelerations, displacements, stiffness, damping ratios, and hysteretic behviour obtained with TDA and with concrete filling. In addition, a design guideline for buckling restrained braced frames with TDA filling is provided.

4.2 Seismic design factors for concrete structures equipped with Innovative Buckling Restrained Braces

4.2.1 Introduction

When a structure dissipates kinetic energy due to a strong ground motion, the damage levels can be identified, the structure is allowed to dissipate the kinetic energy by yielding in specified regions, as dissipating this energy within the elastic range of materials is not cost-effective. (Ko & Field, 2003), to avoid this phenomenon a number of control systems have been investigated. There are three major control systems classes: passive, active, and semi-active (Tehrani, Nazari & Naghshineh, 2022). Among them, passive energy dissipation devices are categorized by a capability to improve energy dissipation in the structural system either by transferring the kinetic energy to heat such as frictional sliding, yielding of metals and viscoelastic solids or fluids or among vibrating modes including supplemental oscillators (Soong & Dargush, 1999). Conventional braces buckle in compression, which leads to progressive degrading behavior and loss of stiffness. To resolve this issue, the unbounded brace, that supports an unbounded layer between surrounding concrete and the steel core, was developed by Professor Wada to take all axial loads. Unbonded braces can provide both stiffness and a stable energy absorption capability, the brace forces are reduced, and they do not need to be designed for buckling (Ko & Field, 2003).

It results in lower costs of new construction or retrofitting existing buildings, with lower forces in the superstructure and foundation, and can be categorized as a passive control system.

Rubberized concrete is the general name for tire-derived aggregate concrete. The idea was to enhance ductility by combining flexible and rigid materials (Tehrani and Miller 2018). Tire-derived aggregate (TDA) is derived from waste tires in a standard range of practical sizes. TDA is defined as shredded scrap tires with a basic geometrical shape with two practical types, Type A "ranging from 75 to 100 mm", and Type B "ranging from 150 to 300 mm" (ASTM D6270-08). Besides the environmental benefits of TDA, it can be used as a lightweight engineering application and the mechanical properties of TDA make it appropriate for a wide range of civil engineering applications. It is also a very durable material and has significant cost advantages. Mechanical properties of Tire-Derived Light Weight Aggregate Concrete (TDLWAC) were investigated using 38 cylindrical and 36 beam specimens (Miller and Tehrani, 2017). The splitting tensile, compressive and flexural strengths, flexural toughness, and impact flexure tests of rubberized lightweight aggregate were examined. The target strength was 21 MPa, Cylinder and beam specimens were contained natural sand fine aggregate, shale lightweight coarse aggregate, cement, and water, then the TDA was added to cylinder and beam specimens by replacement ratios of 0% to 100%. A compression test was carried out using a 500 kN testing machine that was applied 0.24 MPa per second to capture the strain gauge report. ASTM C469 was used to determine the static modulus of elasticity (ASTM C496, 2021), and the stress-strain relationship was determined by the load-deflection data obtained throughout each test. Splitting tensile strength was determined by the load-deflection relationship and in agreement with ASTM C496. It was concluded that the static mechanical properties decreased when the rubber content increased, and these materials were found to be useful where energy absorption was considered an important aspect. Bracings have been used as the most common lateral load resisting system. However, they do not perform well in the nonlinear range of deformation such as low ductility, nonsymmetrical hysteresis curve in compression and tension, and stiffness deterioration as a result of buckling in cyclic loading. Therefore, the new generation of bracing systems known as "Buckling Restrained Braced Frames (BRBF)" have been investigated. These bracing systems have symmetric hysteresis curves, high ductility, and large drift capacity (Asgarian et al. 2009).

In ASCE 7-22, the minimum earthquake lateral force is divided by Seismic Force Resisting System(s) (SFRS) reduction factor known as “the response modification factor”. This factor is regardless of span length, bracing configuration, fundamental period, and the building height. Several studies have been conducted to study the seismic design factors and performance of conventional BRBFs BRBFs (Moni et al. 2016; Mahmoudi and Zaree, 2013; Asgarian and Shokrgozar, 2009). Most of the research carried out in the past focused on the behaviour of buckling restrained braced frames in steel structures, and various approaches have also been proposed to capture their seismic evaluation (Hosseinzadeh et al. 2016; Bai and Ou 2016; Corte et al. 2014; Mahmoudi et al. 2013; Nguyen et al. 2010; Balling et al. 2009; Asgarian et al. 2009; Kumar et al. 2005; Kim et al. 2004; Sabelli et al. 2003). Further studies are required to characterize the capacities of the overall brace frame system to examine the actual behaviour of buckling restrained braces encased still with TDA/Concrete fillings as new design approaches of other types of bracings. In this study, the mechanical properties of tire-derived lightweight aggregate concrete (TDLWAC), as an alternative damping property (Tehrani et al. 2020), were used to model the innovative BRB with encased steel composite containing TDA filling. The seismic force reduction factors including “overstrength”, “ductility”, and “response modification” factors, of four-, eight-, and fourteen-story special reinforced concrete moment frames equipped with BRBF as well as a comparison between the BRB encased steel with TDA infill as a new damping property and the BRB encased steel with concrete infill were then discussed. In addition, the effects of building height and span length for four different bracing configurations, including Single-Leg Braces (SLB), Chevron Inverted V Braces (CIVB), Chevron V Braces (CVB), and Split X braces (SXB), were investigated. Moreover, nonlinear response history analyses using twenty-one scaled ground motions based on ASCE 7 and the fundamental period of each structure are performed to demonstrate the efficiency of these bracing systems.

4.2.2 Analysis Methodology

The lateral force versus deformation for a seismic force-resisting system is presented in Figure 4-1. The first plastic hinge occurred above the required strength by analysis due to specific design rules, limits, and material strengths. The system overstrength capacity is the margin when the peak strength along the curve is greater than the first highlighted yield. When the lateral load increases, plastic hinges are formed, followed by a resistance increase until the peak strength is reached.

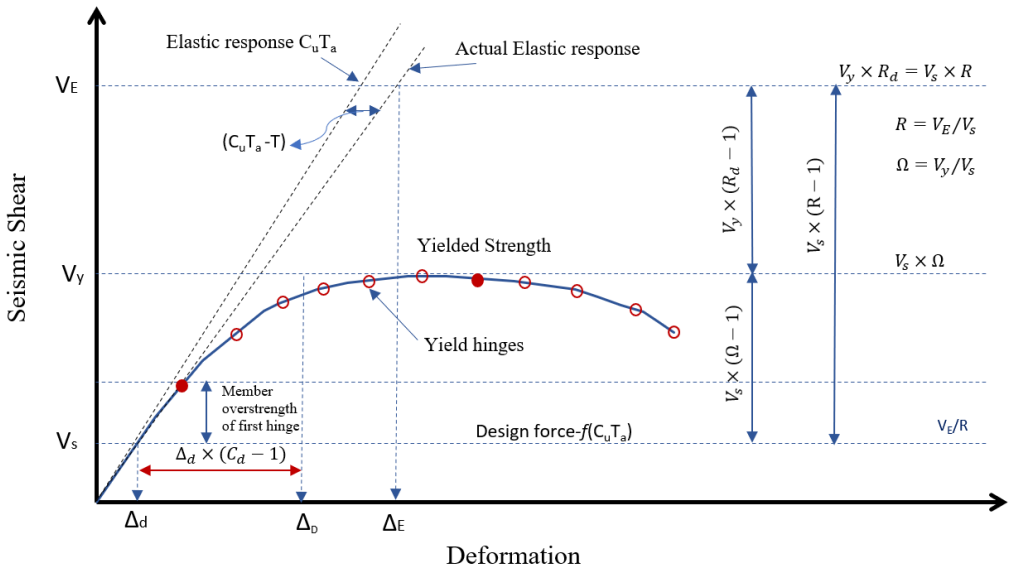

Figure 4-1. Inelastic force deformation (based on ASCE 7, 2022)

In this section, the buildings under consideration are four-, eight-, and 14-story special concrete moment resisting frames equipped with buckling restrained brace with an interstory height of 4.5 m on the ground floor and 3.5 m at all levels and consist of 5-bay in both East-west and North-South directions. The buildings are assumed to be located in Los Angeles, California, on stiff soil (Type D). The height restriction for BRBFs risk category D is limited to 50 m (ASCE 7-22), the maximum height restriction in this study. ASCE 7-22 was used to design the four-, eight-, and 14-story Special reinforced concrete moment frames for BRB encased steel with TDA and concrete infills to evaluate the "overstrength", "ductility", and "response modification" factors. The new material damping properties (TDA) of buckling restrained braces are evaluated and compared with common concrete damping properties. Figure 4-2 displays the elevation, plan, and 3-D view of a 14-story building with various bracing configurations such as Chevron (inverted-V and V), Split X, and single-leg BRBF with span lengths of 6 m and 8 m. The structural models of four-, eight-, and fourteen-story are presented in Figure 4-3 to Figure 4-5. The compressive strength f'c is 30 Mpa, modulus of elasticity E_c is 24,500 Mpa, unit weight of reinforced concrete is 24 kN/m^3, the design live and dead loads for all models are assumed to be 1.5 kN/m^2 and 2.4 kN/m^2, and the snow load acting on the roof is 1.64 kN/m^2.

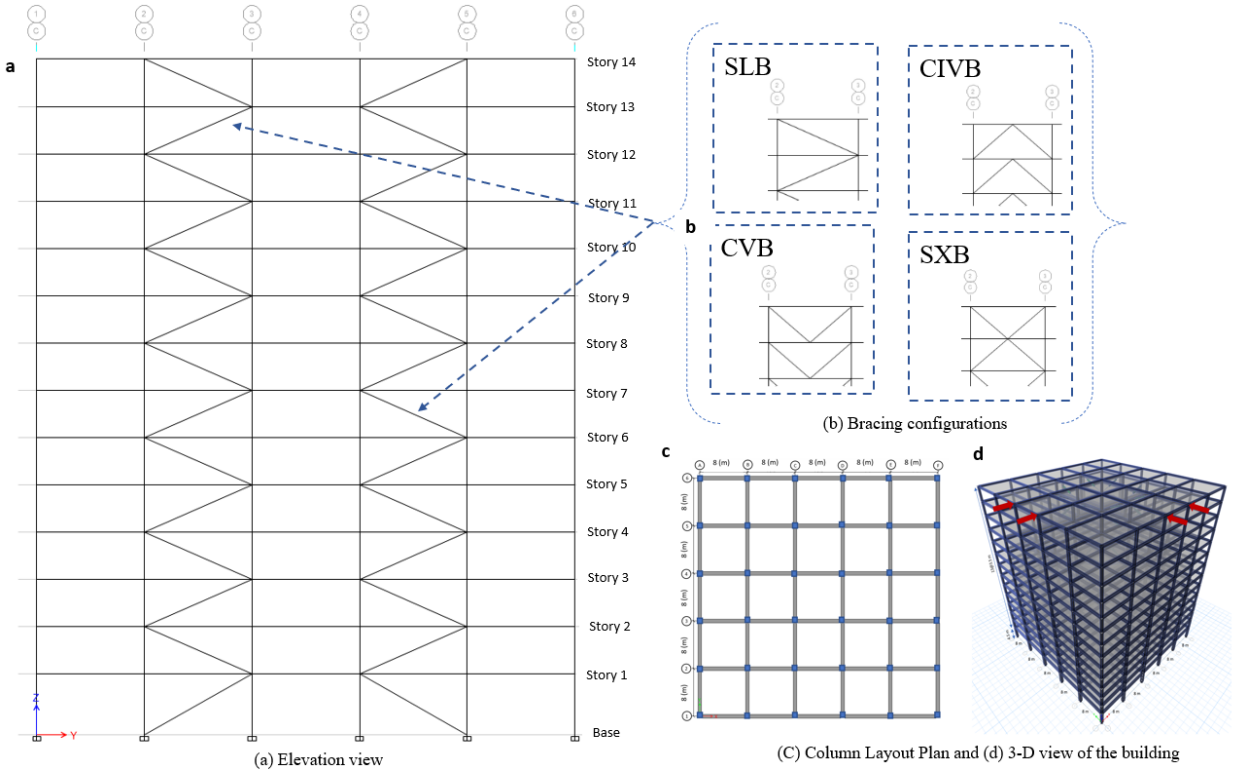

Figure 4-2. Structural models with Single Leg Braces (SLB), Chevron Inverted V Braces (CIVB), Chevron V Braces (CVB) and Split X braces (SXB) and column Layout Plan

The seismic design parameters are presented in Table 4 of Appendix F. The Minimum Design Loads and Associated Criteria for Buildings and Other Structures ASCE 7-22 was used to design four-, eight-, and fourteen-story Special reinforced concrete moment frames equipped with buckling restrained brace, detailing followed the American Concrete Institute (ACI 318-19). The analysis was carried out with the ETABS software (CSI, 2016) to simulate the behavior of reinforced concrete models under static and dynamic loads and estimate the “overstrength”, “ductility”, and “response modification” factors.

The steel core area is calculated based on the axial force (combined loading) over 90% of the yield strength with equation 3.68. The steel core area and design details are presented in Figure 4-6 and Table 4-1.

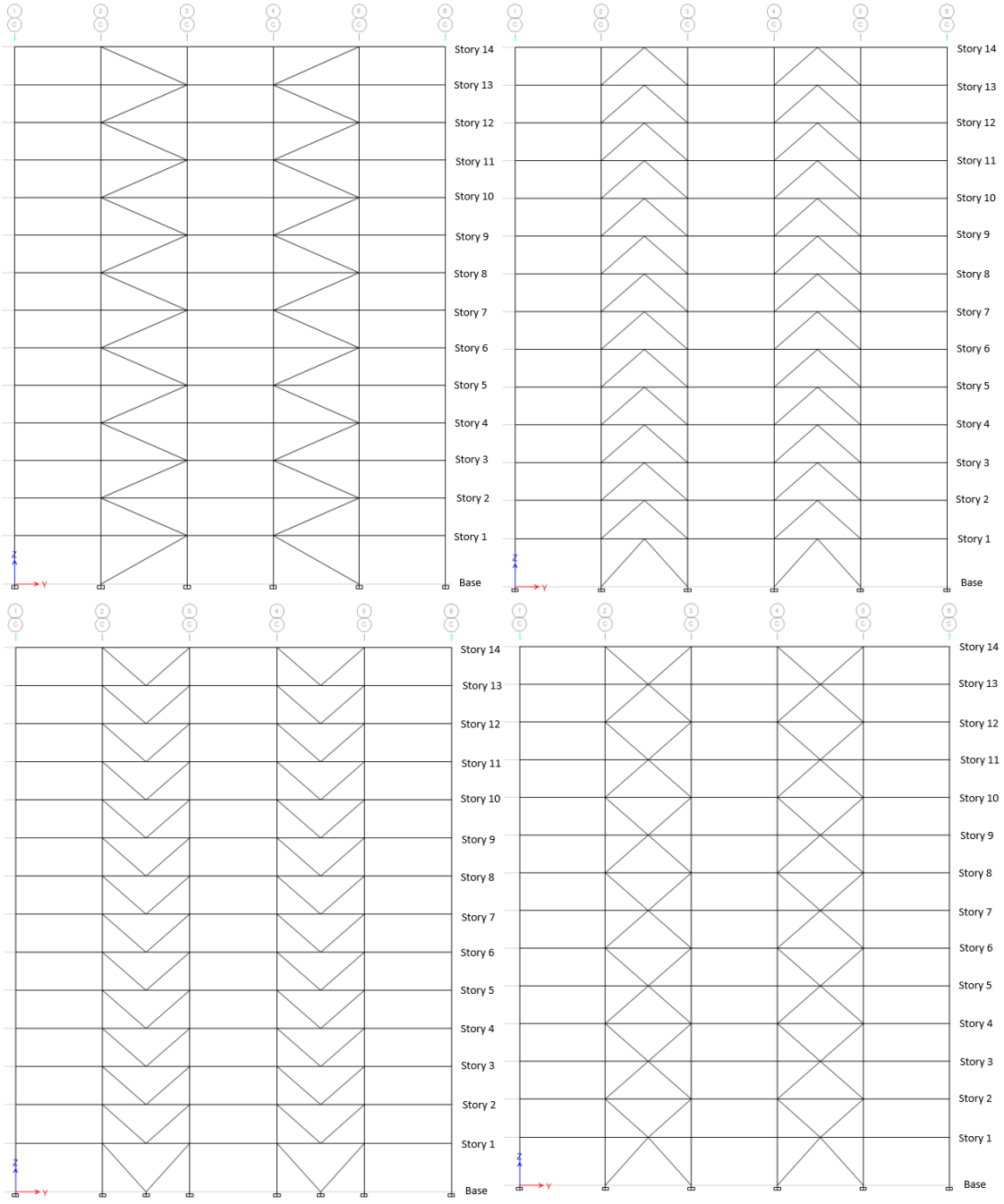

Figure 4-3. Structural model of fourteen-story

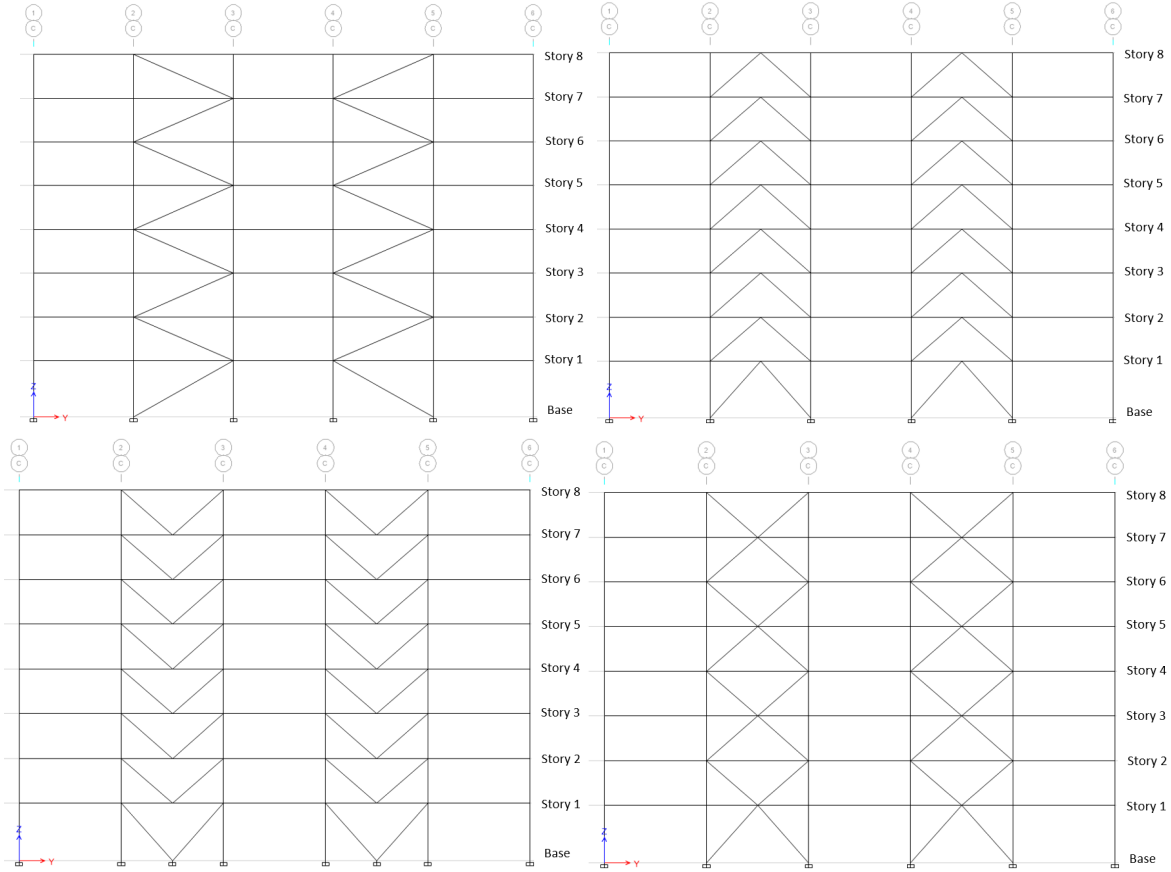

Figure 4-4. Structural model of eight-story

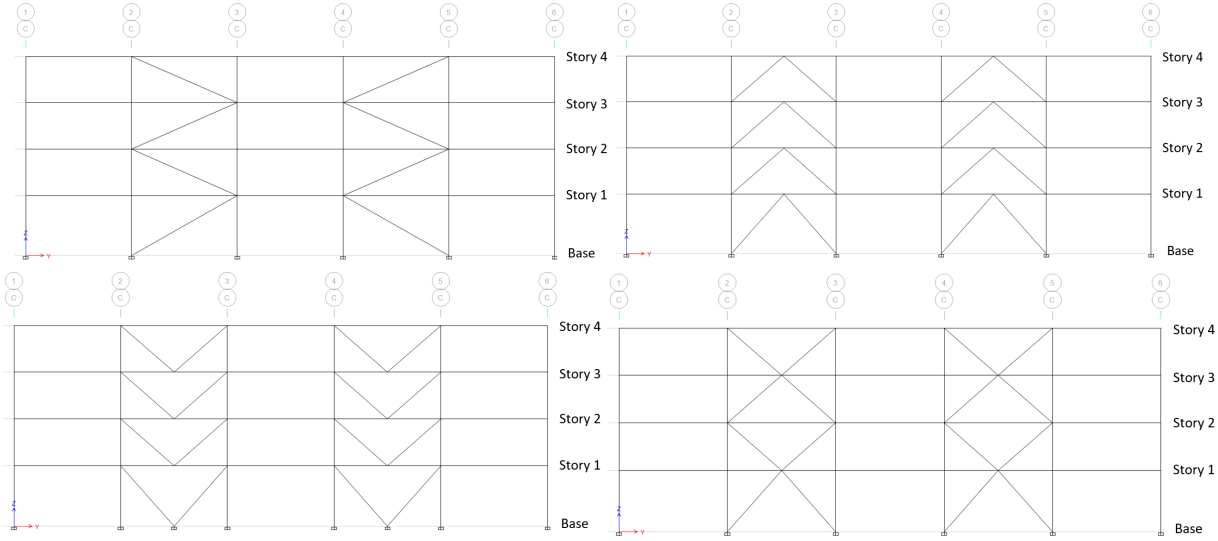

Figure 4-5. Structural model of four-story

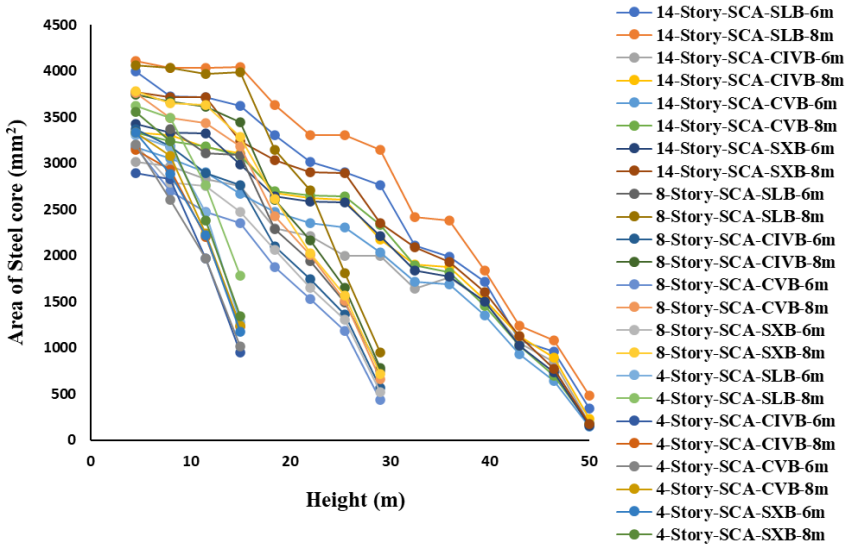

Figure 4-6. Steel Core area (mm^2)

Table 4-1. Design details for different models

		Columns				Beams	
		Interior (Cm)		Exterior (Cm)		Interior (Cm)	
ID	Span / Level	6m	8m	6m	8m	6m	8m
4	4	50×50	55×55	45×45	50×50	40×40	45×45
	3	50×50	55×55	45×45	50×50	40×40	45×45
	2	55×55	60×60	50×50	55×55	45×45	50×50
	1	60×60	65×65	55×55	60×60	45×45	50×50
8	8	50×50	55×55	45×45	50×50	45×45	50×50
	7	50×50	55×55	45×45	50×50	45×45	50×50
	6	65×65	70×70	60×60	65×65	55×50	60×55
	5	65×65	70×70	60×60	65×65	55×50	60×55
	4	70×70	75×75	65×65	70×70	55×50	60×55
	3	70×70	75×75	65×65	70×70	65×55	70×60
	2	75×75	80×80	70×70	75×75	65×55	70×60
	1	75×75	80×80	70×70	75×75	65×55	70×60
14	14	55×55	60×60	50×50	55×55	45×45	50×50
	13	55×55	60×60	50×50	55×55	55×45	60×50
	12	60×60	65×65	55×55	60×60	55×45	60×50
	11	60×60	65×65	55×55	60×60	60×50	65×55
	10	60×60	65×65	55×55	60×60	60×50	65×55
	9	65×65	75×75	60×60	65×65	65×55	70×60
	8	65×65	75×75	60×60	65×65	65×55	70×60
	7	65×65	75×75	65×65	70×70	65×55	70×60
	6	75×75	85×85	65×65	70×70	65×55	70×60
	5	75×75	85×85	65×65	70×70	65×55	70×60
	4	75×75	85×85	65×65	70×70	70×60	75×65
	3	85×85	90×90	70×70	75×75	70×60	75×65
	2	85×85	90×90	70×70	75×75	70×60	75×65
	1	85×85	90×90	70×70	75×75	70×60	75×65

4.2.3 Modal Analysis

The system frequencies and free-vibration mode shapes are provided by the predicted natural modes from the Eigenvalue analysis. The Ritz value analysis, however, identifies modes depending on a particular loading. In this study Ritz value analysis was used to identify the natural periods of the buckling restrained brace frame, because it defines a better basis than eigenvalue, mainly for superposition-based analyses such as response-history or response-spectrum. The fundamental period of the structure is calculated based on the results obtained from the ASCE 7-22 with Empirical equation 4.1.

$$T_a = C_t h_n^x \tag{4.1}$$

Where T_a is the fundamental lateral period, C_t and x are coefficients, and h_n is the height of the structure. The results of the empirical equation $Ta = 0.0731 \times (h_n)^{0.75}$ for h_n = 50 m, 29 m, 15m, and analytical for BRB encased steel with TDA and concrete infills are presented in Table 4-2 and Table 4-3. It can be observed that for BRB encased steel with concrete infills, the empirical equation overestimates the fundamental period for four stories and is almost in a good range with analytical results of eight-and fourteen-story. However, for BRB encased steel with TDA infills, the empirical equation underestimates the fundamental period for all different levels of buildings. The effect of bracing configuration and span length can be neglected due to minor differences.

Table 4-2. Fundamental period of the structures of BRB encased steel with concrete infill

Span Length			**6**				**8**		**T_a**
Bracing	**SLB**	**CIVB**	**CVB**	**SXB**	**SLB**	**CIVB**	**CVB**	**SXB**	**(Sec)**
Story									
4	0.48	0.46	0.48	0.46	0.49	0.46	0.49	0.47	0.55
8	0.91	0.79	0.89	0.84	0.92	0.80	0.90	0.87	0.92
14	1.36	1.30	1.32	1.29	1.37	1.31	1.33	1.30	1.37

Note: Single Leg Braces (SLB), Chevron Inverted V Braces (CIVB), Chevron V Braces (CVB) and Split X braces (SXB)

Table 4-3. Fundamental period of the structures of BRB encased steel with TDA infill

Span Length			**6**				**8**		**T_a**
Bracing	**SLB**	**CIVB**	**CVB**	**SXB**	**SLB**	**CIVB**	**CVB**	**SXB**	**(Sec)**
Story									
4	0.59	0.54	0.54	0.52	0.59	0.55	0.56	0.56	0.55
8	1.08	0.98	1.02	0.99	1.08	0.98	1.02	0.99	0.92
14	1.54	1.46	1.46	1.43	1.55	1.47	1.47	1.44	1.37

Note: Single Leg Braces (SLB), Chevron Inverted V Braces (CIVB), Chevron V Braces (CVB) and Split X braces (SXB)

4.2.4 Nonlinear Pushover Analysis

In this method, the structure is subjected to a lateral load pattern such as static load, acceleration, a lateral force based on the mode shape, as well as any combination of the latter, to achieve the expected structural level of deformation. The structural strength capacities and undesirable features in demand deformation including structural stability, strength, stiffness discontinuities, and additional stresses on brittle elements can be determined using nonlinear pushover analysis (Lawson et al. 1994).

To improve the capture of local P-delta effects, the distributed plasticity employing fiber section "P-M2-M3" along with a finite length hinge zone is used and columns are meshed at intermediate joints and intersecting frames. Subsequently, a nonlinear static pushover analysis was performed to calculate the overstrength and ductility factor of each structure and proceeded until the maximum interstory drift in the frame met 2.5% of the design limit. The results of roof drift ratio versus normalized base shear ratio for BRB encased steel with TDA and concrete infill for different brace configurations are presented in Figure 4-7, Figure 4-8, Figure 4-9, and Figure 4-10. The ductility values are calculated based on pushover results and the idealized lateral force-displacement results as presented in Appendix B. The yield and design strength, overstrength factor, maximum and yield displacement as well as the ductility data are tabulated in Table 4-4 and Table 4-5.

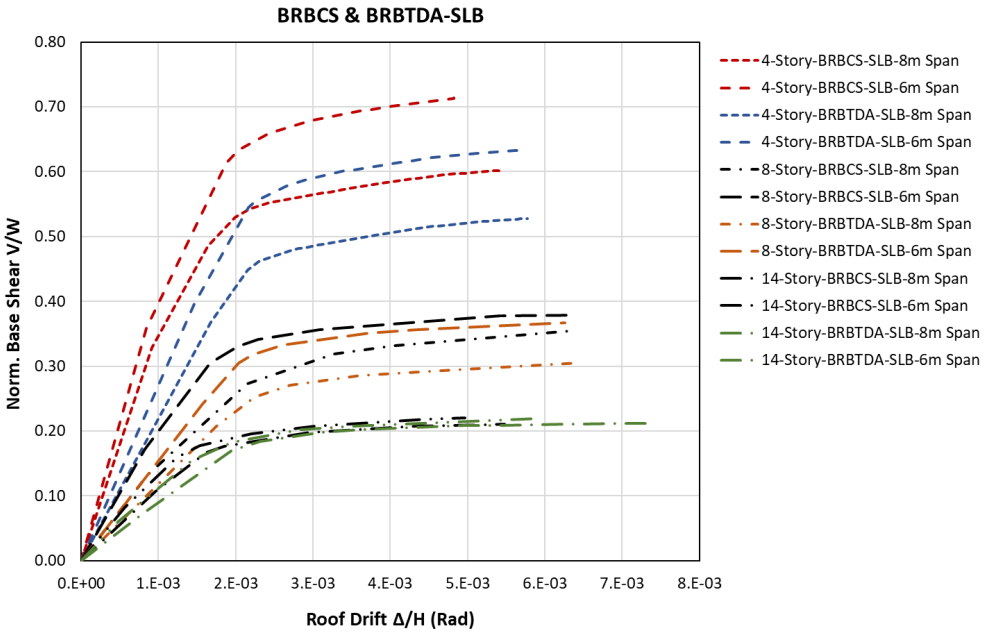

Figure 4-7. Roof drift ratio versus normalized base shear ratio for BRB encased steel with TDA and concrete infills, SLB with 6m and 8m span length (four-, eight-, fourteen-story)

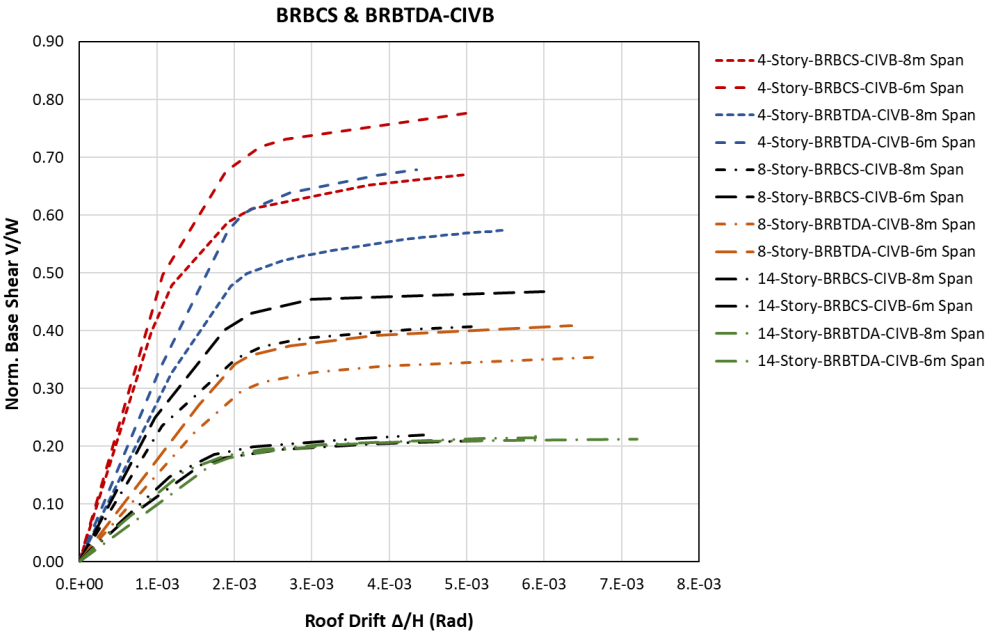

Figure 4-8. Roof drift ratio versus normalized base shear ratio for BRB encased steel with TDA and concrete infills, CIVB with 6m and 8m span length (four-, eight-, fourteen-story)

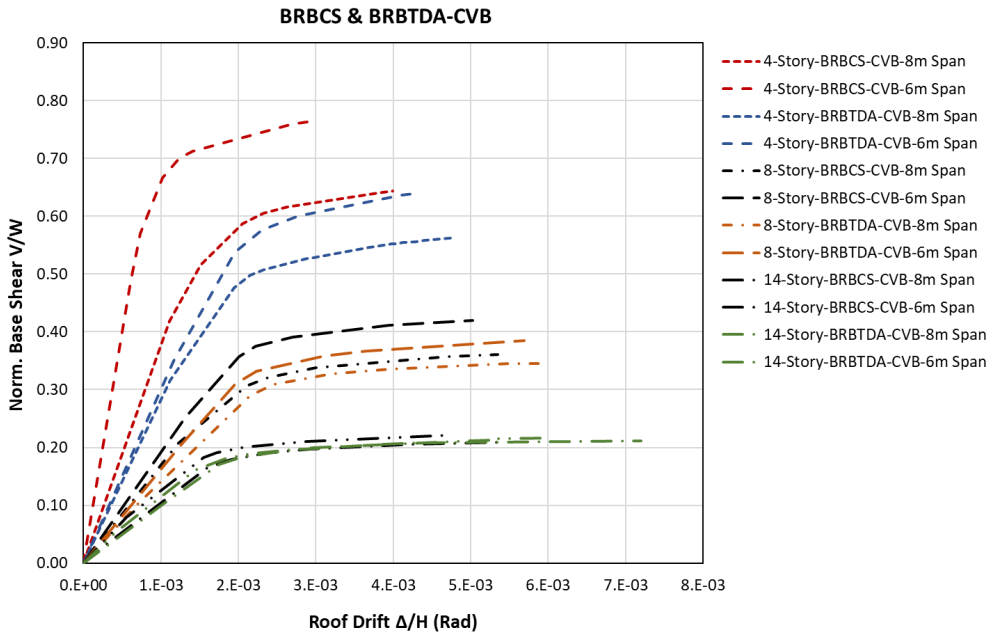

Figure 4-9. Roof drift ratio versus normalized base shear ratio for BRB encased steel with TDA and concrete infills, CVB with 6m and 8m span length (four-, eight-, fourteen-story)

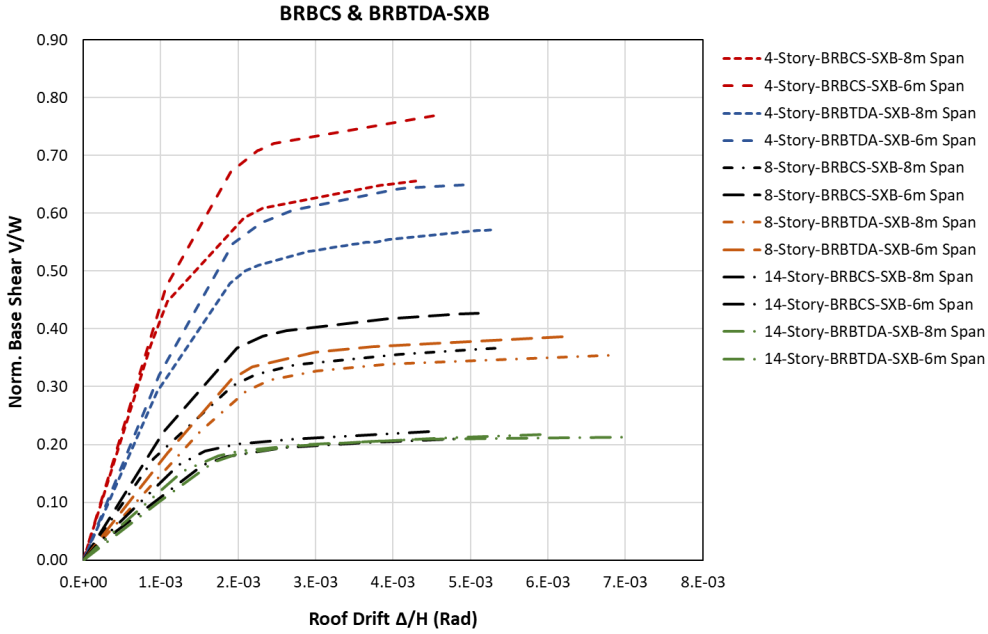

Figure 4-10. Roof drift ratio versus normalized base shear ratio for BRB encased steel with TDA and concrete infills, SXB with 6m and 8m span length (four-, eight-, fourteen-story)

Table 4-4. Pushover analysis results-BRB encased steel with concrete infill

Story	Bracing	Span Length	Yield Strength V_y (kN)	Design Strength V_d (kN)	Overstrength factor R_o	Maximum displacement Δ_{max} (mm)	Yield displacement Δ_y (mm)	Ductility μ
4	SLB	6	7113	5918	1.20	72	21	3.44
		8	8278	6149	1.34	80	22	3.63
	CIVB	6	8314	5911	1.41	65	21	3.09
		8	9130	6139	1.48	6	20	3.48
	CVB	6	8315	5914	1.41	60	24	2.50
		8	9262	6139	1.51	74	22	3.37
	SXB	6	8267	5909	1.39	69	22	3.15
		8	8926	6136	1.45	72	20	3.61
8	SLB	6	8464	7085	1.9	149	49	3.04
		8	9551	7246	1.32	176	56	3.14
	CIVB	6	10468	7877	1.33	138	46	3.01
		8	11403	8240	1.38	149	46	3.24
	CVB	6	11403	8240	1.38	156	57	2.73
		8	10468	7877	1.33	165	53	3.11
	SXB	6	9498	7179	1.33	157	50	3.11
		8	10033	7710	1.31	155	47	3.25
14	SLB	6	8983	8420	1.06	220	71	3.49
		8	10935	8590	1.27	250	78	3.65
	CIVB	6	9208	8447	1.09	222	74	3.78
		8	11209	9084	1.23	260	80	4.03
	CVB	6	9531	8493	1.12	230	78	3.67
		8	11417	8768	1.31	270	84	3.88
	SXB	6	9459	8781	1.07	215	72	3.85
		8	11332	9180	1.24	257	82	3.93

Note: Single Leg Braces (SLB), Chevron Inverted V Braces (CIVB), Chevron V Braces (CVB), and Split X braces (SXB)

Table 4-5. Pushover analysis results-BRB encased steel with TDA infill

Story	Bracing	Span Length	Yield Strength V_y (kN)	Design Strength V_d (kN)	Overstrength factor R_o	Maximum displacement Δ_{max} (mm)	Yield displacement Δ_y (mm)	Ductility μ
4	SLB	6	7008	5222	1.34	85	31	2.68
		8	7723	5409	1.42	101	32	3.07
	CIVB	6	7402	5599	1.32	75	27	2.77
		8	8088	5904	1.36	90	27	3.33
	CVB	6	6785	5460	1.24	75	27	2.77
		8	7973	5990	1.33	88	28	3.14
	SXB	6	6618	5654	1.17	73	24	3.04
		8	7855	6122	1.28	84	26	3.23
8	SLB	6	8383	5976	1.41	205	62	3.47
		8	8806	5997	1.46	220	62	3.54
	CIVB	6	9315	6405	1.45	190	56	3.39
		8	10167	6753	1.51	205	58	3.53
	CVB	6	8697	6171	1.41	186	59	3.28
		8	8806	5997	1.47	197	60	3.15
	SXB	6	8757	6312	1.38	185	56	3.30
		8	10190	6673	1.52	199	58	3.43
14	SLB	6	8995	7708	1.16	295	84	3.49
		8	11470	7819	1.46	370	101	3.65
	CIVB	6	8900	7913	1.12	299	78	3.78
		8	11489	7981	1.43	360	89	4.03
	CVB	6	8887	7897	1.12	298	81	3.67
		8	11422	7971	1.43	360	92	3.88
	SXB	6	8862	8011	1.11	299	77	3.85
		8	11332	8125	1.39	350	89	3.93

Note: Single Leg Braces (SLB), Chevron Inverted V Braces (CIVB), Chevron V Braces (CVB), and Split X braces (SXB)

4.2.5 Calculation of response modification factor components

4.2.5.1 Overstrength factor

Figure 4-11 depicts the overstrength factor for BRB encased steel with TDA and concrete infills for all brace configurations, as determined by the idealized bilinear response of base shear versus displacement. The overstrength factor ranges from 1.10 to 1.52 for the BRB encased steel with TDA and 1.06 to 1.51 for the BRB encased steel with Concrete. The NBCC 2015 specifies an overstrength factor of 1.2, and the ASCE 7-22 prescribed 2.5. These conservative values account for several factors, including member size, structural redundancy, and infill walls (Elnashai and Di Sarno, 2008). In general, overstrength increased in higher span length, which had an average value of 1.42 for BRB encased steel with TDA infill and 1.35 for BRB encased steel with concrete infill.

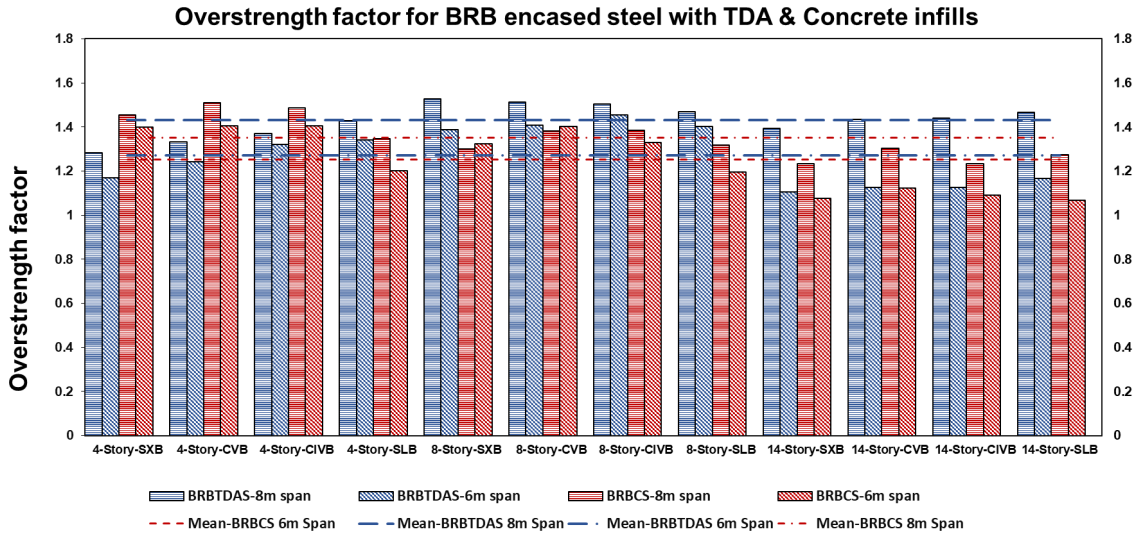

Figure 4-11. Overstrength factor for BRB encased steel with TDA and Concrete infills

4.2.5.2 Ductility factor

Ductility factors for BRB encased steel with TDA and concrete infills are determined using the Miranda and Bertero (1994) approach and compared to the Newmark and Hall (1982) method as presented in Figure 4-12 and Figure 4-13. It is evident that longer span lengths and higher building heights directly affect increasing ductility. The average ductility factors for BRB encased steel with TDA infill have been increased by about 5% compared to concrete infill. The average ductility

factor computed using the Newmark and Hall approach is lower by an average of about 15% than that determined using the Miranda and Bertero method. The effect of bracing configuration can be neglected with the maximum variation of about 3% for fourteen and eight-story buildings and 4% for four-story.

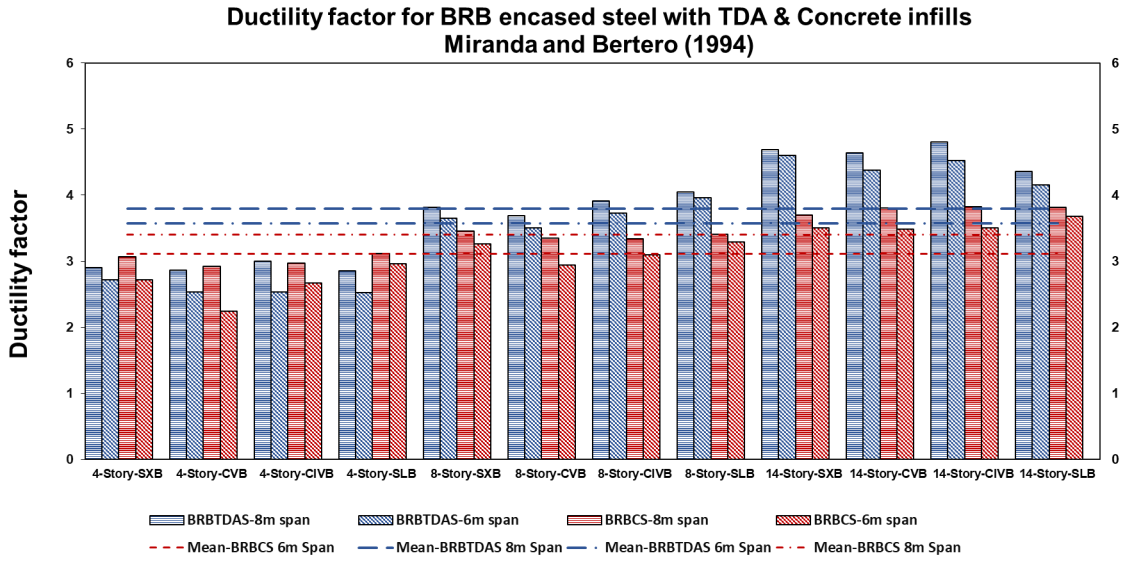

Figure 4-12. Ductility factor for BRB encased steel with TDA and Concrete infills based on Miranda and Bertero (1994) method

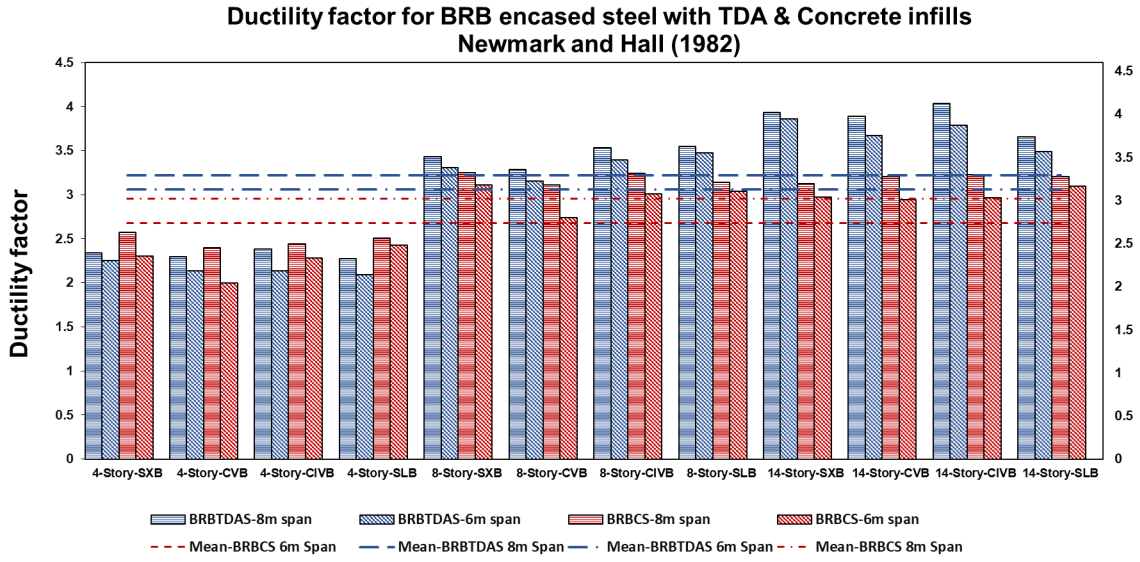

Figure 4-13. Ductility factor for BRB encased steel with TDA and Concrete infills based on Newmark and Hall (1982) method

4.2.5.3 Response modification factor

The results of response modification factors for Miranda and Bertero (1994) and Newmark and Hall (1982) of BRB encased steel with TDA and concrete infills and different frame configurations are tabulated in Table 4-6 and Table 4-7 and presented in Figure 4-14 and Figure 4-15. The Miranda and Bereto method has higher values than Newmark and Hall with an average increase of 17% and 14% for BRB encased steel with TDA and concrete infills. This increase is due to implementing additional components such as soil condition, ductility, and structure's natural period. ASCE 7-22 and NBCC 2015 prescribed the response modification values of 8 and 4.8 for BRBFs. The results show the maximum value of the response modification factor is 6.91 for TDA infill and 4.95 for concrete infill based on Miranda and Bertero; however, these results are decreased to 5.80 and 4.48 for Newmark and Hall method. For BRB encased with TDA and Concrete infills, the mean values are 4.97 and 4.21, respectively. Because different bracing configurations range from 5% to 12%, their effects should be considered.

Table 4-6. Response modification factor for 4-, 8-, 14-Story-BRB encased steel with Concrete infills

Story	Bracing	Span Length	Overstrength factor R_o	Ductility Reduction factor R_μ (Miranda, 1994)	Ductility Reduction factor R_μ (Nemark,1982)	Response modification factor (Miranda, 1994)	Response modification factor (Nemark,1982)
4	SLB	6	1.20	2.96	2.42	3.56	3.05
		8	1.34	3.12	2.51	4.19	3.37
	CIVB	6	1.41	2.67	2.27	3.76	3.21
		8	1.48	2.97	2.44	4.42	3.63
	CVB	6	1.41	2.24	2.00	3.15	2.81
		8	1.51	2.92	2.39	4.42	3.62
	SXB	6	1.39	2.72	2.31	3.79	3.22
		8	1.45	3.06	2.57	4.46	3.74
8	SLB	6	1.9	3.28	3.04	3.93	3.63
		8	1.32	3.41	3.14	4.49	4.14
	CIVB	6	1.33	3.09	3.01	4.11	3.99
		8	1.38	3.33	3.24	4.61	4.48
	CVB	6	1.38	2.94	2.73	4.12	3.83
		8	1.33	3.35	3.11	4.63	4.31
	SXB	6	1.33	3.26	3.11	4.32	4.11
		8	1.31	3.45	3.25	4.49	4.23
14	SLB	6	1.06	3.67	3.09	3.92	3.31
		8	1.27	3.81	3.21	4.85	4.08
	CIVB	6	1.09	3.50	2.96	3.82	3.22
		8	1.23	3.82	3.22	4.72	3.98
	CVB	6	1.12	3.48	2.94	3.91	3.31
		8	1.31	3.80	3.21	4.95	4.17
	SXB	6	1.07	3.50	2.96	3.77	3.19
		8	1.24	3.69	3.12	4.56	3.85

Note: Single Leg Braces (SLB), Chevron Inverted V Braces (CIVB), Chevron V Braces (CVB) and Split X braces (SXB)

Table 4-7. Response modification factor for 4-, 8-, 14-Story-BRB encased steel with TDA infills

Story	Bracing	Span Length	Overstrength factor R_o	Ductility Reduction factor R_μ (Miranda, 1994)	Ductility Reduction factor R_μ (Nemark,1982)	Response modification factor (Miranda, 1994)	Response modification factor (Nemark,1982)
4	SLB	6	1.34	2.52	2.09	3.39	2.81
		8	1.42	2.85	2.27	4.08	3.24
	CIVB	6	1.32	2.53	2.13	3.55	2.82
		8	1.36	2.99	2.38	4.10	3.26
	CVB	6	1.24	2.53	2.13	3.15	2.65
		8	1.33	2.86	2.29	3.81	3.06
	SXB	6	1.17	2.72	2.25	3.18	2.63
		8	1.28	2.90	2.33	3.72	3.99
8	SLB	6	1.41	3.96	3.47	5.56	4.87
		8	1.46	4.04	3.54	5.94	5.21
	CIVB	6	1.45	3.73	3.39	5.42	4.93
		8	1.51	3.90	3.53	5.88	5.32
	CVB	6	1.41	3.50	3.15	4.94	4.44
		8	1.47	3.68	3.28	5.57	4.96
	SXB	6	1.38	3.64	3.31	5.06	4.58
		8	1.52	3.81	3.43	5.81	5.24
14	SLB	6	1.16	4.15	3.49	4.83	4.07
		8	1.46	4.35	3.65	6.38	5.36
	CIVB	6	1.12	4.52	3.78	5.08	4.26
		8	1.43	4.80	4.03	6.91	5.81
	CVB	6	1.12	4.38	3.67	4.93	4.13
		8	1.43	4.63	3.88	6.64	5.57
	SXB	6	1.11	4.60	3.85	5.09	4.26
		8	1.39	4.68	3.93	6.54	5.48

Note: Single Leg Braces (SLB), Chevron Inverted V Braces (CIVB), Chevron V Braces (CVB) and Split X braces (SXB)

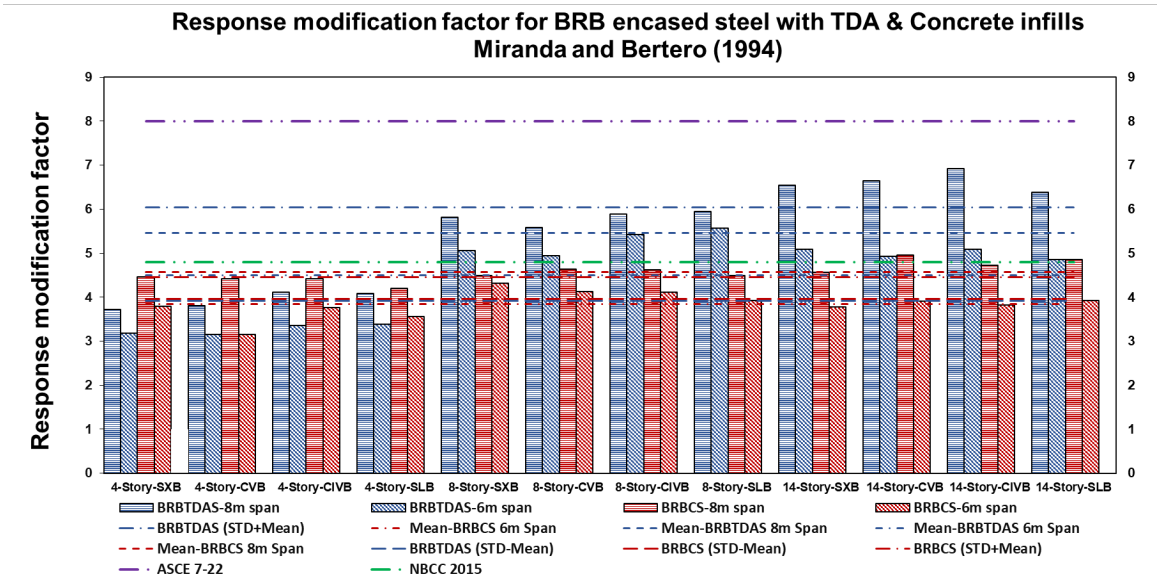

Figure 4-14. Response modification factor for BRB encased steel with TDA and Concrete infills based on Miranda and Bertero (1994) method

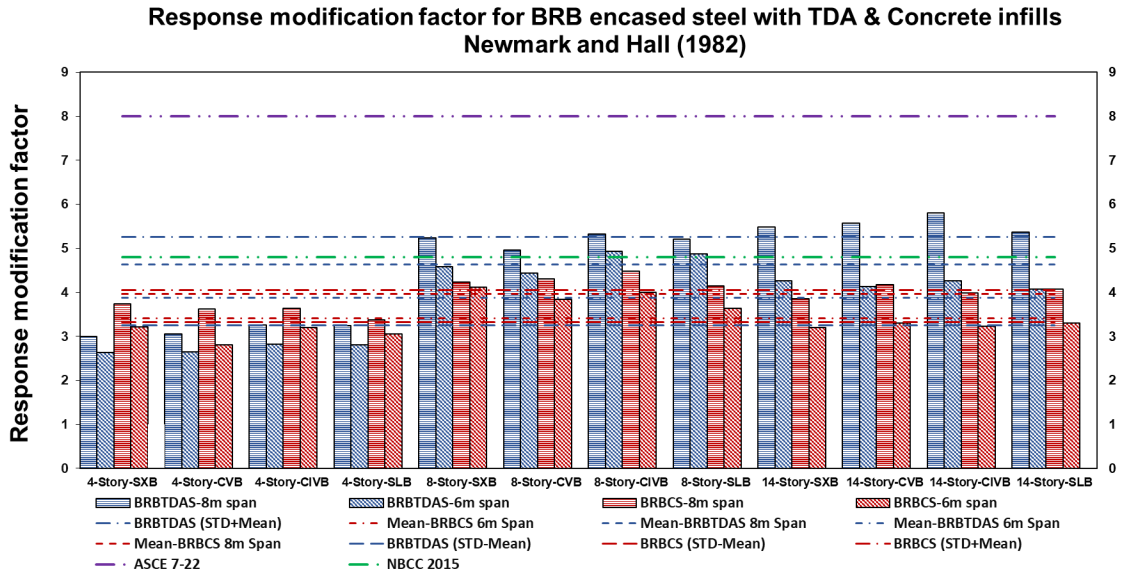

Figure 4-15. Response modification factor for BRB encased steel with TDA and Concrete infills based on Newmark and Hall (1982) method

In addition, deflection amplification factors (C_d) are calculated based on the FEMA P695 (2009) and presented in Appendix C.

4.2.6 Inelastic Response History Analysis

P-Δ effects, structural modeling assumptions, and ground motion parameters are among the important factors which affect the results. The second-order or P-Δ effect is the gravity loads acting on the laterally deformed structure. These effects reduce the initial stiffness of the structure slightly when the structure is in the elastic phase. However, when the structure is in the inelastic phase, they cause a rapid in lateral force resistance with negative stiffness.

4.2.6.1 Ground motion selection

Earthquake ground motions resemble wave signals, and an accelerograph are used to record the ground motions. There are three major aspects of ground motions: amplitude, frequency content, and duration, the ground motion characteristics are presented in Appendix F in Table 4 (Kramer, 1996). The connections between the response of the structure and ground-motion parameters have been explored through different strategies (Gavin et al. 2011, Cordova et al. 2000, Baker 2007). The earlier edition of ASCE 7-05/10 recommended three or seven ground motions for nonlinear response history analysis. When three sets of ground motions were used, the maximum value of peak response of these three ground motions was used to evaluate structural competence. If seven

or more ground motions were used, the mean results were evaluated. These selections are insufficient to address the accuracy of mean or variability in response (ASCE 7-05/10). Therefore, the minimum number of ground motions was increased to eleven in the ASCE 7-16/22 standard. This increased number of ground motions is requierd to have more reliable results in mean structural response. In other words, this is to identify the unacceptable structural response in one or more ground motions, which indicates the structure fails to meet the 10% target collapse reliability. The considered number of ground motion records and the attribute of the selected records are two important aspects of selecting ground motions. To identify the possible dispersion and mean of demand parameters, a large number of ground motion records are required due to the significant scatter of structural response to motions (Stewart et al. 2015; Haselton et al. 2009). The first step of selection involves consideration of important factors, including magnitude, source mechanisms, site soil conditions, usable frequency, period sampling (between 0.001sec to 0.02 sec), and the distance between the site and the source. The second step is to identify the final set of ground motions based on spectral shape, scale factor, and maximum motions from a single event.

In this study, the building is assumed to be located in Los Angeles, California, on stiff soil (Type D) with a latitude and longitude of 34.0522, -118.2436. A single target response spectrum with 5% damped and maximum considered earthquake (MCE_R) was developed by increasing the design response spectrum by 1.5, as presented in Figure 4-16.

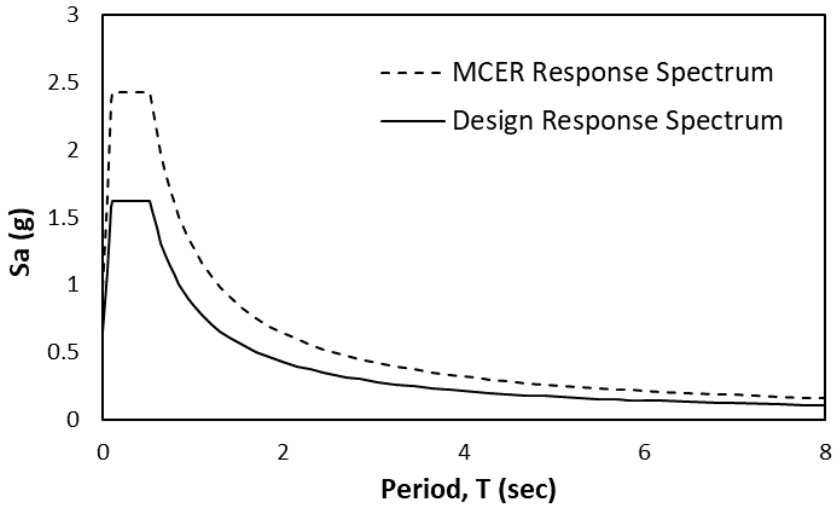

Figure 4-16. Design and MCER response spectrum

For nonlinear dynamics analysis, 21 different ground motion records were selected based on MCE_R target response spectrum from the database of the Pacific Earthquake Engineering Research Center (PEER) database, as presented in Table 4-8.

Table 4-8. Summary of Metadata of Selected Records

ID	Scale Factor	Earthquake	Year	Station Name	Magnitude	Mechanism	Arias Intensity (cm/sec, OA)	Arias Intensity (cm/sec, MA)	PGA (g)
1	1.0797	Gazli USSR	1976	Karakyr	6.8	Reverse	5.28	13.19	0.702
2	1.3647	Imperial Valley-06	1979	Bonds Corner	6.53	Strike slip	3.98	14.91	0.598
3	1.3146	Nahanni Canada	1985	Site 1	6.76	Reverse	3.88	8.64	1.108
4	1.6071	Superstition Hills-02	1987	Parachute Test Site	6.54	Strike slip	3.74	17.34	0.432
5	1.7282	Loma Prieta	1989	BRAN	6.93	Reverse Oblique	5.36	20.59	0.456
6	1.622	Erzican Turkey	1992	Erzincan	6.69	Strike slip	1.53	10.62	0.386
7	0.9724	Cape Mendocino	1992	Cape Mendocino	7.01	Reverse	5.96	8.49	1.493
8	1.6892	Northridge-01	1994	Beverly Hills-14145 Mulhol	6.69	Reverse	3.08	17.91	0.443
9	1.228	Kobe Japan	1995	KJMA	6.9	Strike slip	8.39	16.09	0.834
10	1.1306	Chi-Chi Taiwan	1999	CHY028	7.62	Reverse Oblique	5.34	17.22	0.636
11	1.3235	Duzce Turkey	1999	Bolu	7.14	Strike slip	3.72	12.12	0.739
12	1.4563	Manjil Iran	1990	Abbar	7.37	Strike slip	4.64	31.79	0.514
13	1.7718	Tottori Japan	2000	SMNH01	6.61	Strike slip	5.29	18.07	0.733
14	1.1297	Bam Iran	2003	Bam	6.6	Strike slip	8.02	18.22	0.807
15	0.7919	Niigata Japan	2004	NIG019	6.63	Reverse	14.51	17.35	1.166
16	1.3327	Chuetsu oki Japan	2007	Kashiwazaki City Center	6.8	Reverse	2.81	16.73	0.482
17	1.0688	Iwate Japan	2008	AKTH04	6.9	Reverse	11.82	19.25	1.343
18	1.587	El Mayor Cucapah Mexico	2010	MICHOACAN DE OCAMPO	7.2	Strike slip	6.01	29.53	0.537
19	1.0332	Darfield New Zealand	2010	GDLC	7	Strike slip	4.49	10.71	0.764
20	1.6745	Duzce Turkey	1999	IRIGM 496	7.14	Strike slip	13.36	20.66	1.031
21		Tohoku	1923		7.9	Subduction	11.59	78.15	0.427

Note: Original Accelerograms (OA), Matched Accelerograms (MA)

4.2.6.2 Ground motion scaling

Spectral matching and amplitude scaling are two methods for aligning time series with the intended response spectrum. Spectral matching is the process of matching the time series frequency content to the desired response spectrum. The scaling procedure, on the other hand, is the adjusting initial time series by the scaling factor, after which the matched spectrum in a specific time range equals or surpasses the expected response spectrum (Gavin et al. 2011). The previous

version of ASCE 7-05/10 specified the desired period of range for the lower bond (0.2T) and the higher bond (1.5T) to reflect the period elongation as well as the higher mode effects. The higher bond was increased to 2.0T in the new version of ASCE 7-16/22, to reflect a higher inelastic response by considering the maximum considered earthquake response. Where T is the maximum fundamental period of the building in both transitional directions as well as the fundamental torsional period. The lower bound period of 0.2T should capture the periods required for 90% mass participation in both building directions. This additional requirement ensures that the ground motions can capture response in higher modes for long period structures.

The accelerograms for each structure were scaled according to the maximum considered earthquake (MCE_R) with a period range of 0.2T to 2.0T using the applicable tool in SeismoMatch 2018 software, as shown in Figure 4-17, Figure 4-18, and Figure 4-19.

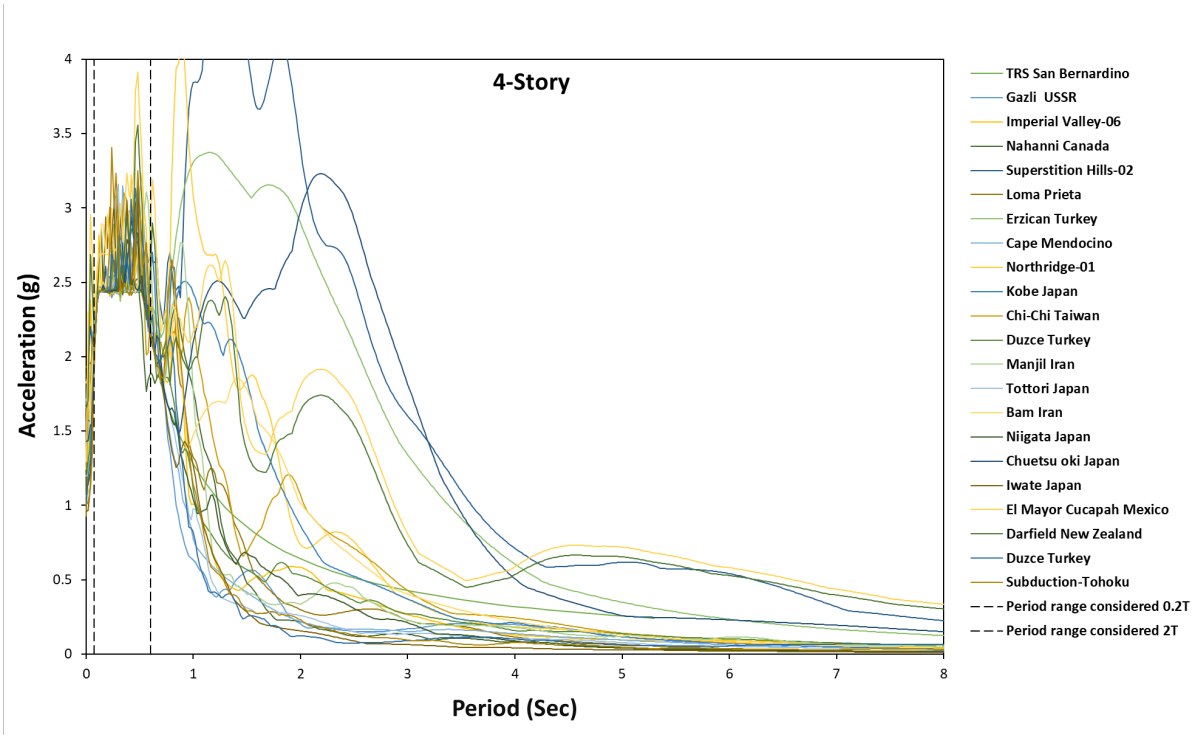

Figure 4-17. Matched accelerograms based on the target response spectrum (four-story)

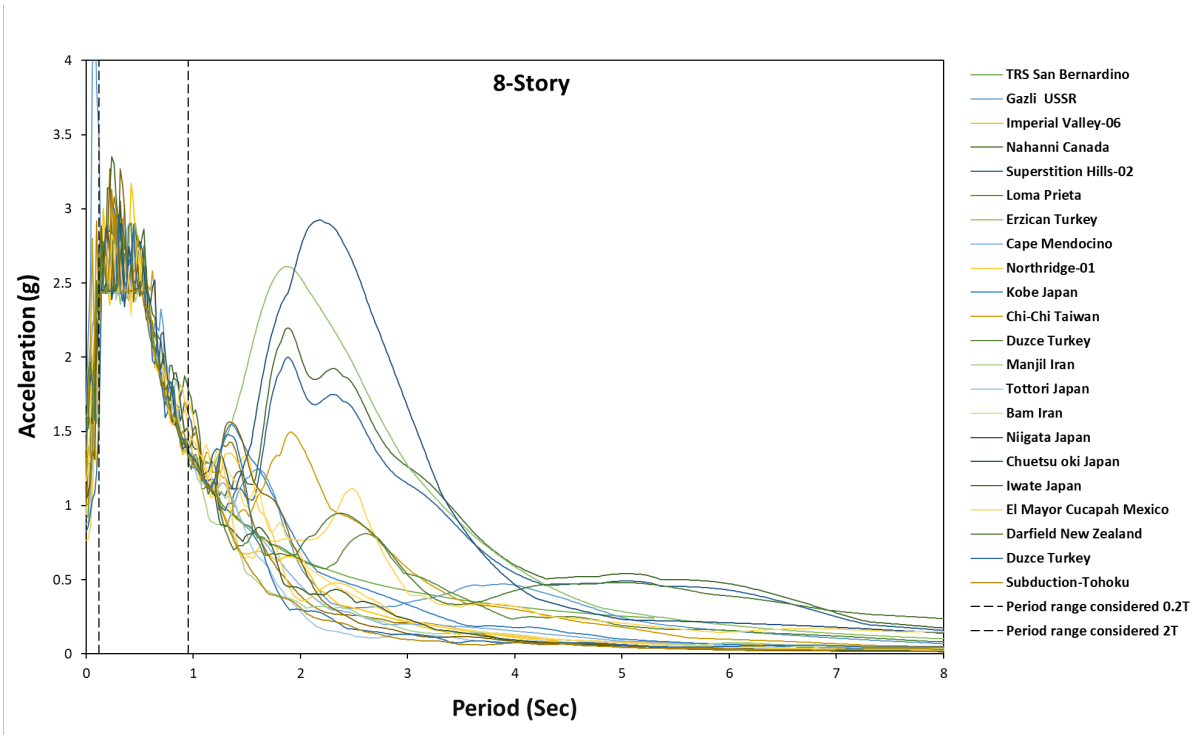

Figure 4-18. Matched accelerograms based on the target response spectrum (eight-story)

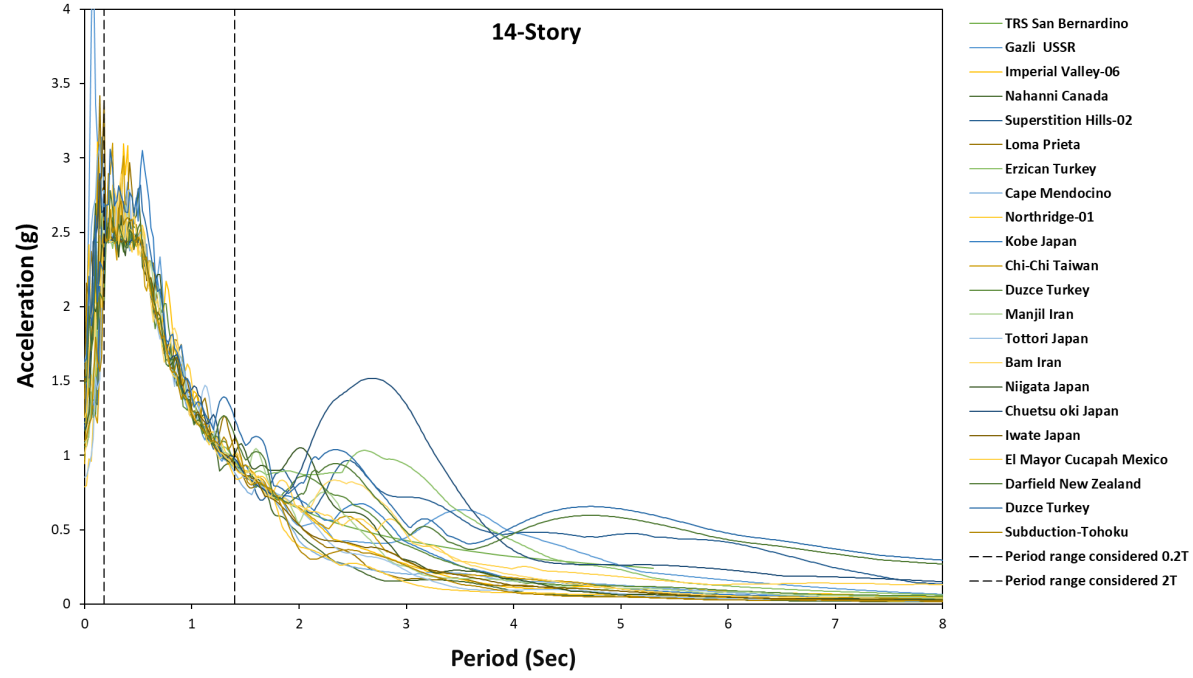

Figure 4-19. Matched accelerograms based on the target response spectrum (fourteen-story)

4.2.7 Inter-story, and base shear demand results

Figure 4-20, Figure 4-21, and Figure 4-22 present the Standard deviation plus the mean values of twenty-one ground motions records for different bracing configurations of BRB encased steel with TDA and Concrete infills at varying building heights and span lengths. The tenth level of fourteen-story for the BRB with encased steel with TDA infill has a maximum mean peak value of 2.11% and 2.18% of the interstory demands for 6m and 8m span of SLB. However, the maximum mean interstory demand decreased to 2.23% and 2.32% at a similar level for the BRB with encased steel with concrete infill for 6m and 8m span of SLB. The maximum mean interstory demands for the BRB encased steel with TDA infill are 2.19% and 2.28% at the fourth level of eight-story for SLB 6m and 8m span lengths, respectively, while the maximum mean interstory demands for the BRB encased steel with concrete infill of SLB are 2% and 2.07% at the sixth level of eight-story. The third level of four stories for the BRB with encased steel with TDA infill of SLB has a maximum mean value of 2.12% and 2.34% for 6m and 8m span lengths, and a similar level has a maximum mean value of 1.94% and 2.17% for the BRB encased steel with Concrete infill for 6m and 8m span of SLB. Maximum mean value drifts demand was observed at the third, fourth, and tenth levels for BRB encased steel with TDA and concrete infills. In general, the drift demand has a higher value for the BRB with encased steel with TDA compared to the BRB with encased steel with concrete. Appendix D represents the interstory drift for twenty-one ground motions records of all models.

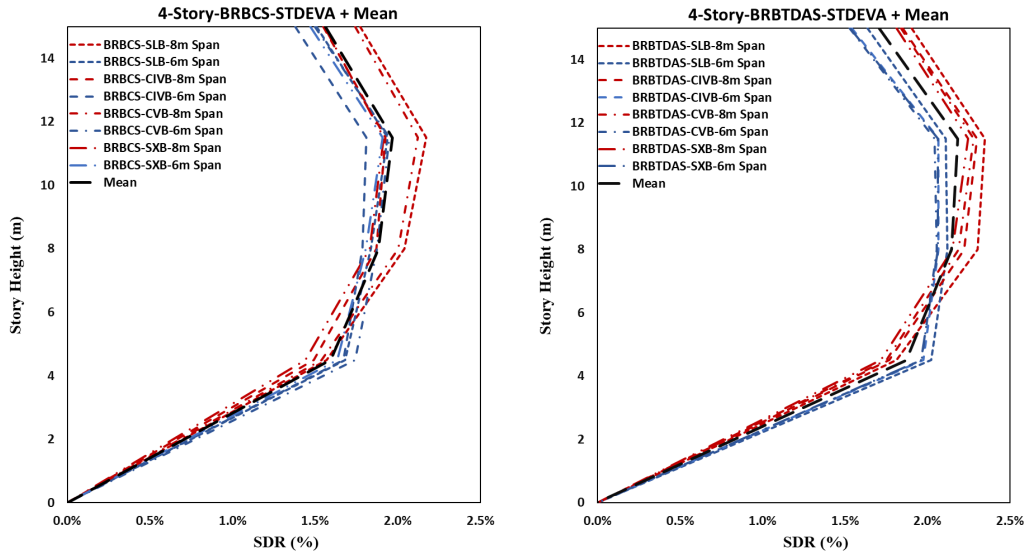

Figure 4-20. Standard deviation and the mean values of inter-story drift ratio for 4-Story BRB encased steel with TDA and concrete infills for span lengths of 6m and 8m

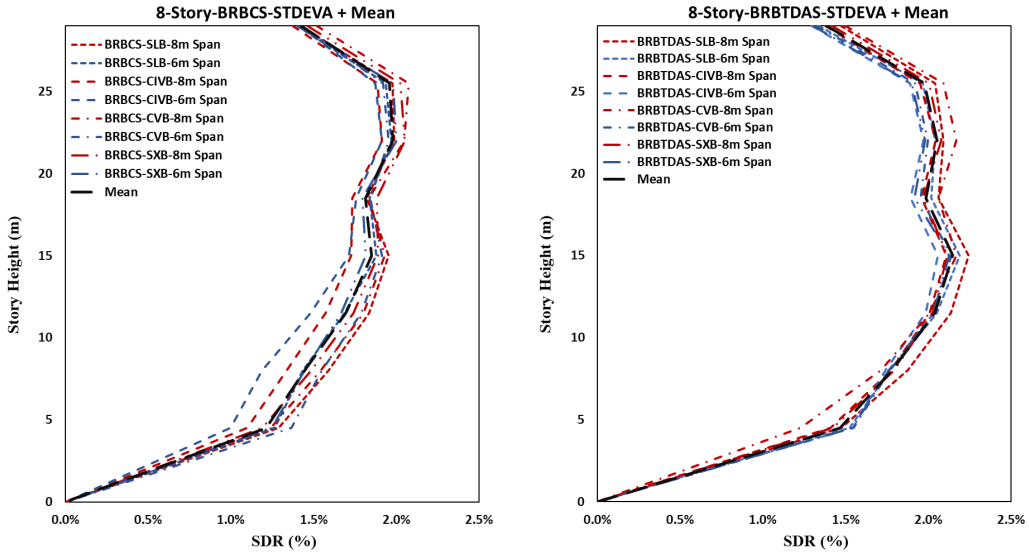

Figure 4-21. Standard deviation and the mean values of interstory drift ratio for 8-Story BRB encased steel with TDA and concrete infills for span lengths of 6m and 8m

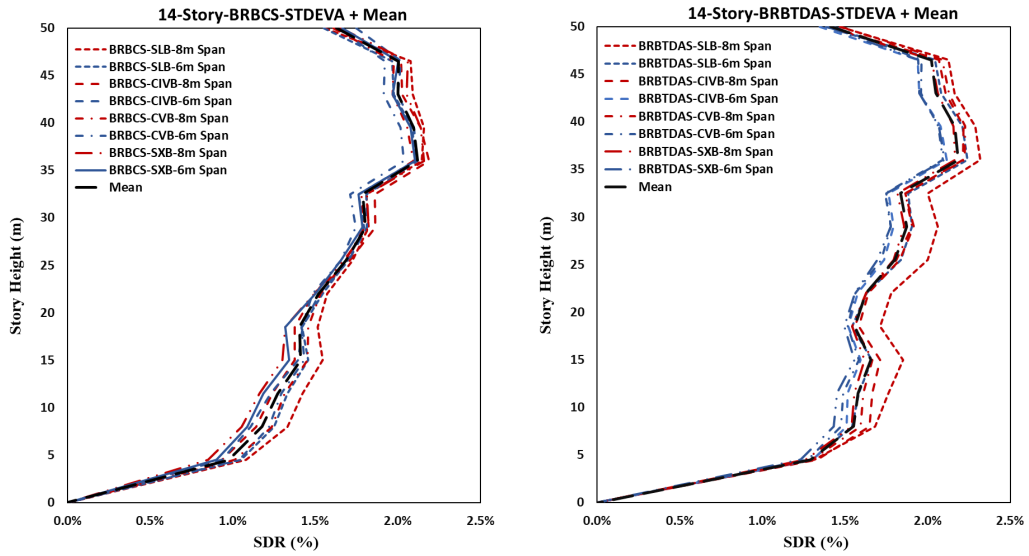

Figure 4-22. Standard deviation and the mean values of interstory drift ratio for 14-Story BRB encased steel with TDA and concrete infills for span lengths of 6m and 8m

4.2.8 Base shear demand

The maximum base shear demands were calculated based on the nonlinear response history analysis and presented in Appendix E. It can be observed that the smaller span lengths have lower base shear demands compared with longer span lengths, and the base shear demands increase with the increase of building height and varies with different bracing configurations.

The mean base shear demands for BRB encased steel with TDA and Concrete infills with different span lengths, bracing configurations, and various heights are presented in Figure 4-23. Overall, the base shear demands are reduced for the BRB encased steel with TDA infill than the concrete infill and are higher in longer span length.

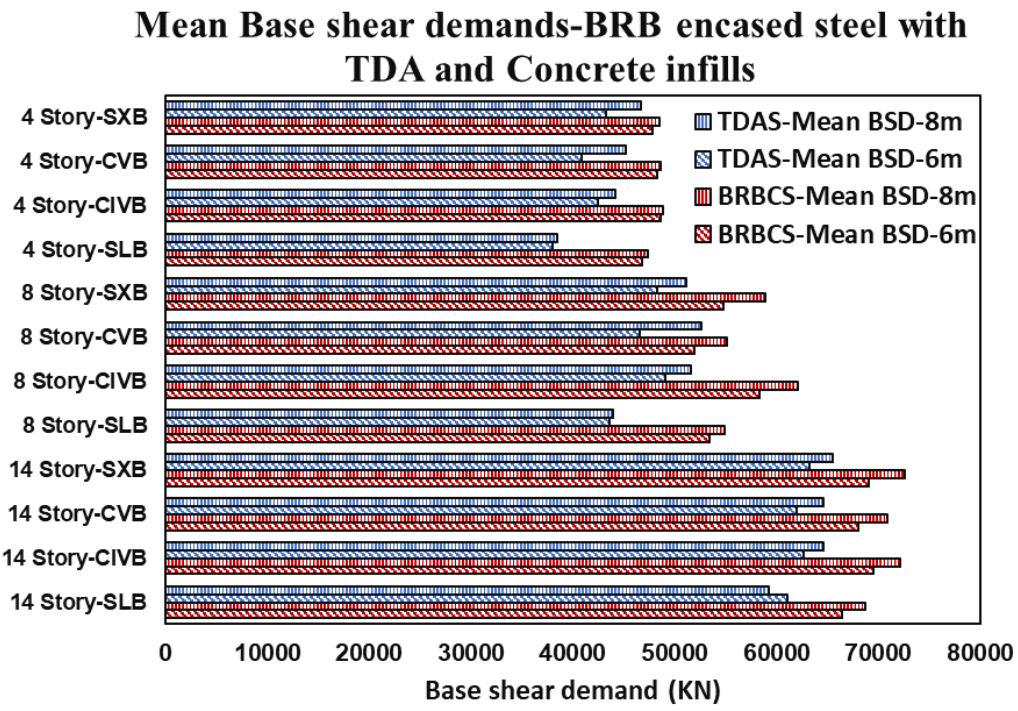

Figure 4-23. Mean Base Shear Demand (BSD) for BRB encased steel with TDA and concrete fillings and different span length

In addition, the base shear capacity over demand ratio is presented in Figure 4-24 and Figure 4-25. This ratio is higher for 8m-span than 6m-span length. The mean base shear demand values for BRB encased with TDA infill are 1.49 and 1.38 for 8m and 6m spans, respectively, these values increase to 1.63, and 1.45 for 8m and 6m spans of BRB encased in the concrete infill. Buildings equipped with BRB encased with TDA reduced the base shear capacity over demand by an average of 7% compared to concrete infill.

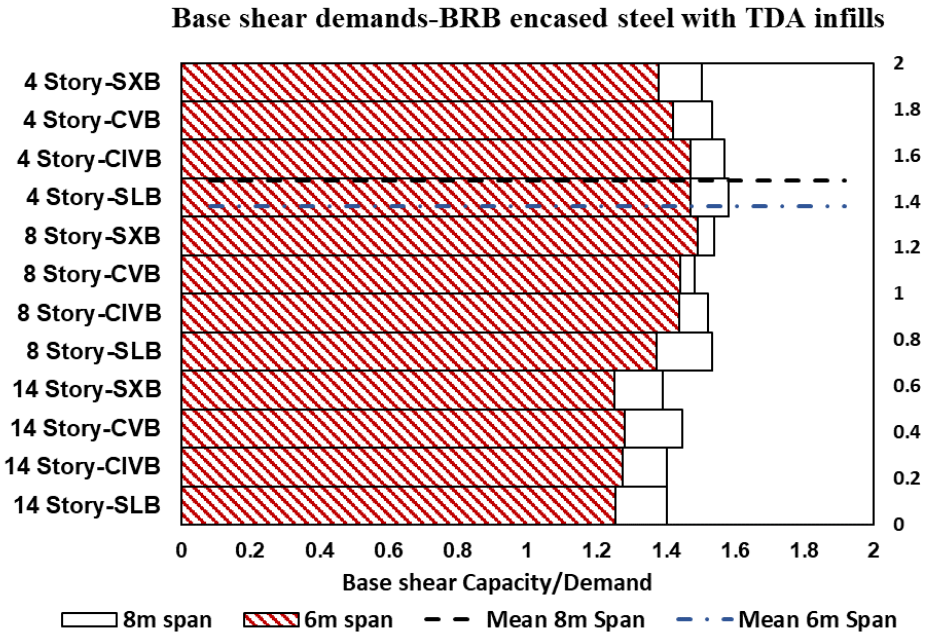

Figure 4-24. Base shear Capacity over demand for 4-, 8-, 14-story BRB encased steel with TDA filling for SLB, CIVB, CVB, and SXB bracing configurations

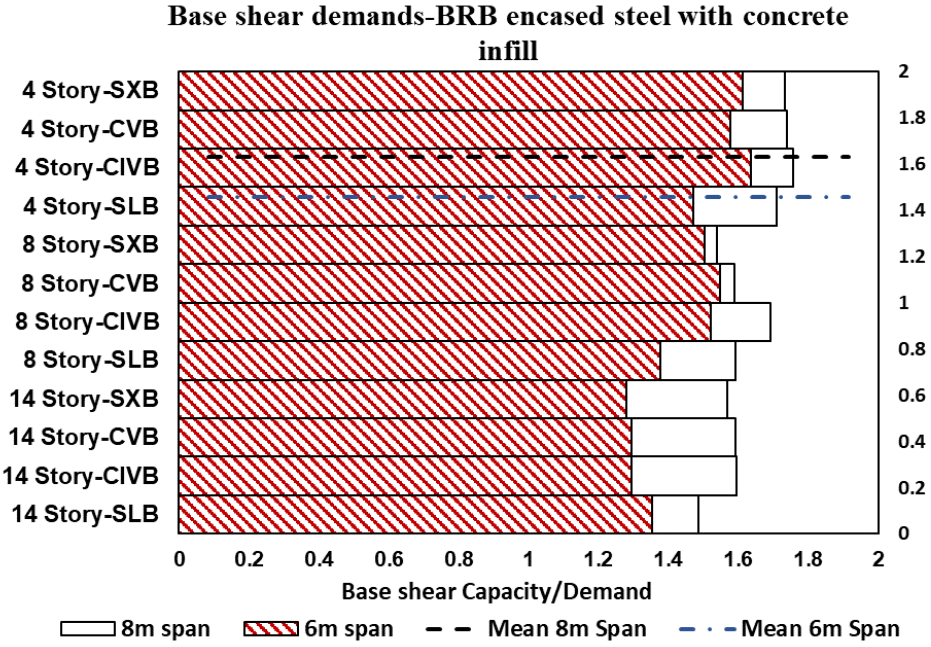

Figure 4-25. Base shear Capacity over demand for 4-, 8-, 14-story BRB encased steel with concrete filling for SLB, CIVB, CVB, and SXB bracing configurations

4.2.9 Conclusions

The seismic design factors for novel Buckling Restrained Braces employing tire-derived lightweight aggregate concrete as a filling material were explored in this study. Four, eight, and fourteen-story special concrete moment frames were designed based on the ASCE 7-22 and ACI 318-19. The effects of different bracing configurations, including chevron (inverted-V and V), Split X, and single-leg BRB with different span lengths of 6 m and 8 m, were discussed. Overstrength, ductility, and response modification factors of forty-eight different frames were evaluated and discussed. Furthermore, nonlinear response history analysis was used to evaluate the performance of these buildings utilizing twenty-one distinct ground motion recordings. Interpretation of inter-story and roof drifts, as well as their capacity over demand ratios, were presented. The following highlights are concluded:

The average fundamental periods of BRB encased steel with Concrete considering different span lengths and bracing configurations are 0.47(s), 0.86(s), and 1.32(s) for four, eight, and fourteen-story SCMF. These values are increased to 0.55(s), 1.01(s), and 1.47(s) for four, eight, and fourteen-story SCMF of BRB encased steel with TDA. In general, the empirical equation-calculated fundamental period of the structures is more conservative than the eigenvalue analysis of the structures for BRB encased steel with Concrete infill. It underestimates the period of the structure in higher buildings equipped with BRB encased steel with TDA. The fundamental period of BRB encased steel with TDA infill is about 15% higher than BRB encased steel with concrete infill. Furthermore, while computing the natural period of the structures, the effect of bracing configuration can be ignored.

The overstrength factor ranges from 1.10 to 1.52 and 1.06 to 1.51 for the BRB encased steel with TDA and Concrete infills. The prescribed overstrength factor in ASCE 7-22 and NBCC 2015 is 2.5 and 1.2. ASCE 7-22 has a conservative value that accounts for several factors, including member size, effects of structural redundancy, and infill walls (Elnashai and Di Sarno 2008). Moreover, Span length directly affects the overstrength factor, and a longer span length results in a greater overstrength factor.

The ductility factors are calculated and compared using the Miranda and Bertero (1994) and Newmark and Hall (1982) methods. It has been revealed that a longer span length and a higher

building height increase the ductility factor. The BRB encased steel with TDA infill has increased the average ductility factors by 5% compared to the BRB encased steel with concrete infill. The average ductility factor calculated using the Newmark and Hall (1982) method is approximately 15% lower than that derived using the Miranda and Bertero (1994) method. Additionally, because the variance in bracing configuration impact is less than 4%, their effect can be ignored.

The calculated mean value of RMF based on the Miranda and Bertero (1994) method for BRB encased with TDA infill is 4.97 and 4.21 for concrete infill, the computed mean value of RMF based on Newmark and Hall (1982) approach is 4.25, and 3.68 for BRB encased with TDA and concrete infills. Miranda and Bertero (1994) method achieves a better result than Newmark and Hall (1982) method because they consider more parameters such as soil condition, ductility, and the natural period of the structure. The response modification factor increases as the building height and span length increase. The response modification factor for BRB encased with TDA and concrete infills was in the range of 3.15 to 5.56, with a mean value minus standard deviation of about 4 in both cases. Accordingly, ASCE 7-22 and NBCC 2015 specified response modification values of 8 and 4.8 for BRBFs. As a result, for structures with a height equal to or less than 50m, a response modification factor of 4 is recommended, which covers about 95 percent of the cases. It is evident that different bracing configurations range from 5% to 12%; hence their effect shall be addressed.

The maximum drift demand of nonlinear response history analysis increases with the height. For four-story BRBFs, the maximum mean value of interstory demand was exhibited in the third level, while it is shifted to the fourth and tenth level for eight and fourteen-story. It can be observed the higher height of the structure move the maximum interstory drifts to a higher level, and the longer span length increases the story drift ratios. Interstory demands are higher for BRB encased steel with TDA infill than BRB encased steel with concrete infill.

Base shear demands increase with larger span length and height and vary with different framing configurations. Furthermore, compared to concrete infill, the base shear demands for BRB encased steel with TDA infill are reduced in shorter span lengths and higher in longer span lengths.

Further numerical and experimental studies are required to evaluate the effects of BRBFs with TDA filling in SCMF using different mechanical properties of Tire-Derived Light Weight

Aggregate Concrete (TDLWAC) to evaluate their seismic parameters and performance under real excitations.

4.3 Numerical investigation of the seismic performance of an innovative type of buckling restrained brace (BRB)

4.3.1 Introduction

Buckling Restrained Braced Frames (BRBF) could be an alternative to conventional braced frames due to their poor performance during past earthquakes, including buckling failure, limited ductility, fraction in connections, and unsymmetrical hysteresis behavior. A typical BRBF, consisting of a ductile steel core embedded in concrete and encased concrete with steel tube, attempts to avoid brittle failure modes. The steel core provides the required yielding mechanism while the tube prevents buckling of the core, increasing the ductility of the system. Modified concrete using waste tire chip has lower strength and stiffness yet high toughness. When its strength is too low, it is impossible to use waste tire rubber-filled concrete for construction purposes. The possible increase in strength and stiffness with a reduced cost by using waste tires in the form of fibers instead of chips was studied (Li et al. 2004).

In this section, the application of an innovative single-leg BRB with TDA and with concrete infill is verified against the experimental tests performed at the Structures Laboratory of California State University (CSU), Fresno (Pathan et al. 2021). Based on the experimental tests, four models for BRB with TDA filling and with concrete filling are developed utilizing ETABS and OpenSees software. The evaluations include the modeling of a full-scale experimental frame equipped with a single leg buckling restrained brace with TDA and concrete infills. The models are subjected to artificial loadings such as harmonic, periodic, and impulse loadings, as well as different ground motion loadings. The results compare experimental and analytical studies, including acceleration, displacement, stiffness, damping ratios, as well as hysteretic behaviour of BRB with TDA and with concrete infill. Furthermore, a design guideline for buckling restricted brace frames with TDA filling is provided.

4.3.2 Tire-Derived Aggregate (TDA)

Mechanical properties of TDA and concrete were conducted using six cylindrical specimens (0.1m × 0.2 m) as per ASTM C39 and C78 and ASTM C496 (Tehrani et al. 2020). Compression and split tensile tests were carried out using the 500 kN "Tinius Olsen universal testing" rig as presented in Figure 4-26. The loads for the compression test were applied at a rate of 0.24 MPa per second and a rate of 48.9 kN per second for the tensile test, respectively.

Figure 4-26. compression and tensile tests of TDA and concrete (Tehrani et al. 2020)

The results of compression and tensile strength tests for TDA and concrete are presented in Table 4-9.

Table 4-9. Cylinder test results for concrete and TDA (Tehrani et al. 2020)

Cylinder testing	**Compression Strength (MPA)**	**Tensile strength (kN)**
Concrete	34.6	11.2
TDA	10.6	0.36

4.3.3 Buckling Restrained Braces

Buckling restrained braces frames (BRBF) can be categorized as one of the new types of seismic force-resisting systems; single-leg and concentratedly braced frames are the two most common bracing configurations. Although BRBF is comparable to conventional CBF in geometric arrangement, there are apparent differences, including the connections, members, hysteresis behavior, and ductility. BRBFs consist of ductile steel core in concrete or mortar encased with a

steel tube, and the steel core dissipates energy through regular tension-compression yield cycles, providing the yielding mechanism as presented in Figure 4-27. Bracing elements limit the buckling of the steel core to achieve this behavior (Kersting et al. 2015; ANSI/AISC 341-16).

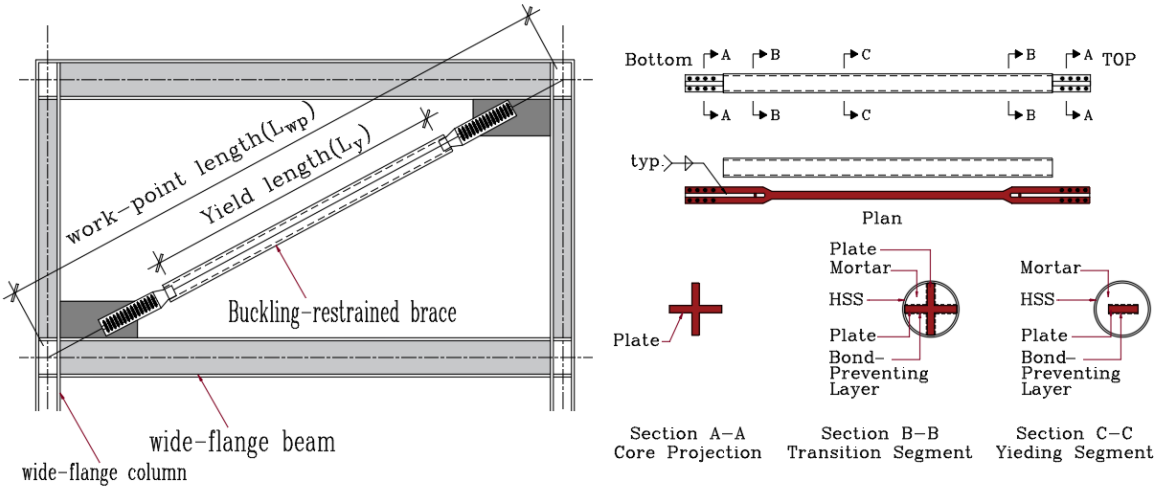

Figure 4-27. Single leg buckling restrained bracing and details (Kersting et al. 2016; ANSI/AISC 341-16)

The main objective of this research is to demonstrate the effectiveness of TDA as a filling material compared to conventional concrete filling. Details of the experimental buckling restrained brace, having 7'-7.0" (2.31 m) effective and a total length of 8'-3.0" (2.51 m), and the cross section of the buckling restrained brace (3.4 in (8.64 cm) × 4.6 in (11.68 cm)), are presented in Figure 4-28. The steel core cross-section, an A36 plate, measures 2.45 in × 0.125 in (6.23 cm × 0.32 cm), which is designed to resist a lateral load of 27.7 kN (6.24 Kips).

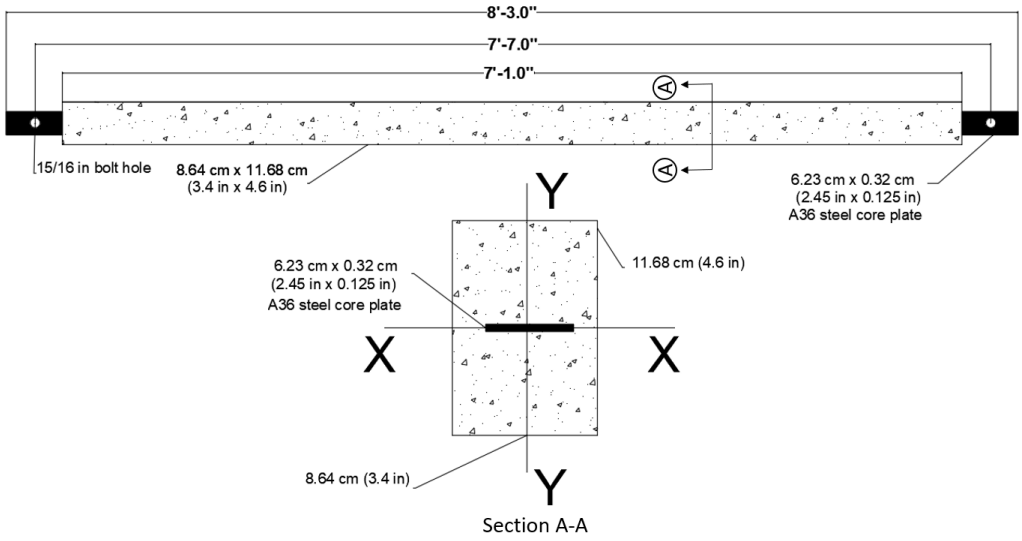

Figure 4-28. The experimental model of Buckling Restrained Brace (Tehrani et.al. 2020)

Initial stiffness (K_{in}) of the buckling restrained brace for both TDA and concrete fillings are calculated based on Equation 4.2 using experimental results, in which A_{sc} is the steel core, E is the modulus of elasticity, L_{wp} is the work point length, which can be predicated on the assumption of minor angle changes, in which the axial deformation, Δ_{bx}, is equal to drift angle, q_x, multiplied by work point length, L_{wp}, and sin(2α), where α is the BRB angle. Next, the yield length ratio may be computed by dividing the yielding region length, L_y, by the work point length L_{wp}. Initial stiffness is calculated based on the modulus elasticity of the steel core (A36), and for both BRB with TDA and concrete fillings is 12,478.65 kN/m (71.255 kip/in).

$$k_{in} = \frac{A_{sc}E}{L_{wp}} \tag{4.2}$$

4.3.4 Experimental setup

The setup consists of one bay in the X direction with a 2.02m (6.6 feet) span length and two bays in the Y direction; each has a span length of 0.762 m (2.5 feet), the height of the frame is 2.44 m (8 feet). W6×9 and W6×15 (A992) are used for columns and beams. Two concrete blocks were installed on the top of the frame, with each block weighing 1035 Kg. The lateral translation was controlled by two wires with a capacity of 4.4 kN (1 Kips), and the shake table is 2.44 m × 2.06 m (8 ft × 6.75 ft) in X and Y directions as presented in Figure 4-29.

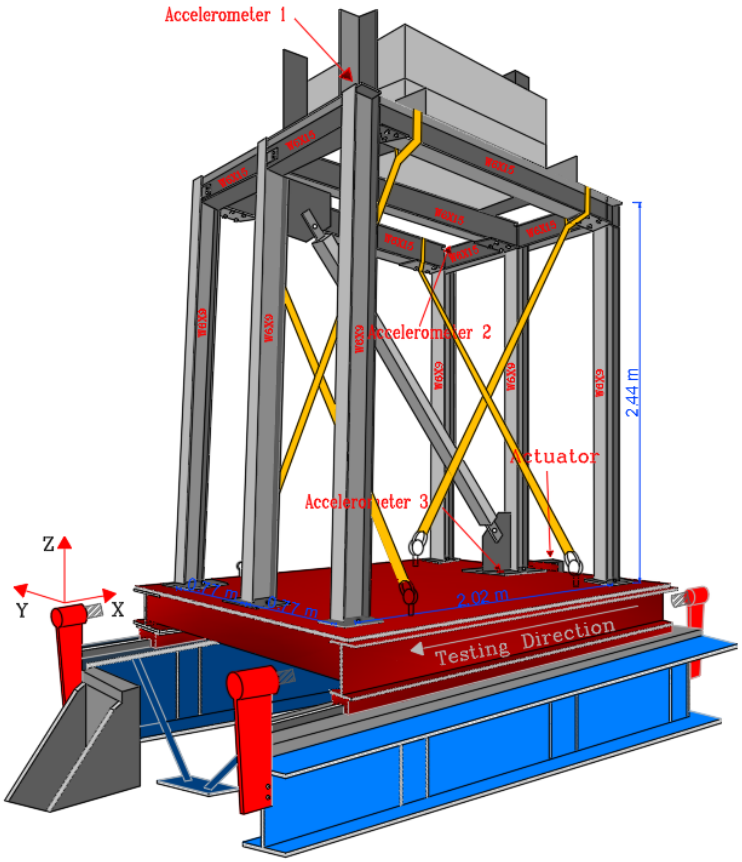

Figure 4-29. A 3-D view of the frame (based on Pathan, 2021)

Three accelerometers were used to measure the vibrations of the frame. These instruments were installed on the North-East, South-West, and base of the frame as shown in Figure 4-30.

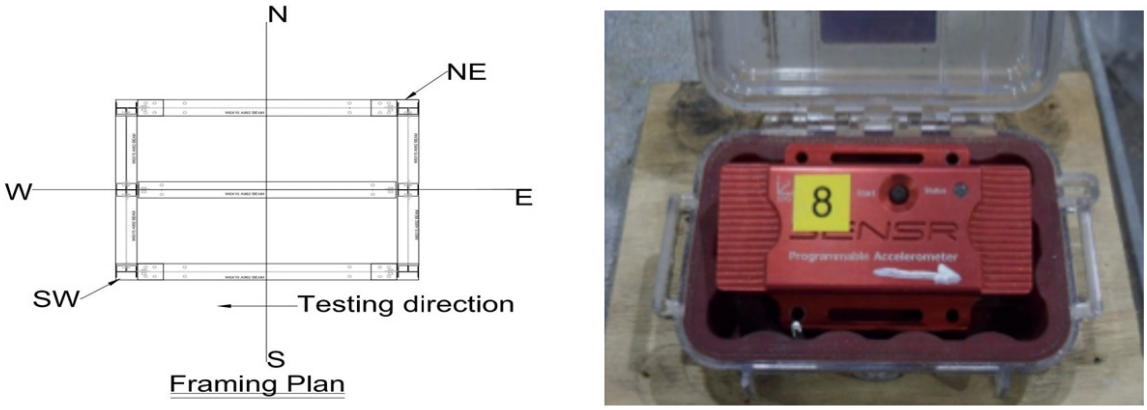

Figure 4-30. Accelerometer's installation (Pathan, 2021)

4.3.5 Simulation of experimental and analytical work

4.3.5.1 Introduction

In this section four models are created based on the experimental tests, the study parameters are including acceleration, displacement, stiffness, damping ratios, and hysteretic behavior for BRB with TDA infill versus conventional concrete infill.

4.3.5.2 Displacement's history loadings

The frame was subjected to the FEMA loadings with maximum displacements of 0.80" (20.32 mm) with different time steps of 0.00625 Sec, 0.003125 Sec, 0.0125 Sec, and the maximum displacement of 1.60" (40.46 mm displacement, which is two times 20.32 mm) which is named as FEMA-2D with the time step of 0.0125 Sec, 0.2" (5 mm) sweep loading, and impulse loading as well as different scaled ground motions as presented in Figure 4-31and Figure 4-32.

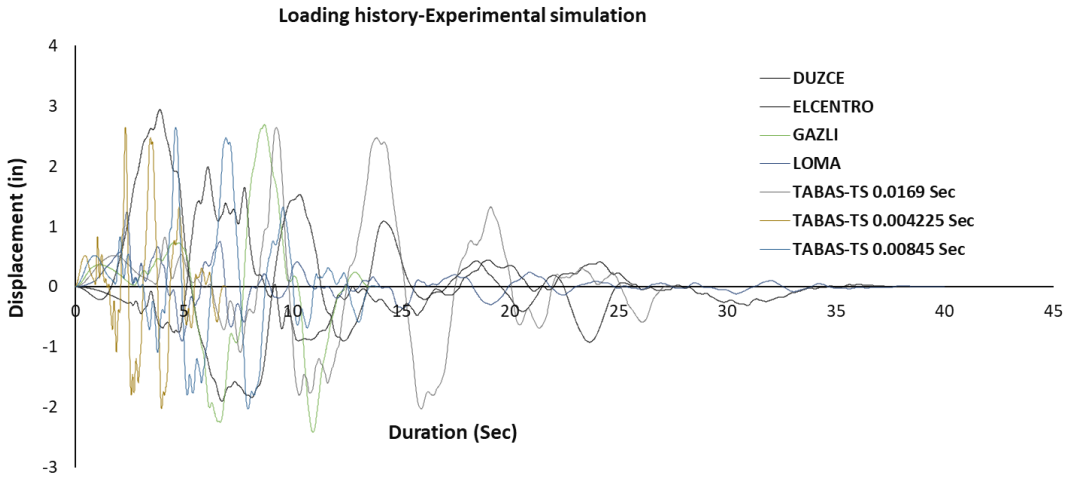

Figure 4-31. Ground motions loadings history

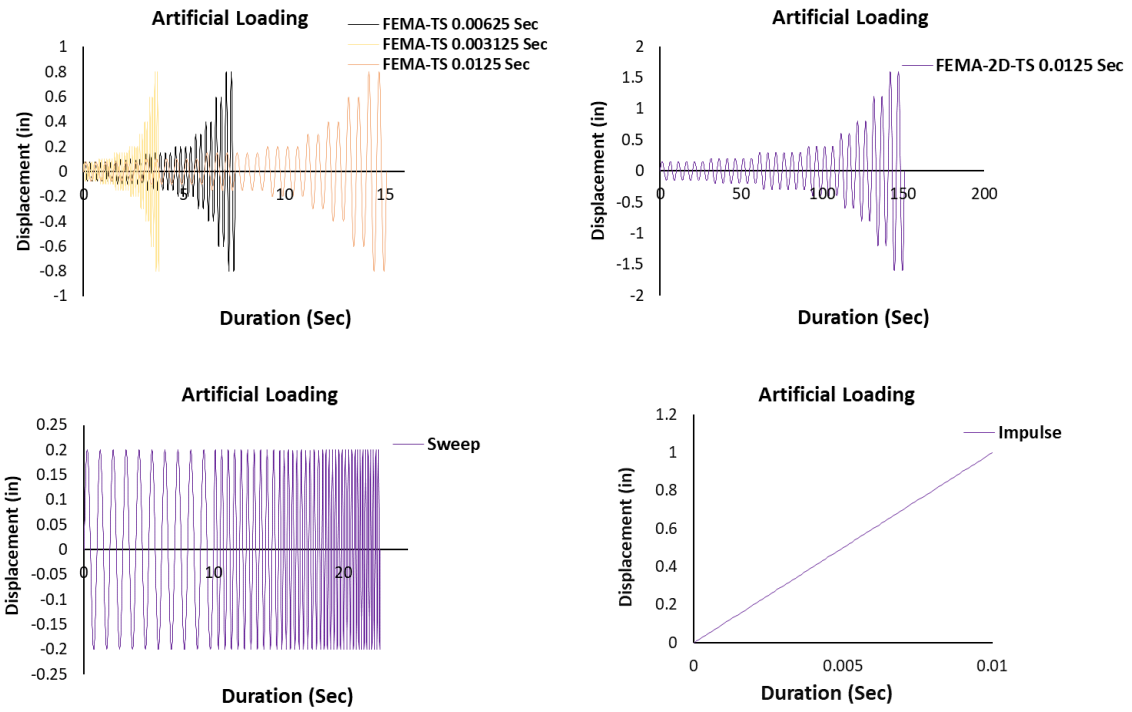

Figure 4-32. Artificial loadings history

Time steps of each loading are calculated based on the ASCE 41-17; these values are tabulated in Table 4-10.

Table 4-10. Selected time steps for acceleration and displacement

Loadings	**TS (Sec.)**	**T/100 (Sec.)**	***T_{90} (Sec.)**	**Selected TS-Acceleration (Sec.) (Min: TS, T/100, T_{90}, and 0.01_s)**	**Selected TS-Displacement (Sec.)**
DUZCE	0.0050	0.0023	0.145	0.0023	0.0050
ELCENTRO	0.0050	0.0023	0.145	0.0023	0.0050
GAZLI	0.0066	0.0023	0.145	0.0023	0.0066
LOMA	0.0050	0.0023	0.145	0.0023	0.0050
TABAS 1	0.0169	0.0023	0.145	0.0023	0.0169
TABAS 2	0.004225	0.0023	0.145	0.0023	0.0042
TABAS 3	0.00845	0.0023	0.145	0.0023	0.0084
FEMA 1	0.00625	0.0023	0.145	0.0023	0.0062
FEMA 2	0.003125	0.0023	0.145	0.0023	0.0031
FEMA 3	0.0125	0.0023	0.145	0.0023	0.0125
FEMA-2D-4	0.0125	0.0023	0.145	0.0023	0.0125
Sweep	0.0125	0.0023	0.145	0.0023	0.0125

*T is the fundamental period of the structure and T_{90} is the highest mode when T reaches at 90% of modal mass participation

4.3.5.3 Simulation of experimental model

Four numerical models are created based on the experimental tests using ETABS and OpenSees software. The existing blocks' weight is imposed as two-point loads of 2.3 kip (10.21 kN) on the central beam (2-L1&L2) and four-point loads of 1.15 kip (5.1 kN) on the outside beams (1&3-L1&L2) and demonstrated in Figure 4-33.

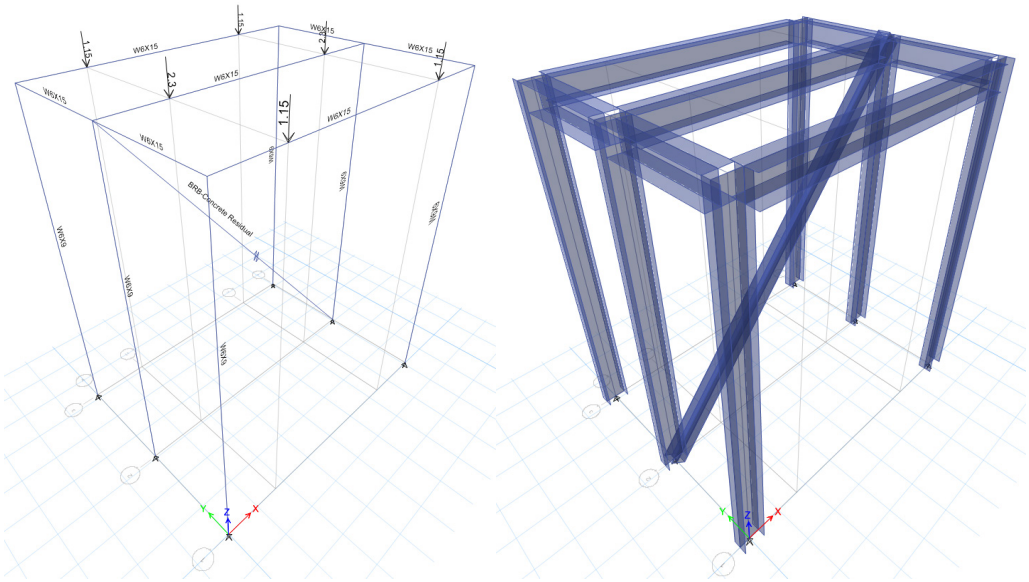

Figure 4-33. Simulation of the experimental frame using ETABS software

OpenSees is an open source and object-oriented software for earthquake engineering. The structural response can be simulated using finite element computer applications (McKenna, 1997). The simulated experimental BRB frame with TDA and concrete is presented in Figure 4-34.

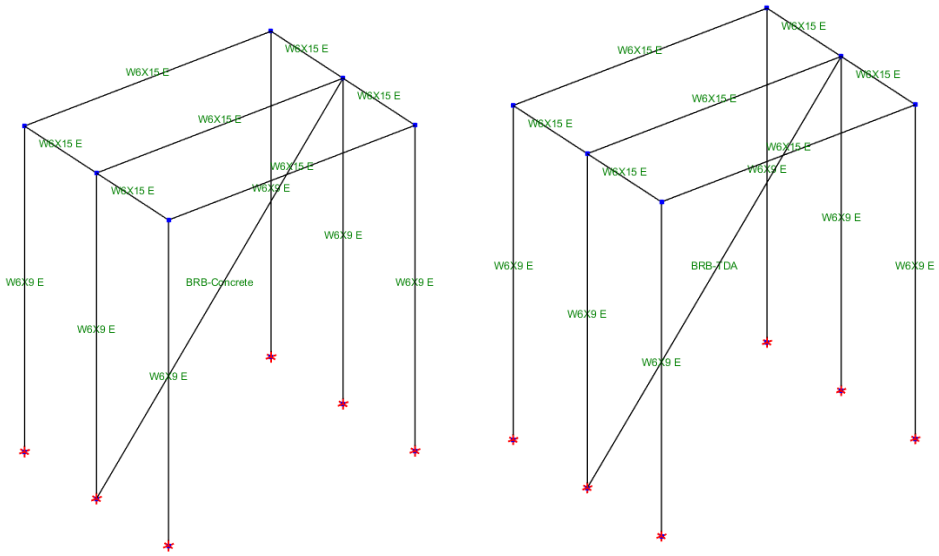

Figure 4-34. Simulation of the experimental frame using OpenSees software

The stress-strain curve was defined using the concrete material in OpenSees as presented in Figure 4-35. In this figure, fpc is the concrete compressive strength, fpsc is the concrete strain, fpcu is the concrete crushing strength, epsU is the concrete strain at the crushing point, ft is the tensile strength, and Ets is the tension softening stiffness (Yassin, 1994).

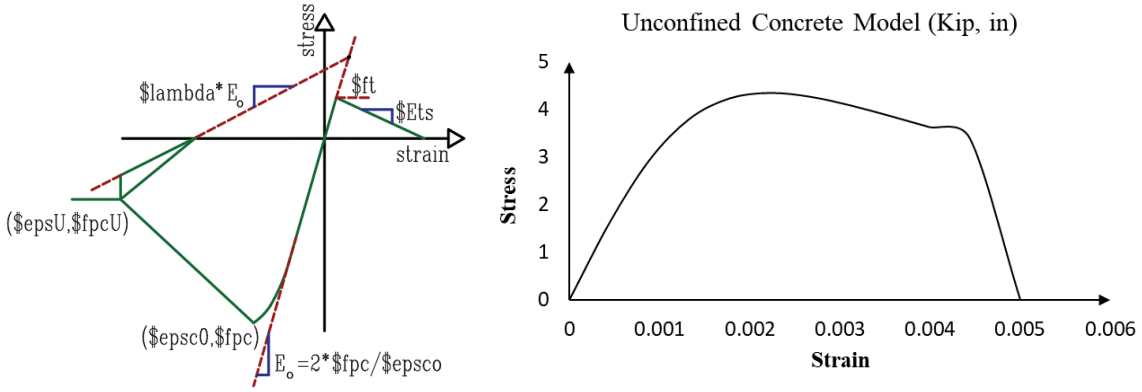

Figure 4-35. Concrete stress-strain curve (based on Yassin, 1994)

4.3.6 Results and discussions

The roof acceleration history for BRB with concrete and TDA fillings based on the experimental findings in tension, compression, and the average of tension and compression as well as the analytical results using ETABS and OpenSees software are presented in Figure 4-36 to

Figure 4-40 (conventional concrete filling) and Figure 4-41 to Figure 4-46 (TDA filling). All diagrams show a quite good agreement between experimental and analytical results. Figure 4-47and Figure 4-48 present the outcomes of the maximum roof acceleration for BRB with TDA and concrete fillings. The highest roof acceleration for BRB with concrete infill was achieved with Lomaprieta ground motion, with a maximum of 0.49 g and 0.44 g in tension and compression, respectively, and an average acceleration of 0.46 g (experimental result) and 0.42 g (simulation). The frame subjected to El Centro ground motion for BRB with concrete infill experienced a minimum acceleration of 0.24 g in tension and 0.25 g in compression, with an average acceleration of 0.245 g for the experimental study and a comparable value of 0.23 g for the analytical work. Tabas (TS-0.004225) had a maximum acceleration of 0.83 g and 0.64 g in tension and compression, respectively, an average of 0.735 g for experimental research and 0.89 g for analytical work for the BRB with TDA. Duzce was determined to have the lowest acceleration of BRB with TDA filling, with an average of 0.075 g in tension and compression for experimental and 0.08 g for analytical studies.

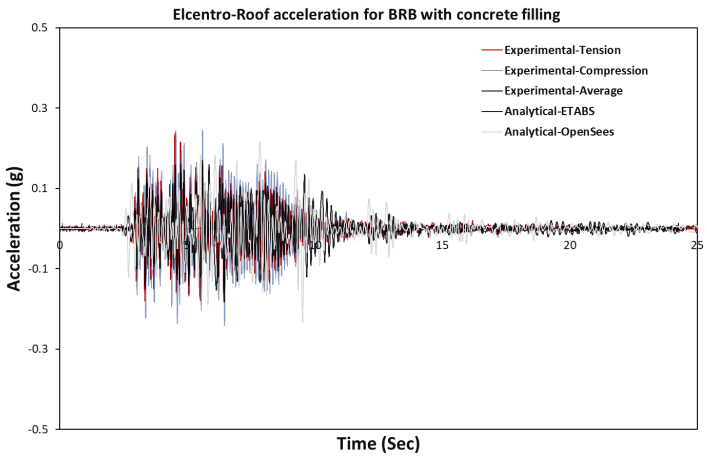

Figure 4-36. Roof acceleration for BRB with concrete filling subjected to El Centro

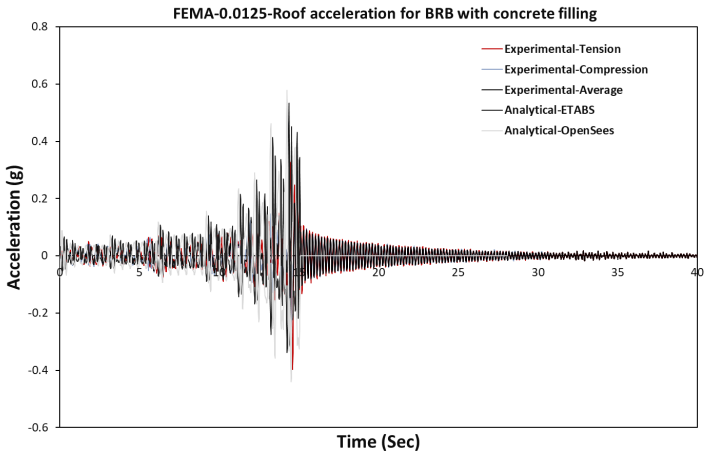

Figure 4-37. Roof acceleration for BRB with concrete filling subjected to FEMA-0.0125

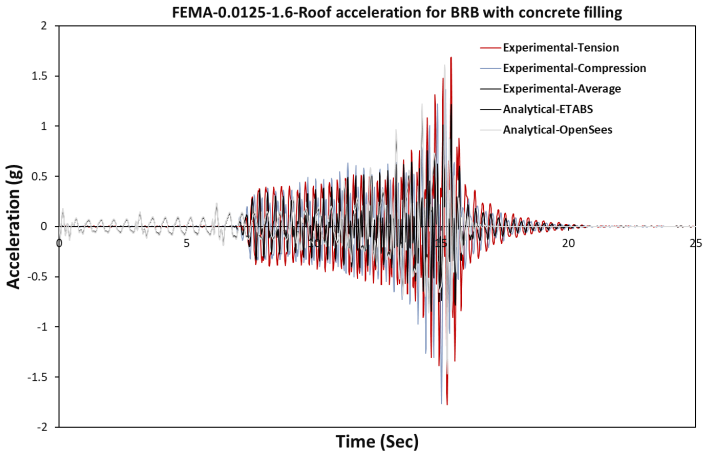

Figure 4-38. Roof acceleration for BRB with concrete filling subjected to FEMA-0.0125-1.6

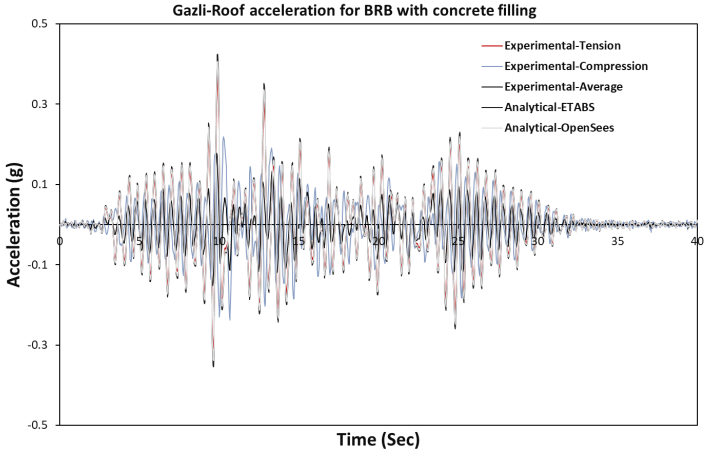

Figure 4-39. Roof acceleration for BRB with concrete filling subjected to Gazli

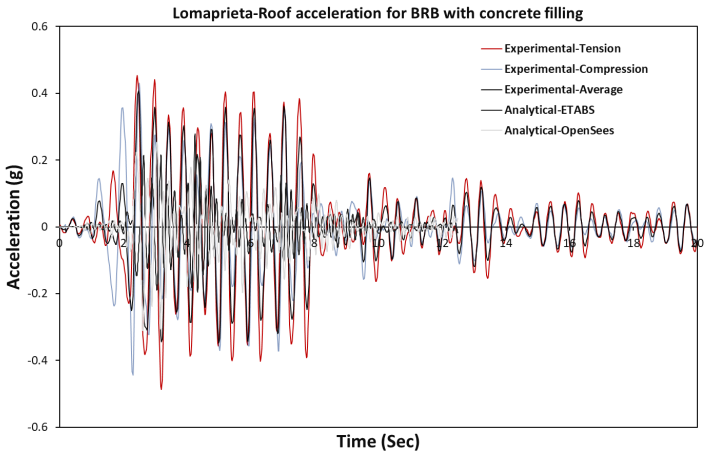

Figure 4-40. Roof acceleration for BRB with concrete filling subjected to Loma Prieta

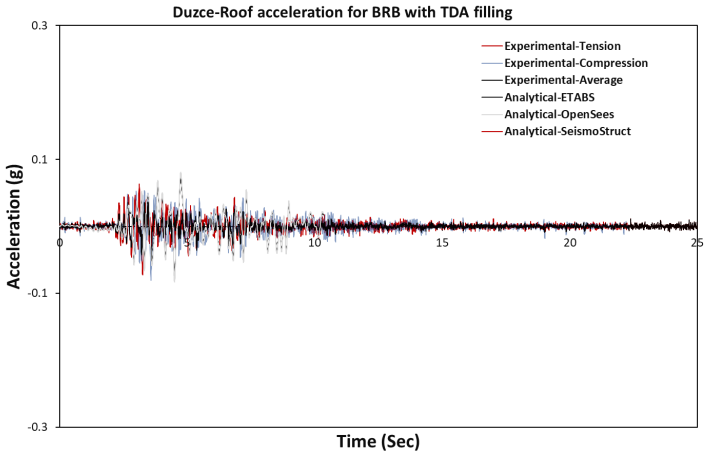

Figure 4-41. Roof acceleration for BRB with TDA filling subjected to Duzce

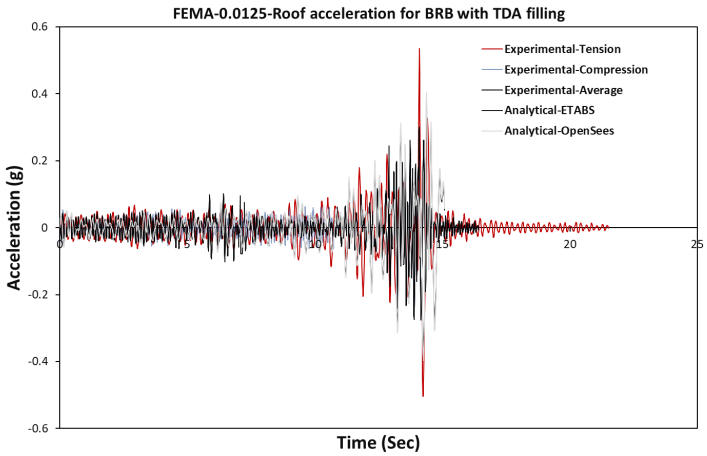

Figure 4-42. Roof acceleration for BRB with TDA filling subjected to FEMA-0.0125

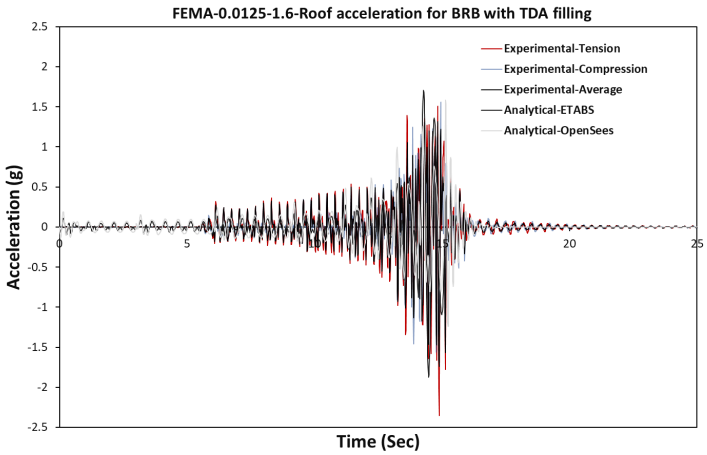

Figure 4-43. Roof acceleration for BRB with TDA filling subjected to FEMA-0.0125-1.6

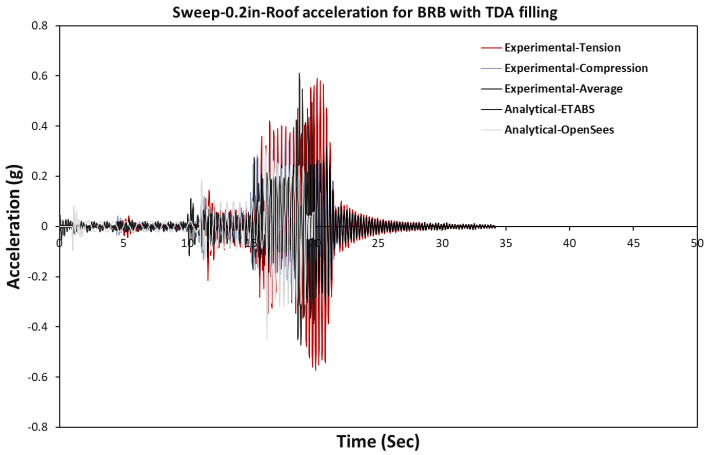

Figure 4-44. Roof acceleration for BRB with TDA filling subjected to Sweep-0.2in

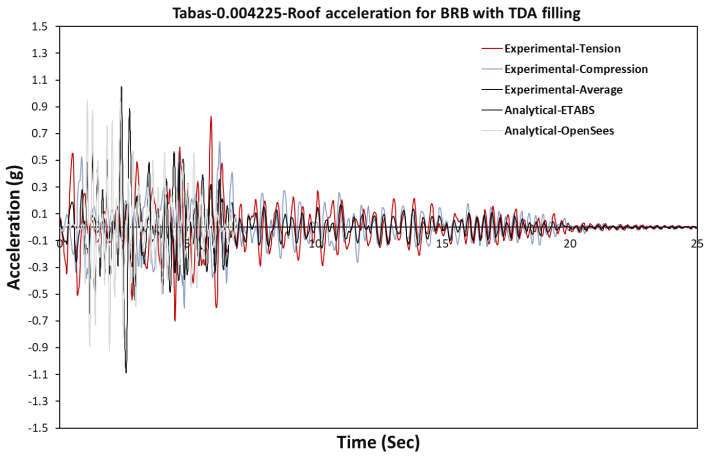

Figure 4-45. Roof acceleration for BRB with TDA filling subjected to Tabas-0.004225

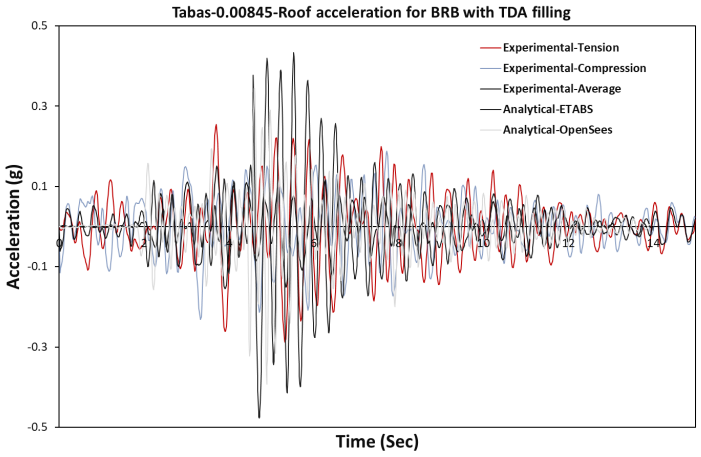

Figure 4-46. Roof acceleration for BRB with TDA filling subjected to Tabas-0.00845

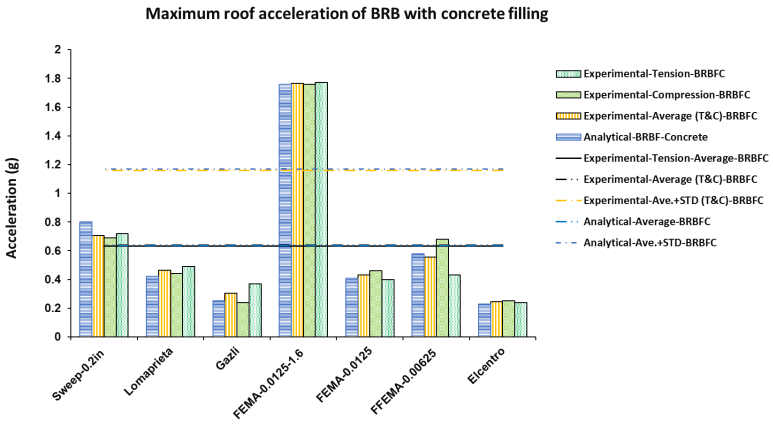

Figure 4-47. Selected maximum roof acceleration for BRB with concrete filling

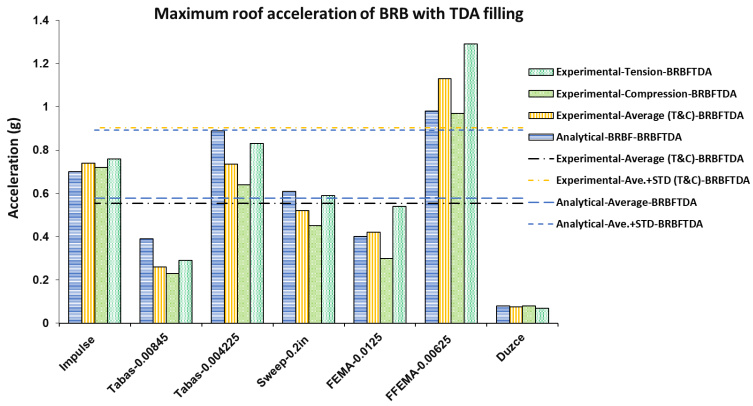

Figure 4-48. Selected maximum roof acceleration for BRB with TDA filling

Hysteresis loops of BRB with TDA and concrete infills are presented in Figure 4-49. BRB with TDA infill observed less energy than BRB with concrete infill. Based on the literature, adding rubber content in concrete mixtures causes a reduction in flexural and compression. A similar conclusion is made in experimental work due to the effects of unbinding the rubber content within concrete mixtures.

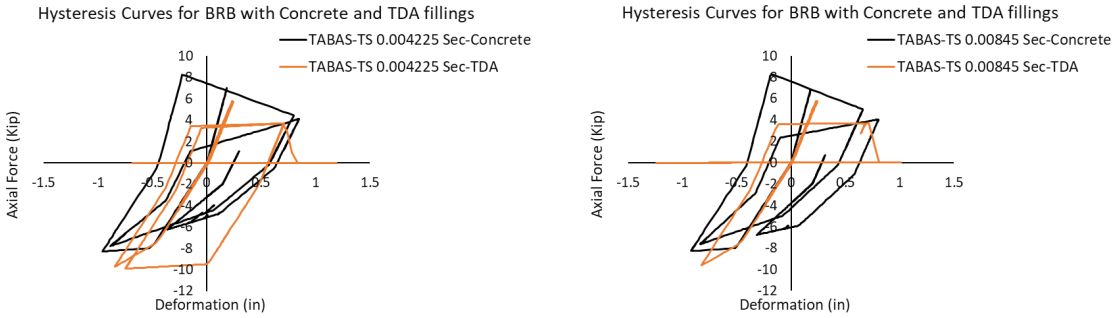

Figure 4-49. Results of hysteresis curves for BRB with TDA and concrete infills subjected to Tabas motion (TS-0.004225/0.00845)

Figure 4-50 compares the backbone curve of the analytical versus the experimental test of both BRB models with TDA and concrete fillings under FEMA 4 loading. The results of analytical and experimental results have the same trend, and it was observed that BRB with TDA filling is less ductile compared to the conventional one.

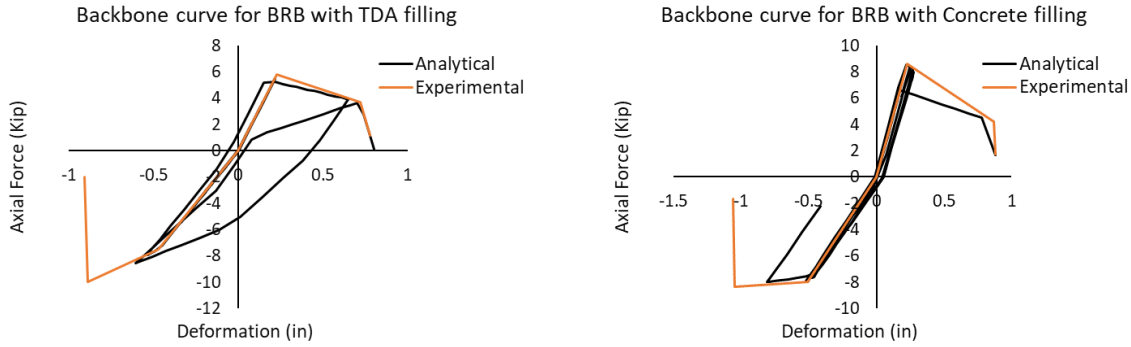

Figure 4-50. Comparison of hysteresis curves of analytical and experimental works for BRB

Maximum roof displacements of BRB with TDA and concrete infills are presented in Figure 4-51and Figure 4-52. The BRB frame equipped with concrete infill showed the maximum roof displacements of 3.08 (in) (7.82 cm) in tension and 2.97 (in) (7.54 cm) in compression under Gazli

ground motion, and the minimum roof displacements of 0.38 (in) (0.96 cm) and 0.28 (in) (0.72 cm) subjected to sweep loading. Analytical work had the highest and lowest displacement of 2.75 (in) (6.98 cm) and 0.49 (in) (1.24 cm) subjected to Gazali and sweep loading. The BRB frame with TDA under Tabas (TS-0.00845) ground motion demonstrated the maximum displacement of 2.67 (in) (6.78 cm) and 2.3 (in) (5.84 cm) in tension and compression for experimental and 2.7 (in) (6.85 cm) for analytical. The minimum roof displacement was 0.63 (in) (1.61 cm) in tension and 0.43 (in) (1.10 cm) in compression for the experimental frame and 0.7 (in) (1.77 cm) for the simulated work subjected to FEMA-0.0125 loading.

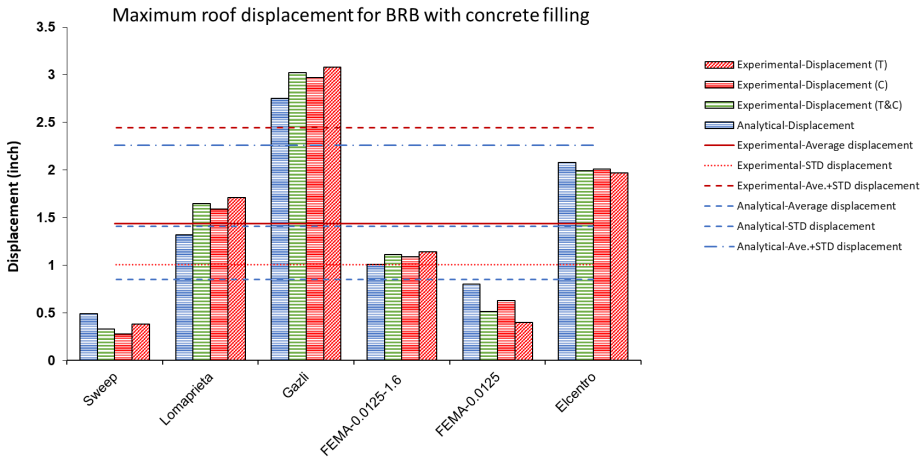

Figure 4-51. Maximum displacements for BRB with concrete filling

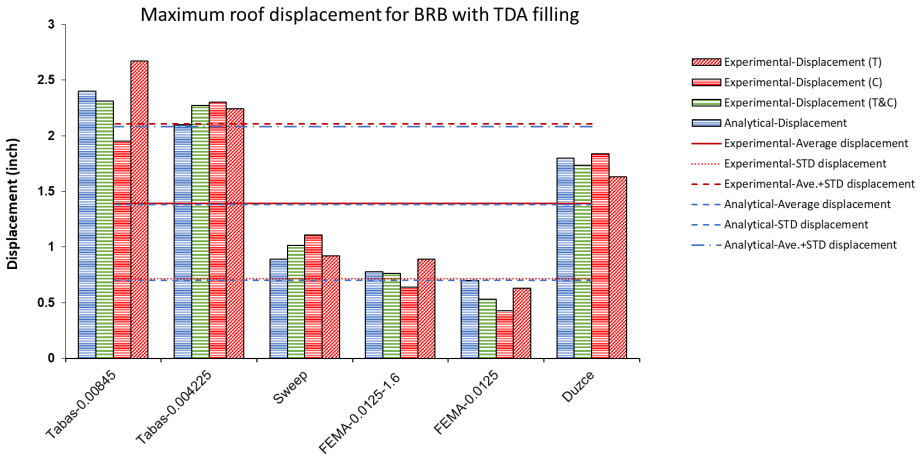

Figure 4-52. Maximum displacements for BRB with TDA filling

The effective stiffness is calculated based on 1-inch impulse loading; the damping of the system is calculated from FEMA 4 loading based on the deformation response figure. The average effective stiffness of BRB with concrete filling for experimental and analytical are 26.5 Kip/inch (4,640.8 kN/m) and 28 Kip/inch (4,903.5 kN/m). The effective stiffness was reduced to 20 Kip/inch (3,502.5 kN/m) and 21 Kip/inch (3,677.6 kN/m) for BRB with TDA filling in experimental and analytical works. The damping ratios for BRB with TDA filling increased dramatically compared with the BRB with concrete filling. These results are presented in Table 4-11. The BRB with TDA showed increased damping of about 25% compared to the conventional system.

Table 4-11. Buckling restrained brace frame damping and stiffness

Description	**Damping ratio (%)**			
	Experimental		**Analytical**	
	Tension	Compression	Tension	Compression
BRBF with TDA filling	16%	26%	25%	25%
BRBF with concrete filling	13%	17%	14%	14%
	Stiffness			
	Experimental		**Analytical**	
	Tension	Compression	Tension	Compression
BRBF with TDA filling	19(Kips/in) 3,327.4 kN/m	21(Kips/in) 3,677.6 kN/m	21(Kips/in) 3,677.6 kN/m	21(Kips/in) 3,677.6 kN/m
BRBF with concrete filling	26(Kips/in) 4,553.3 kN/m	27(Kips/in) 4,728.4 kN/m	28(Kips/in) 4,903.5 kN/m	28(Kips/in) 4,903.5 kN/m

4.3.7 Design guideline

ASCE 7 defines system design parameters and system-independent criteria, seismic hazard levels, redundancy, limitations, and irregularity conditions. AISC 341 provides design and detailing guidelines for individual members, connections, and requirements to ensure the desired ductile behavior. A BRBF system is expected to withstand significant inelastic deformation demands. Therefore, ASCE 7 has the most prominent response modification coefficient (R = 8). The following steps and design procedures are recommended for BRBF with TDA infill:

The application of ductile tire-derived lightweight aggregate concrete improves the overall performance of the system. Mechanical properties of both TDA and concrete (compressive, flexural, and splitting tensile strength, toughness, modulus of elasticity, etc.) shall be evaluated prior to the design to achieve this phenomenon. This study uses the mechanical properties of TDA,

and concrete based on the experimental tests by Tehrani and Miller (2018), and Tehrani et al. (2020).

The BRBF reduction factors depend on building height and bracing configurations. Calculating the response modification factor from pushover response curves is suggested to achieve more realistic results. However, according to the current American code, ASCE 7, BRBFs shall be designed based on the prescribed reduced reduction factor R. Then, select the appropriate load combinations.

The strength of the steel core is defined as either the actual yield stress of the steel core from a coupon test or the specified minimum yield stress of the steel core. The steel core shall be designed to resist axial forces in the brace (AISC 341).

Analysis and design of BRB and control inelastic design level of BRB strain and drift based on ASCE 7 and AISCE 41 provisions. The greater value of either $0.02 \times h_{sx}$ or $2 \times \Delta_x$ shall be considered for the expected deformation, where h_{sx} is the story height, and Δ_x is the story drift.

The forces on the BRB are afterward transferred to the connections, columns, and beams. Therefore, the design of the beams, columns, and connections should follow adjusted brace strength and remain in the elastic zone. Furthermore, all beam to column joints must guarantee the extra shear strength caused by extra forces in adjoining braces.

4.3.8 Conclusion

This investigation compares experimental and analytical works on a single-story steel frame with buckling restrained brace infill with TDA and concrete. The effectiveness of tire-derived aggregates (TDA) as an alternative material was presented. From the study, the following main conclusions can be drawn:

Analytical and experimental investigations on buckling restrained braces with TDA infill demonstrate an increase in frame damping of around 25% compared to conventional a damping rate of some 14%. When a system requires more damping, both experimental and analytical works suggest using BRB with TDA infill.

BRB with TDA filling, in general, reduced acceleration by about 20% compared to conventional concrete filling. In the experimental research, the average plus standard deviation acceleration values for BRB with concrete and TDA fillings were 1.15 g and 0.91g, respectively, and 1.16 g and 0.89g in the analytical study.

The average plus standard deviation of the displacement of the frame with BRB with concrete infill was 2.44 (in) (6.20 cm) for experimental and 2.26 (in) (5.74 cm) for analytical studies, respectively. For experimental and analytical research, these values for BRB with TDA infill were changed to 2.10 (in) (5.33 cm) and 2.08 (in) (5.28 cm). As a result, the frame equipped with BRB with TDA filling has less ductility versus BRB with conventional concrete filling.

Comparison of hysteresis curves of analytical and experimental works exhibited almost the same trend in their backbone curves for BRB with TDA and concrete infills subjected to FFEMA 4 loading. It was also determined that the amount of energy absorbed by BRB with TDA infill is smaller than that recorded by BRB with concrete infill, implying that BRB with TDA infill has less ductility than conventional concrete.

More experimental tests and numerical analyses are required in the future to determine the effect of BRB with TDAFRC infill on the system performance, which may improve ductility by adding fibers.

CHAPTER 5

Summary, Conclusions, and Recommendations for Future Work

5.1 Summary

The purpose of this thesis is to investigate the effectiveness of an innovative type of buckling restrained brace with TDA infill. Based on the literature review and to the best of the author's knowledge, the effects of BRB with TDA infill on structural performance have not been previously addressed, numerically and experimentally. Furthermore, waste tiers have become a major problem both locally and worldwide; nevertheless, employing waste materials such as TDA may contribute to sustainability by lowering CO_2 emissions and embodied energy. This research provides numerical and experimental evidence on the structural response equipped with BRB with TDA infill and with conventional concrete infill which helps to enrich the knowledge in this area.

The seismic design factors of four-, eight- and 14-story special reinforced concrete moment frames equipped with buckling restrained braces encased steel with TDA infill and with conventional concrete infill are evaluated and discussed in terms of the effect of different heights, span length, and bracing configurations. The results covered a comparison between the innovative BRB and the conventional BRB including response modification, overstrength, and ductility factors. Furthermore, inelastic response history analysis was performed to evaluate the performance of BRBF using available experimental stress-strain characteristics of tire-derived lightweight aggregate concrete as an alternative material. The numerical studies included the followings:

- Mechanical properties of Tire-Derived Light Weight Aggregate Concrete (TDLWAC) were determined using 38 cylindrical and 36 beam specimens (Tehrani et al. 2020), these mechanical properties as an alternative damping property are used to model an innovative type of BRB encased steel composite containing TDA.
- ASCE /SEI 7-22 and ACI 318-19 are used for the design of four-, eight-, and 14-story special concrete moment frames.
- The effects of building height, span length as well as bracing configurations including Single-Leg Braces (SLB), Chevron Inverted V Braces (CIVB), Chevron V Braces

(CVB) and Split X braces (SXB) for BRB encased steel with TDA and with conventional concrete infill are investigated. Forty-eight models are created based on the four-, eight-, and 14-story special concrete moment frames equipped with BRB encased steel with TDA and with concrete infills (Twenty-four models in each category).

- Modal analysis and nonlinear static analysis are performed, and yield strength, as well as design strength, are calculated to determine the overstrength factor of each model.
- Ductility and ductility reduction factors are calculated based on Miranda and Bertero (1994) and Newmark and Hall (1982) methods, using fundamental period, yield displacement, and maximum displacement.
- Inelastic response history analysis is performed to verify the overall performance of the BRBFs.
- Twenty-one different earthquake records including subduction records are selected based on the MCE_R target response spectrum from the Pacific Earthquake Engineering Research Center (PEER) database. The accelerograms were scaled using the applicable tool in SeismoMatch 2018 software based on the maximum consider earthquake response spectrum (MCE_R), and within the recommended period range of 0.2T to 2.0T.
- A compression is made between BRB encased steel with TDA infill and BRB encased steel with concrete infill.

The collaborated experimental test was performed at the Structures Laboratory of California State University (CSU), Fresno (Pathan et al. 2021). The collaborated experimental test was performed using a shake table with the dimension of 2.44 m × 2.06 m (8 ft × 6.75 ft). The experimental frame consists of one bay in X direction with a 2.02m (6.6 feet) span length and two bays in Y direction each has a span length of 0.762 m (2.5 feet), the height of the frame is 2.44 m (8 feet). Two concrete blocks with a total weight of 2070 Kg were installed on top of the frame. The frame is subjected to harmonic, periodic, impulse, and ground motion excitations. The response of six large-scale buckling restrained braces with TDA infill and with conventional concrete infills for a one-story steel frame were evaluated experimentally on a shake table. Then the application of an innovative BRB with TDA and with concrete infills was verified numerically and compared with the experimental test. For this purpose, four models were developed utilizing ETABS and OpenSees software, and the results examined acceleration, displacement, stiffness,

damping ratios, as well as the hysteretic behaviour of BRB with TDA and with concrete infill to evaluate the effectiveness of the proposed model. Additionally, a design guideline for BRBFs with TDA filling is provided. The following procedures were incorporated in the collaborative experimental test and numerical simulation:

- Compression and split tensile tests are conducted using 6 cylindrical specimens as per ASTM C39 and C78 and ASTM C496 to evaluate the mechanical properties of TDA and Concrete (Tehrani et al. 2020).
- The effective and total lengths of the buckling restrained brace are 2.31 m (7'-7.0") and 2.51 m (8'-3.0"), respectively. Buckling load and predicted buckling load are computed using the effective length of the brace. The steel core cross-section is 1.99 cm^2 (0.304 in^2), which is calculated to resist the lateral load of 27.7 kN (6.24 Kips).
- Using the compression and split tensile tests of TDA and concrete, three BRBs with TDA filling and three BRBs with concrete filling were constructed. The experimental frame was equipped with each BRB at a time and was subjected to FEMA loadings with maximum displacements of 20.32 mm (0.80") with different time steps of 0.00625 Sec, 0.003125 Sec, 0.0125 Sec, and the maximum displacement of 40.46 mm (1.60" displacement) which is named as FEMA-2D with the time step of 0.0125 Sec, 5 mm (0.2") increasing frequency sweep loading as well as the ground motions namely as El-Centro, Loma Prieta, Tabas, Gazli, and Duzce. Vibration signals of the frame are measured by three accelerometers.
- From the hysteresis curves of BRB with TDA and conventional concrete filing subjected to cycling loading, the ductility and toughness are determined. The strength adjustment factors ω and ωβ are calculated from the backbone curve.
- Seismospect is used to calculate the response spectrum, final damping ratios are calculated in tension and compression for BRBs with TDA and with concrete fillings, and finally, the debonding and failure mode of each six BRBs are discussed.
- ETABS and OpenSees software are used to simulate the experimental tests, discussion covers a comparison of acceleration, displacement, drift, stiffness, damping ratios, as well as the hysteretic behaviour of BRB with TDA infill and with conventional concrete infill.

5.2 Conclusions

The following conclusions are based on the analytical study of seismic design factors for concrete moment structures equipped with Innovative Buckling Restrained Braces (IBRB), as well as a numerical investigation of an innovative type of BRB with TDA and with concrete infills based on the collaborated experimental test.

5.2.1 Analytical study of seismic design factors and a performance evaluation of CMRF with BRB

- The empirical equation for the determination of the fundamental period of the structure is more conservative than the eigenvalue analysis for BRB encased steel with TDA infill. Overall, the substitution of conventional concrete infill with TDA concrete infill in BRB encased steel increases the fundamental period of the structure.
- The bracing configuration has a negligible effect on the fundamental period of analytical models.
- The calculated overstrength factors based on the pushover analysis had a range from 1.10 to 1.52 for BRB encased steel with TDA, which was very close to a similar range of 1.06 to 1.51 for BRB encased steel with concrete. ASCE 7-22 and NBCC 2015 prescribed the overstrength factor of 2.5 and 1.2. These conservative values account for member size, structural redundancy, and the effects of infill walls.
- The ductility is determined using two different methods based on Miranda and Bertero (1994) and Nemark and Hall (1982). The longer span length and higher building height increased the ductility factor.
- The BRBs encased steel with TDA and concrete infills have higher ductility results using Miranda and Bertero (1994) method compared to Nemark and Hall (1982) method. Miranda and Bertero (1994) method considers more parameters, including ductility and fundamental period, as well as soil type; and thus, provides more insightful results, hence this method is recommended to calculate ductility and response modification factor.
- The average ductility factor calculated for BRBs encased steel with TDA infill has increased by an average of 5% compared to conventional BRBs. Furthermore, the effect

of bracing configurations might be ignored as their impact on the ductility factor is below 4%.

- The mean response modification factor for BRBs encased steel with TDA infill is 4.97 and 4.21 for BRBs encased steel with conventional concrete infill. In all cases, the response modification factor for BRB encased steel with TDA and with concrete infills was in the range of 3.15 to 5.56, with a mean value minus standard deviation of about 4. ASCE 7-22 and NBCC 2015 recommend the response modification factor of 8 and 4.8 for BRBFs, respectively. In this study, the response modification factor of 4 is proposed for structures with a height equal to or less than 50 m. Moreover, the effects of bracing configuration had a range of 5% to 12% on RMF and should be considered for calculating the response modification factor.
- Nonlinear response history analysis showed the height of the structure increases the ductility demand. For eight- and fourteen-story buildings, the maximum story drift was at the fourth and tenth levels, respectively, whereas the four-story building experienced the maximum interstory demand at the third level. In general, the interstory demand for BRB encased steel with TDA infill is higher compared to the conventional BRB.
- Span length, height, and various brace configurations have a direct effect on the base shear demands. The base shear increases by span length and height and varies with different brace configurations. It was observed that the base shear demands are reduced in the BRBFs encased steel with TDA compared to the conventional BRBFs.

5.2.2 Numerical investigation of the experimental frame

The effectiveness of BRB with TDA filling versus conventional BRB was examined both analytically and experimentally, generating the following results:

- Buckling restrained brace with TDA infill increases the damping of the system by about 25% compared to the conventional BRB. Therefore, both experimental and analytical works recommend using BRB with TDA when increasing the damping of the system is required.
- The average plus standard deviation acceleration values for BRB with TDA and conventional concrete fillings in the experimental research were 0.91g and 1.15g,

respectively, while the analytical investigations showed similar values of 0.89g and 1.16g.

- The mean+ STDEVA values of the maximum displacements of BRB with TDA infill are lower than the BRB with concrete infill; these results are consistent with experimental tests. As a result, as compared to BRB with concrete filling, the frame equipped with BRB with TDA filling has lower ductility.
- The hysteresis behavior indicated the BRB with TDA infill is less ductile and observed less energy than the BRB with concrete infill.
- The backbone curve of Experimental and analytical is calculated based on the FEMA 4 loading, the results indicated a very good agreement between experimental and analytical works for BRB with TDA and with concrete fillings.

5.3 Recommendations for Future Research

It is crucial to find different applications for utilizing scrap tiers that cause considerable environmental damage on a large scale (Tehrani et al. 2019). This research introduced another application for the reuse of TDA in buckling restrained braces which contributes to sustainability. They can be used in retrofit of new as well as existing structures where the primary concern is the damping of the system. Further numerical and experimental studies are required to examine the effects of BRBFs with TDA filling in special CMRF employing different mechanical characteristics of Tire-Derived Light Weight Aggregate Concrete (TDLWAC) to evaluate their seismic parameters and performance under actual seismic ground motions. Additional experimental tests and numerical studies are required to assess the ductility of BRB with TDAFRC infill by adding fibers.

References

ACI 130. (2019). “Report on the Role of Materials in Sustainable Concrete Construction.” Reported by ACI Committee 130.

ACI 318-19. (2019). “Building Code Requirements for Structural Concrete and Commentary.” ACI Committee 318.

Ahn, I.S., Cheng, L., Fox, P.J., Wright, J., Patenaude, S., Fujii, B. (2015). “Material Properties of Large-Size Tire Derived Aggregate for Civil Engineering Applications.” Journal of Materials in Civil Engineering, Vol. 27, No. 9, pp.04014258-11. https://doi.org/10.1061/(ASCE)MT.1943-5533.0001225.

Aiello, M.A., Leuzzi, F. (2010). “Waste tyre rubberized concrete: Properties at fresh and hardened state.” Waste Management, 30, 1696–1704. https://doi.org/10.1016/j.wasman.2010.02.005.

Alam, M.S., Moni, M., and Tesfamariam, S. (2012). “Seismic overstrength and ductility of concrete buildings reinforced with superelastic shape memory alloy rebar.” Engineering Structures, 34, 8–20.

Al-Tayeb, M.M., Abu Bakar, B.H., Akil, H.M., Ismail, H. (2013). “Performance of Rubberized and Hybrid Rubberized Concrete Structures under Static and Impact Load Conditions.” Experimental Mechanics, Vol. 53, No. 3, pp.377–384. https://doi.org/10.1007/s11340-012-9651-z.

ANSI/AISC 341-16. (2016). “Seismic Provisions for Structural Steel Buildings.” American Institute of Steel Construction, Chicago, Illinois 60601.

ANSI/AISC 360-05. (2005). “Specification for Structural Steel Buildings, American Institute of Steel Construction.” Chicago, Illinois 60601.

Arias, A. (1970). “A measure of earthquake intensity, In Seismic Design for Nuclear Power Plants.” R. Hansen, Ed., MIT Press, Cambridge, MA, USA, pp. 438-483.

ASCE/SEI 41-17. (2017). “Seismic evaluation and retrofit of existing buildings.” American Society of Civil Engineers, Reston, Virginia.

ASCE/SEI 41–17. (2017). “Seismic evaluation and retrofit of existing buildings.” American Society of Civil Engineers, Reston, Virginia, USA.

ASCE/SEI 7-05. (2005). “Minimum Design Loads for Buildings and Other Structures.” American Society of Civil Engineers.

ASCE/SEI 7-10. (2010). “Minimum Design Loads for Buildings and Other Structures.” American Society of Civil Engineers.

ASCE/SEI 7-16. (2016). “Minimum Design Loads for Buildings and Other Structures.” American Society of Civil Engineers.

ASCE/SEI 7-22. (2022). “Minimum Design Loads and Associated Criteria for Buildings and Other Structures.” American Society of Civil Engineers, ASCE standard.

Asgarian, B., Shokrgozar, H.R. (2009). “BRBF response modification factor.” Journal of Constructional Steel Research 2009; 65:290–8, https://doi.org/10.1016/j.jcsr.2008.08.002.

Aslani, F. (2016). “Mechanical Properties of Waste Tire Rubber Concrete.” Journal of Materials in Civil Engineering, Vol. 28, No. 3, 2016, pp. 04015152-14. https://doi.org/10.1061/(ASCE)MT.1943-5533.0001429.

ASTM C39. (2015). “Standard Test Method for Compressive Strength of Cylindrical Concrete Specimens.” ASTM International, www.astm.org.

ASTM C469. (2021). “Standard Test Method for Static Modulus of Elasticity and Poisson's Ratio of Concrete in Compression.” https://www.astm.org/c0469_c0469m-14e01.html.

ASTM C78. (2018). “Standard Test Method for Flexural Strength of Concrete.” West Conshohocken, PA, USA.

ASTM D6270. (2008). “Standard Practice for Use of Scrap Tires in Civil Engineering Applications.” https://www.astm.org/d6270-08.html.

Atahan, A.O, Yücel, A.Ö. (2012). “Crumb rubber in concrete: Static and dynamic evaluation.” Construction and Building Materials, 36:617–622. https://doi.org/10.1016/j.conbuildmat.2012.04.068.

Atahan, A.O., Sevim, U.K. (2008). “Testing and comparison of concrete barriers containing shredded waste tire chips.” Materials Letters, 62:3754–3757. https://doi.org/10.1016/j.matlet.2008.04.068.

ATC 3-06. (1982). “Tentative provisions for the development of seismic regulations for buildings.” ATC publication, V.Series, United States. National Bureau of Standards. Special publication, 510.

ATC 40. (1996). “Seismic Evaluation and Retrofit of Concrete Buildings.” Volume 1, ATC-40 Report, Applied Technology Council, Redwood City, California.

ATC 58-1. (2003). “Sponsored workshop on communicating earthquake risk.” Applied Technology Council, www.ATCouncil.org.

ATC 72-1. (2019). “Nonlinear modeling of tall buildings, Pacific Earthquake Engineering Research Center.” https://peer.berkeley.edu/peeratc-72-1-report-released-about-nonlinear-modeling-tall-buildings.

ATC-19. (1995). “Structural response modification factors.” Applied Technology Council, Redwood city, California.

ATC-34. (1995). “A critical review of current approaches to earthquake-resistant design.” Applied Technology Council, NCEER Project No. 92-4601.

Atkinson, G.M., Adams J. (2013). “Ground motion prediction equations for application to the 2015 Canadian national seismic hazard maps.” Can. J. Civ. Eng. 40, 988- 998.

AZOCleantech. (2021). “Tackling the Global Tire Waste Problem with Pretred.” https://www.azocleantech.com/article.aspx?ArticleID=1227.

Bai, J., Ou, J. (2016). “Earthquake-resistant design of buckling-restrained braced RC moment frames using performance-based plastic design method.” Engineering Structures, 107:66–79. https://doi.org/10.1016/j.engstruct.2015.10.048.

Baker J.W. (2007). “Correlation of ground motion intensity parameters used for predicting structural and geotechnical response.” Applications of Statistics and Probability in Civil Engineering, Taylor & Francis Group, London, ISBN 978-0-415-45134-5.

Balling, R.J., Balling, L.J., Richards, P.W. (2009). “Design of Buckling-Restrained Braced Frames Using Nonlinear Time History Analysis and Optimization.” J Struct Eng, 135:461–8. https://doi.org/10.1061/(ASCE)ST.1943-541X.0000007.

Bignozzi, M.C., Sandrolini, F. (2006). “Tyre rubber waste recycling in self-compacting concrete.” Cement and Concrete Research, 36, 735–739. https://doi.org/10.1016/j.cemconres.2005.12.011.

Bolt, B.A. (1973). “Duration of strong motion.” Conference on Earthquake Engineering, Santiago, Chile, pp. 1304-1315.

Bolt, B.A. (2003). “Earthquakes.” Fifth Edition, W. H. Freeman, New York, ISBN 978-0-7167-5618-7.

Boore, D.M. and Joyner, W.B. (1982). “The empirical prediction of ground motion.” Bulletin of the Seismological Society of America,72 (6, Part B), S43-S60.

Boore, D.M., & Atkinson, G.M. (2008). “Ground-motion prediction equations for the average horizontal component of PGA, PGV, and 5%-damped PSA at spectral periods between 0.01 s and 10.0 s.” Earthquake spectra, 24(1), 99-138.

Boore, D.M., Joyner, W.B., Fumal, T.E. (1993). “Estimation of response spectra and peak accelerations from western North American earthquakes: an interim report.”

Brzev, S., Pao, J. (2016). “Reinforced concrete design: a practical approach.” Pearson Education, Third edition.

Campbell, K.W. (1985). “Strong motion attenuation relationships: A ten-year prospective.” Earthquake Spectra, 1 (4), 759-804.

Caterino, N., Spizzuoco, M., Occhiuzzi, A. (2013). “Promptness and dissipative capacity of MR dampers: Experimental investigations.” Structural Control and Health Monitoring 20:1424–1440. https://doi.org/10.1002/stc.1578.

Chang, F.K., Krinitzsky, E.L. (1977). “Duration, spectral content, and predominant period of strong motion earthquake records from western United States.” Army Corps of Engineers Waterways Experiment Station, Vicksburg, Mississippi, Paper 5-73-1.

Chopra, A.K. (2012). “Dynamics of structures: theory and applications to earthquake engineering.” 4th ed. Prentice Hall, Upper Saddle River.

Constantinou, M.C., Soong, T.T., Dargush, G.F. (1996). “Passive Energy Dissipation Systems for Structural Design and Retrofit.” MCEER Monograph No. 1, University at Buffalo, ISBN 0-9656682-1-5.

Constantinou, M.C., Symans, M.D. (1993). “Seismic response of buildings with supplemental damping.” Journal of Structural Design of Tall Buildings, 2:77–92.

Cordova, P.P., Deierlein, G.G., Mehanny, S.S.F., and Cornell, C.A. (2000). “Development of a two-parameter seismic intensity measure and probabilistic assessment procedure.” 2nd U.S.-Japan Workshop on Performance-based Earthquake Engineering Methodology for Reinforced Concrete Building Structures, Sapporo, Hokkaido, Japan,187–206.

Corebrace. (2020). “Superior seismic performance.” https://corebrace.com.

CSA (2019). “Design of concrete structures.” CSA A23.3-19, Canadian Standards Association, Rexdale, Ontario.

CSI (2016). “Integrated Building Design Software.” ETABS. CSI Analysis Reference Manual, Computers and Structures, Inc., California, USA, Retrieved from https://www.csiamerica.com/products/etabs.

Dallard, P., Fitzpatrick, A.J., Flint, A., Le Bourva, S., Low, A., Ridsdill, R.M., Willford, M. (2001). “The London Millennium Footbridge.” the structural engineer, Volume 79/No.22.

Deierlein, G.G., Reinhorn, A.M., Willford, M.R. (2010). “Nonlinear structural analysis for seismic design.” NEHRP seismic design technical brief 4, 1–36.

Della Corte, G., D’Aniello, M., Landolfo, R. (2015). “Field Testing of All-Steel Buckling-Restrained Braces Applied to a Damaged Reinforced Concrete Building.” J Struct Eng, 141: D4014004. https://doi.org/10.1061/(ASCE)ST.1943-541X.0001080.

Dolce, M., Santarsiero, G. (2004). “Development of regulations for seismic isolation and passive energy dissipation of buildings and bridges in Italy and Europe.” 13th World Conference on Earthquake Engineering, Vancouver, B.C., Canada, No. 2991.

Douglas, J. (2006). “Errata of and additions to Ground motion estimation equations 1964- 2003.” ESEE Research Report No.01- 6, Department of Civil Engineering and Environmental Engineering, Imperial College, London, UK.

Earthquakes General Interest Publication. (2016), “USGC.” https://pubs.usgs.gov/gip/earthq1/plate.html.

Elnashai, A.S., Di Sarno, L. (2008). “Fundamentals of earthquake engineering.” John Wiley & Sons.

Elnashai, A.S., Di Sarno, L. (2015). “Fundamentals of earthquake engineering: from source to fragility.” John Wiley & Sons.

Elwood K.J., Eberhard M.O. (2006). „Effective Stiffness of Reinforced Concrete Columns.” Pacific Earthquake Engineering Research Center (PEER), Research Digest No.2006-1.

Elwood, K.J., Matamoros, A.B., Wallace, J.W., Lehman, D.E., Heintz, J.A., Mitchell, A.D., Moore, M.A., Valley, M.T., Lowes, L.N., Comartin, C.D., Moehle, J.P. (2007). “Update to ASCE/SEI 41 Concrete Provisions.” Earthquake Spectra, 23, 493–523.

ETRMA. (2022). “European Tyre and rubber manufacturers association.” https://www.etrma.org/key-topics/circulareconomy.

European Committee for Standardization, Eurocode 8. (2002). “Design Provisions for Earthquake Resistance of Structures.” Part 1.1: General rules, seismic actions and rules for buildings, ENV19981-1.

Fajfar, P., Fischinger, M. (1988). “N2 a method for non-linear seismic analysis of regular structures.” Proc. 9th World Conf Earthquake Engineering, Vol. 5, Tokyo-Kyoto, Japan, 111-116.

FEMA 273. (1997). “NEHRP Guidelines for the Seismic Rehabilitation of Buildings.” Developed by the Building Seismic Safety Council for the Federal Emergency Management Agency (Report No. FEMA 273), Washington, D.C.

FEMA 274. (1997). “NEHRP Commentary on the Guidelines for the Seismic Rehabilitation of Buildings.” Developed by the Building Seismic Safety Council for the Federal Emergency Management Agency (Report No. FEMA 274), Washington, D.C.

FEMA 356. (2000). “Prestandard and Commentary for the Seismic Rehabilitation of Buildings.” Federal Emergency Management Agency, prepared by ASCE, Washington, D.C.

FEMA P695. (2009). “Quantification of building seismic performance factors.” Federal Emergency Management Agency, Washington, D.C.

FEMA P749. (2010). “Earthquake-Resistant Design Concepts.” An Introduction to the NEHRP Recommended Seismic Provisions for New Buildings and Other Structures, Building Seismic Safety Council, Washington, District of Columbia, USA.

FEMA-440. (2005). “Improvement of nonlinear static seismic analysis procedures.” Federal Emergency Management Agency, Washington, D.C.

Freeman, S.A. (1990). “On the correlation of code forces to earthquake demands.” proceedings of the 4th U.S.- Japan workshop on improvement of building structural design and construction practices, ATC 15-3, Redwood city, California.

Gavin, H.P., Dickinson, B.W. (2011). “Generation of Uniform-Hazard Earthquake Ground Motions.” J. Struct. Eng., 137, 423–432.

Ghaaowd, I., McCartney, J.S., Thielmann, S.S., Sanders, M.J., Fox, P.J. (2017). "Shearing Behavior of Tire-Derived Aggregate with Large Particle Size. I: Internal and Concrete Interface Direct Shear." J. Geotech. Geoenviron. Eng., 143(10): 04017078. https://doi.org/10.1061/(ASCE)GT.1943-5606.0001775.

Green, R.A., Hall, W. J. (1994). "An overview of selected seismic hazard analysis methodologies." Civil Engineering Studies SRS-592.

Gunay M.S. (2011). "A practical guide to nonlinear static analysis." university of California, Berkeley.

Güneyisi, E., Gesoğlu, M., and Özturan, T. (2004). "Properties of rubberized concretes containing silica fume." Cement and Concrete Research, Vol. 34, No. 12, pp. 2309–2317.

Gupta, A.K. (1990). "Response spectrum method in seismic analysis and design of structures." new directions in civil engineering, Blackwell Scientific Publications, Boston.

Hachem, M.M. (2004). BISPEC: "Interactive Software for the Computation of Unidirectional and Bidirectional Nonlinear Earthquake Spectra." Presented at the Structures Congress, American Society of Civil Engineers, Nashville, Tennessee, United States, pp. 1–12. https://doi.org/10.1061/40700(2004)180.

Hancock, J., Bommer, J.J. (2006). "A state-of-knowledge review of the influence of strong-motion duration on structural damage." Earthquake spectra, 22(3), 827-845.

Haselton, C.B., Baker, J.W., Bozorgnia, Y., Goulet, C.A., Kalkan, E., Luco, N., Shantz, T., Shome, N., Stewart, J.P., Tothong, P., Watson-Lamprey, J. (2009). "Evaluation of ground motion selection and modification methods: Predicting median interstory drift response of buildings." PEER report, 1, pp.1-288.

Haselton, C.B., Liel, A.B., Lange, S.T., Deierlein, G.G. (2007). "Beam-Column Element Model Calibrated for Predicting Flexural Response Leading to Global Collapse of RC Frame Buildings." PEER Report No. 2007, Pacific Earthquake Engineering Research Center College of Engineering, University of California, Berkeley.

Hertz, D.L. (1991). “An analysis of rubber under strain from an engineering perspective.” Elastomerics.

Hosseinzadeh, S.h., Mohebi, B. (2016). “Seismic evaluation of all-steel buckling restrained braces using finite element analysis.” Journal of Constructional Steel Research, 119:76–84. https://doi.org/10.1016/j.jcsr.2015.12.014.

Housner, G.W. (1973). “Important features of earthquake ground motions.” Proceedings of the 5th World Conference on Earthquake Engineering, Rome, Italy, Vol. 1, pp. CLIX–CLXVIII.

https://opensees.berkeley.edu/wiki/index.php/OpenSees_User.

Hudson, D.E. (1979). “Reading and Interpreting Strong Motion Accelerograms.” Earthquake Engineering Research Institute, Berkeley, California, 112 pp.

Humphrey, D., Blumenthal, M. (2010). “The Use of Tire-Derived Aggregate in Road Construction Applications.” Green Streets and Highways, Denver, Colorado, United States: American Society of Civil Engineers, pp.299–313. https://doi.org/10.1061/41148(389)25.

Hwang, H., and Shinozuka, M. (1994). “Effect of large earthquakes on the design of buildings in eastern United States.” Proceedings of the fifth U.S national conference on earthquake engineering, Chicago, Illinois.

ICBO. (1961, 1985, 1988, 1994). “Uniform Building Code.” International Conference of Building Officials, Whittier, California, 90601.

Idriss, I.M. (1978). “Characteristics of earthquake ground motions.” Proceedings of the Geotechnical Engineering Division Specialty Conference: Earthquake Engineering and Soil Dynamics, ASCE, III, 1151-1265.

International Code Council. (2000). “International Building Code.” Section 1623, Seismically Isolated Structures.

Issa, C.A., Salem, G. (2013). “Utilization of recycled crumb rubber as fine aggregates in concrete mix design.” Construction and Building Materials, 42, 48–52. https://doi.org/10.1016/j.conbuildmat.2012.12.054.

Kanai, K. (1983). “Engineering Seismology.” University of Tokyo Press, Tokyo, Japan.

Kennett, J.P. (1982). “Marine Geology.” Prentice-Hall, Englewood Cliffs, New Jersey.

Kersting, R.A., Fahnestock, L.A., Lopez, W.A. (2015). “Seismic design of steel buckling-restrained braced frames: a guide for practicing engineers.” National Institute of Standards and Technology, Gaithersburg, MD, NIST GCR 15-917-34.

Khatib, Z.K., Bayomy, F.M. (1999). “Rubberized Portland Cement Concrete.” Journal of Materials in Civil Engineering, Vol. 11, No.3, 206–213, https://doi.org/10.1061/(ASCE)0899-1561(1999)11:3(206).

Kim, T.W., Foutch, D.A., LaFave, J.M., Wilcoski, J. (2004). “Performance assessment of reinforced concrete structural walls for seismic loads.” University of Illinois Engineering Experiment Station. College of Engineering. University of Illinois at Urbana-Champaign.

Ko, E., and Field, C. (2003). “The Unbonded Brace™: From Research to Californian Practice.” SEAOC convention.

Kramer, S.L. (1996). “Geotechnical earthquake engineering.” Prentice-Hall international series in civil engineering and engineering mechanics, Prentice Hall, Upper Saddle River, New Jersey, 07458.

Krawinkler, H. (1997). “A framework for performance-based earthquake resistive design.” EERC CUREe Symposium in Honor of Vitelmo V. Bertero, Berkeley, California.

Krawinkler, H., and Seneviratna, G.D.P.K. (1998). “Pros and cons of a pushover analysis of seismic performance evaluation.” Engineering Structures, 20(4–6), 452–464.

Krawinkler, H., Nassar, A. A. (1992). “Nonlinear Seismic Analysis and Design of Reinforced Concrete Buildings.” CRC Press, ISBN9780429176753.

Kumar, R.G., Kumar, S.R., Kalyanaraman, V. (2005). “Behaviour of frames with non-Buckling bracings under earthquake loading.” Journal of Constructional Steel Research, 63:254–62. https://doi.org/10.1016/j.jcsr.2006.04.012.

Kurtis, K. (2007). “Structure of the Hydrated Cement Paste.” Georgia Institute of Technology, Atlanta.

Lawson, R. S., Vance, V., Krawinkler, H. (1994). “Nonlinear static pushover analysis - why, when and how?” Proc. 5th US Conf. Earthquake Engineering, Vol. 1, Chicago, IL, 283-292.

Li, G., Garrick, G., Eggers, J., Abadie, C., Stubblefield, M.A., Pang, S.S. (2004). “Waste tire fiber modified concrete.” Composites Part B: Engineering, 35:305–312. https://doi.org/10.1016/j.compositesb.2004.01.002.

Lignos, D.G. (2014). “Nonlinear structural analysis for buildings.” Department of Civil Engineering and Applied Mechanics Structural Systems and Deflection Decomposition, MacDonald Engineering Building, McGill.

Lignos, D.G., Krawinkler, H., and Whittaker, A.S. (2011). “Prediction and validation of sideway collapse of two scale models of a 4-storey steel moment frame.” Earthquake Engineering and Structural Dynamics (EESD), 40(7), 807–825.

Lilhanand, K., Tseng, W.S. (1988). “Development and application of realistic earthquake time histories compatible with multiple-damping design spectra.” In Proceedings of the 9th world conference on earthquake engineering, Vol. 2, pp. 819-824.

Liu, F., Chen, G., Li, L., Guo, Y. (2012). “Study of impact performance of rubber reinforced concrete, Construction and Building Materials.” 36, 604–616. https://doi.org/10.1016/j.conbuildmat.2012.06.014.

Locher, F.W. (1994). “The properties of rubberized concretes, Cement and Concrete Research.” Vol. 25, No. 2, pp. 304-310.

Mahaney, J.A., Paret, T.F., Kehoe, B.E., Freeman, S.A. (1993). “The capacity spectrum method for evaluating structural response during the Loma Prieta earthquake.” In Mitigation and damage to the built environment, pp. 501-10.

Mahmoudi, M., Zaree, M. (2013). “Determination the Response Modification Factors of Buckling Restrained Braced Frames.” Procedia Engineering 2013; 54:222–31. https://doi.org/10.1016/j.proeng.2013.03.020.

Mallet, R. (1862). “Great Neapolitan Earthquake of 1857. The First Principles of Observational Seismology.” Vol. 1, Chapman and Hall, London, UK.

Mazzolani, F.M. (2001). “Passive control technologies for seismic-resistant buildings in Europe.” Progress in Structural Engineering and Materials 3, 277–287. https://doi.org/10.1002/pse.83.

McKenna, F. (1997). “Object-oriented finite element programming: frameworks for analysis, algorithms and parallel computing.” PhD thesis, Civil Engineering, University of California, Berkley, Ca.

Miller, N.M., Tehrani, F.M. (2017). „Mechanical properties of rubberized lightweight aggregate concrete.” Construction and Building Materials, 147:264–271. https://doi.org/10.1016/j.conbuildmat.2017.04.155.

Miranda, E. (1991). “Evaluation of seismic performance of a ten story RC building during the whittier narrows earthquake.” Ph.D. dissertation, Department of Civil Engineering, University of California, Berkeley, CA.

Miranda, E., Bertero, V.V. (1994). “Evaluation of Strength Reduction Factors for Earthquake Resistant Design.” Earthquake Spectra, 10(2), 357–379.

Mohammed, B.S. (2010). “Structural behavior and m–k value of composite slab utilizing concrete containing crumb rubber.” Construction and Building Materials, 24, 1214–1221. https://doi.org/10.1016/j.conbuildmat.2009.12.018.

Mohammed, B.S., Anwar Hossain, K.M., Eng Swee, J.T., Wong, G., Abdullahi, M. (2012). “Properties of crumb rubber hollow concrete block.” Journal of Cleaner Production, 23, 57–67. https://doi.org/10.1016/j.jclepro.2011.10.035.

Moni, M., Moradi, S., and Alam, M. S. (2016). “Response modification factors for steel buckling restrained braced frames designed as per the 2010 National Building Code of Canada.” Canadian Journal of Civil Engineering, 43(8), 702–715.

Mwafy, A.M. (2001). “Seismic performance of code-designed RC buildings.” PhD Thesis, Department of Civil and Environmental Engineering, Imperial College of Science, Technology and Medicine, London.

NBCC. (2015). “National Building Code of Canada.” National Research Council of Canada, Ottawa, ON.

Newmark, N.M., Hall, W.J. (1982). “Earthquake Spectra and Design.” EERI Monograph, Earthquake Engineering Research Institute, Berkeley, California.

Next Generation Attenuation Relationship. (NGA, 2008). PEER Center, https://apps.peer.berkeley.edu/ngawest/nga_models.html.

Nguyen, A.H., Chintanapakdee, C., Hayashikawa, T. (2010). “Assessment of current nonlinear static procedures for seismic evaluation of BRBF buildings.” Journal of Constructional Steel Research, 66:1118–27. https://doi.org/10.1016/j.jcsr.2010.03.001.

Oaks, E.D.H. (2004). “Preparation for the Second Coming 3.” General Conference.

Occhiuzzi, A., Spizzuoco, M., Serino, G. (2002). “Semi-active MR dampers in TMD’s for vibration control of footbridges, Part1: Numerical modelling and control algorithm.” footbridge 2002, design and dynamic behaviour of footbridges, Paris.

Occhiuzzi, A., Spizzuoco, M., Serino, G. (2003). “Experimental analysis of magnetorheological dampers for structural control.” Smart Materials and Structures, 12-703.

Osteras, J.D., and Krawinkler, H.(1990). “Strength and ductility consideration in seismic design.” Blume earthquake engineering center, Report 90, Stanford university, California.

Pathan, N. B. (2021). “Seismic Behavior of Buckling Restrained Braced Frames.” Master of Science in Civil Engineering in the Lyles College of Engineering California State University, Fresno.

Paulay T., Priestley M. J. N. (1992). “Seismic Design of Reinforced Concrete and Masonry Buildings.” John Wiley and Sons, Inc.

PEER Ground Motion Database. (2019). PEER Center, https://ngawest2.berkeley.edu.

Ricciardelli, F., Occhiuzzi, A., Clemente, P. (2000). “Semi-active Tuned Mass Damper control strategy for wind-excited structures.” Journal of Wind Engineering and Industrial Aerodynamics, 88, 57–74. https://doi.org/10.1016/S0167-6105(00)00024-6.

Richter, C.F. (1961). “Elementary seismology.” W. H. Freeman and Company, San Francisco, Geological Journal, Vol. 2, No. 2, pp. xi–xiii.

RILEM. (2022). “GLOBE - Global Consensus on Sustainability in the Built Environment.” Available at: https://www.rilem.net/globe.

Sabelli, R., Mahin, S., Chang, C. (2003). “Seismic demands on steel braced frame buildings with buckling restrained braces.” Engineering Structures, 25:655–66. https://doi.org/10.1016/S0141 0296(02)00175-X.

Sajidi, M., Sozen, M.A. (1981). “Simple nonlinear seismic analysis of R/C structures.” J. Struct. Div., ASCE, 107 (ST5), 937-951.

SEAOC. (1959, 1974, 1985, 1988, 1990). “Recommended lateral force requirements and commentary.” seismology committee, Structural Engineers Association of California, Sacramento, California.

SEAOC. (1995). “Vision 2000, A framework for performance-based engineering.” Sacramento, CA, Structural Engineers Association of California.

Seed, H.B., Idriss, 1.M. (1982). “Ground Motions and Soil Liquefaction During Earthquakes.” Earthquake Engineering Research Institute, Berkeley, California, p.134.

Seiler, C.H., Fischer, O., Distl, H., Braun, C. (2003). “Semi-aktive Schwingungsdämpfer Entwicklung und Anwendung einer neuen Technologie.” Beton- und Stahlbetonbau 98, 605–614. https://doi.org/10.1002/best.200302580.

Seiler, C.H., Fischer, O., Huber, P. (2002). “Semi-active MR dampers in TMD’s for vibration control of footbridges, Part 2: Numerical analysis and practical realisation.” footbridge 2002, design and dynamic behaviour of footbridges, Paris.

SeismoSoft. (2018). “Earthquake Software for Response Spectrum Matching.” Pavia, Italy, www.seismosoft.com.

SeismoSoft. (2018).SeismoStruct-User Manual For version 7.0 Pavia, Italy, www.seismosoft.com.

Siddique, R., Naik, T.R. (2004). “Properties of concrete containing scrap-tire rubber-an overview.” Waste Management 24:563–569. https://doi.org/10.1016/j.wasman.2004.01.006.

Son, K.S., Hajirasouliha, I., Pilakoutas, K. (2011). “Strength and deformability of waste tyre rubber-filled reinforced concrete columns.” Construction and Building Materials, 25:218–226. https://doi.org/10.1016/j.conbuildmat.2010.06.035.

Soong, T.T., and Dargush, G. F. (1999). “Passive Energy Dissipation and Active Control.” Boca Raton: Structural Engineering Handbook, CRC Press LLC, 1–28.

Soong, T.T., Constantinou, M.C. (1994). “Passive and Active Structural Vibration Control in Civil Engineering.” Springer, New York.

Spizzuoco, M., Occhiuzzi, A., Serino, G. (2004). “Performance of a Semi-Active MR Control System for Earthquake Protection.” 13th world Conference on Earthquake Engineering, Vancouver, B.C., Canada, No.2025.

Stewart, J.P., Douglas, J., Javanbarg, M., Bozorgnia, Y., Abrahamson, N.A., Boore, D.M., Campbell, K.W., Delavaud, E., Erdik, M. and Stafford, P.J. (2015). “Selection of ground motion prediction equations for the global earthquake model.” Earthquake Spectra, 31(1), pp.19-45.

Suhendro, B. (2014). “Toward Green Concrete for Better Sustainable Environment.” Procedia Engineering, 95: 305–320. https://doi.org/10.1016/j.proeng.2014.12.190.

Sukontasukkul, P. (2009). “Use of crumb rubber to improve thermal and sound properties of pre-cast concrete panel.” Construction and Building Materials, Vol.23, No.2, 1084–1092. https://doi.org/10.1016/j.conbuildmat.2008.05.021.

Symans, M.D., and Constantinou, M.C. (1997). “Semi-active control systems for seismic protection of structures: a state-of-the-art review.” Eng. Struct. 21, 469-487.

Tall Buildings Initiative. (2017). “Guidelines for Performance-Based Seismic Design of Tall Buildings.” Pacific Earthquake Engineering Research Center. College of Engineering. University of California: Berkeley, CA, USA. 2017.

Technical Manual. (1986). “Seismic Guidelines for Essential Buildings.” Change 1, Army TM 5-809-10-1, Navy NAVFAC P-355.1, Air Force AFM 88-3, Chap. 13, Sec A, Departments of the Army, Navy, and Air Force.

Tehrani, F.M., Carreon, J., Miller, N. (2019). “An Investigation of Tire-derived Lightweight Aggregate Concrete.” Sustainable Concrete with Beneficial Byproducts, SP-334-5.

Tehrani, F.M., Masswadi, N.A., Miller, N.M., Sadrinezhad, A. (2020). “An Experimental Investigation of Dynamic Properties of Fiber-Reinforced Tire-Derived Lightweight-Aggregate Concrete.” European Journal of Engineering and Technology Research, 5(6), pp.702-707. https://doi.org/10.24018/ejers.2020.5.6.1967.

Tehrani, F.M., Miller, N.M. (2018). “Tire-Derived Aggregate Cementitious Materials: A Review of Mechanical Properties.” in Saleh, H.E.-D.M., Rahman, R.O.A. (Eds.), Cement-Based Materials. https://doi.org/10.5772/intechopen.74313.

Tehrani, F.M., Nazari, M., Naghshineh, A. (2020). “Role of Seismic Isolation and Protection Devices in Enhancing Structural Resilience.” EMI ORC MOP Part III Chapter 21.

Topçu, I.B., Avcular, N. (1997). “Collision behaviours of rubberized concrete.” Cement and Concrete Research, Vol. 27, No. 12, pp.1893–1898. https://doi.org/10.1016/S0008-8846(97)00204-4.

Toutanji H.A. (1996). “The use of rubber tire particles in concrete to replace mineral aggregates.” Cement and Concrete Composites 18:135–139. https://doi.org/10.1016/0958-9465(95)00010-0.

Toutanji, H. A., and El-Korchi, T. (1996). “Tensile and Compressive Strength of Silica Fume-Cement Pastes and Mortars.” Cement, Concrete, and Aggregates, Vol. 18, No. 2, 1996, pp. 78-84.

Treloar, L.R.G. (1994). “Stress-Strain Data for Vulcanized Rubber under Various Types of Deformation.” Transactions of the Faraday Society, Vol. 40, 1944, pp. 59-70.

Tremblay, R., Filiatrault, A., Bruneau, M., Nakashima, M., Prion, H.G., Devall, R. (1996). “Seismic design of steel building: lessons from the 1995 Hyogo-ken Nanbu earthquake.” Can. J. Civ. Eng. 23(3), 727–756.

Trifunac, M.D. and Brady, A.G. (1976). “Correlations of peak, velocity and displacement with earthquake magnitude, distance and site conditions.” Earthquake Engineering and Structural Dynamics, 4 (5), 455- 471.

Tseng, W.S., Lihanand, K., Ostadan, F., Tuann, S.Y. (1991). “Post-earthquake analysis and data correlation for the 1/4-scale containment model of the Lotung experiment (No. EPRI-NP-7305-M).” Electric Power Research Inst., Palo Alto, CA (United States); Bechtel Corp., San Francisco, CA.

U.S. Geological Survey (USGS). (2011). “Historical Statistics for Mineral and Material Commodities in the United States.” https://minerals.usgs.gov/minerals/pubs/historicalstatistics.

Uang, C.M., Bertero, V.V., (1988). “Use of Energy as a Design Criterion in Earthquake-Resistant Design.” Technical Report UCB/EERC-88/18, University of California, Berkeley, CA.

Uang, C.M., and Maaroug, A. (1993). “Safety and economy considerations of UBC seismic force reduction factors.” Proceeding of the 1993 national earthquake conference. Memphis, Tennessee.

Uang, C.M., Maarouf, A. (1994). “Deflection Amplification Factor for Seismic Design Provisions.” Journal of Structural Engineering, V. 120, No. 8, pp. 2423–36.

UNESCO. (2022). “Sustainable Development.” UNESCO. Available at: https://en.unesco.org/themes/education-sustainable-development/what-is-esd/sd.

UPSeis. (2022). https://www.mtu.edu/geo/community/seismology/learn/earthquake-epicenter.

USGS. (2022). “The Modified Mercalli Intensity Scale.” https://www.usgs.gov.

WDK. (2022). “ Wirtschaftsverband der deutschen Kautschukindustrie e.V., Secondary Raw Materials.” https://wdk.brandbox.de/sekundaer-rohstoffe-unterseite-von-tee.

Whittaker, A.S., Uang, C.M., and Bertero V.V. (1987). “Earthquake simulation tests and associated studies of a 0.3-scale model of a six-story eccentrically braces steel structure.” Earthquake engineering research center, Report No. UCB/EERC-87/02, University of California, Berkeley, California.

Williams, J. (2017). “What can the world do with 1.5 billion waste tyres?” The Earthbound Report. https://earthbound.report/2017/06/29/what-can-the-world-do-with-1-5-billion-wastetyres/.

Wood, L. A. (1977). “Uniaxial Extension and Compression in Stress-Strain Relationships of Rubber.” Journal of Research of the National Bureau of Standards, Vol. 82, pp. 57-63.

Xue, J., Shinozuka, M. (2013). “Rubberized concrete: A green structural material with enhanced energy-dissipation capability.” Construction and Building Materials, 42, 196–204. https://doi.org/10.1016/j.conbuildmat.2013.01.005.

Yang, H., Jiang, L., Zhang, Y., and Pu, Q. (2013). “Flexural Strength of Cement Paste Beam under Chemical Degradation: Experiments and Simplified Modeling.” Journal of Materials in Civil Engineering, Vol. 25, pp. 555-562.

Yassin, M. H. M. (1994). “Nonlinear analysis of pre-stressed concrete structures under monotonic and cyclic loads.” Dissertation. University of California. Berkeley, California.

Zheng, L., Huo, X.S., Yuan, Y. (2008). “Strength, Modulus of Elasticity, and Brittleness Index of Rubberized Concrete.” Journal of Materials in Civil Engineering, Vol. 20, No. 11, pp. 692–699. https://doi.org/10.1061/(ASCE)0899-1561(2008)20:11(692).

Appendix A: Acceleration, velocity, and displacement

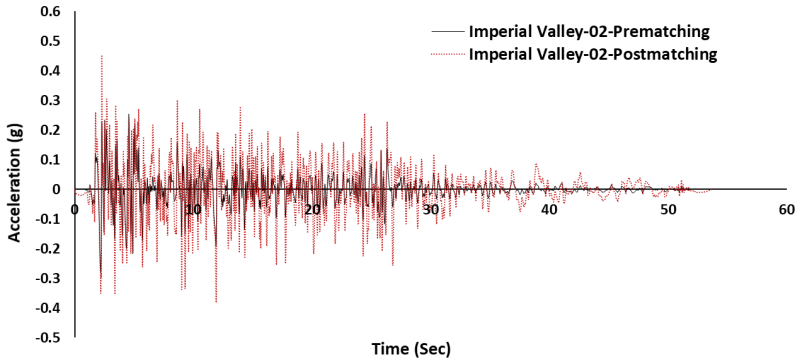

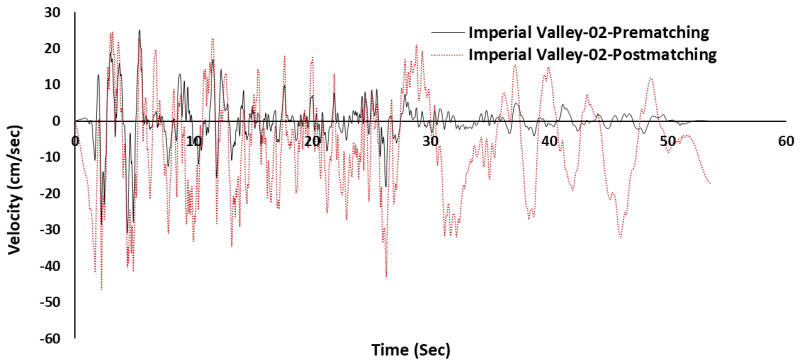

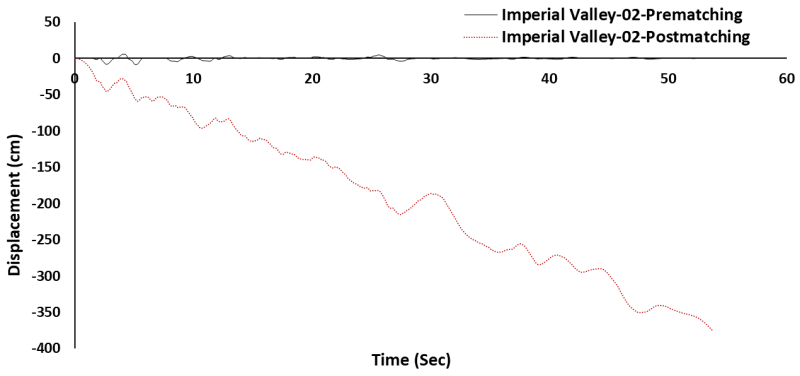

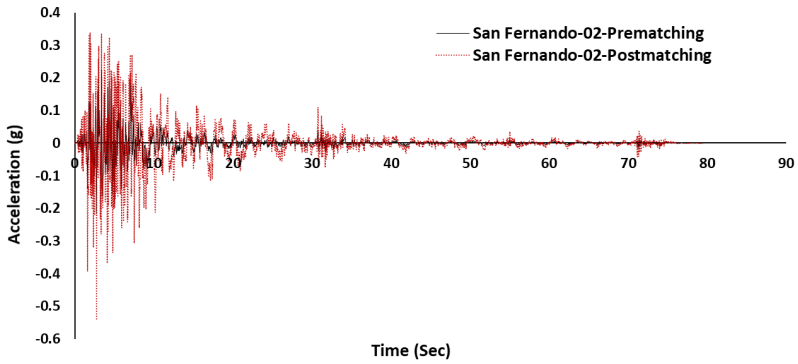
San Fernando-02-Prematching
San Fernando-02-Postmatching
Acceleration (g)
Time (Sec)

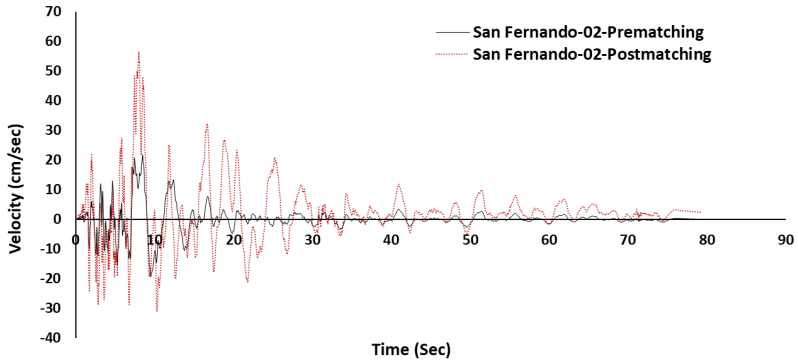
San Fernando-02-Prematching
San Fernando-02-Postmatching
Velocity (cm/sec)
Time (Sec)

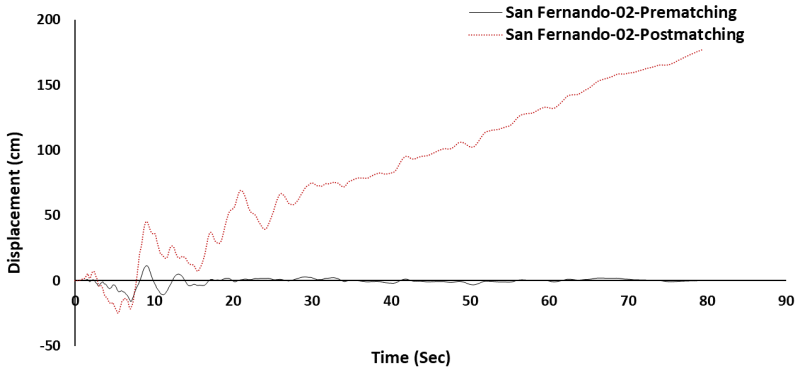
San Fernando-02-Prematching
San Fernando-02-Postmatching
Displacement (cm)
Time (Sec)

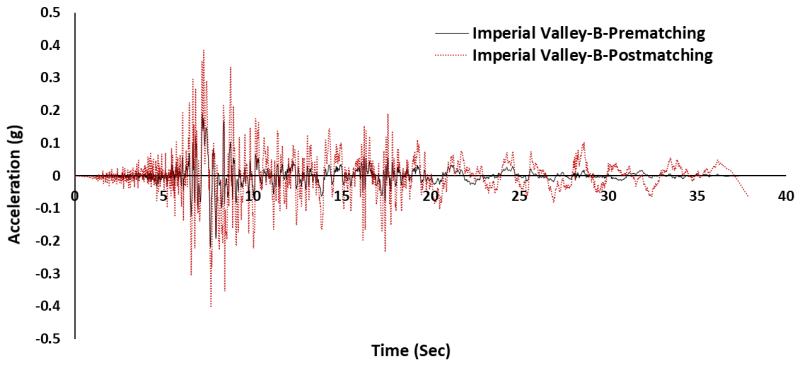
Imperial Valley-B-Prematching
Imperial Valley-B-Postmatching
Acceleration (g)
0.5
0.4
0.3
0.2
0.1
0
-0.1
-0.2
-0.3
-0.4
-0.5
0
5
10
15
20
25
30
35
40
Time (Sec)

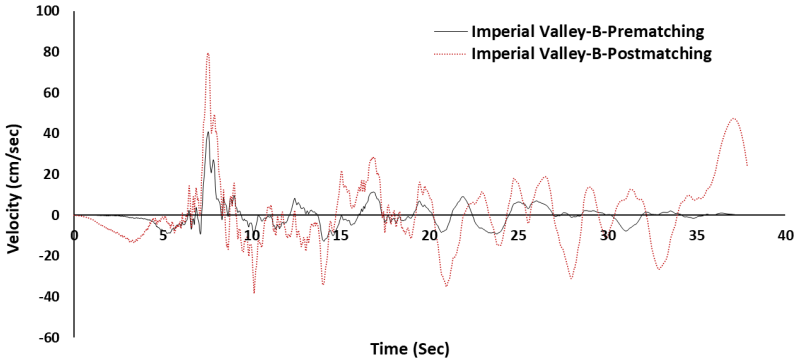
Imperial Valley-B-Prematching
Imperial Valley-B-Postmatching
Velocity (cm/sec)
100
80
60
40
20
0
-20
-40
-60
0
5
10
15
20
25
30
35
40
Time (Sec)

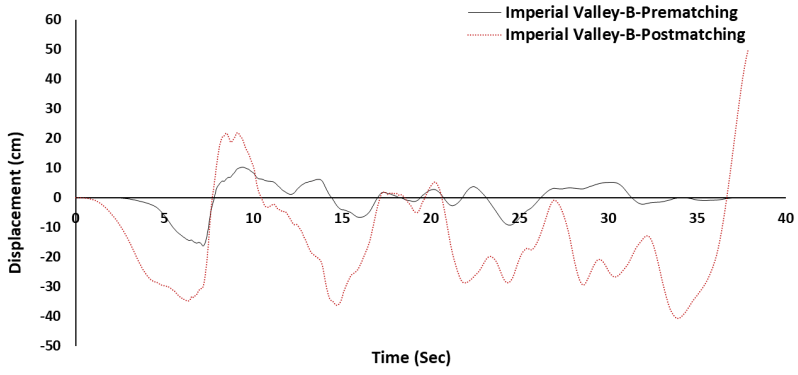
Imperial Valley-B-Prematching
Imperial Valley-B-Postmatching
Displacement (cm)
60
50
40
30
20
10
0
-10
-20
-30
-40
-50
0
5
10
15
20
25
30
35
40
Time (Sec)

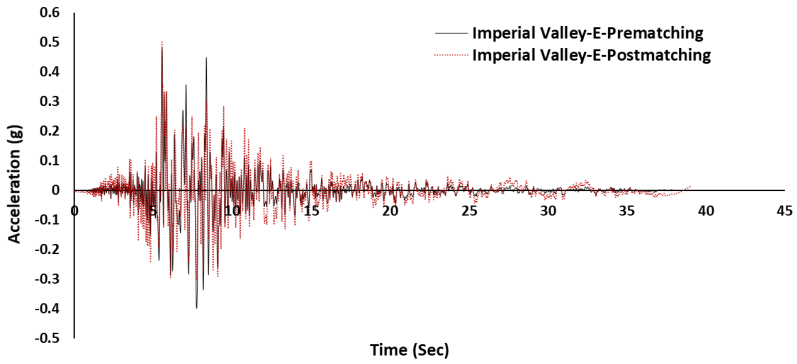
Imperial Valley-E-Prematching
Imperial Valley-E-Postmatching
Acceleration (g)
Time (Sec)

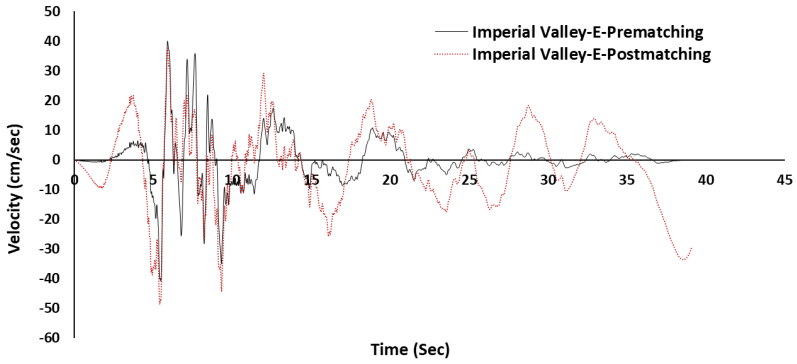
Imperial Valley-E-Prematching
Imperial Valley-E-Postmatching
Velocity (cm/sec)
Time (Sec)

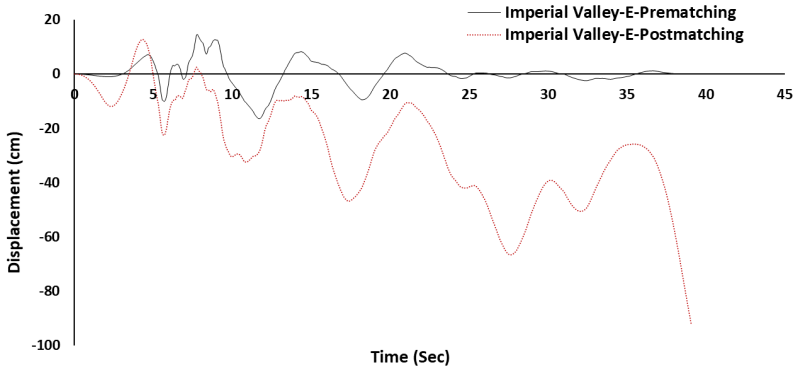
Imperial Valley-E-Prematching
Imperial Valley-E-Postmatching
Displacement (cm)
Time (Sec)

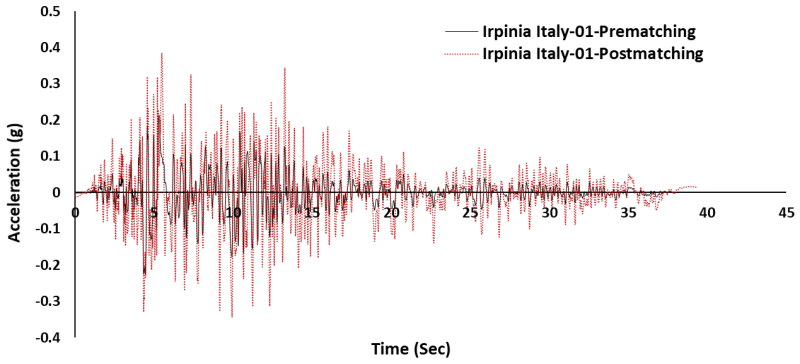
Irpinia Italy-01-Prematching
Irpinia Italy-01-Postmatching
Acceleration (g)
Time (Sec)

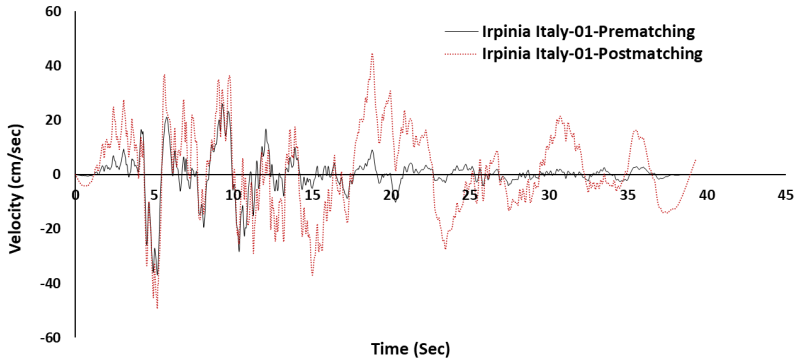
Irpinia Italy-01-Prematching
Irpinia Italy-01-Postmatching
Velocity (cm/sec)
Time (Sec)

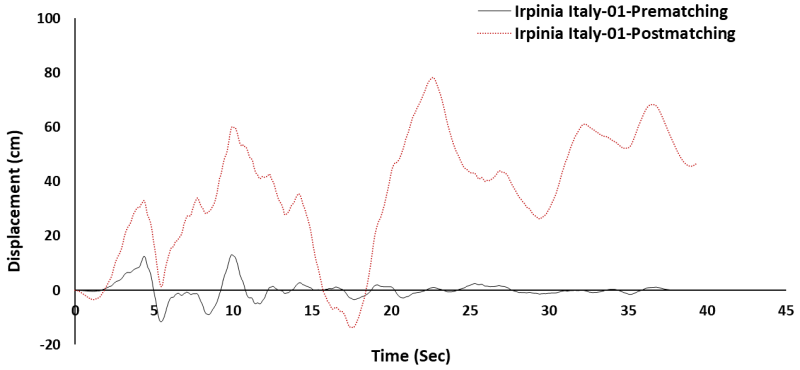
Irpinia Italy-01-Prematching
Irpinia Italy-01-Postmatching
Displacement (cm)
Time (Sec)

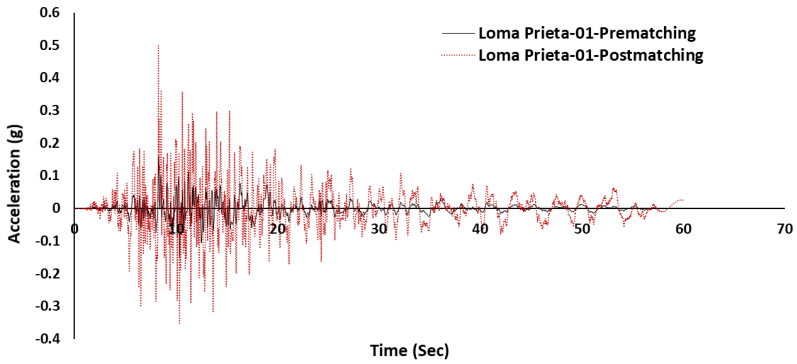
Loma Prieta-01-Prematching
Loma Prieta-01-Postmatching
Acceleration (g)
Time (Sec)

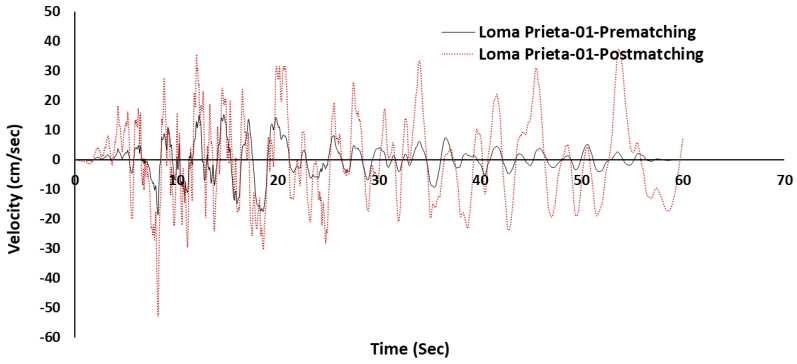
Loma Prieta-01-Prematching
Loma Prieta-01-Postmatching
Velocity (cm/sec)
Time (Sec)

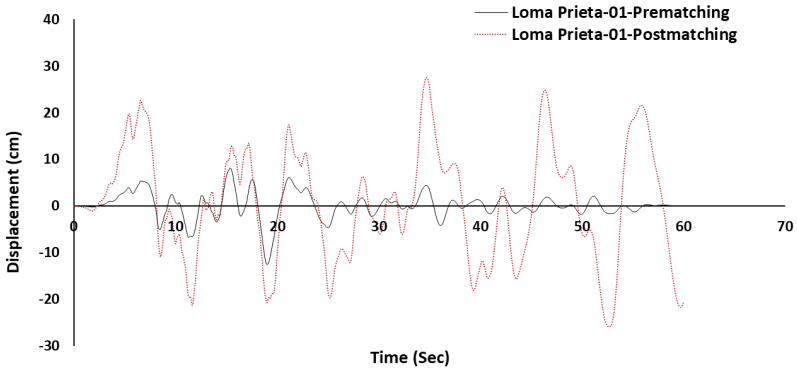
Loma Prieta-01-Prematching
Loma Prieta-01-Postmatching
Displacement (cm)
Time (Sec)

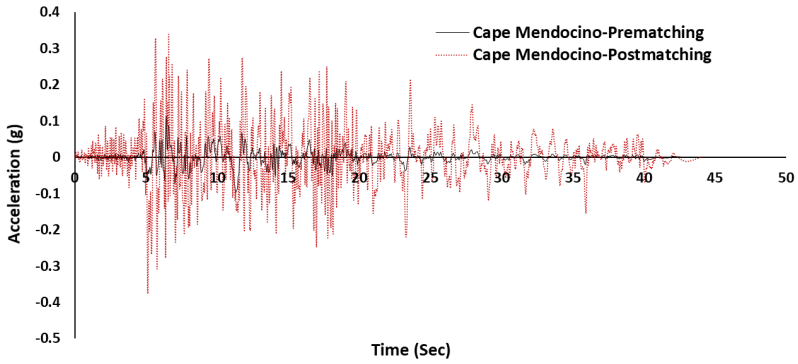
Cape Mendocino-Prematching
Cape Mendocino-Postmatching
Acceleration (g)
Time (Sec)

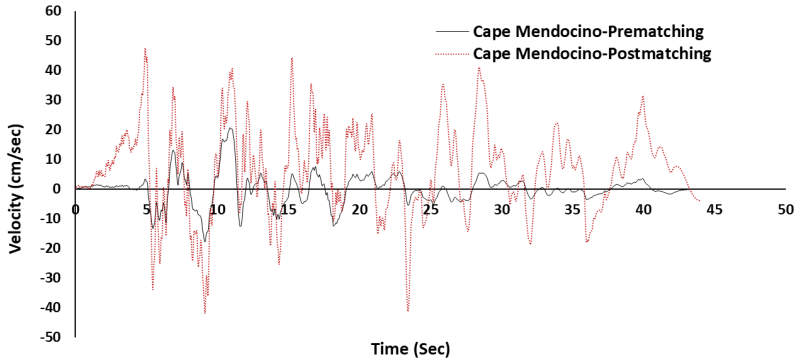
Cape Mendocino-Prematching
Cape Mendocino-Postmatching
Velocity (cm/sec)
Time (Sec)

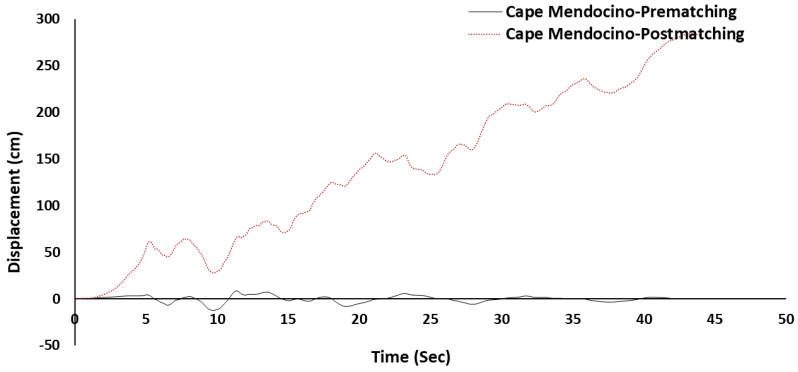
Cape Mendocino-Prematching
Cape Mendocino-Postmatching
Displacement (cm)
Time (Sec)

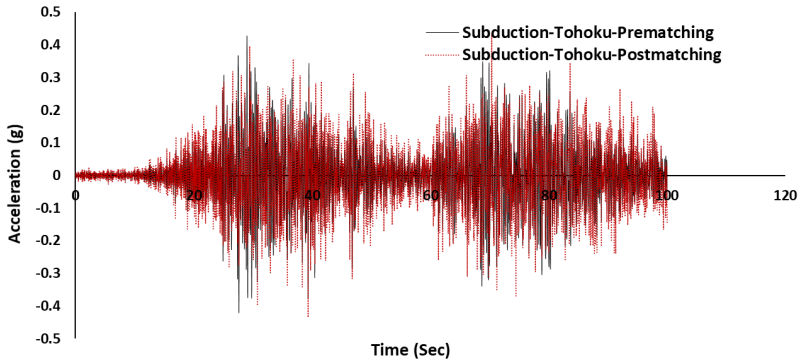
Subduction-Tohoku-Prematching
Subduction-Tohoku-Postmatching
Acceleration (g)
0.5
0.4
0.3
0.2
0.1
0
-0.1
-0.2
-0.3
-0.4
-0.5
0
20
40
60
80
100
120
Time (Sec)

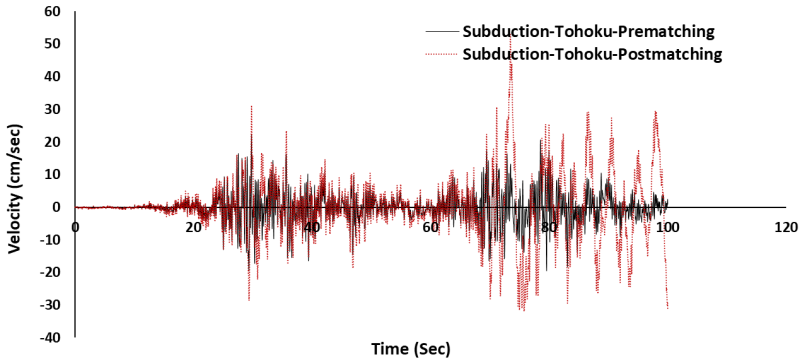
Subduction-Tohoku-Prematching
Subduction-Tohoku-Postmatching
Velocity (cm/sec)
60
50
40
30
20
10
0
-10
-20
-30
-40
0
20
40
60
80
100
120
Time (Sec)

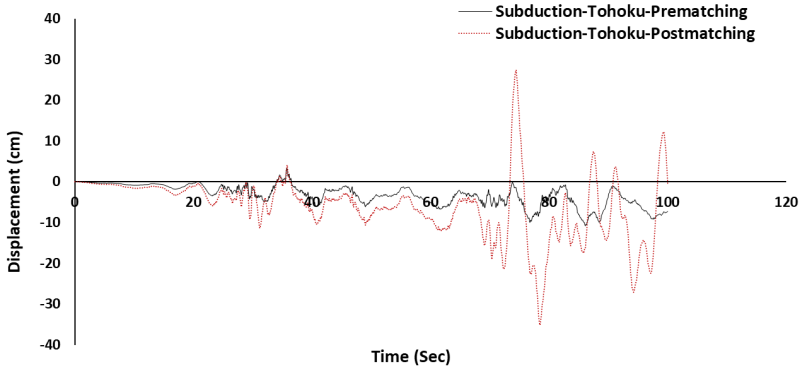
Subduction-Tohoku-Prematching
Subduction-Tohoku-Postmatching
Displacement (cm)
40
30
20
10
0
-10
-20
-30
-40
0
20
40
60
80
100
120
Time (Sec)

Appendix B: Ductility (μ)

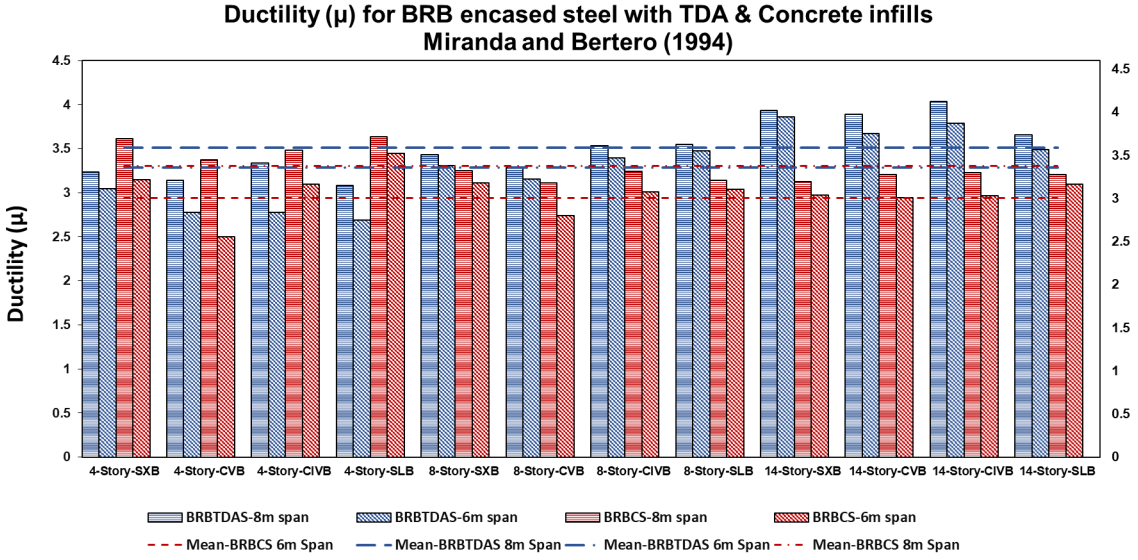

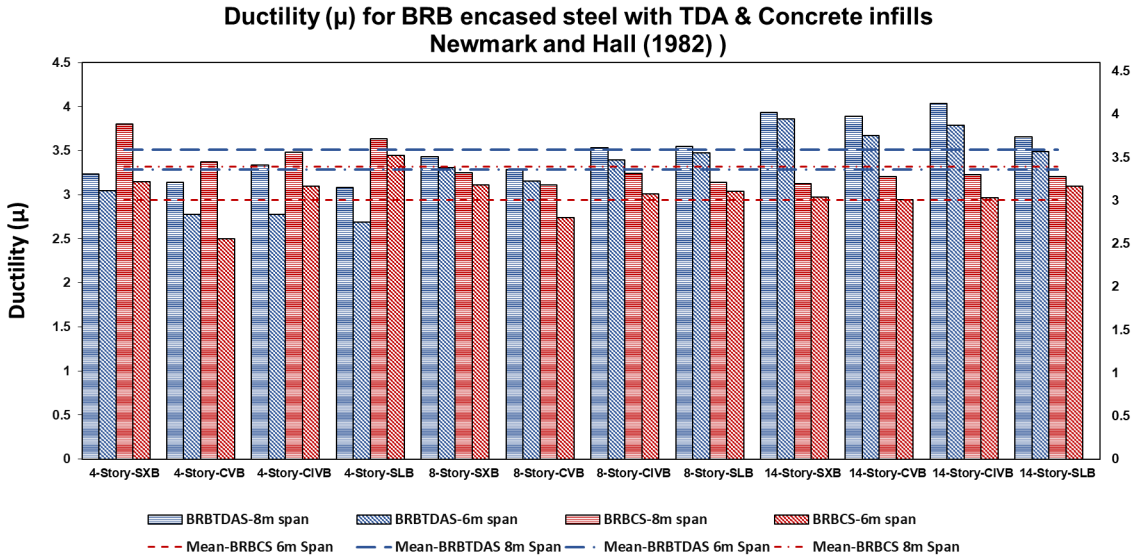

Appendix C: Deflection Amplification Factor (C_d)

The deflection amplification factor is determined based on the reduced response modification factor by the damping factor (FEMA P695, 2009). The ASCE 7-22 suggest the deflection amplification factor of 5 for steel buckling restrained braced frames, the recommended value based on Miranda and Bertero method is 3 for BRB with TDA infill and the height restriction of 50 meters.

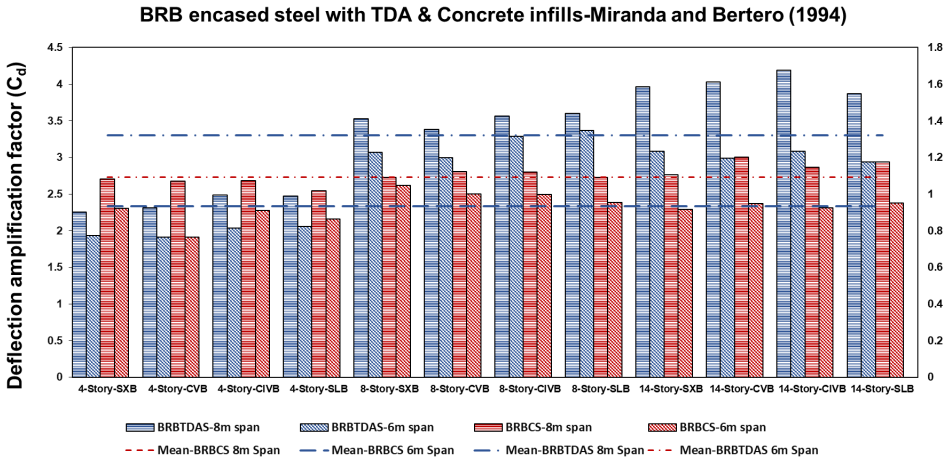

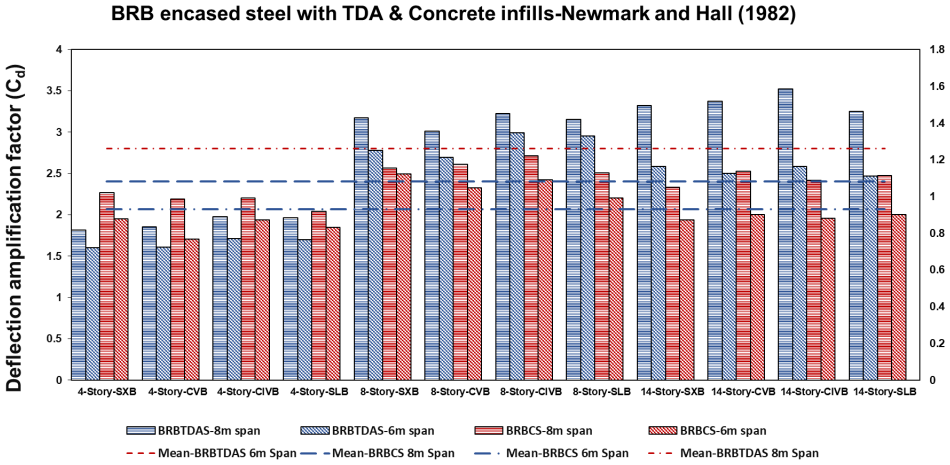

Appendix D: Interstory drift ratio

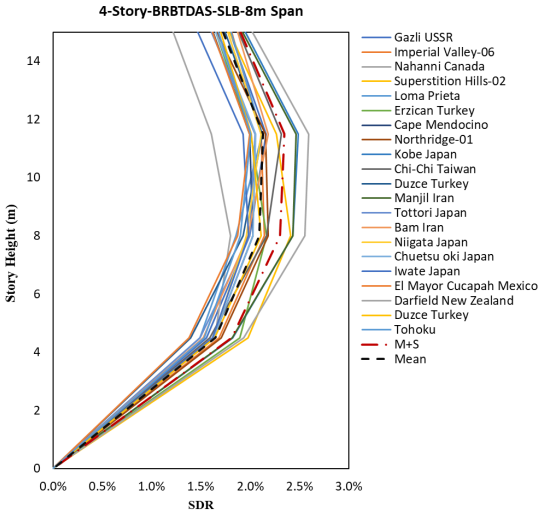

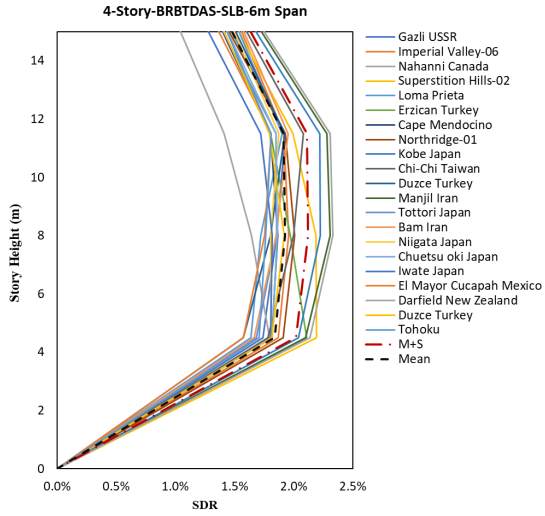

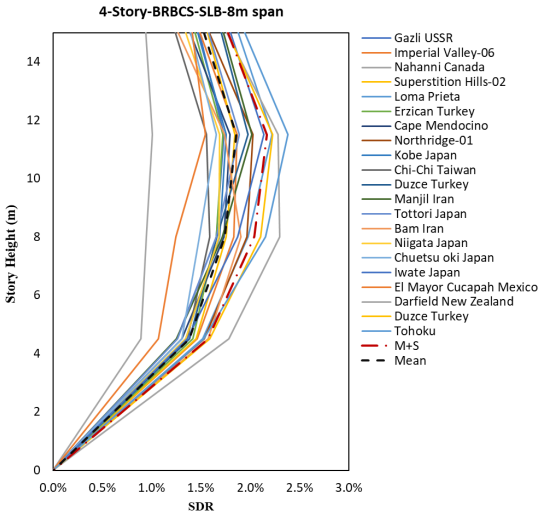

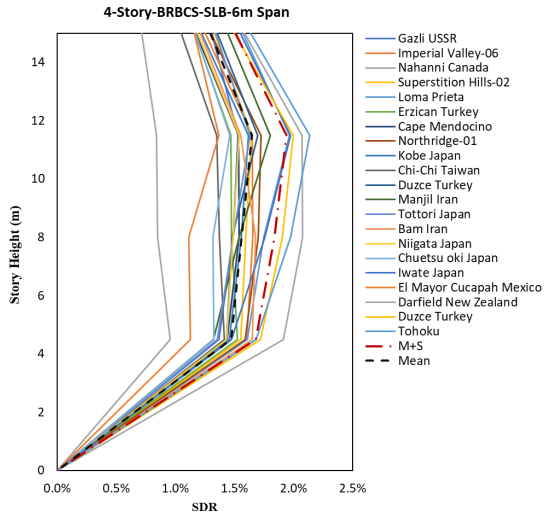

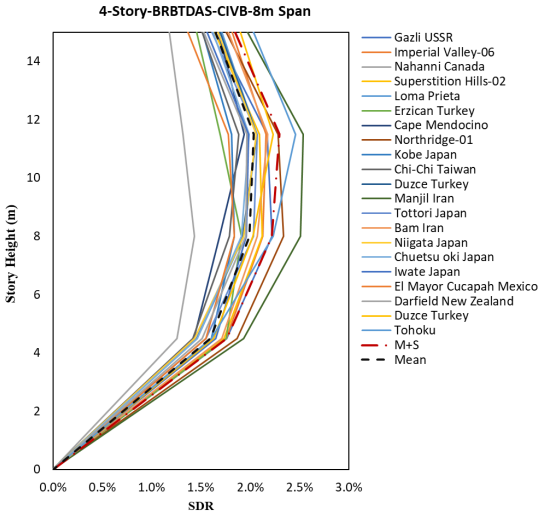
4-Story-BRBTDAS-CIVB-8m Span
Story Height (m)
SDR
0.0%
0.5%
1.0%
1.5%
2.0%
2.5%
3.0%
0
2
4
6
8
10
12
14
Gazli USSR
Imperial Valley-06
Nahanni Canada
Superstition Hills-02
Loma Prieta
Erzican Turkey
Cape Mendocino
Northridge-01
Kobe Japan
Chi-Chi Taiwan
Duzce Turkey
Manjil Iran
Tottori Japan
Bam Iran
Niigata Japan
Chuetsu oki Japan
Iwate Japan
El Mayor Cucapah Mexico
Darfield New Zealand
Duzce Turkey
Tohoku
M+S
Mean

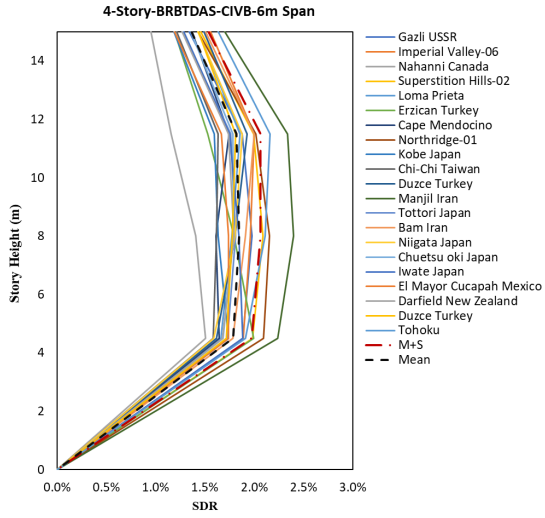
4-Story-BRBTDAS-CIVB-6m Span
Story Height (m)
SDR
0.0%
0.5%
1.0%
1.5%
2.0%
2.5%
3.0%
0
2
4
6
8
10
12
14
Gazli USSR
Imperial Valley-06
Nahanni Canada
Superstition Hills-02
Loma Prieta
Erzican Turkey
Cape Mendocino
Northridge-01
Kobe Japan
Chi-Chi Taiwan
Duzce Turkey
Manjil Iran
Tottori Japan
Bam Iran
Niigata Japan
Chuetsu oki Japan
Iwate Japan
El Mayor Cucapah Mexico
Darfield New Zealand
Duzce Turkey
Tohoku
M+S
Mean

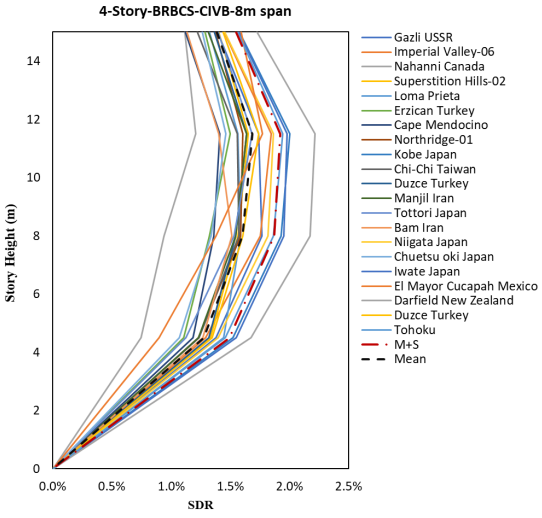
4-Story-BRBCS-CIVB-8m span
Story Height (m)
SDR
0.0%
0.5%
1.0%
1.5%
2.0%
2.5%
0
2
4
6
8
10
12
14
Gazli USSR
Imperial Valley-06
Nahanni Canada
Superstition Hills-02
Loma Prieta
Erzican Turkey
Cape Mendocino
Northridge-01
Kobe Japan
Chi-Chi Taiwan
Duzce Turkey
Manjil Iran
Tottori Japan
Bam Iran
Niigata Japan
Chuetsu oki Japan
Iwate Japan
El Mayor Cucapah Mexico
Darfield New Zealand
Duzce Turkey
Tohoku
M+S
Mean

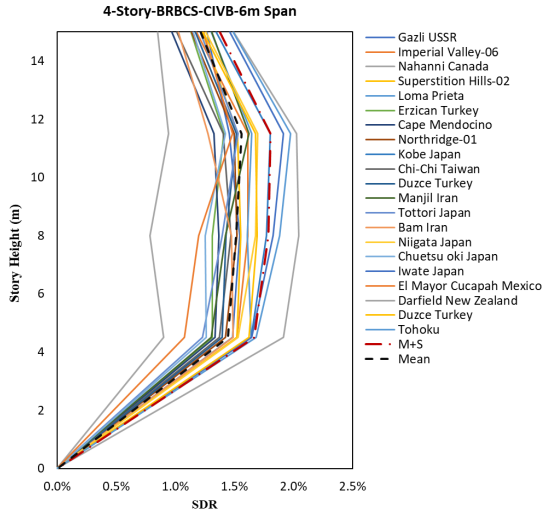
4-Story-BRBCS-CIVB-6m Span
Story Height (m)
SDR
0.0%
0.5%
1.0%
1.5%
2.0%
2.5%
0
2
4
6
8
10
12
14
Gazli USSR
Imperial Valley-06
Nahanni Canada
Superstition Hills-02
Loma Prieta
Erzican Turkey
Cape Mendocino
Northridge-01
Kobe Japan
Chi-Chi Taiwan
Duzce Turkey
Manjil Iran
Tottori Japan
Bam Iran
Niigata Japan
Chuetsu oki Japan
Iwate Japan
El Mayor Cucapah Mexico
Darfield New Zealand
Duzce Turkey
Tohoku
M+S
Mean

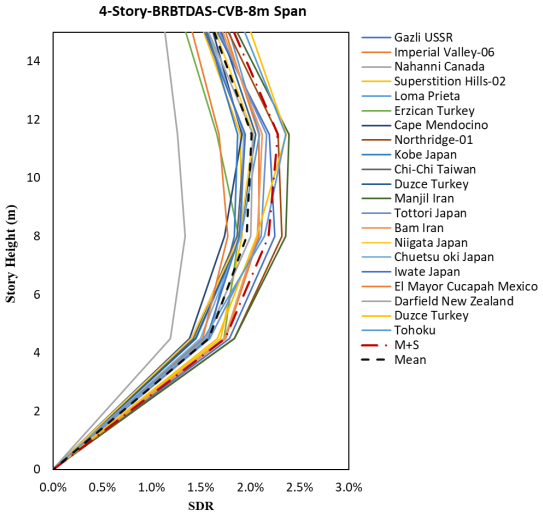
4-Story-BRBTDAS-CVB-8m Span
Story Height (m)
SDR
0.0%
0.5%
1.0%
1.5%
2.0%
2.5%
3.0%
0
2
4
6
8
10
12
14
Gazli USSR
Imperial Valley-06
Nahanni Canada
Superstition Hills-02
Loma Prieta
Erzican Turkey
Cape Mendocino
Northridge-01
Kobe Japan
Chi-Chi Taiwan
Duzce Turkey
Manjil Iran
Tottori Japan
Bam Iran
Niigata Japan
Chuetsu oki Japan
Iwate Japan
El Mayor Cucapah Mexico
Darfield New Zealand
Duzce Turkey
Tohoku
M+S
Mean

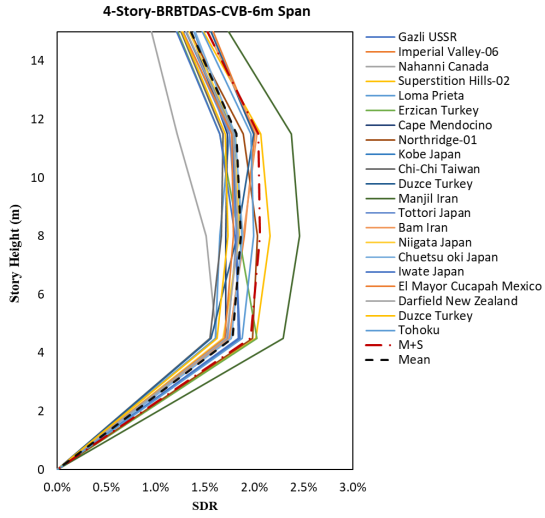
4-Story-BRBTDAS-CVB-6m Span
Story Height (m)
SDR
0.0%
0.5%
1.0%
1.5%
2.0%
2.5%
3.0%
0
2
4
6
8
10
12
14
Gazli USSR
Imperial Valley-06
Nahanni Canada
Superstition Hills-02
Loma Prieta
Erzican Turkey
Cape Mendocino
Northridge-01
Kobe Japan
Chi-Chi Taiwan
Duzce Turkey
Manjil Iran
Tottori Japan
Bam Iran
Niigata Japan
Chuetsu oki Japan
Iwate Japan
El Mayor Cucapah Mexico
Darfield New Zealand
Duzce Turkey
Tohoku
M+S
Mean

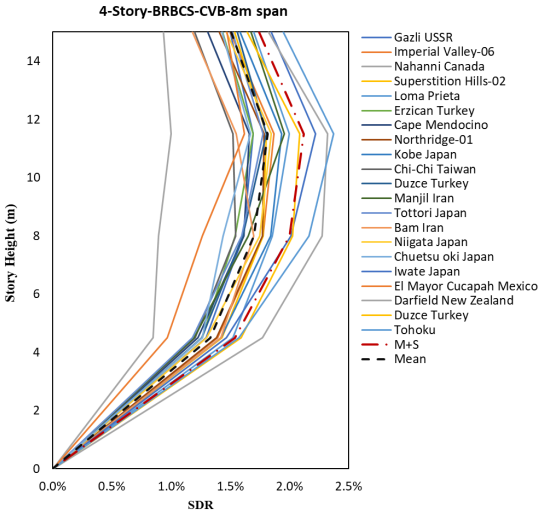
4-Story-BRBCS-CVB-8m span
Story Height (m)
SDR
0.0%
0.5%
1.0%
1.5%
2.0%
2.5%
0
2
4
6
8
10
12
14
Gazli USSR
Imperial Valley-06
Nahanni Canada
Superstition Hills-02
Loma Prieta
Erzican Turkey
Cape Mendocino
Northridge-01
Kobe Japan
Chi-Chi Taiwan
Duzce Turkey
Manjil Iran
Tottori Japan
Bam Iran
Niigata Japan
Chuetsu oki Japan
Iwate Japan
El Mayor Cucapah Mexico
Darfield New Zealand
Duzce Turkey
Tohoku
M+S
Mean

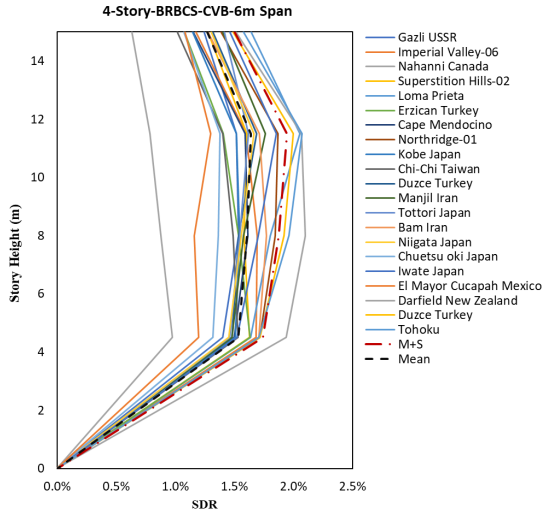
4-Story-BRBCS-CVB-6m Span
Story Height (m)
SDR
0.0%
0.5%
1.0%
1.5%
2.0%
2.5%
0
2
4
6
8
10
12
14
Gazli USSR
Imperial Valley-06
Nahanni Canada
Superstition Hills-02
Loma Prieta
Erzican Turkey
Cape Mendocino
Northridge-01
Kobe Japan
Chi-Chi Taiwan
Duzce Turkey
Manjil Iran
Tottori Japan
Bam Iran
Niigata Japan
Chuetsu oki Japan
Iwate Japan
El Mayor Cucapah Mexico
Darfield New Zealand
Duzce Turkey
Tohoku
M+S
Mean

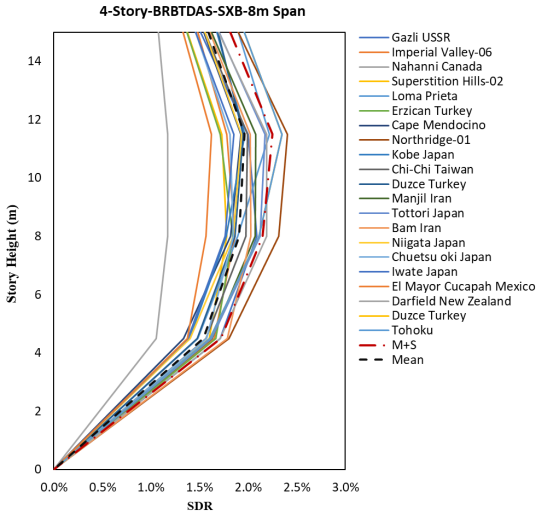
4-Story-BRBTDAS-SXB-8m Span
Story Height (m)
SDR
0.0%
0.5%
1.0%
1.5%
2.0%
2.5%
3.0%
0
2
4
6
8
10
12
14
Gazli USSR
Imperial Valley-06
Nahanni Canada
Superstition Hills-02
Loma Prieta
Erzican Turkey
Cape Mendocino
Northridge-01
Kobe Japan
Chi-Chi Taiwan
Duzce Turkey
Manjil Iran
Tottori Japan
Bam Iran
Niigata Japan
Chuetsu oki Japan
Iwate Japan
El Mayor Cucapah Mexico
Darfield New Zealand
Duzce Turkey
Tohoku
M+S
Mean

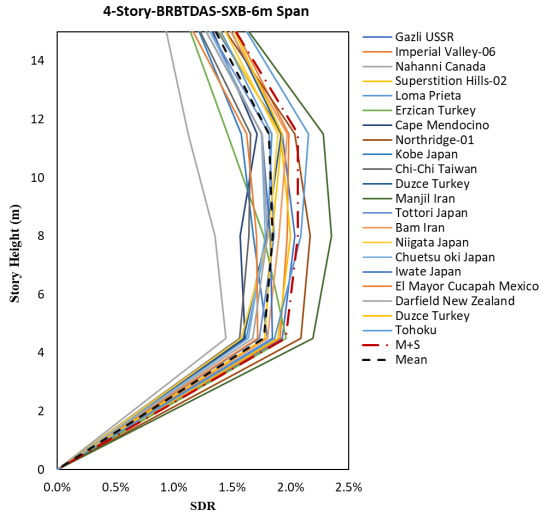
4-Story-BRBTDAS-SXB-6m Span
Story Height (m)
SDR
0.0%
0.5%
1.0%
1.5%
2.0%
2.5%
0
2
4
6
8
10
12
14
Gazli USSR
Imperial Valley-06
Nahanni Canada
Superstition Hills-02
Loma Prieta
Erzican Turkey
Cape Mendocino
Northridge-01
Kobe Japan
Chi-Chi Taiwan
Duzce Turkey
Manjil Iran
Tottori Japan
Bam Iran
Niigata Japan
Chuetsu oki Japan
Iwate Japan
El Mayor Cucapah Mexico
Darfield New Zealand
Duzce Turkey
Tohoku
M+S
Mean

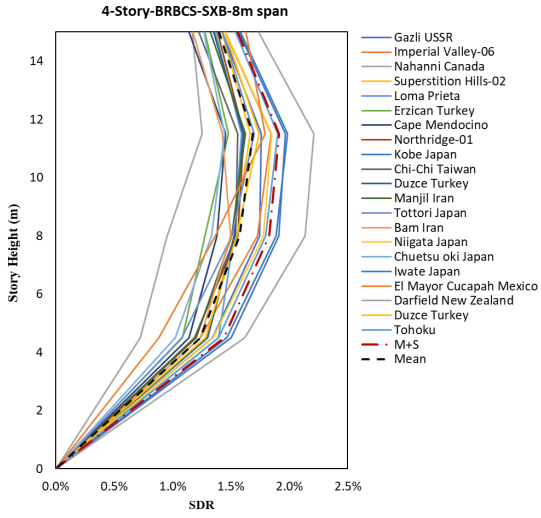
4-Story-BRBCS-SXB-8m span
Story Height (m)
SDR
0.0%
0.5%
1.0%
1.5%
2.0%
2.5%
0
2
4
6
8
10
12
14
Gazli USSR
Imperial Valley-06
Nahanni Canada
Superstition Hills-02
Loma Prieta
Erzican Turkey
Cape Mendocino
Northridge-01
Kobe Japan
Chi-Chi Taiwan
Duzce Turkey
Manjil Iran
Tottori Japan
Bam Iran
Niigata Japan
Chuetsu oki Japan
Iwate Japan
El Mayor Cucapah Mexico
Darfield New Zealand
Duzce Turkey
Tohoku
M+S
Mean

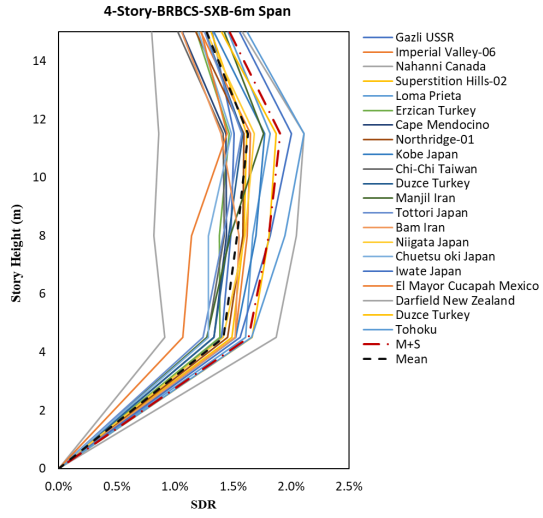
4-Story-BRBCS-SXB-6m Span
Story Height (m)
SDR
0.0%
0.5%
1.0%
1.5%
2.0%
2.5%
0
2
4
6
8
10
12
14
Gazli USSR
Imperial Valley-06
Nahanni Canada
Superstition Hills-02
Loma Prieta
Erzican Turkey
Cape Mendocino
Northridge-01
Kobe Japan
Chi-Chi Taiwan
Duzce Turkey
Manjil Iran
Tottori Japan
Bam Iran
Niigata Japan
Chuetsu oki Japan
Iwate Japan
El Mayor Cucapah Mexico
Darfield New Zealand
Duzce Turkey
Tohoku
M+S
Mean

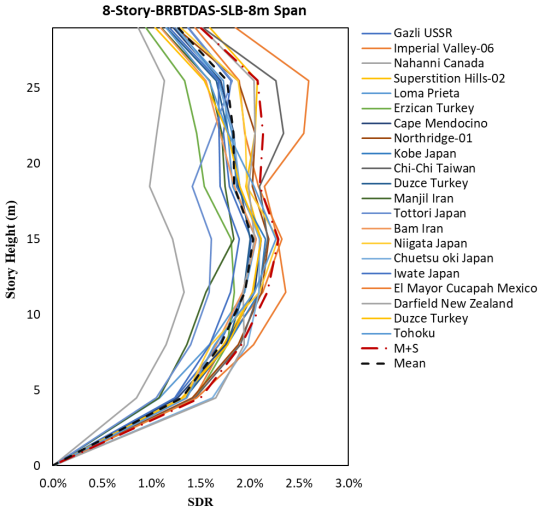
8-Story-BRBTDAS-SLB-8m Span
Story Height (m)
SDR
0
5
10
15
20
25
0.0%
0.5%
1.0%
1.5%
2.0%
2.5%
3.0%
Gazli USSR
Imperial Valley-06
Nahanni Canada
Superstition Hills-02
Loma Prieta
Erzican Turkey
Cape Mendocino
Northridge-01
Kobe Japan
Chi-Chi Taiwan
Duzce Turkey
Manjil Iran
Tottori Japan
Bam Iran
Niigata Japan
Chuetsu oki Japan
Iwate Japan
El Mayor Cucapah Mexico
Darfield New Zealand
Duzce Turkey
Tohoku
M+S
Mean

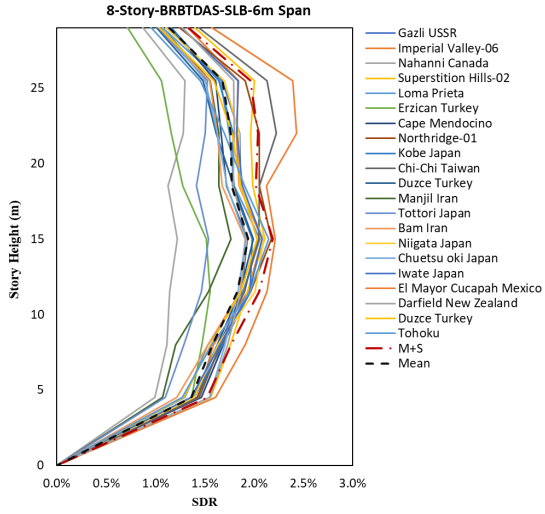
8-Story-BRBTDAS-SLB-6m Span
Story Height (m)
SDR
0
5
10
15
20
25
0.0%
0.5%
1.0%
1.5%
2.0%
2.5%
3.0%
Gazli USSR
Imperial Valley-06
Nahanni Canada
Superstition Hills-02
Loma Prieta
Erzican Turkey
Cape Mendocino
Northridge-01
Kobe Japan
Chi-Chi Taiwan
Duzce Turkey
Manjil Iran
Tottori Japan
Bam Iran
Niigata Japan
Chuetsu oki Japan
Iwate Japan
El Mayor Cucapah Mexico
Darfield New Zealand
Duzce Turkey
Tohoku
M+S
Mean

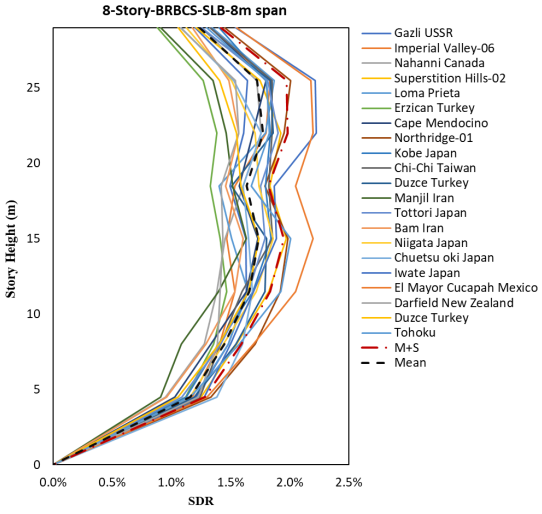
8-Story-BRBCS-SLB-8m span
Story Height (m)
SDR
0
5
10
15
20
25
0.0%
0.5%
1.0%
1.5%
2.0%
2.5%
Gazli USSR
Imperial Valley-06
Nahanni Canada
Superstition Hills-02
Loma Prieta
Erzican Turkey
Cape Mendocino
Northridge-01
Kobe Japan
Chi-Chi Taiwan
Duzce Turkey
Manjil Iran
Tottori Japan
Bam Iran
Niigata Japan
Chuetsu oki Japan
Iwate Japan
El Mayor Cucapah Mexico
Darfield New Zealand
Duzce Turkey
Tohoku
M+S
Mean

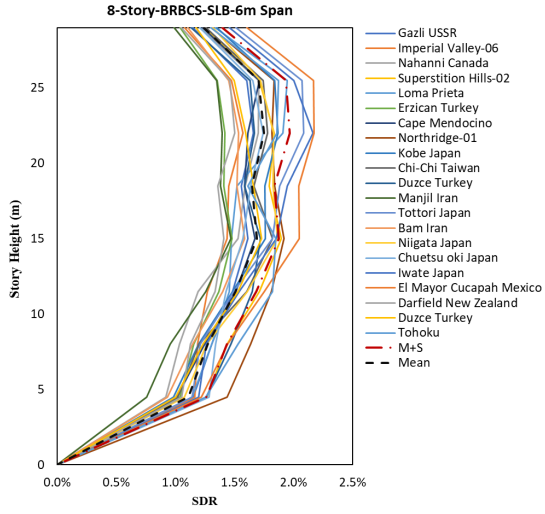
8-Story-BRBCS-SLB-6m Span
Story Height (m)
SDR
0
5
10
15
20
25
0.0%
0.5%
1.0%
1.5%
2.0%
2.5%
Gazli USSR
Imperial Valley-06
Nahanni Canada
Superstition Hills-02
Loma Prieta
Erzican Turkey
Cape Mendocino
Northridge-01
Kobe Japan
Chi-Chi Taiwan
Duzce Turkey
Manjil Iran
Tottori Japan
Bam Iran
Niigata Japan
Chuetsu oki Japan
Iwate Japan
El Mayor Cucapah Mexico
Darfield New Zealand
Duzce Turkey
Tohoku
M+S
Mean

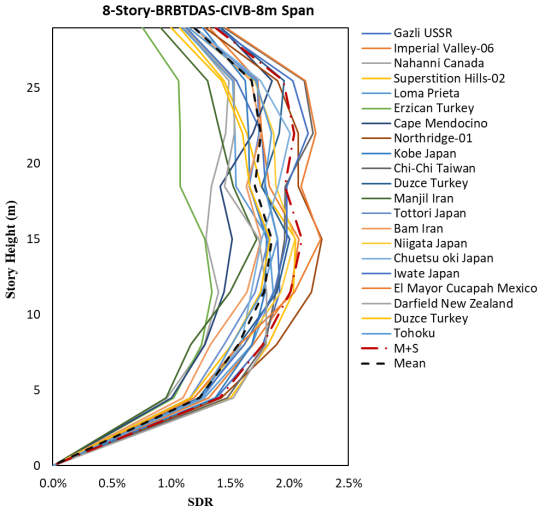
8-Story-BRBTDAS-CIVB-8m Span
Story Height (m)
SDR
0
5
10
15
20
25
0.0%
0.5%
1.0%
1.5%
2.0%
2.5%
Gazli USSR
Imperial Valley-06
Nahanni Canada
Superstition Hills-02
Loma Prieta
Erzican Turkey
Cape Mendocino
Northridge-01
Kobe Japan
Chi-Chi Taiwan
Duzce Turkey
Manjil Iran
Tottori Japan
Bam Iran
Niigata Japan
Chuetsu oki Japan
Iwate Japan
El Mayor Cucapah Mexico
Darfield New Zealand
Duzce Turkey
Tohoku
M+S
Mean

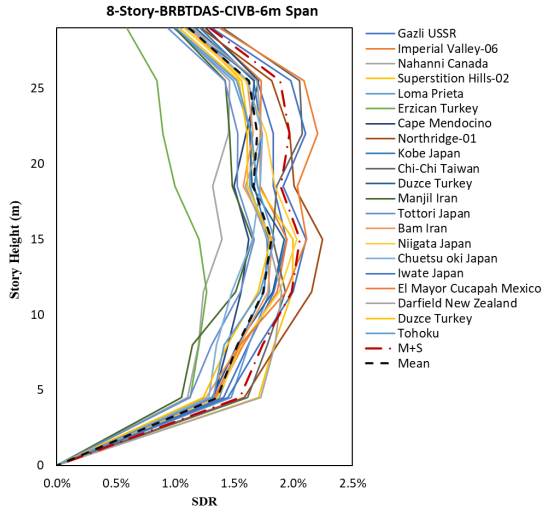
8-Story-BRBTDAS-CIVB-6m Span
Story Height (m)
SDR
0
5
10
15
20
25
0.0%
0.5%
1.0%
1.5%
2.0%
2.5%
Gazli USSR
Imperial Valley-06
Nahanni Canada
Superstition Hills-02
Loma Prieta
Erzican Turkey
Cape Mendocino
Northridge-01
Kobe Japan
Chi-Chi Taiwan
Duzce Turkey
Manjil Iran
Tottori Japan
Bam Iran
Niigata Japan
Chuetsu oki Japan
Iwate Japan
El Mayor Cucapah Mexico
Darfield New Zealand
Duzce Turkey
Tohoku
M+S
Mean

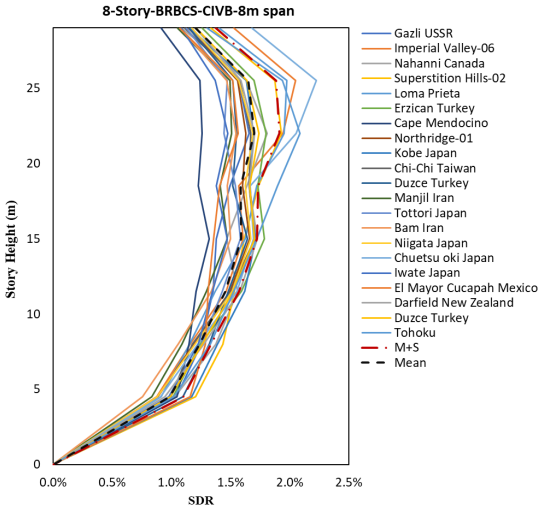
8-Story-BRBCS-CIVB-8m span
Story Height (m)
SDR
0
5
10
15
20
25
0.0%
0.5%
1.0%
1.5%
2.0%
2.5%
Gazli USSR
Imperial Valley-06
Nahanni Canada
Superstition Hills-02
Loma Prieta
Erzican Turkey
Cape Mendocino
Northridge-01
Kobe Japan
Chi-Chi Taiwan
Duzce Turkey
Manjil Iran
Tottori Japan
Bam Iran
Niigata Japan
Chuetsu oki Japan
Iwate Japan
El Mayor Cucapah Mexico
Darfield New Zealand
Duzce Turkey
Tohoku
M+S
Mean

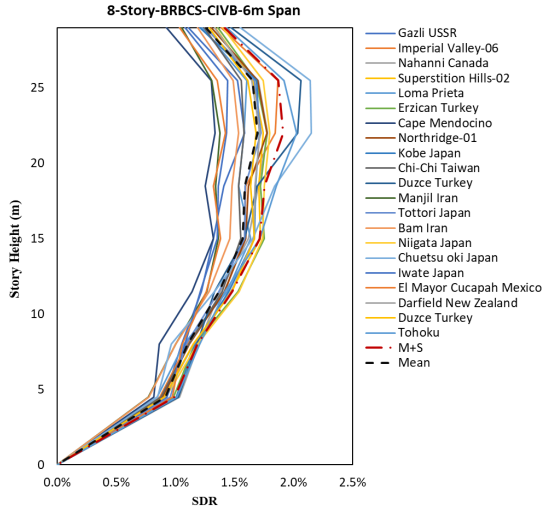
8-Story-BRBCS-CIVB-6m Span
Story Height (m)
SDR
0
5
10
15
20
25
0.0%
0.5%
1.0%
1.5%
2.0%
2.5%
Gazli USSR
Imperial Valley-06
Nahanni Canada
Superstition Hills-02
Loma Prieta
Erzican Turkey
Cape Mendocino
Northridge-01
Kobe Japan
Chi-Chi Taiwan
Duzce Turkey
Manjil Iran
Tottori Japan
Bam Iran
Niigata Japan
Chuetsu oki Japan
Iwate Japan
El Mayor Cucapah Mexico
Darfield New Zealand
Duzce Turkey
Tohoku
M+S
Mean

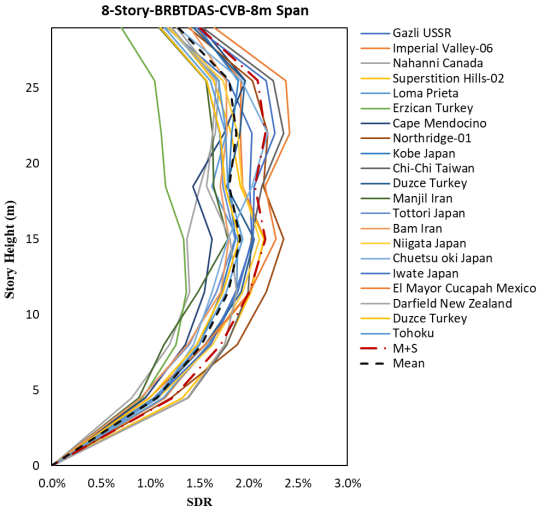
8-Story-BRBTDAS-CVB-8m Span
Story Height (m)
SDR
0.0% 0.5% 1.0% 1.5% 2.0% 2.5% 3.0%
0 5 10 15 20 25
Gazli USSR
Imperial Valley-06
Nahanni Canada
Superstition Hills-02
Loma Prieta
Erzican Turkey
Cape Mendocino
Northridge-01
Kobe Japan
Chi-Chi Taiwan
Duzce Turkey
Manjil Iran
Tottori Japan
Bam Iran
Niigata Japan
Chuetsu oki Japan
Iwate Japan
El Mayor Cucapah Mexico
Darfield New Zealand
Duzce Turkey
Tohoku
M+S
Mean

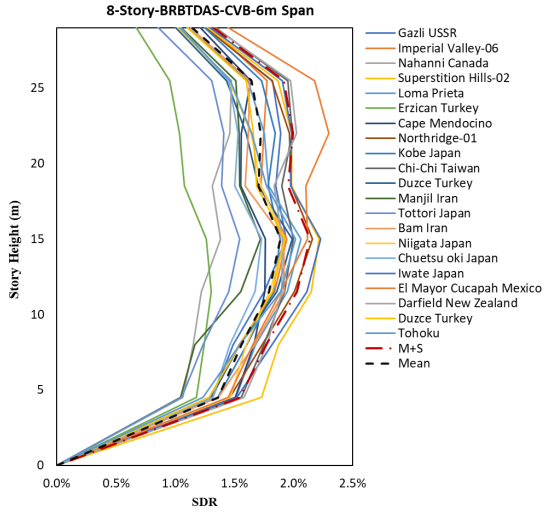
8-Story-BRBTDAS-CVB-6m Span
Story Height (m)
SDR
0.0% 0.5% 1.0% 1.5% 2.0% 2.5%
0 5 10 15 20 25
Gazli USSR
Imperial Valley-06
Nahanni Canada
Superstition Hills-02
Loma Prieta
Erzican Turkey
Cape Mendocino
Northridge-01
Kobe Japan
Chi-Chi Taiwan
Duzce Turkey
Manjil Iran
Tottori Japan
Bam Iran
Niigata Japan
Chuetsu oki Japan
Iwate Japan
El Mayor Cucapah Mexico
Darfield New Zealand
Duzce Turkey
Tohoku
M+S
Mean

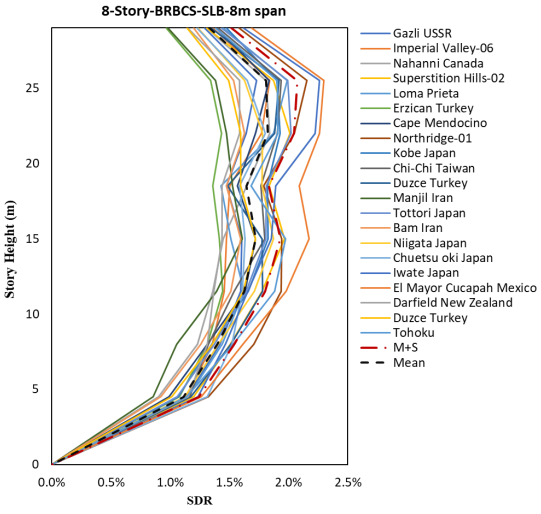
8-Story-BRBCS-SLB-8m span
Story Height (m)
SDR
0.0% 0.5% 1.0% 1.5% 2.0% 2.5%
0 5 10 15 20 25
Gazli USSR
Imperial Valley-06
Nahanni Canada
Superstition Hills-02
Loma Prieta
Erzican Turkey
Cape Mendocino
Northridge-01
Kobe Japan
Chi-Chi Taiwan
Duzce Turkey
Manjil Iran
Tottori Japan
Bam Iran
Niigata Japan
Chuetsu oki Japan
Iwate Japan
El Mayor Cucapah Mexico
Darfield New Zealand
Duzce Turkey
Tohoku
M+S
Mean

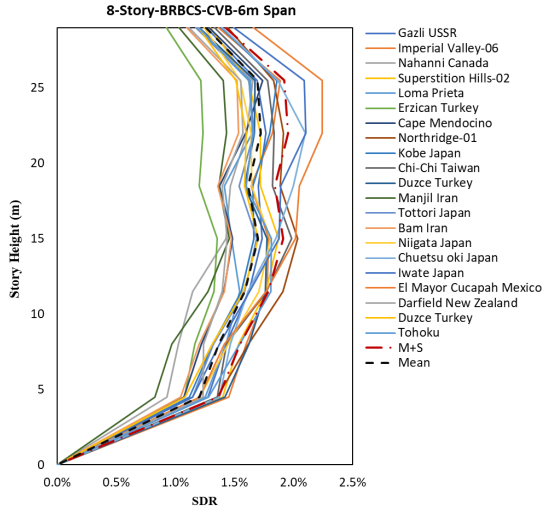
8-Story-BRBCS-CVB-6m Span
Story Height (m)
SDR
0.0% 0.5% 1.0% 1.5% 2.0% 2.5%
0 5 10 15 20 25
Gazli USSR
Imperial Valley-06
Nahanni Canada
Superstition Hills-02
Loma Prieta
Erzican Turkey
Cape Mendocino
Northridge-01
Kobe Japan
Chi-Chi Taiwan
Duzce Turkey
Manjil Iran
Tottori Japan
Bam Iran
Niigata Japan
Chuetsu oki Japan
Iwate Japan
El Mayor Cucapah Mexico
Darfield New Zealand
Duzce Turkey
Tohoku
M+S
Mean

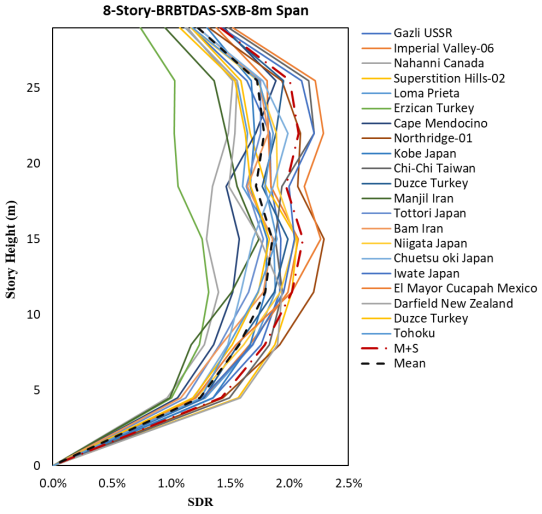
8-Story-BRBTDAS-SXB-8m Span
Story Height (m)
SDR
0
5
10
15
20
25
0.0%
0.5%
1.0%
1.5%
2.0%
2.5%
Gazli USSR
Imperial Valley-06
Nahanni Canada
Superstition Hills-02
Loma Prieta
Erzican Turkey
Cape Mendocino
Northridge-01
Kobe Japan
Chi-Chi Taiwan
Duzce Turkey
Manjil Iran
Tottori Japan
Bam Iran
Niigata Japan
Chuetsu oki Japan
Iwate Japan
El Mayor Cucapah Mexico
Darfield New Zealand
Duzce Turkey
Tohoku
M+S
Mean

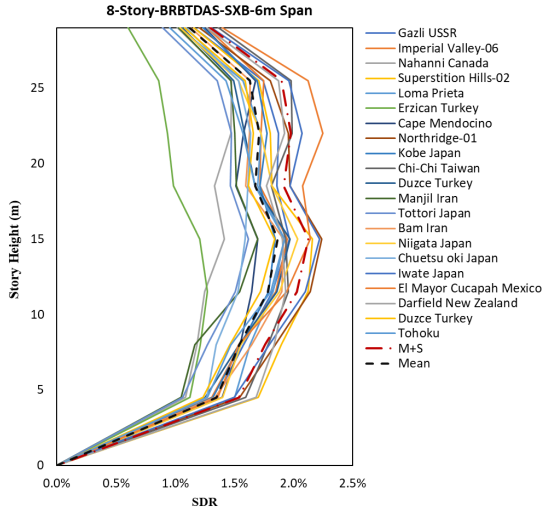
8-Story-BRBTDAS-SXB-6m Span
Story Height (m)
SDR
0
5
10
15
20
25
0.0%
0.5%
1.0%
1.5%
2.0%
2.5%
Gazli USSR
Imperial Valley-06
Nahanni Canada
Superstition Hills-02
Loma Prieta
Erzican Turkey
Cape Mendocino
Northridge-01
Kobe Japan
Chi-Chi Taiwan
Duzce Turkey
Manjil Iran
Tottori Japan
Bam Iran
Niigata Japan
Chuetsu oki Japan
Iwate Japan
El Mayor Cucapah Mexico
Darfield New Zealand
Duzce Turkey
Tohoku
M+S
Mean

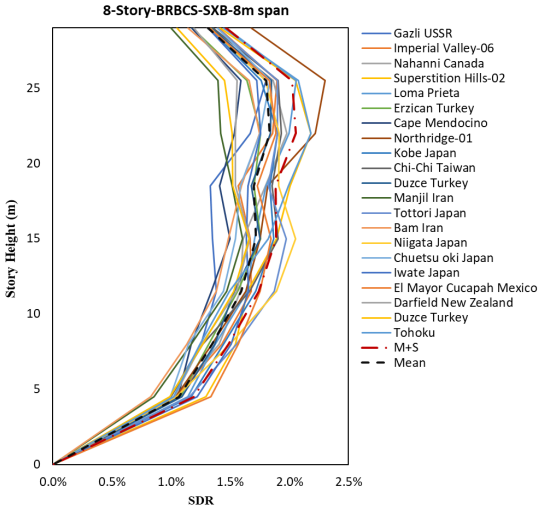
8-Story-BRBCS-SXB-8m span
Story Height (m)
SDR
0
5
10
15
20
25
0.0%
0.5%
1.0%
1.5%
2.0%
2.5%
Gazli USSR
Imperial Valley-06
Nahanni Canada
Superstition Hills-02
Loma Prieta
Erzican Turkey
Cape Mendocino
Northridge-01
Kobe Japan
Chi-Chi Taiwan
Duzce Turkey
Manjil Iran
Tottori Japan
Bam Iran
Niigata Japan
Chuetsu oki Japan
Iwate Japan
El Mayor Cucapah Mexico
Darfield New Zealand
Duzce Turkey
Tohoku
M+S
Mean

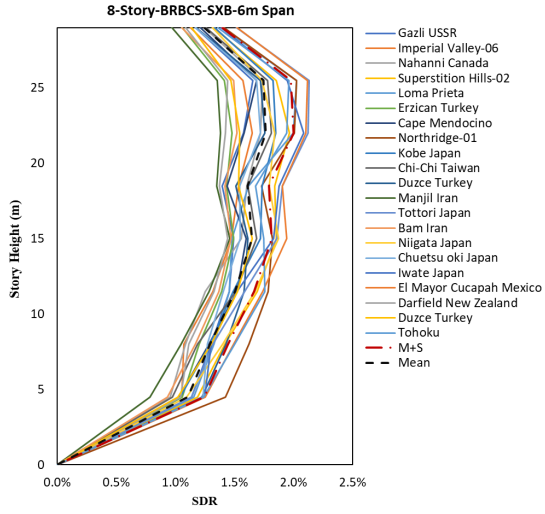
8-Story-BRBCS-SXB-6m Span
Story Height (m)
SDR
0
5
10
15
20
25
0.0%
0.5%
1.0%
1.5%
2.0%
2.5%
Gazli USSR
Imperial Valley-06
Nahanni Canada
Superstition Hills-02
Loma Prieta
Erzican Turkey
Cape Mendocino
Northridge-01
Kobe Japan
Chi-Chi Taiwan
Duzce Turkey
Manjil Iran
Tottori Japan
Bam Iran
Niigata Japan
Chuetsu oki Japan
Iwate Japan
El Mayor Cucapah Mexico
Darfield New Zealand
Duzce Turkey
Tohoku
M+S
Mean

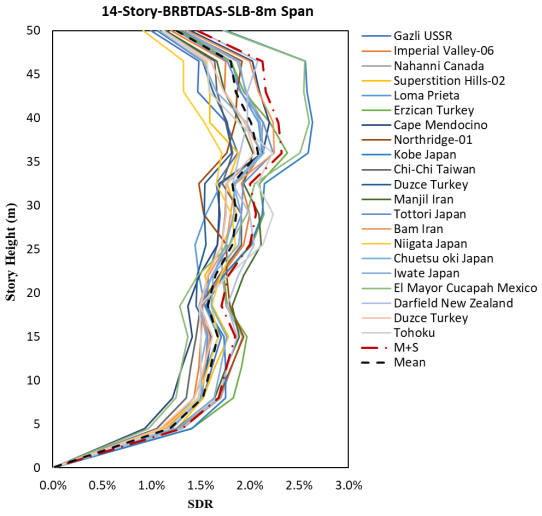
14-Story-BRBTDAS-SLB-8m Span
Story Height (m)
SDR
0.0% 0.5% 1.0% 1.5% 2.0% 2.5% 3.0%
0 5 10 15 20 25 30 35 40 45 50
Gazli USSR
Imperial Valley-06
Nahanni Canada
Superstition Hills-02
Loma Prieta
Erzican Turkey
Cape Mendocino
Northridge-01
Kobe Japan
Chi-Chi Taiwan
Duzce Turkey
Manjil Iran
Tottori Japan
Bam Iran
Niigata Japan
Chuetsu oki Japan
Iwate Japan
El Mayor Cucapah Mexico
Darfield New Zealand
Duzce Turkey
Tohoku
M+S
Mean

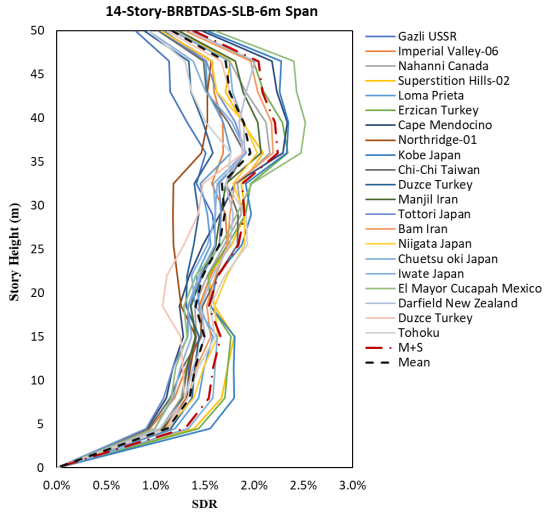
14-Story-BRBTDAS-SLB-6m Span
Story Height (m)
SDR
0.0% 0.5% 1.0% 1.5% 2.0% 2.5% 3.0%
0 5 10 15 20 25 30 35 40 45 50
Gazli USSR
Imperial Valley-06
Nahanni Canada
Superstition Hills-02
Loma Prieta
Erzican Turkey
Cape Mendocino
Northridge-01
Kobe Japan
Chi-Chi Taiwan
Duzce Turkey
Manjil Iran
Tottori Japan
Bam Iran
Niigata Japan
Chuetsu oki Japan
Iwate Japan
El Mayor Cucapah Mexico
Darfield New Zealand
Duzce Turkey
Tohoku
M+S
Mean

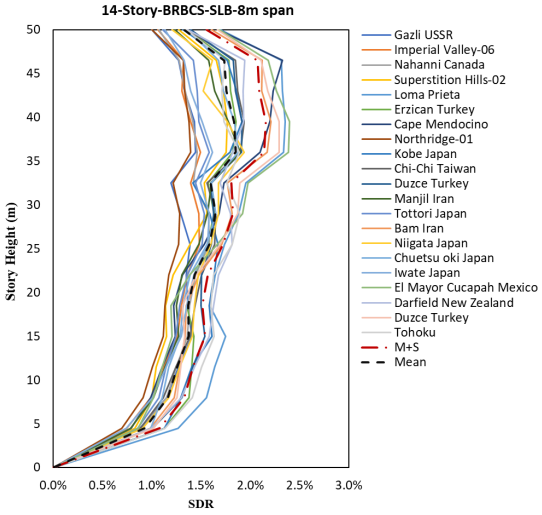
14-Story-BRBCS-SLB-8m span
Story Height (m)
SDR
0.0% 0.5% 1.0% 1.5% 2.0% 2.5% 3.0%
0 5 10 15 20 25 30 35 40 45 50
Gazli USSR
Imperial Valley-06
Nahanni Canada
Superstition Hills-02
Loma Prieta
Erzican Turkey
Cape Mendocino
Northridge-01
Kobe Japan
Chi-Chi Taiwan
Duzce Turkey
Manjil Iran
Tottori Japan
Bam Iran
Niigata Japan
Chuetsu oki Japan
Iwate Japan
El Mayor Cucapah Mexico
Darfield New Zealand
Duzce Turkey
Tohoku
M+S
Mean

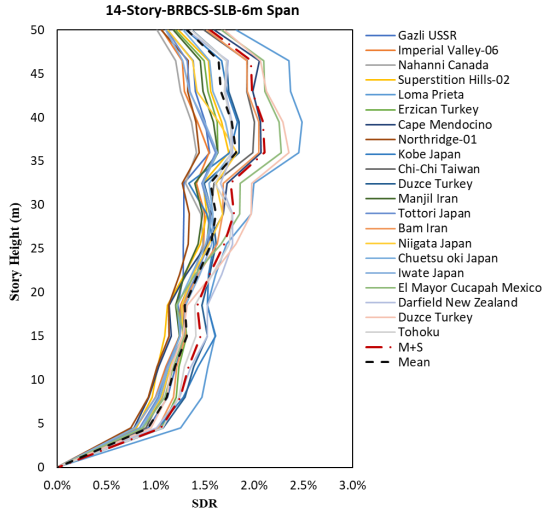
14-Story-BRBCS-SLB-6m Span
Story Height (m)
SDR
0.0% 0.5% 1.0% 1.5% 2.0% 2.5% 3.0%
0 5 10 15 20 25 30 35 40 45 50
Gazli USSR
Imperial Valley-06
Nahanni Canada
Superstition Hills-02
Loma Prieta
Erzican Turkey
Cape Mendocino
Northridge-01
Kobe Japan
Chi-Chi Taiwan
Duzce Turkey
Manjil Iran
Tottori Japan
Bam Iran
Niigata Japan
Chuetsu oki Japan
Iwate Japan
El Mayor Cucapah Mexico
Darfield New Zealand
Duzce Turkey
Tohoku
M+S
Mean

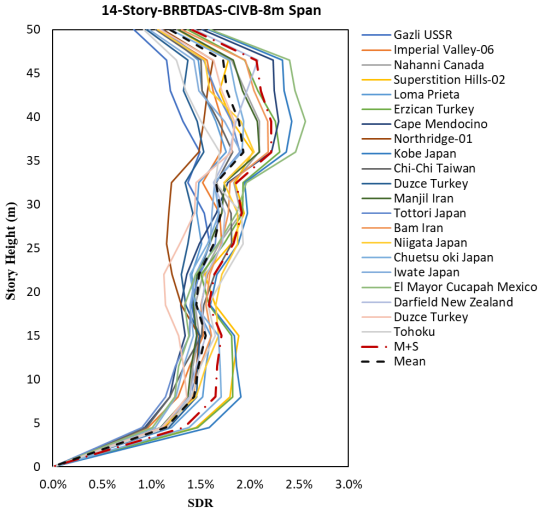
14-Story-BRBTDAS-CIVB-8m Span
Story Height (m)
SDR
0
5
10
15
20
25
30
35
40
45
50
0.0%
0.5%
1.0%
1.5%
2.0%
2.5%
3.0%
Gazli USSR
Imperial Valley-06
Nahanni Canada
Superstition Hills-02
Loma Prieta
Erzican Turkey
Cape Mendocino
Northridge-01
Kobe Japan
Chi-Chi Taiwan
Duzce Turkey
Manjil Iran
Tottori Japan
Bam Iran
Niigata Japan
Chuetsu oki Japan
Iwate Japan
El Mayor Cucapah Mexico
Darfield New Zealand
Duzce Turkey
Tohoku
M+S
Mean

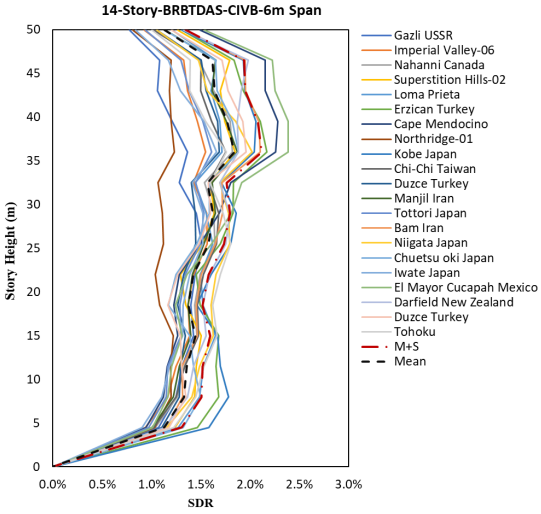
14-Story-BRBTDAS-CIVB-6m Span
Story Height (m)
SDR
0
5
10
15
20
25
30
35
40
45
50
0.0%
0.5%
1.0%
1.5%
2.0%
2.5%
3.0%
Gazli USSR
Imperial Valley-06
Nahanni Canada
Superstition Hills-02
Loma Prieta
Erzican Turkey
Cape Mendocino
Northridge-01
Kobe Japan
Chi-Chi Taiwan
Duzce Turkey
Manjil Iran
Tottori Japan
Bam Iran
Niigata Japan
Chuetsu oki Japan
Iwate Japan
El Mayor Cucapah Mexico
Darfield New Zealand
Duzce Turkey
Tohoku
M+S
Mean

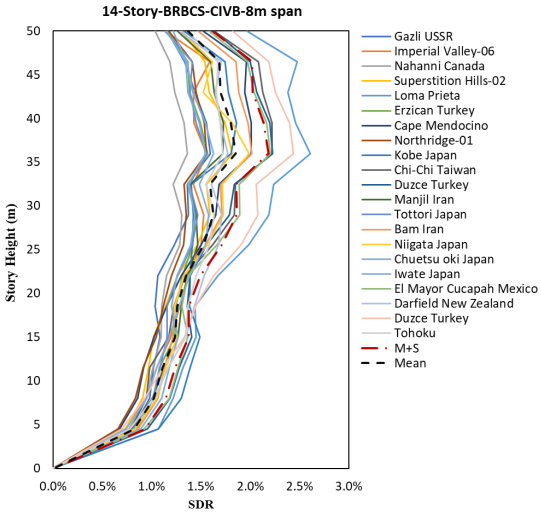
14-Story-BRBCS-CIVB-8m span
Story Height (m)
SDR
0
5
10
15
20
25
30
35
40
45
50
0.0%
0.5%
1.0%
1.5%
2.0%
2.5%
3.0%
Gazli USSR
Imperial Valley-06
Nahanni Canada
Superstition Hills-02
Loma Prieta
Erzican Turkey
Cape Mendocino
Northridge-01
Kobe Japan
Chi-Chi Taiwan
Duzce Turkey
Manjil Iran
Tottori Japan
Bam Iran
Niigata Japan
Chuetsu oki Japan
Iwate Japan
El Mayor Cucapah Mexico
Darfield New Zealand
Duzce Turkey
Tohoku
M+S
Mean

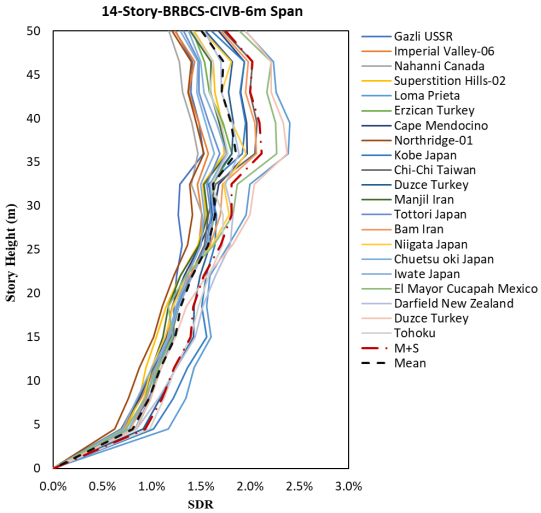
14-Story-BRBCS-CIVB-6m Span
Story Height (m)
SDR
0
5
10
15
20
25
30
35
40
45
50
0.0%
0.5%
1.0%
1.5%
2.0%
2.5%
3.0%
Gazli USSR
Imperial Valley-06
Nahanni Canada
Superstition Hills-02
Loma Prieta
Erzican Turkey
Cape Mendocino
Northridge-01
Kobe Japan
Chi-Chi Taiwan
Duzce Turkey
Manjil Iran
Tottori Japan
Bam Iran
Niigata Japan
Chuetsu oki Japan
Iwate Japan
El Mayor Cucapah Mexico
Darfield New Zealand
Duzce Turkey
Tohoku
M+S
Mean

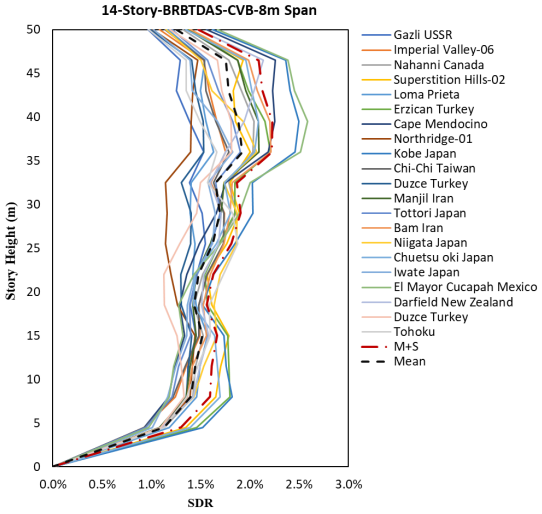
14-Story-BRBTDAS-CVB-8m Span
Story Height (m)
SDR
0.0% 0.5% 1.0% 1.5% 2.0% 2.5% 3.0%
0 5 10 15 20 25 30 35 40 45 50
Gazli USSR
Imperial Valley-06
Nahanni Canada
Superstition Hills-02
Loma Prieta
Erzican Turkey
Cape Mendocino
Northridge-01
Kobe Japan
Chi-Chi Taiwan
Duzce Turkey
Manjil Iran
Tottori Japan
Bam Iran
Niigata Japan
Chuetsu oki Japan
Iwate Japan
El Mayor Cucapah Mexico
Darfield New Zealand
Duzce Turkey
Tohoku
M+S
Mean

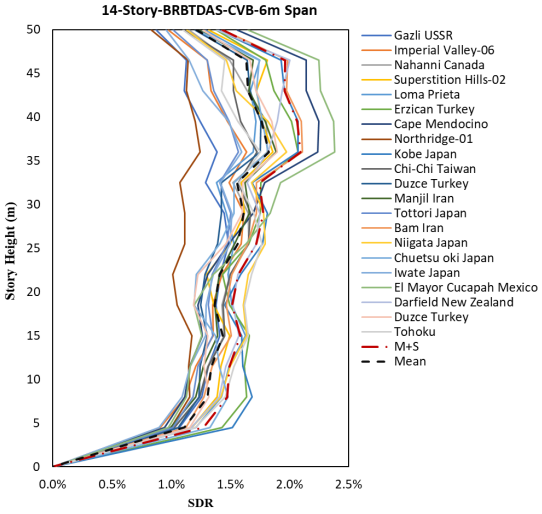
14-Story-BRBTDAS-CVB-6m Span
Story Height (m)
SDR
0.0% 0.5% 1.0% 1.5% 2.0% 2.5%
0 5 10 15 20 25 30 35 40 45 50
Gazli USSR
Imperial Valley-06
Nahanni Canada
Superstition Hills-02
Loma Prieta
Erzican Turkey
Cape Mendocino
Northridge-01
Kobe Japan
Chi-Chi Taiwan
Duzce Turkey
Manjil Iran
Tottori Japan
Bam Iran
Niigata Japan
Chuetsu oki Japan
Iwate Japan
El Mayor Cucapah Mexico
Darfield New Zealand
Duzce Turkey
Tohoku
M+S
Mean

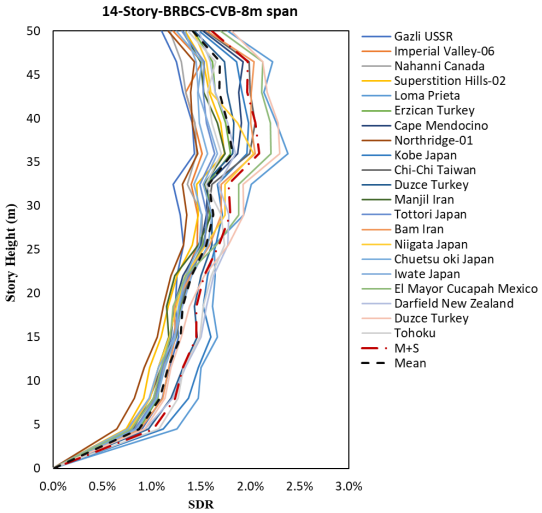
14-Story-BRBCS-CVB-8m span
Story Height (m)
SDR
0.0% 0.5% 1.0% 1.5% 2.0% 2.5% 3.0%
0 5 10 15 20 25 30 35 40 45 50
Gazli USSR
Imperial Valley-06
Nahanni Canada
Superstition Hills-02
Loma Prieta
Erzican Turkey
Cape Mendocino
Northridge-01
Kobe Japan
Chi-Chi Taiwan
Duzce Turkey
Manjil Iran
Tottori Japan
Bam Iran
Niigata Japan
Chuetsu oki Japan
Iwate Japan
El Mayor Cucapah Mexico
Darfield New Zealand
Duzce Turkey
Tohoku
M+S
Mean

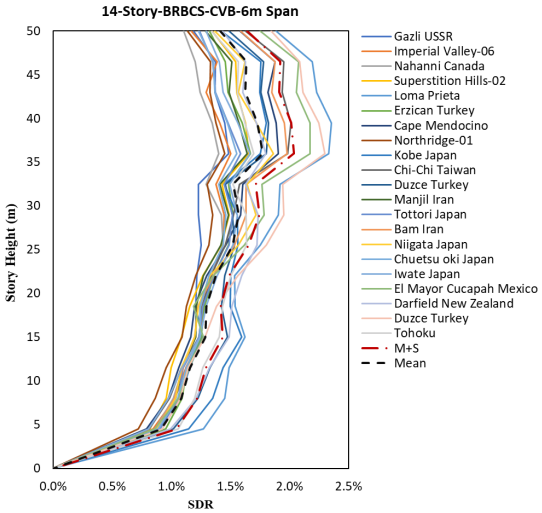
14-Story-BRBCS-CVB-6m Span
Story Height (m)
SDR
0.0% 0.5% 1.0% 1.5% 2.0% 2.5%
0 5 10 15 20 25 30 35 40 45 50
Gazli USSR
Imperial Valley-06
Nahanni Canada
Superstition Hills-02
Loma Prieta
Erzican Turkey
Cape Mendocino
Northridge-01
Kobe Japan
Chi-Chi Taiwan
Duzce Turkey
Manjil Iran
Tottori Japan
Bam Iran
Niigata Japan
Chuetsu oki Japan
Iwate Japan
El Mayor Cucapah Mexico
Darfield New Zealand
Duzce Turkey
Tohoku
M+S
Mean

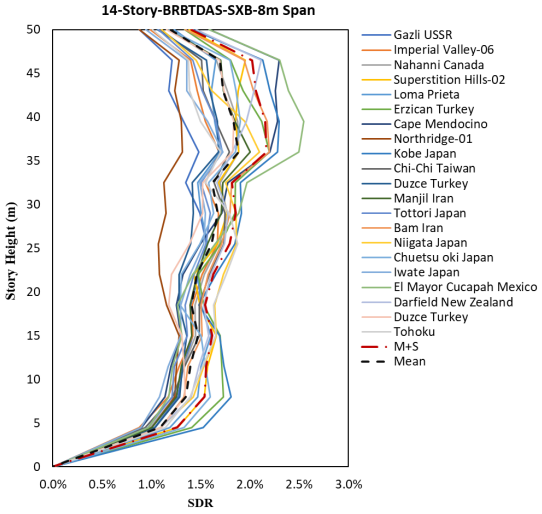
14-Story-BRBTDAS-SXB-8m Span
Story Height (m)
SDR
0
5
10
15
20
25
30
35
40
45
50
0.0%
0.5%
1.0%
1.5%
2.0%
2.5%
3.0%
Gazli USSR
Imperial Valley-06
Nahanni Canada
Superstition Hills-02
Loma Prieta
Erzican Turkey
Cape Mendocino
Northridge-01
Kobe Japan
Chi-Chi Taiwan
Duzce Turkey
Manjil Iran
Tottori Japan
Bam Iran
Niigata Japan
Chuetsu oki Japan
Iwate Japan
El Mayor Cucapah Mexico
Darfield New Zealand
Duzce Turkey
Tohoku
M+S
Mean

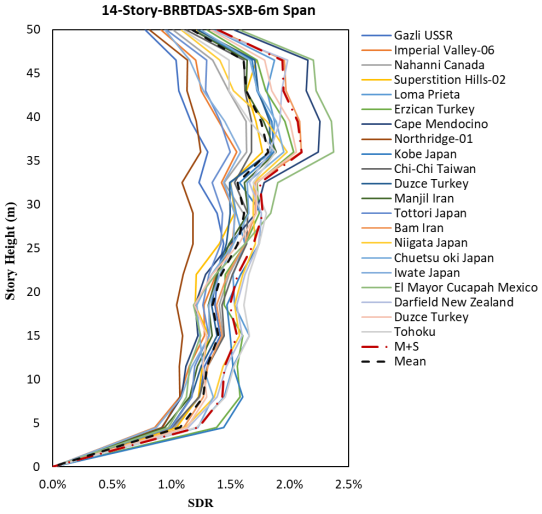
14-Story-BRBTDAS-SXB-6m Span
Story Height (m)
SDR
0
5
10
15
20
25
30
35
40
45
50
0.0%
0.5%
1.0%
1.5%
2.0%
2.5%
Gazli USSR
Imperial Valley-06
Nahanni Canada
Superstition Hills-02
Loma Prieta
Erzican Turkey
Cape Mendocino
Northridge-01
Kobe Japan
Chi-Chi Taiwan
Duzce Turkey
Manjil Iran
Tottori Japan
Bam Iran
Niigata Japan
Chuetsu oki Japan
Iwate Japan
El Mayor Cucapah Mexico
Darfield New Zealand
Duzce Turkey
Tohoku
M+S
Mean

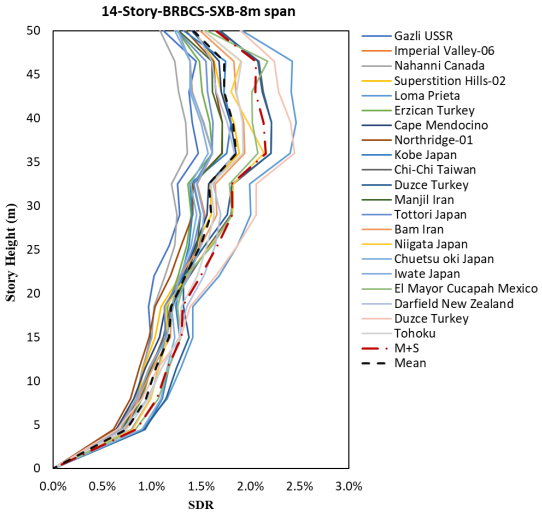
14-Story-BRBCS-SXB-8m span
Story Height (m)
SDR
0
5
10
15
20
25
30
35
40
45
50
0.0%
0.5%
1.0%
1.5%
2.0%
2.5%
3.0%
Gazli USSR
Imperial Valley-06
Nahanni Canada
Superstition Hills-02
Loma Prieta
Erzican Turkey
Cape Mendocino
Northridge-01
Kobe Japan
Chi-Chi Taiwan
Duzce Turkey
Manjil Iran
Tottori Japan
Bam Iran
Niigata Japan
Chuetsu oki Japan
Iwate Japan
El Mayor Cucapah Mexico
Darfield New Zealand
Duzce Turkey
Tohoku
M+S
Mean

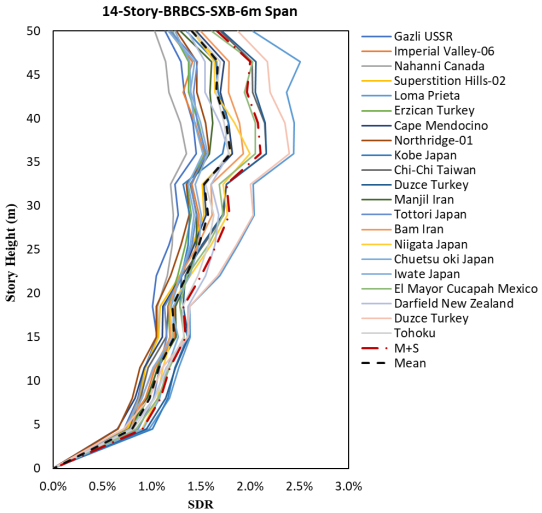
14-Story-BRBCS-SXB-6m Span
Story Height (m)
SDR
0
5
10
15
20
25
30
35
40
45
50
0.0%
0.5%
1.0%
1.5%
2.0%
2.5%
3.0%
Gazli USSR
Imperial Valley-06
Nahanni Canada
Superstition Hills-02
Loma Prieta
Erzican Turkey
Cape Mendocino
Northridge-01
Kobe Japan
Chi-Chi Taiwan
Duzce Turkey
Manjil Iran
Tottori Japan
Bam Iran
Niigata Japan
Chuetsu oki Japan
Iwate Japan
El Mayor Cucapah Mexico
Darfield New Zealand
Duzce Turkey
Tohoku
M+S
Mean

Appendix E: Base shear demand

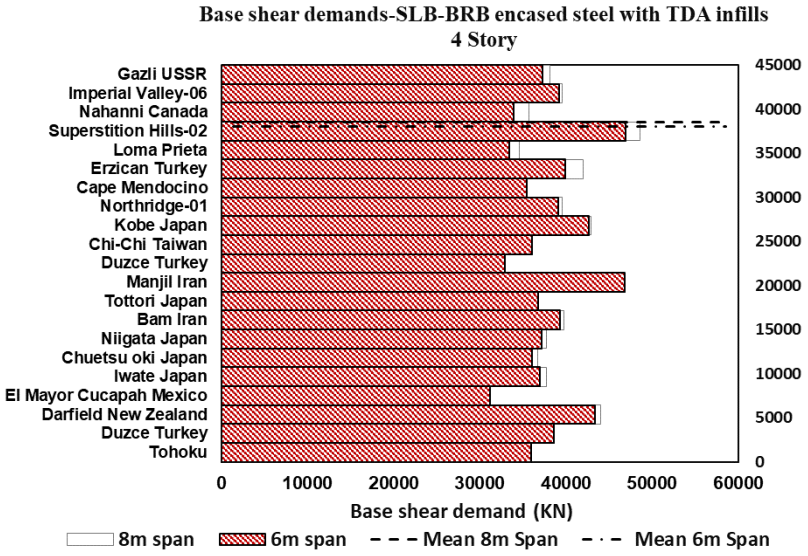

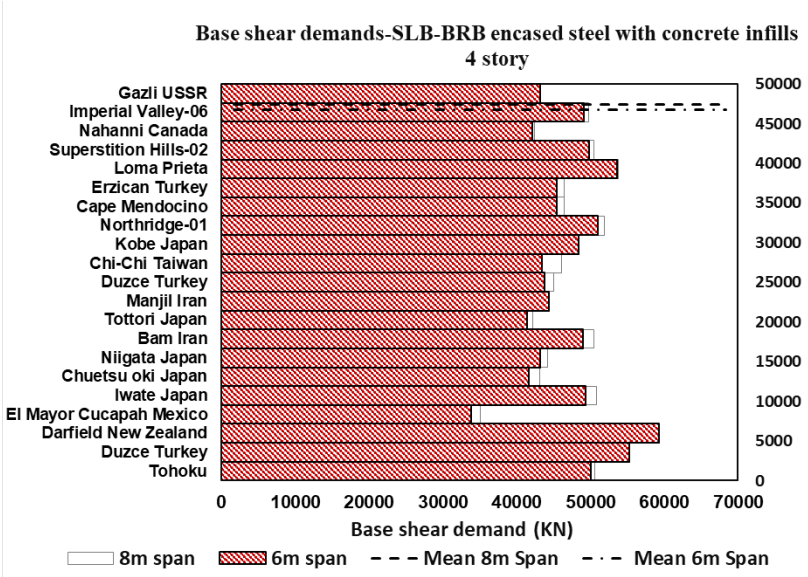

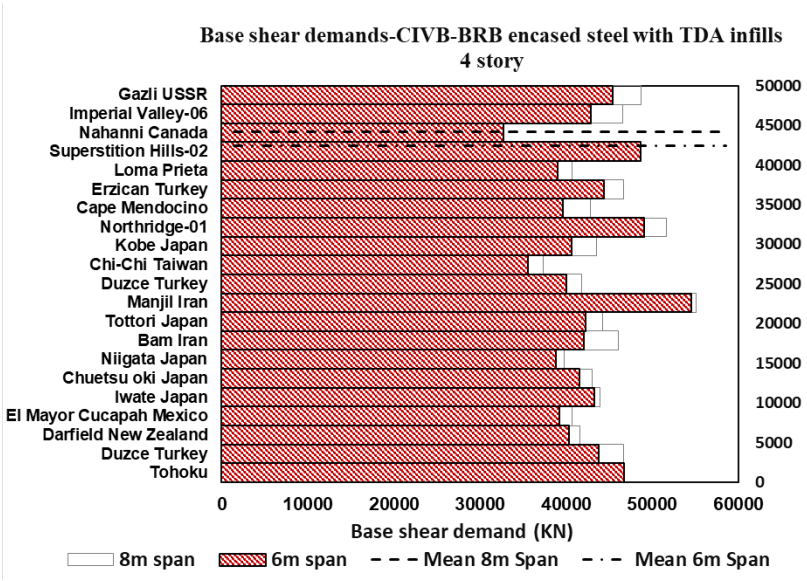
Base shear demands-CIVB-BRB encased steel with TDA infills
4 story
Gazli USSR
Imperial Valley-06
Nahanni Canada
Superstition Hills-02
Loma Prieta
Erzican Turkey
Cape Mendocino
Northridge-01
Kobe Japan
Chi-Chi Taiwan
Duzce Turkey
Manjil Iran
Tottori Japan
Bam Iran
Niigata Japan
Chuetsu oki Japan
Iwate Japan
El Mayor Cucapah Mexico
Darfield New Zealand
Duzce Turkey
Tohoku
0
10000
20000
30000
40000
50000
60000
0
5000
10000
15000
20000
25000
30000
35000
40000
45000
50000
Base shear demand (KN)
8m span
6m span
Mean 8m Span
Mean 6m Span

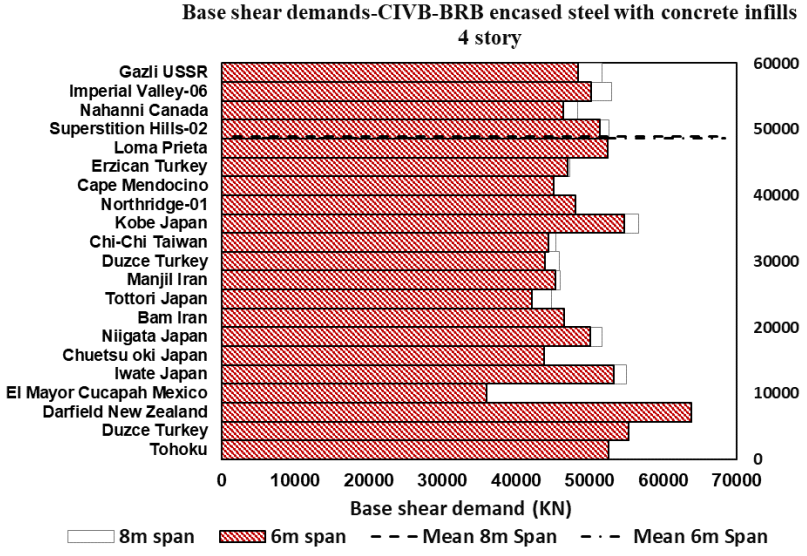
Base shear demands-CIVB-BRB encased steel with concrete infills
4 story
Gazli USSR
Imperial Valley-06
Nahanni Canada
Superstition Hills-02
Loma Prieta
Erzican Turkey
Cape Mendocino
Northridge-01
Kobe Japan
Chi-Chi Taiwan
Duzce Turkey
Manjil Iran
Tottori Japan
Bam Iran
Niigata Japan
Chuetsu oki Japan
Iwate Japan
El Mayor Cucapah Mexico
Darfield New Zealand
Duzce Turkey
Tohoku
0
10000
20000
30000
40000
50000
60000
70000
0
10000
20000
30000
40000
50000
60000
Base shear demand (KN)
8m span
6m span
Mean 8m Span
Mean 6m Span

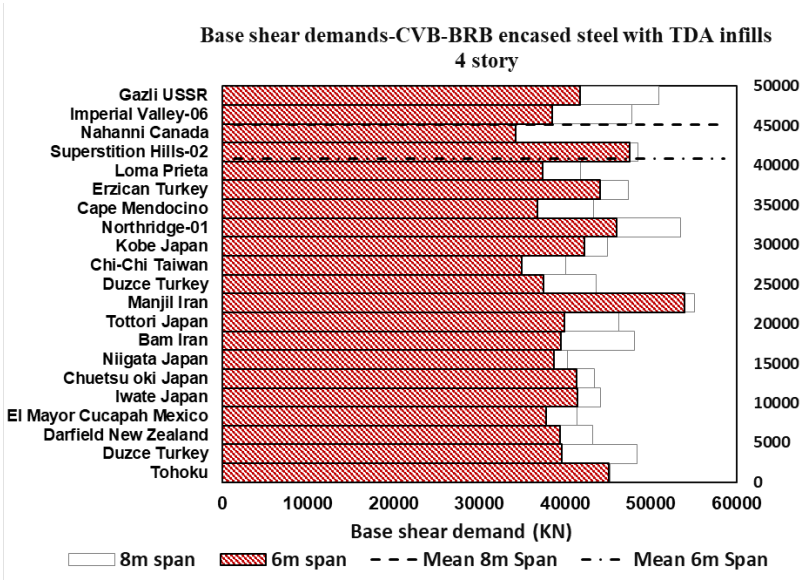
Base shear demands-CVB-BRB encased steel with TDA infills
4 story
Gazli USSR
Imperial Valley-06
Nahanni Canada
Superstition Hills-02
Loma Prieta
Erzican Turkey
Cape Mendocino
Northridge-01
Kobe Japan
Chi-Chi Taiwan
Duzce Turkey
Manjil Iran
Tottori Japan
Bam Iran
Niigata Japan
Chuetsu oki Japan
Iwate Japan
El Mayor Cucapah Mexico
Darfield New Zealand
Duzce Turkey
Tohoku
0
10000
20000
30000
40000
50000
60000
0
5000
10000
15000
20000
25000
30000
35000
40000
45000
50000
Base shear demand (KN)
8m span
6m span
Mean 8m Span
Mean 6m Span

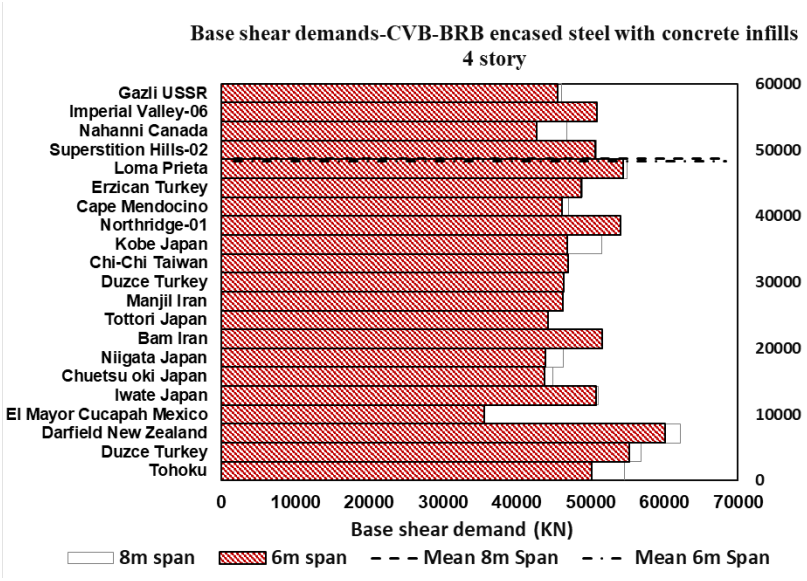
Base shear demands-CVB-BRB encased steel with concrete infills
4 story
Gazli USSR
Imperial Valley-06
Nahanni Canada
Superstition Hills-02
Loma Prieta
Erzican Turkey
Cape Mendocino
Northridge-01
Kobe Japan
Chi-Chi Taiwan
Duzce Turkey
Manjil Iran
Tottori Japan
Bam Iran
Niigata Japan
Chuetsu oki Japan
Iwate Japan
El Mayor Cucapah Mexico
Darfield New Zealand
Duzce Turkey
Tohoku
0
10000
20000
30000
40000
50000
60000
70000
0
10000
20000
30000
40000
50000
60000
Base shear demand (KN)
8m span
6m span
Mean 8m Span
Mean 6m Span

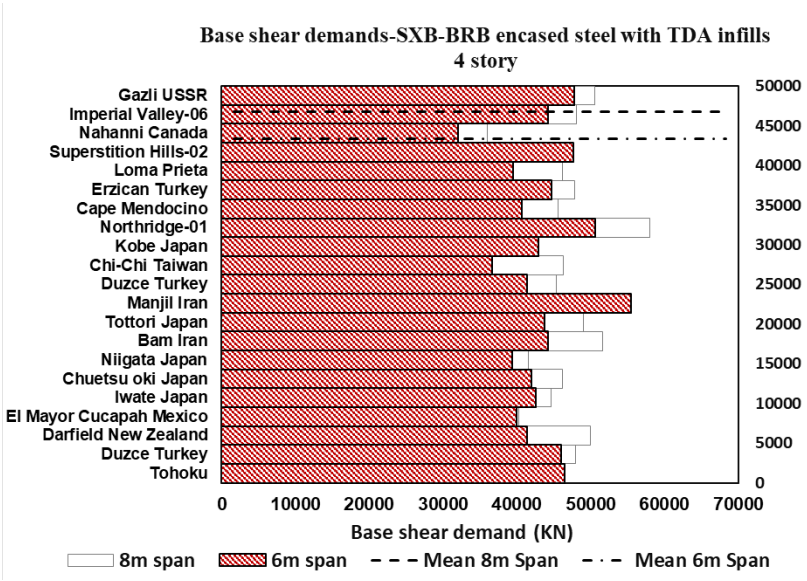
Base shear demands-SXB-BRB encased steel with TDA infills
4 story
Gazli USSR
Imperial Valley-06
Nahanni Canada
Superstition Hills-02
Loma Prieta
Erzican Turkey
Cape Mendocino
Northridge-01
Kobe Japan
Chi-Chi Taiwan
Duzce Turkey
Manjil Iran
Tottori Japan
Bam Iran
Niigata Japan
Chuetsu oki Japan
Iwate Japan
El Mayor Cucapah Mexico
Darfield New Zealand
Duzce Turkey
Tohoku
0
10000
20000
30000
40000
50000
60000
70000
Base shear demand (KN)
8m span
6m span
Mean 8m Span
Mean 6m Span

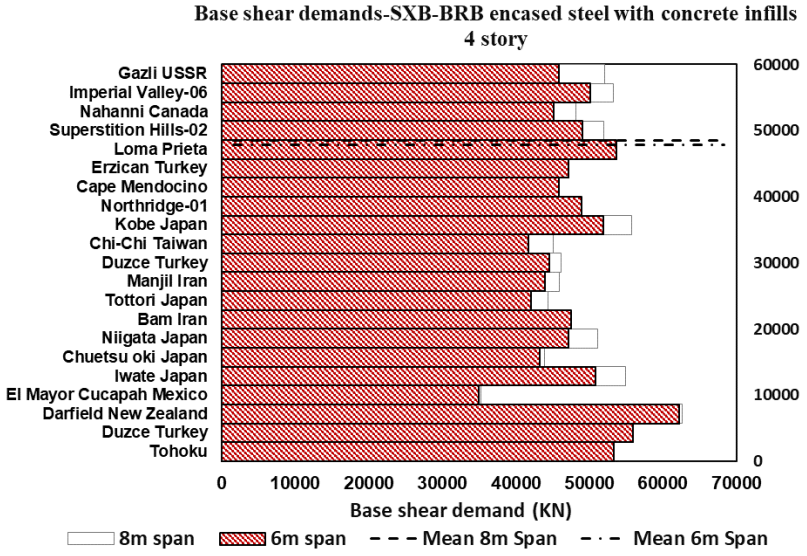
Base shear demands-SXB-BRB encased steel with concrete infills
4 story
Gazli USSR
Imperial Valley-06
Nahanni Canada
Superstition Hills-02
Loma Prieta
Erzican Turkey
Cape Mendocino
Northridge-01
Kobe Japan
Chi-Chi Taiwan
Duzce Turkey
Manjil Iran
Tottori Japan
Bam Iran
Niigata Japan
Chuetsu oki Japan
Iwate Japan
El Mayor Cucapah Mexico
Darfield New Zealand
Duzce Turkey
Tohoku
0
10000
20000
30000
40000
50000
60000
70000
Base shear demand (KN)
8m span
6m span
Mean 8m Span
Mean 6m Span

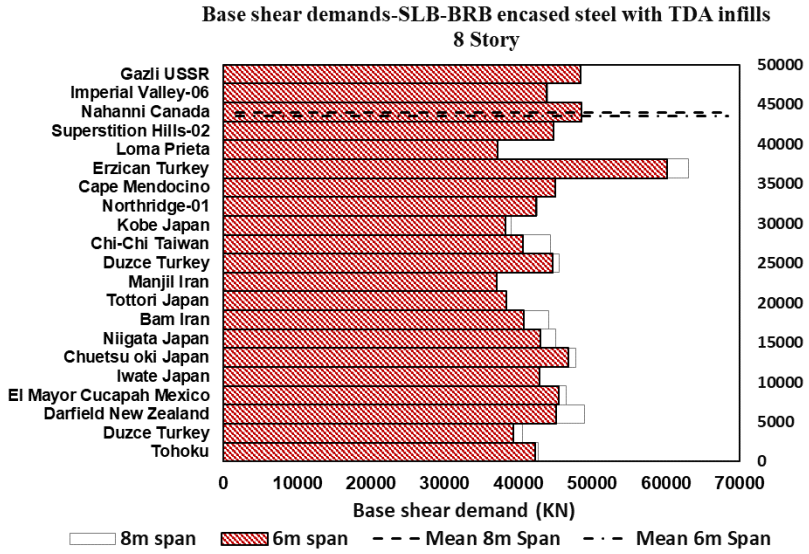
Base shear demands-SLB-BRB encased steel with TDA infills
8 Story
Gazli USSR
Imperial Valley-06
Nahanni Canada
Superstition Hills-02
Loma Prieta
Erzican Turkey
Cape Mendocino
Northridge-01
Kobe Japan
Chi-Chi Taiwan
Duzce Turkey
Manjil Iran
Tottori Japan
Bam Iran
Niigata Japan
Chuetsu oki Japan
Iwate Japan
El Mayor Cucapah Mexico
Darfield New Zealand
Duzce Turkey
Tohoku
0 10000 20000 30000 40000 50000 60000 70000
50000 45000 40000 35000 30000 25000 20000 15000 10000 5000 0
Base shear demand (KN)
8m span
6m span
Mean 8m Span
Mean 6m Span

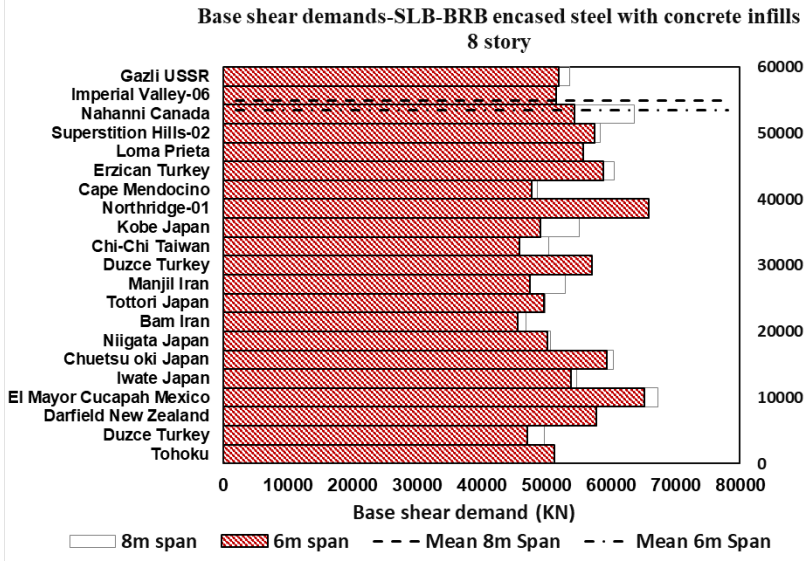
Base shear demands-SLB-BRB encased steel with concrete infills
8 story
Gazli USSR
Imperial Valley-06
Nahanni Canada
Superstition Hills-02
Loma Prieta
Erzican Turkey
Cape Mendocino
Northridge-01
Kobe Japan
Chi-Chi Taiwan
Duzce Turkey
Manjil Iran
Tottori Japan
Bam Iran
Niigata Japan
Chuetsu oki Japan
Iwate Japan
El Mayor Cucapah Mexico
Darfield New Zealand
Duzce Turkey
Tohoku
0 10000 20000 30000 40000 50000 60000 70000 80000
60000 50000 40000 30000 20000 10000 0
Base shear demand (KN)
8m span
6m span
Mean 8m Span
Mean 6m Span

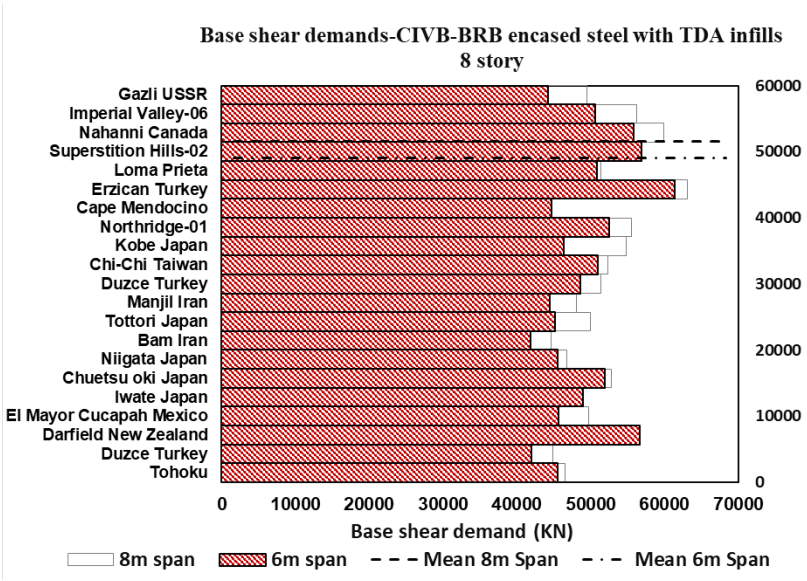
Base shear demands-CIVB-BRB encased steel with TDA infills
8 story
Gazli USSR
Imperial Valley-06
Nahanni Canada
Superstition Hills-02
Loma Prieta
Erzican Turkey
Cape Mendocino
Northridge-01
Kobe Japan
Chi-Chi Taiwan
Duzce Turkey
Manjil Iran
Tottori Japan
Bam Iran
Niigata Japan
Chuetsu oki Japan
Iwate Japan
El Mayor Cucapah Mexico
Darfield New Zealand
Duzce Turkey
Tohoku
0
10000
20000
30000
40000
50000
60000
70000
Base shear demand (KN)
8m span
6m span
Mean 8m Span
Mean 6m Span

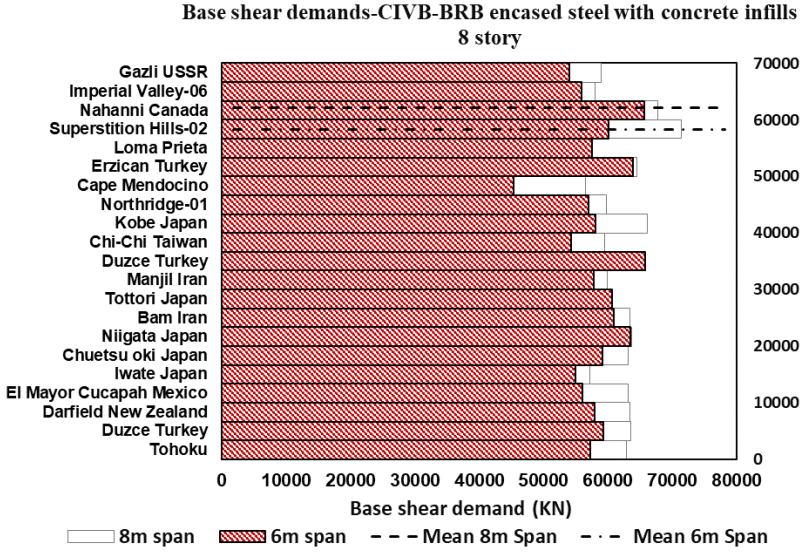
Base shear demands-CIVB-BRB encased steel with concrete infills
8 story
Gazli USSR
Imperial Valley-06
Nahanni Canada
Superstition Hills-02
Loma Prieta
Erzican Turkey
Cape Mendocino
Northridge-01
Kobe Japan
Chi-Chi Taiwan
Duzce Turkey
Manjil Iran
Tottori Japan
Bam Iran
Niigata Japan
Chuetsu oki Japan
Iwate Japan
El Mayor Cucapah Mexico
Darfield New Zealand
Duzce Turkey
Tohoku
0
10000
20000
30000
40000
50000
60000
70000
80000
Base shear demand (KN)
8m span
6m span
Mean 8m Span
Mean 6m Span

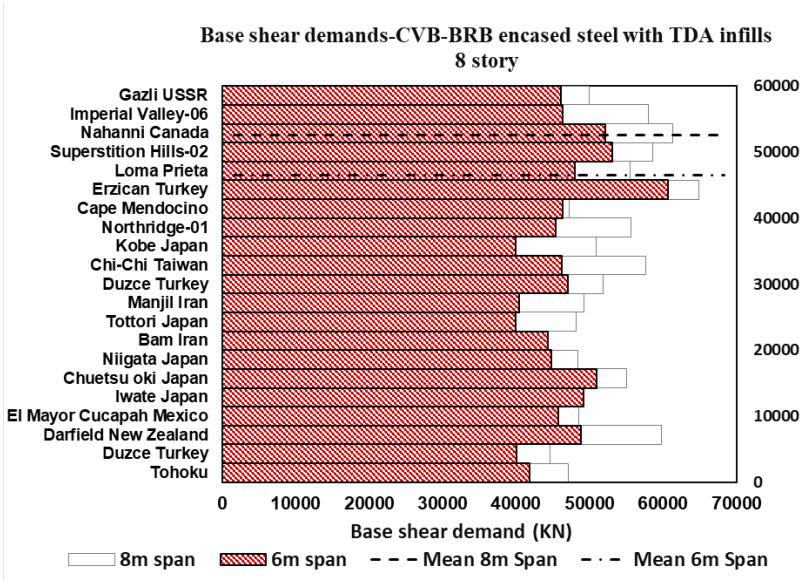
Base shear demands-CVB-BRB encased steel with TDA infills
8 story
Gazli USSR
Imperial Valley-06
Nahanni Canada
Superstition Hills-02
Loma Prieta
Erzican Turkey
Cape Mendocino
Northridge-01
Kobe Japan
Chi-Chi Taiwan
Duzce Turkey
Manjil Iran
Tottori Japan
Bam Iran
Niigata Japan
Chuetsu oki Japan
Iwate Japan
El Mayor Cucapah Mexico
Darfield New Zealand
Duzce Turkey
Tohoku
0
10000
20000
30000
40000
50000
60000
70000
Base shear demand (KN)
8m span
6m span
Mean 8m Span
Mean 6m Span

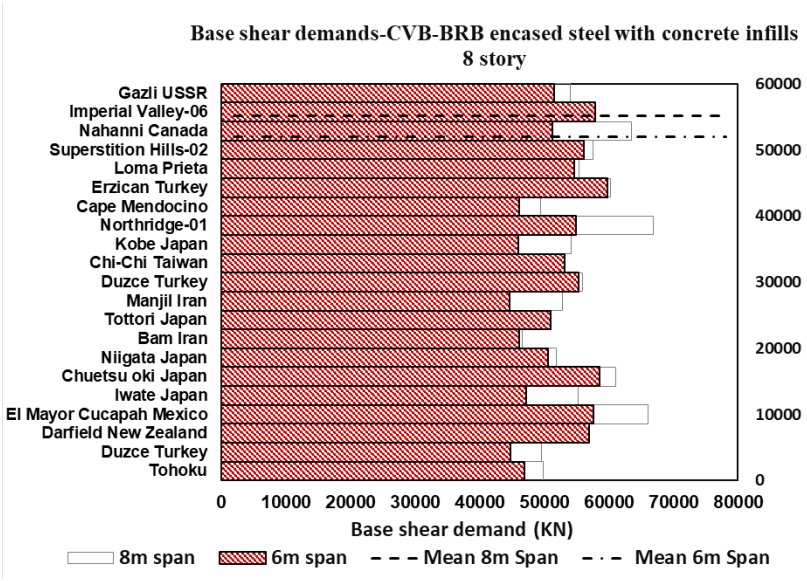
Base shear demands-CVB-BRB encased steel with concrete infills
8 story
Gazli USSR
Imperial Valley-06
Nahanni Canada
Superstition Hills-02
Loma Prieta
Erzican Turkey
Cape Mendocino
Northridge-01
Kobe Japan
Chi-Chi Taiwan
Duzce Turkey
Manjil Iran
Tottori Japan
Bam Iran
Niigata Japan
Chuetsu oki Japan
Iwate Japan
El Mayor Cucapah Mexico
Darfield New Zealand
Duzce Turkey
Tohoku
0
10000
20000
30000
40000
50000
60000
70000
80000
Base shear demand (KN)
8m span
6m span
Mean 8m Span
Mean 6m Span

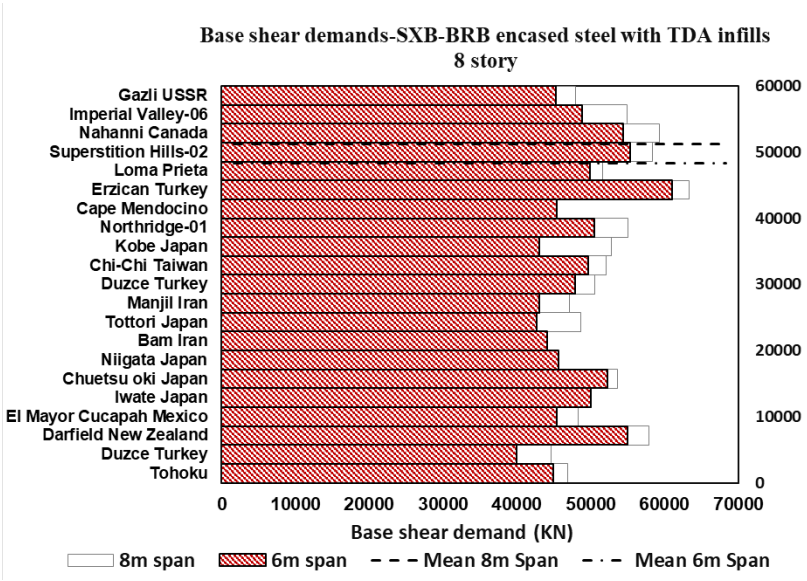
Base shear demands-SXB-BRB encased steel with TDA infills
8 story
Gazli USSR
Imperial Valley-06
Nahanni Canada
Superstition Hills-02
Loma Prieta
Erzican Turkey
Cape Mendocino
Northridge-01
Kobe Japan
Chi-Chi Taiwan
Duzce Turkey
Manjil Iran
Tottori Japan
Bam Iran
Niigata Japan
Chuetsu oki Japan
Iwate Japan
El Mayor Cucapah Mexico
Darfield New Zealand
Duzce Turkey
Tohoku
0 10000 20000 30000 40000 50000 60000 70000
Base shear demand (KN)
8m span
6m span
Mean 8m Span
Mean 6m Span

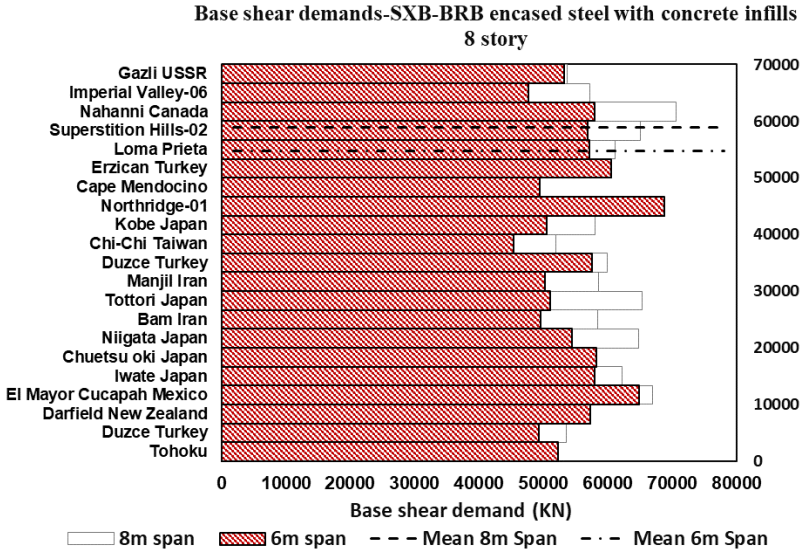
Base shear demands-SXB-BRB encased steel with concrete infills
8 story
Gazli USSR
Imperial Valley-06
Nahanni Canada
Superstition Hills-02
Loma Prieta
Erzican Turkey
Cape Mendocino
Northridge-01
Kobe Japan
Chi-Chi Taiwan
Duzce Turkey
Manjil Iran
Tottori Japan
Bam Iran
Niigata Japan
Chuetsu oki Japan
Iwate Japan
El Mayor Cucapah Mexico
Darfield New Zealand
Duzce Turkey
Tohoku
0 10000 20000 30000 40000 50000 60000 70000 80000
Base shear demand (KN)
8m span
6m span
Mean 8m Span
Mean 6m Span

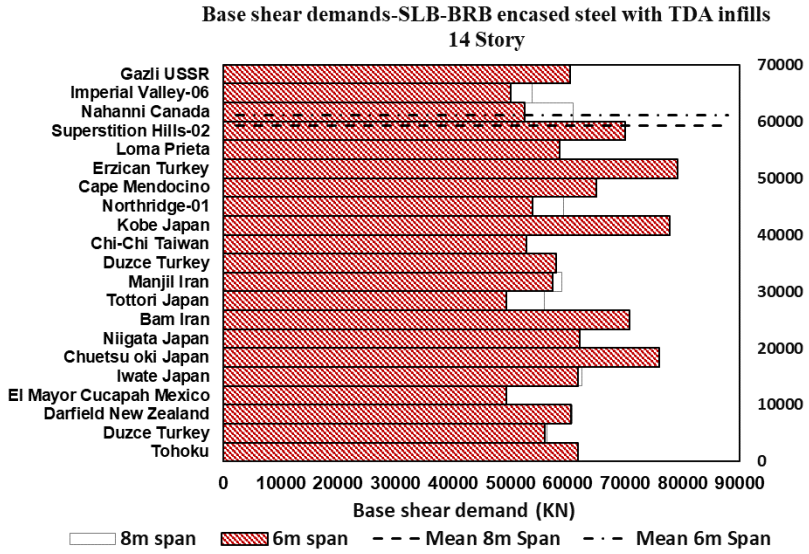
Base shear demands-SLB-BRB encased steel with TDA infills
14 Story
Gazli USSR
Imperial Valley-06
Nahanni Canada
Superstition Hills-02
Loma Prieta
Erzican Turkey
Cape Mendocino
Northridge-01
Kobe Japan
Chi-Chi Taiwan
Duzce Turkey
Manjil Iran
Tottori Japan
Bam Iran
Niigata Japan
Chuetsu oki Japan
Iwate Japan
El Mayor Cucapah Mexico
Darfield New Zealand
Duzce Turkey
Tohoku
0 10000 20000 30000 40000 50000 60000 70000 80000 90000
Base shear demand (KN)
8m span
6m span
Mean 8m Span
Mean 6m Span

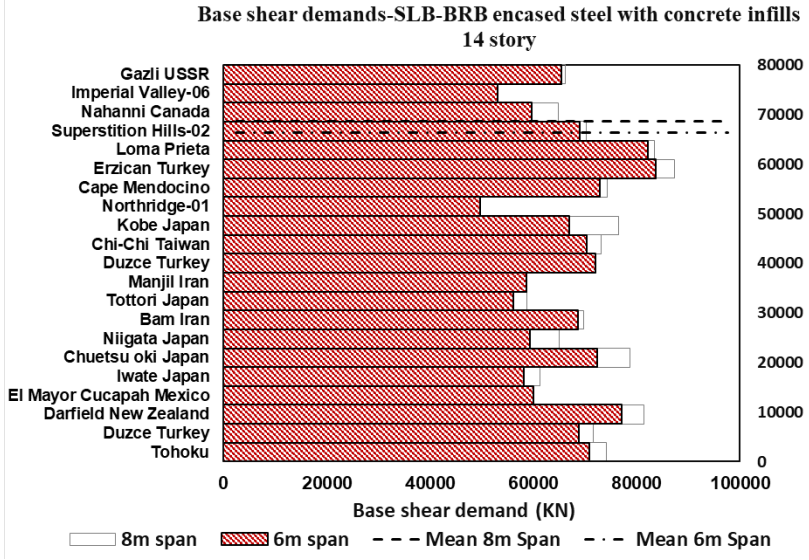
Base shear demands-SLB-BRB encased steel with concrete infills
14 story
Gazli USSR
Imperial Valley-06
Nahanni Canada
Superstition Hills-02
Loma Prieta
Erzican Turkey
Cape Mendocino
Northridge-01
Kobe Japan
Chi-Chi Taiwan
Duzce Turkey
Manjil Iran
Tottori Japan
Bam Iran
Niigata Japan
Chuetsu oki Japan
Iwate Japan
El Mayor Cucapah Mexico
Darfield New Zealand
Duzce Turkey
Tohoku
0 20000 40000 60000 80000 100000
Base shear demand (KN)
8m span
6m span
Mean 8m Span
Mean 6m Span

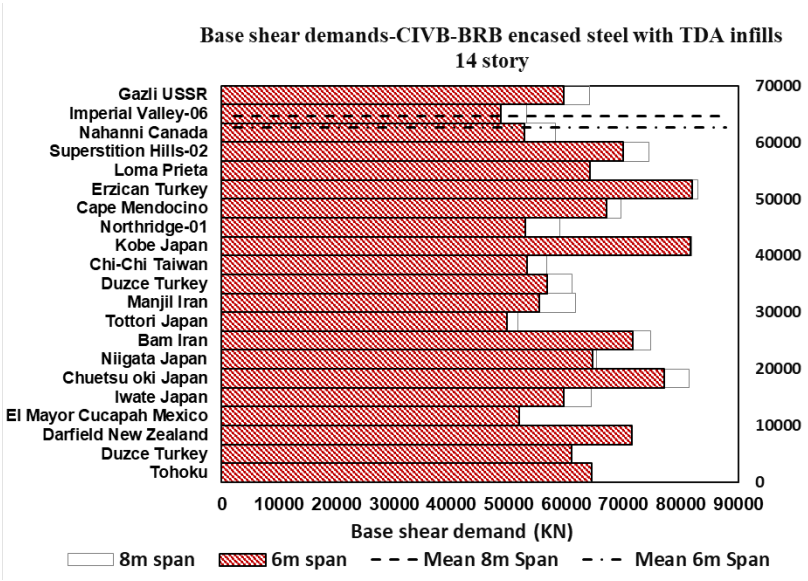
Base shear demands-CIVB-BRB encased steel with TDA infills
14 story
Gazli USSR
Imperial Valley-06
Nahanni Canada
Superstition Hills-02
Loma Prieta
Erzican Turkey
Cape Mendocino
Northridge-01
Kobe Japan
Chi-Chi Taiwan
Duzce Turkey
Manjil Iran
Tottori Japan
Bam Iran
Niigata Japan
Chuetsu oki Japan
Iwate Japan
El Mayor Cucapah Mexico
Darfield New Zealand
Duzce Turkey
Tohoku
0 10000 20000 30000 40000 50000 60000 70000 80000 90000
Base shear demand (KN)
8m span
6m span
Mean 8m Span
Mean 6m Span

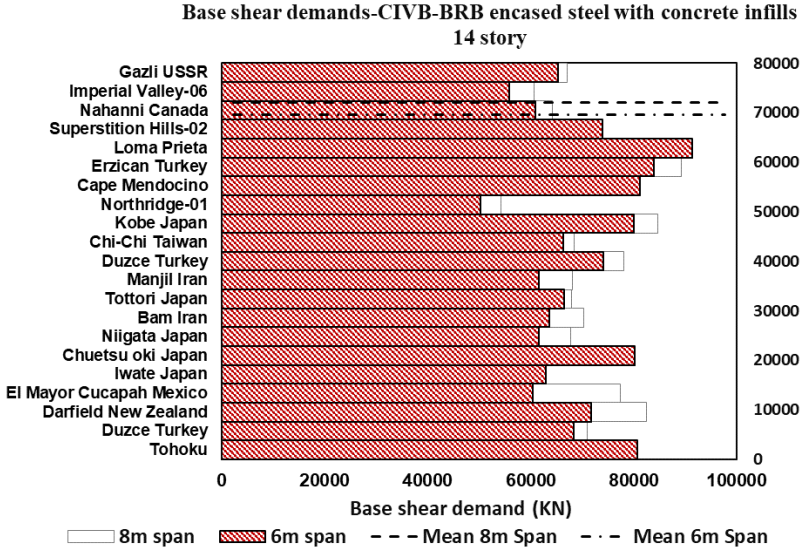
Base shear demands-CIVB-BRB encased steel with concrete infills
14 story
Gazli USSR
Imperial Valley-06
Nahanni Canada
Superstition Hills-02
Loma Prieta
Erzican Turkey
Cape Mendocino
Northridge-01
Kobe Japan
Chi-Chi Taiwan
Duzce Turkey
Manjil Iran
Tottori Japan
Bam Iran
Niigata Japan
Chuetsu oki Japan
Iwate Japan
El Mayor Cucapah Mexico
Darfield New Zealand
Duzce Turkey
Tohoku
0 20000 40000 60000 80000 100000
Base shear demand (KN)
8m span
6m span
Mean 8m Span
Mean 6m Span

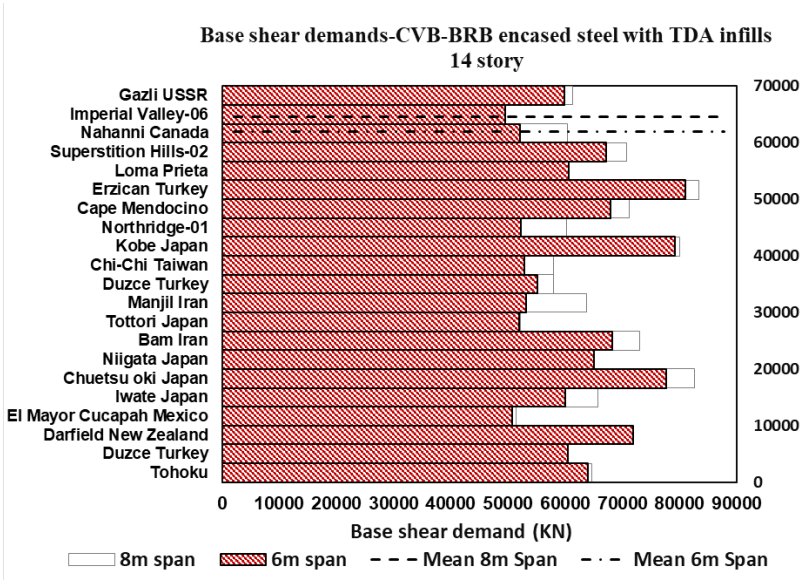
Base shear demands-CVB-BRB encased steel with TDA infills
14 story
Gazli USSR
Imperial Valley-06
Nahanni Canada
Superstition Hills-02
Loma Prieta
Erzican Turkey
Cape Mendocino
Northridge-01
Kobe Japan
Chi-Chi Taiwan
Duzce Turkey
Manjil Iran
Tottori Japan
Bam Iran
Niigata Japan
Chuetsu oki Japan
Iwate Japan
El Mayor Cucapah Mexico
Darfield New Zealand
Duzce Turkey
Tohoku
0 10000 20000 30000 40000 50000 60000 70000 80000 90000
Base shear demand (KN)
8m span
6m span
Mean 8m Span
Mean 6m Span

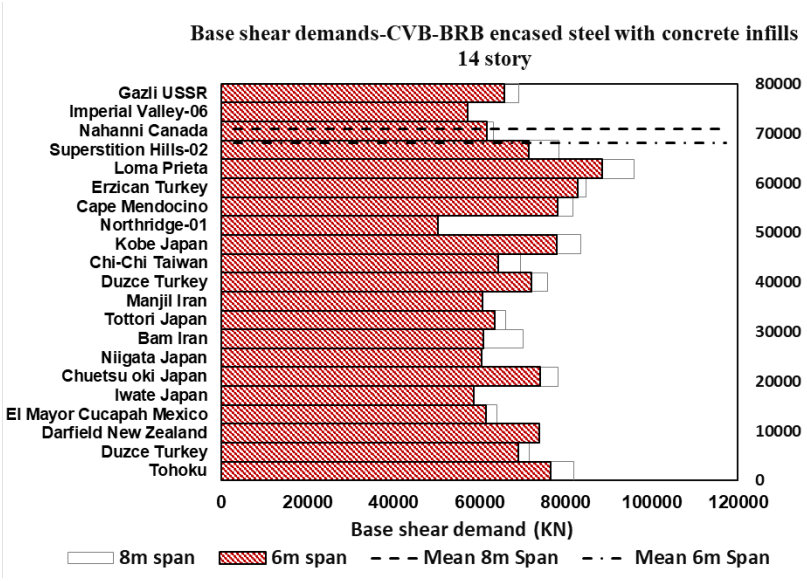
Base shear demands-CVB-BRB encased steel with concrete infills
14 story
Gazli USSR
Imperial Valley-06
Nahanni Canada
Superstition Hills-02
Loma Prieta
Erzican Turkey
Cape Mendocino
Northridge-01
Kobe Japan
Chi-Chi Taiwan
Duzce Turkey
Manjil Iran
Tottori Japan
Bam Iran
Niigata Japan
Chuetsu oki Japan
Iwate Japan
El Mayor Cucapah Mexico
Darfield New Zealand
Duzce Turkey
Tohoku
0 20000 40000 60000 80000 100000 120000
Base shear demand (KN)
8m span
6m span
Mean 8m Span
Mean 6m Span

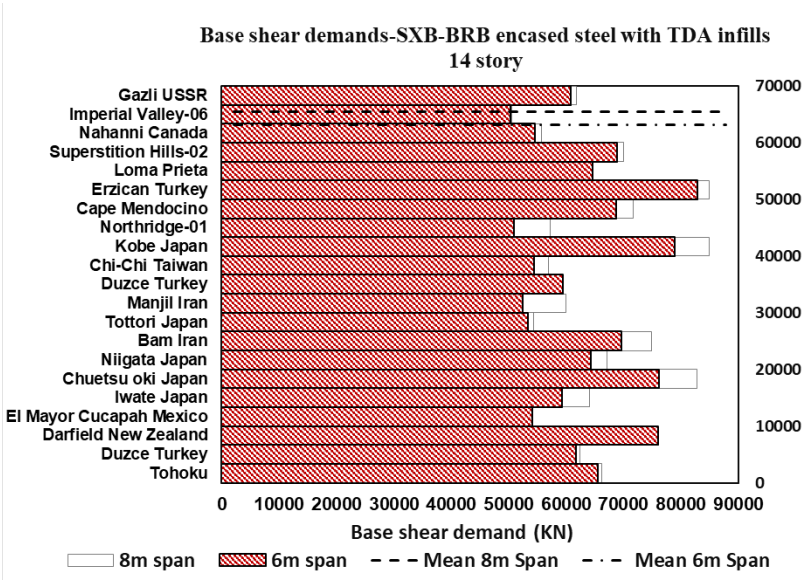
Base shear demands-SXB-BRB encased steel with TDA infills
14 story
Gazli USSR
Imperial Valley-06
Nahanni Canada
Superstition Hills-02
Loma Prieta
Erzican Turkey
Cape Mendocino
Northridge-01
Kobe Japan
Chi-Chi Taiwan
Duzce Turkey
Manjil Iran
Tottori Japan
Bam Iran
Niigata Japan
Chuetsu oki Japan
Iwate Japan
El Mayor Cucapah Mexico
Darfield New Zealand
Duzce Turkey
Tohoku
0 10000 20000 30000 40000 50000 60000 70000 80000 90000
70000
60000
50000
40000
30000
20000
10000
0
Base shear demand (KN)
8m span
6m span
Mean 8m Span
Mean 6m Span

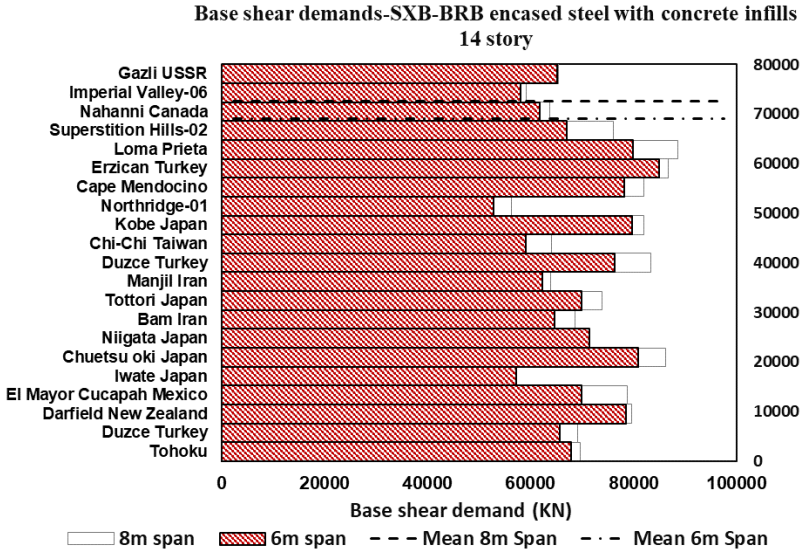
Base shear demands-SXB-BRB encased steel with concrete infills
14 story
Gazli USSR
Imperial Valley-06
Nahanni Canada
Superstition Hills-02
Loma Prieta
Erzican Turkey
Cape Mendocino
Northridge-01
Kobe Japan
Chi-Chi Taiwan
Duzce Turkey
Manjil Iran
Tottori Japan
Bam Iran
Niigata Japan
Chuetsu oki Japan
Iwate Japan
El Mayor Cucapah Mexico
Darfield New Zealand
Duzce Turkey
Tohoku
0 20000 40000 60000 80000 100000
80000
70000
60000
50000
40000
30000
20000
10000
0
Base shear demand (KN)
8m span
6m span
Mean 8m Span
Mean 6m Span

Appendix F: Calculation Note (ACI 318-19)

F.1: Introduction

The important design criteria procedures of 4-, 8- and 14-story Special reinforced concrete moment frames equipped with BRBF are presented here.

F.1.1: Purpose and Objective

This appendix is included the structural calculation notes for analysis and design of 4-, 8- and 14-story Special reinforced concrete moment frames (SMFs) equipped with BRBF.

F.1.2: Codes and Standards

- Loading Codes
  - Minimum Design Loads and Associated Criteria for Buildings and Other Structures, American Society of Civil Engineering, ASCE/SEI 7-22.
- Design Codes
  - Building Code Requirements for Structural Concrete, (ACI Committee 318, 2019)

F.2: Assumptions

F.2.1.1: Methods of Design

Concrete buildings have been designed in compliance with ACI-318-14/19 considering the Strength Design method.

F.2.1.2: Material properties

F.2.1.2.1: Concrete

The minimum compressive characteristic strength at 28 days on the cylindrical specimen, f_c', of the reinforced concrete is assumed to be 30 MPa is used for cast in place concrete. The unit weight of reinforced concrete, w_c, is taken as 24 kN/m^3 (2400 kg/m^3). The initial modulus of elasticity E_c based on ACI 318-19 is calculated from equation 1, where w_c is the density of normal

weight concrete in kg/m^3, E_c is equal to 27692 MPa (282379 kgf/cm^2) and the Poisson ratio, υ, is equal to 0.2.

$$E_c = w_c^{1.5} 0.043 \sqrt{f_c'} = 2400^{1.5} 0.043 \sqrt{30} = 27692\ (MPa) \quad (1)$$

The minimum compressive characteristic strength at 28 days on a cylindrical specimen for lean concrete is considered equal to 14 MPa.

F.2.1.2.2: Cement

In accordance with the geotechnical and soil investigation report, it is recommended to use cement type II.

F.2.1.2.3: Bars

Based on ACI 318-19 deformed bars shall conform to ASTM A615M (carbon steel), ASTM A706M (low alloy steel), ASTM A996M (axle and rail steel), ASTM A955M (stainless steel), or ASTM A1035M (low carbon chromium steel). The yield strength of reinforcing steel, f_y, is assumed to be 400 MPa. For deformed steel bar, Grade 60 (A615Gr60, F_y=4000 Kg/cm2, F_u= 6000 Kg/cm2) in accordance with ASTM 615M or equivalent material is used. The modulus of elasticity, E_s, is equal to 29,000,000 psi (ACI, 20.2.2.2).

- Probable flexural strength (M_{pr})

The probable flexural strength of members was determined assuming tensile stress in the longitudinal bars of at least 1.25f_y.

F.2.1.2.4: Anchor Bolts

Material for anchor bolts, plates, and steel shapes for insert shall be ASTM A307 weldable type in accordance with ASTM standard or alternative equivalent.

F.3: The Geotechnical and Soil Investigation Report of the Area

Refer to geotechnical and soil investigation data (OSOP).

F.4: Foundation Type

Foundation shape has been considered square footing (OSOP).

F.5: Allowable Bearing Capacity of Soil

There are several diagrams used to determine the allowable bearing capacity of all foundation types. If the moment is applied to the foundation, the reaction of the soil beneath will not be uniform. In such a case, the stress at the center of soil reaction should not be exceeded more than the allowable limits (OSOP).

F.6: Concrete Cover

The concrete cover protects the reinforcement from weather and other effects including ground, moisture, temperature, etc., Specified concrete covers for cast in place concrete members are demonstrated in Table 1. In this study, concrete is exposed to weather and the specified cover is 50 mm, it is estimated to the outer edge of stirrups, spirals, or ties when transverse reinforcement surrounds main bars or the outmost layer of bars.

Table 1. Concrete cover (ACI 318-19)

Concrete exposure	Member	Reinforcement	Specified cover, mm
Cast against and permanently in contact with ground	All	All	75
Exposed to weather or in contact with ground	All	No. 19 through No. 57 bars	50
		No. 16 bar, MW200 or MD200 wire, and smaller	40
Not exposed to weather or in contact with ground	Slabs, joists, and walls	No. 43 and No. 57 bars	40
		No. 36 bar and smaller	20
	Beams, columns, pedestals, and tension ties	Primary reinforce-ment, stirrups, ties, spirals, and hoops	40

F.7: Computer Programs

ETABS ver.15.2.2 software has been used to model, analyze, and design concrete buildings.

F.8: Calculation

F.8.1: Design Input

ASCE 7-22 has three categories for concrete moment resisting systems including special reinforced concrete moment frames (SMFs), intermediate reinforced concrete moment frames (IMFs), and ordinary reinforced concrete moment frames (OMFs). In this study and based on Table 2, SMFs have been used in order to reach a large ductility in high seismic regions, this can be defined by sway special in the program.

Table 2. Concrete moment frames parameters (ASCE 7-22)

	Response modification factor, R	**Overstrength Factor, Ω_o**	**Deflection amplification Factor C_d**	**Structural system limitations based on seismic design category**				
				B	C	D	E	F
SMFs	8	3	5.5	NL	NL	NL	NL	NL
IMFs	5	3	4.5	NL	NL	NP	NP	NP
OMFs	3	3	2.5	NL	NP	NP	NP	NP

Note: NL (Not Limited), NP (Not Permitted)

F.8.2: Geometry

The buildings are symmetrical in both directions. The total height of the ground floor in each building is 4.5m and the height of the rest of the floors in each building is 3.5m. Figure 1 is geometry of different structures.

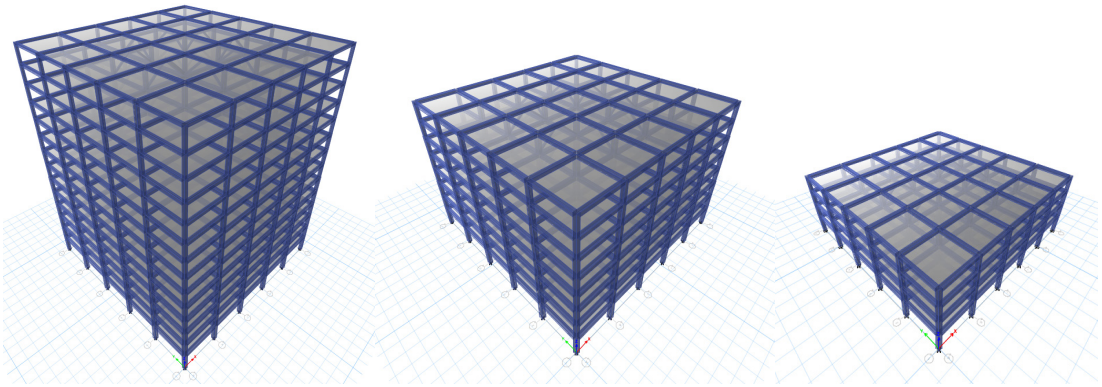

Figure 1. The geometry of Structure (14-Storey, 8-Storey, and 4-Story)

F.8.3: Loading

The design live and dead loads for all models are assumed to be 1.5 kN/m^2 and 2.4 kN/m^2, and the snow load acting on the roof is 1.64 kN/m^2.

F.8.3.1: Live load

Except for the roof uniform live loads, loads exceeding 4.79 kN/m^2, garages, assembly uses, and limitations on one-way slabs, reduction in uniform live loads can be calculated in accordance with equation 2, in which L_o is the unreduced design live load (m^2), K_{LL} is the factor live load element factor from Table 3 and A_T is the tributary area in m^2.

$$L = L_0\left(0.25 + \frac{4.75}{\sqrt{K_{LL}A_T}}\right) \quad (2)$$

Table 3. Live load element factor (ACI 318-19)

Element	K_{LL}[a]
Interior columns	4
Exterior columns without cantilever slabs	4
Edge columns with cantilever slabs	3
Corner columns with cantilever slabs	2
Edge beams without cantilever slabs	2
Interior beams	2
All other members not identified, including	1
Edge beams with cantilever slabs	
Cantilever beams	
One-way slabs	
Two-way slabs	
Members without provisions for continuous shear transfer normal to their span	

[a]In lieu of the preceding values, K_{LL} is permitted to be calculated.

F.8.3.2: Snow load

The flat roof snow load, P_f, can be calculated from equation 3

$$P_f = 0.7C_eC_tI_sP_g = 0.7 \times 0.8 \times 1.0 \times 1.2 \times 5 \times 0.0479 = 0.161 \text{ kN/m}^2 \quad (3)$$

Herein, C_e, C_s, C_t, I_s are exposure, slope, thermal, and important factors, P_g is the ground snow load. The buildings are located in unobstructed areas, therefore surface roughness is D (section 26.7.2) C_e = 0.8. C_t=1.0 is from Table 7.3-2, I_s=1.2 from Table 1.5-2 and risk category. p_g can be calculated from Figure 2 and is equal to 5 lb⁄ft^2.

Minimum snow load, p_m, for low slope roofs can be determined from equation 4 (Section C7.3-4).

$$P_m = I_s P_g \qquad for \qquad P_g \leq 0.96\ KN/m^2 \tag{4}$$

Figure 2. Ground snow loads, p_g, based on location (lb/ft^2, multiply by 0.0479 kN/m^2)

In this study, the snow load is assumed to be 1.64 kN/m^2.

F.8.3.3: Earthquake Load

The structures are office buildings that are equipped with the "radio dispatcher facility" with the risk category of IV, and a site class D-stiff soil. Seismic design parameters are presented in Table 4.

Table 4. Seismic design parameters (ASCE 7-22)

Type	Value	Description
S_S(g)	2.432	MCE_R for 0.2 second
S_1(g)	0.853	MCE_R for 1.0 second
S_{MS}(g)	2.432	Site modified spectral acceleration
S_{M1}(g)	1.279	Site modified spectral acceleration
S_{DS}(g)	1.622	Numeric seismic design value at 0.2 second
S_{D1}(g)	0.853	Numeric seismic design value at 1.0 second
F_a	1	Site amplification factor at 0.2 second
F_v	1.5	Site amplification factor at 1.0 second
PGA(g)	0.92	MCE_G peak ground acceleration
T_L(Sec)	8	Long period

The seismic base shear, V, is calculated from equation 5. where C_s is the seismic response coefficient shall be determined in accordance with equation 6, and W is the seismic weight.

$$V = C_s W \tag{5}$$

$$C_s = \frac{S_{DS}}{\left(\frac{R}{I_e}\right)} = \frac{1.622}{\left(\frac{8}{1.25}\right)} = 0.253 \tag{6}$$

Where S_{DS} is the short period design spectral acceleration, R is the response modification factor, and I_e is the importance factor at risk category III (Table 5). The seismic response coefficient shall satisfy equations 7 to 11.

Table 5. Importance factors (ASCE 7-22)

Risk Category from Table 1.5-1	Snow Importance Factor, I_s	Ice Importance Factor—Thickness, I_i	Ice Importance Factor—Wind, I_w	Seismic Importance Factor, I_e
I	0.80	0.80	1.00	1.00
II	1.00	1.00	1.00	1.00
III	1.10	1.15	1.00	1.25
IV	1.20	1.25	1.00	1.50

$T \leq T_L = 8$ sec therefore C_s is calculated from equations 7-11.

$$For\ 4-story\ C_s \le \frac{S_{D1}}{T\left(\frac{R}{I_e}\right)} = \frac{0.853}{0.37\left(\frac{8}{1.25}\right)} = 0.360\ \text{ for } T \le T_L \tag{7}$$

$$For\ 8-story\ C_s \le \frac{S_{D1}}{T\left(\frac{R}{I_e}\right)} = \frac{0.853}{0.61\left(\frac{8}{1.25}\right)} = 0.218\ \text{ for } T \le T_L \tag{8}$$

$$For\ 14-story\ C_s \le \frac{S_{D1}}{T\left(\frac{R}{I_e}\right)} = \frac{0.853}{0.92\left(\frac{8}{1.25}\right)} = 0.144\ \text{ for } T \le T_L \tag{9}$$

$$C_s \ge 0.044 S_{DS} I_e = 0.044 \times 1.622 \times 1.25 = 0.0892 \ge 0.01 \tag{10}$$

$$C_s \ge 0.5 S_1/(R/I_e) = 0.5 \times 0.853/(8/1.25) = \ 0.066 \text{ for } S_1 \ge \ 0.6g \tag{11}$$

Where S_{D1} is the "design spectral response acceleration at a period of 1.0 second", T is the fundamental period, T_L is the long transition period, and S_1 is the "maximum considered earthquake spectral response acceleration".

The approximate fundamental period, Ta, shall be determined with equation 12. where C_t and x are coefficients from Table 6, and h_n is the structural height. The seismic response coefficients of different buildings are presented in Table 7.

$$T_a = C_t h_n^x \tag{12}$$

Table 6. Approximate period parameters C_t and x (ASCE 7-22)

Structure Type	C_t	x
Moment-resisting frame systems in which the frames resist 100% of the required seismic force and are not enclosed or adjoined by components that are more rigid and will prevent the frames from deflecting where subjected to seismic forces:		
Steel moment-resisting frames	0.028 (0.0724)[a]	0.8
Concrete moment-resisting frames	0.016 (0.0466)[a]	0.9
Steel eccentrically braced frames in accordance with Table 12.2-1 lines B1 or D1	0.03 (0.0731)[a]	0.75
Steel buckling-restrained braced frames	0.03 (0.0731)[a]	0.75
All other structural systems	0.02 (0.0488)[a]	0.75

[a]Metric equivalents are shown in parentheses.

Table 7. Calculation of Seismic response coefficient and K values of the buildings

Story	Ta (Sec)	$C_s = \frac{S_{DS}}{\left(\frac{R}{I_e}\right)}$	$C_s \leq \frac{S_{D1}}{T\left(\frac{R}{I_e}\right)}$	$C_s \geq 0.044 S_{DS} I_e$	Selected C_s	K
4	0.37	0.253	0.360	0.089	0.253	1
8	0.61	0.253	0.218	0.089	0.218	1.05
14	0.92	0.253	0.144	0.089	0.144	1.21

The distribution of the seismic force, F_x, along the height of the building can be estimated from equation 13. C_{vx} is the vertical distribution factor and can be determined from equation 14.

$$F_x = C_{vx} V \tag{13}$$

$$C_{vx} = \frac{w_x h_x^k}{\sum_{i=1}^{n} w_i h_i^k} \tag{14}$$

Where V is the design lateral force, w_i and w_x are the effective seismic weight to level i or x, h_i and h_x are the height from the base to the desired level, k is an exponent and depends on the period, K=1 for T ≤ 0.5s, K=2 for T ≥ 2.5s, and for structure having period between 0.5 and 2.5s, k is 2 or can be determined by linear interpolation K=(2-1)*(T-0.5)/(2.5-0.5)+1.

The equivalent static force procedures as well as different brace configurations axial forces are presented in Table 8 and Table 9.

Table 8. Equivalent static force analysis results of BRBF with encased steel composite containing concrete

			Seismic shear forces (kN)		Brace axial forces (kN)		Seismic Weight (kN)	
Story	**Bracing**	**Level**	**6 m Span**	**8 m Span**	**6 m Span**	**8 m Span**	**6 m Span**	**8 m Span**
4	SLB	4	2193	2265	587	708	12413	16114
		3	3956	4095	980	1119	12413	16114
		2	5205	5400	1600	1700	12413	16114
		1	5918	6149	1900	2025	12413	16114
4	CIVB	4	2192	2262	430	490	12384	16065
		3	3953	4088	810	853	12384	16065
		2	5200	5391	1070	1170	12384	16065
		1	5911	6139	1270	1470	12384	16065
4	CVB	4	2194	2262	420	431	12395	16065
		3	3956	4088	810	818	12395	16065
		2	5203	5391	1010	1120	12395	16065
		1	5914	6139	1350	1450	12395	16065
4	SXB	4	2192	2262	420	462	12374	16053
		3	3952	4086	800	819	12374	16053
		2	5197	5388	1010	1130	12374	16053
		1	5909	6136	1320	1420	12374	16053
8	SLB	8	1558	1592	280	517	25386	32424
		7	2964	3031	670	879	25386	32424
		6	4147	4239	1080	1409	25386	32424
		5	5153	5271	1230	1575	25386	32424
		4	5937	6073	1690	2070	25386	32424
		3	6510	6658	2130	2250	25386	32424
		2	6890	7045	2135	2322	25386	32424
		1	7085	7246	2210	2340	25572	32457
8	CIVB	8	1699	1769	198	305	25572	32465
		7	3243	3377	615	702	25572	32465
		6	4549	4739	849	946	25572	32465
		5	5670	5914	1100	1261	25572	32465
		4	6553	6841	1510	1574	25572	32465
		3	7206	7528	1710	1750	25572	32465
		2	7645	7992	1810	1860	25572	32465
		1	7877	8240	2010	2130	25572	32465
8	CVB	8	1507	1595	122	225	25385	32247
		7	2864	3032	446	539	25385	32247
		6	4002	4242	621	788	25385	32247
		5	4968	5277	842	983	25385	32247
		4	5719	6082	1040	1236	25385	32247
		3	6264	6669	1170	1353	25385	32247
		2	6622	7059	1180	1380	25385	32247
		1	6804	7260	1480	1540	25385	32247
8	SXB	8	1574	1675	163	261	25385	32247
		7	2997	3191	519	614	25385	32247
		6	4193	4471	677	880	25385	32247
		5	5215	5572	977	1140	25385	32247
		4	6011	6432	1150	1340	25385	32247
		3	6594	7064	1438	1520	25385	32247
		2	6980	7488	1450	1590	25385	32247
		1	7179	7710	1783	1890	25385	32247
14	SLB	14	1130	1149	27	66	48167	61088
		13	2256	2279	370	418	48167	61088
		12	3268	3328	592	667	48167	61088
		11	4213	4295	816	946	48167	61088
		10	5041	5142	1004	1238	48167	61088
		9	5797	5917	1059	1242	48167	61088
		8	6447	6583	1241	1559	48167	61088
		7	6990	7137	1350	1689	48167	61088
		6	7433	7589	1390	1714	48167	61088
		5	7798	7961	1575	1832	48167	61088
		4	8069	8236	1850	2119	48167	61088
		3	8256	8426	1960	2268	48167	61088
		2	8369	8539	2070	2417	48167	61088
		1	8420	8590	2330	2494	48167	61088
14	CIVB	14	1133	1198	20	58	48198	61096
		13	2262	2399	260	280	48198	61096
		12	3279	3481	390	438	48198	61096
		11	4227	4497	590	626	48198	61096
		10	5058	5390	797	810	48198	61096
		9	5816	6209	811	850	48198	61096
		8	6468	6915	1020	1040	48198	61096
		7	7013	7507	1148	1191	48198	61096
		6	7458	7991	1152	1229	48198	61096
		5	7824	8392	1241	1325	48198	61096
		4	8096	8691	1474	1581	48198	61096
		3	8283	8900	1578	1678	48198	61096
		2	8396	9026	1802	1812	48198	61096
		1	8447	9084	1990	2016	48198	61096
14	CVB	14	1137	1168	47	48	48198	61096
		13	2271	2336	215	225	48198	61096
		12	3292	3387	343	355	48198	61096
		11	4245	4372	512	542	48198	61096
		10	5080	5235	710	715	48198	61096
		9	5843	6026	750	762	48198	61096
		8	6499	6705	940	957	48198	61096
		7	7047	7272	1021	1071	48198	61096
		6	7495	7735	1052	1156	48198	61096
		5	7864	8117	1140	1178	48198	61096
		4	8138	8401	1207	1448	48198	61096
		3	8327	8597	1307	1496	48198	61096
		2	8441	8715	1440	1590	48198	61096
		1	8493	8768	1490	1700	48198	61096
14	SXB	14	1165	1207	45	55	48198	61096
		13	2329	2418	234	266	48198	61096
		12	3379	3510	344	394	48198	61096
		11	4360	4536	590	630	48198	61096
		10	5223	5437	690	744	48198	61096
		9	6011	6265	790	889	48198	61096
		8	6692	6979	1010	1093	48198	61096
		7	7626	7578	1180	1285	48198	61096
		6	7729	8069	1190	1295	48198	61096
		5	8115	8475	1207	1468	48198	61096
		4	8403	8780	1227	1505	48198	61096
		3	8603	8992	1540	1906	48198	61096
		2	8725	9121	1780	1950	48198	61096
		1	8781	9180	2134	2331	48198	61096

Note: Single Leg Braces (SLB), Chevron Inverted V Braces (CIVB), Chevron V Braces (CVB), and Split X braces (SXB)

Table 9. Equivalent static force analysis results of BRBF with encased steel composite containing TDA

			Seismic shear forces (kN)		Brace axial forces (kN)		Seismic Weight (kN)	
Story	**Bracing**	**Level**	**6 m Span**	**8 m Span**	**6 m Span**	**8 m Span**	**6 m Span**	**8 m Span**
4	SLB	4	1971	2029	403	560	12309	16018
		3	3533	3646	776	870	12309	16018
		2	4619	4778	999	1100	12309	16018
		1	5222	5409	1040	1140	12309	16018
4	CIVB	4	2099	2196	300	388	12326	15992
		3	3772	3956	620	694	12326	15992
		2	4942	5200	890	924	12326	15992
		1	5599	5904	910	990	12326	15992
4	CVB	4	2052	2225	320	390	12303	15980
		3	3684	4010	620	704	12303	15980
		2	4823	5273	820	970	12303	15980
		1	5460	5990	1010	1050	12303	15980
4	SXB	4	2118	2268	370	424	12303	15980
		3	3807	4090	700	750	12303	15980
		2	4989	5384	908	1020	12303	15980
		1	5654	6122	1050	1120	12303	15980
8	SLB	8	1356	1368	236	300	25183	32132
		7	2566	2586	471	570	25183	32132
		6	3570	3596	611	853	25183	32132
		5	4414	4446	720	990	25183	32132
		4	5060	5094	974	1257	25183	32132
		3	5522	5556	980	1250	25183	32132
		2	5818	5852	1060	1270	25183	32132
		1	5960	5997	1090	1280	25183	32132
8	CIVB	8	1436	1504	178	245	25183	32132
		7	2723	2855	428	519	25235	32146
		6	3798	3984	550	683	25235	32146
		5	4706	4944	660	821	25235	32146
		4	5406	5686	870	1085	25235	32146
		3	5912	6222	910	1138	25235	32146
		2	6241	6574	1004	1157	25235	32146
		1	6405	6753	1060	1180	25235	32146
8	CVB	8	1393	1502	136	208	25240	32230
		7	2640	2851	373	476	25240	32230
		6	3678	3978	481	632	25240	32230
		5	4552	4935	589	763	25240	32230
		4	5224	5675	740	1004	25240	32230
		3	5705	6209	780	1081	25240	32230
		2	6017	6560	850	1100	25240	32230
		1	6171	6739	1000	1500	25240	32230
8	SXB	8	1419	1490	164	226	25240	32095
		7	2690	2827	410	493	25240	32095
		6	3750	3943	520	638	25240	32095
		5	4645	4891	650	823	25240	32095
		4	5334	5624	780	1035	25240	32095
		3	5830	6152	868	1145	25240	32095
		2	6152	6498	880	1150	25240	32095
		1	6312	6673	1010	1190	25240	32095
14	SLB	14	1061	1087	107	151	47463	63013
		13	2110	2161	303	340	47463	63013
		12	3050	3123	340	390	47463	63013
		11	3923	4015	540	580	47463	63013
		10	4684	4790	626	750	47463	63013
		9	5374	5492	665	760	47463	63013
		8	5965	6090	870	990	47463	63013
		7	6454	6582	913	1040	47463	63013
		6	6850	6978	950	1042	47463	63013
		5	7174	7300	1042	1145	47463	63013
		4	7410	7533	1141	1272	47463	63013
		3	7571	7689	1171	1270	47463	63013
		2	7666	7780	1174	1270	47463	63013
		1	7708	7819	1260	1293	47463	63013
14	CIVB	14	1082	1093	57	72	47510	60274
		13	2151	2175	267	281	47510	60274
		12	3111	3144	330	356	47510	60274
		11	4005	4049	474	478	47510	60274
		10	4786	4838	555	590	47510	60274
		9	5495	5556	518	600	47510	60274
		8	6103	6170	629	685	47510	60274
		7	6608	6678	630	819	47510	60274
		6	7019	7090	697	825	47510	60274
		5	7354	7426	723	844	47510	60274
		4	7600	7673	867	980	47510	60274
		3	7769	7840	890	1000	47510	60274
		2	7869	7938	935	1040	47510	60274
		1	7913	7981	950	1050	47510	60274
14	CVB	14	1080	1091	47	55	47529	60294
		13	2149	2174	201	219	47529	60294
		12	3108	3143	294	323	47529	60294
		11	4000	4047	425	457	47529	60294
		10	4779	4834	532	573	47529	60294
		9	5487	5552	540	597	47529	60294
		8	6093	6164	640	734	47529	60294
		7	6597	6672	725	832	47529	60294
		6	7006	7082	740	835	47529	60294
		5	7340	7418	780	850	47529	60294
		4	7586	7664	840	970	47529	60294
		3	7754	7830	915	1003	47529	60294
		2	7853	7929	960	1020	47529	60294
		1	7897	7971	1000	1050	47529	60294
14	SXB	14	1091	1106	50	55	47529	60294
		13	2172	2205	232	242	47529	60294
		12	3143	3189	322	354	47529	60294
		11	4046	4108	474	505	47529	60294
		10	4836	4911	558	609	47529	60294
		9	5554	5642	580	658	47529	60294
		8	6170	6268	697	740	47529	60294
		7	6682	6787	811	910	47529	60294
		6	7099	7208	815	915	47529	60294
		5	7440	7552	833	955	47529	60294
		4	7691	7806	940	1019	47529	60294
		3	7863	7978	1048	1169	47529	60294
		2	7966	8080	1050	1170	47529	60294
		1	8011	8125	1080	1187	47529	60294

Note: Single Leg Braces (SLB), Chevron Inverted V Braces (CIVB), Chevron V Braces (CVB), and Split X braces (SXB)

Horizontal Seismic load effect, E_h, shall be calculated from equation 15 where Q_E is the effects of seismic forces from V, and ρ is the redundancy factor.

$$E_h = \rho Q_E \tag{15}$$

The redundancy factor is defined by the design system Rho in ETABS and shall equal 1.0 based on sections 12.3.4.1 and 12.3.4.2 of ASCE 7-22.

The vertical seismic load effect, E_v, can be determined from equation 16, where SDS is the design spectral response acceleration, and the effect of the dead load is considered D.

$$E_v = 0.2 S_{DS} D = 0.2 \times 1.622 \times D = 0.33D \tag{16}$$

To consider the effect of vertical seismic load, 0.33 can be added to the dead load multiplier in the load combination.

F.8.3.3.1: Direction of loading

The direction of designed seismic forces shall produce the most critical load effects (ASCE 7-22), and members and foundations of structures with nonparallel system irregularities shall be designed "for 100% of the forces in one direction plus 30% of the forces in perpendicular direction".

F.8.3.3.2: Load Combination

Referring to ASCE 7-22, Loads Combinations for structures, components and foundation in design strength is equal or exceed the effects of factor loads as follows:

I. 1.4D
II. 1.2D+1.6L+0.5(L_r or S or R)
III. 1.2D + 1.6(L_r or S or R) +(1.0L or 0.5W)
IV. 1.2D + 1.0W + 1.0L + 0.5(L_r or S or R)
V. 0.9D + 1.0W
VI. 1.2D +1.0E_v + 1.0E_h + 1.0L + 0.2S
VII. 0.9D – 1.0E_v + 1.0E_h

Note: Since the seismic load weight on the buildings considers half of the wall above plus half of the wall below, these walls are converted to uniform loads in ETABS which is valid only for stories with similar heights. However, on the roof, we need to consider the half of the wall below plus the surrounding wall above which has an average height of about 110 cm. This can be considered by defining a mass load in the load pattern and using it in the mass source with multiplier one. This load shall be excluded from load combination to avoid the calculation of extra loads on the top floor's beams.

F.8.3.3.3: Effective seismic weight

Dead loads are included the weights of all materials and construction as well as the weight of fixed service equipment. W is the effective seismic weight of structure including the dead load plus other loads including:

- 25% LL (Live Load) of the floor for storage shall be considered and can be ignored if it adds no more than 5% to ESW and opens public garages.
- The greater value of the actual partition weight or 0.48 kN/m^2 (10 psf).
- Total operating weight (OW).
- 20% SL (Snow Load), where the flat roof snow load exceeds 1.44 kN/m^2 (30 psf).
- Weight of "landscaping at roof gardens"

F.9: Analysis and Design

F.9.1: Design Ratios

A rough design has been performed for the structure. Mainly the columns are of importance to tolerate the loads on the structure. The following picture demonstrated the design ratios of the selected sections. The minimum depth of non-prestressed beams for normal weight concrete and grade 420 reinforcement are presented in Table 10.

Table 10. Minimum beam depth (ACI 318-19)

Support Condition	**Minimum h**
Simply supported	l/16
One end continuous	l/18.5
Both end continuous	l/21
Cantilever	l/8

If the condition above is not satisfied the deflection shall be calculated and controlled based on ACI 318-19, section 24.2, and for other types of reinforcement refer to sections 9.3.1.1.1 through 9.3.1.1.3. In these models, the minimum beam depths are limited to 43 cm and 38 cm for one and both ends continuous.

Rebar percentage for 12Φ20 (an example), ρ can be calculated as below: ρ=As/bd=12*π*20^2/4/450*450=0.018=1.8% (this value shall be greater than 1 % and less than 3.5%). The cross-sectional area and moment of inertia of members shall be calculated from Table 11.

Table 11. Moment of inertia and cross-sectional area (ACI 318-19)

Member	Moment of Inertia	Cross section area
Columns	$0.70I_g$	
Walls	$0.70I_g$	
	$0.35I_g$	$1.0A_g$
Beams	$0.35I_g$	
Flat plates and slabs	$0.25I_g$	

F.9.2: Column Design

The column design procedures are including, generate a biaxial interacting surface as shown in Figure 3, this coordination can be calculated by rotating a plane of linear strain in three dimensions. Calculate the capacity ratio and column shear reinforcement design.

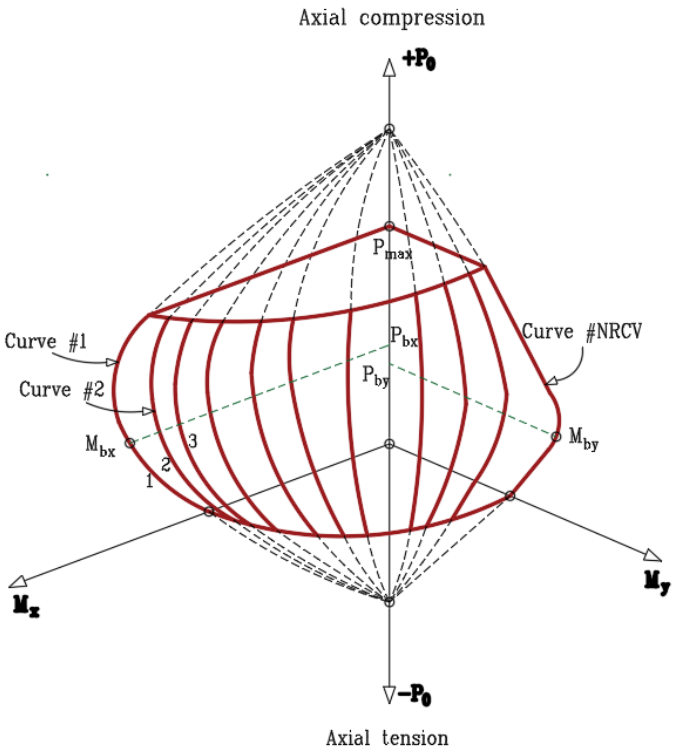

Figure 3. Column biaxial interacting surface (based on ACI 318 & CSI)

F.9.2.1: Column capacity ratio

This capacity is calculated for each design load station at each column. The first step is to calculate the factored moment and forces to obtain the factor axial load, P_u, factor moment about 2-axis, M_{u2}, and factor moment about 3-axis M_{u3}. If there are small factor moments, the design of slender columns shall be based on minimum eccentricity in equation 17, where h is the corresponding dimension in the column (ACI 318-19, 6.6.5.4)

$$M_{2,min} = P_u(0.6 + 0.03h) \tag{17}$$

The moment magnification factors are calculated from equation 18, based on factor moment due to loads the cause non-sway, M_{ns}, and sway M_s.

$$M = M_{ns} + \delta_s M_s \tag{18}$$

The moment magnifier, δ_s, shall be calculated from equations 19, 20, and 21.

$$\delta_s = \frac{1}{1-Q} \geq 1 \tag{19}$$

$$\delta_s = \frac{1}{1-\frac{\sum P_u}{0.75\sum P_c}} \geq 1 \tag{20}$$

$$Second-order\ elastic\ analysis \tag{21}$$

For the second order, the combination shall correspond to 1.2DL+1.6LL (ACI 5.3.1). P_u is the factored vertical load, P_c is the critical buckling load that can be calculated from equation 22.

$$P_c = \frac{\pi^2 (EI)_{eff}}{(kl_u)^2} \geq 1 \tag{22}$$

$$EI_{eff} = \frac{0.4E_c I_g}{1+\beta_{dns}} \tag{23}$$

$$\beta_{dns} = \frac{maximum\ factored\ axial\ sustained\ load}{maximum\ factored\ axial\ total\ load} \leq 1.0 \tag{24}$$

Where K is the effective length factor, l_u is the unsupported length of the column. The capacity ratio shows the stress condition in the column and is presented in Figure 4. The capacity ratio is calculated by determining the points L and C. If OL=OC column is stressed, OL<OC Column capacity is adequate and OL>OC column is overstressed.

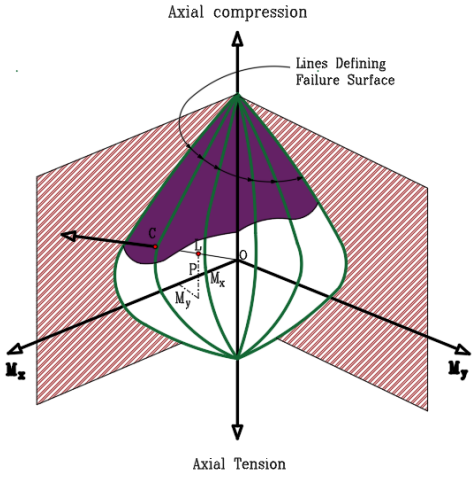

Figure 4. Column capacity ratio (ACI 318 & CSI)

For non-prestressed columns area of minimum and maximum longitudinal reinforcement shall be $0.01A_g$ and $0.08A_g$, the 0.08 applies to all sections including the splice regions. Longitudinal reinforcement in columns shall not be greater than 4 percent for lap splice zones (ACI 10.6.1.1). For “parallel reinforcement in a horizontal layer", spacing is the maximum value of 25mm, d_b, and $1.33d_{agg}$. For longitudinal reinforcement columns, the distance between bars shall be the maximum value of 40mm, 1.5db, and $1.33d_{agg}$ (ACI 25.2).

F.9.3: Beam Design

The beam design procedures are involving the design of flexural, shear, and torsion reinforcement. Web shear and flexural shear are two types of inclined cracking as presented in Figure 5. When the concrete tensile strength is less than principal tensile stresses web shear cracking occurs in a member’s interior point, and when the shear plus flexural tensile are greater than the tensile strength of the concrete, the flexural shear cracking begins to form.

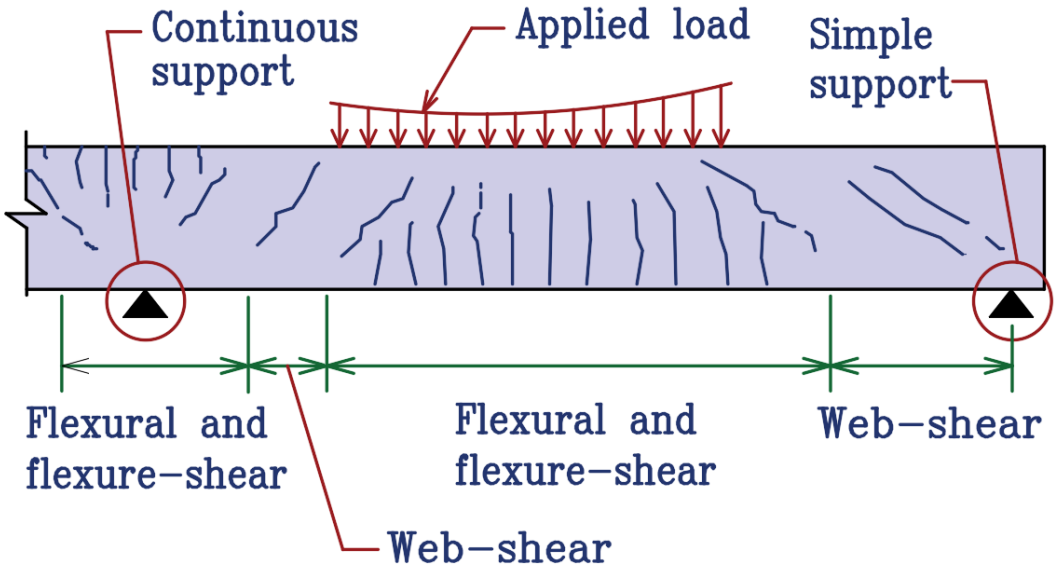

Figure 5. Concrete beams cracking (based on ACI 318-19)

F.9.3.1: Beam Flexural reinforcement

Simplified strain and stress diagrams for both rectangular and T beams are presented in Figure 6.

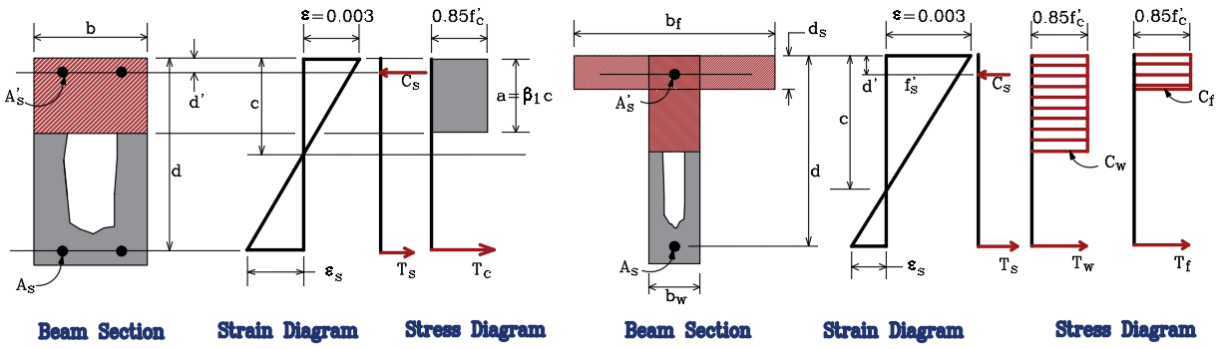

Figure 6. Rectangular beam and T-beam (ACI 318 & CSI)

Strain in concrete shall be calculated based on the assumption that is relative to the distance from the neutral axis, peak strain at the extreme concrete compression fiber, ε_{max}, is assumed to be 0.003 (ACI 22.2). ACI 318-19 allows ε_{min} to be equal to 0.004, however, in ACI 318-19 this value shall be in compliance with Figure 7 and Table 21.2.2 of ACI 318. Where $\varepsilon_{ty}=f_y/E_s$ for grade 60 and equal to 0.002.

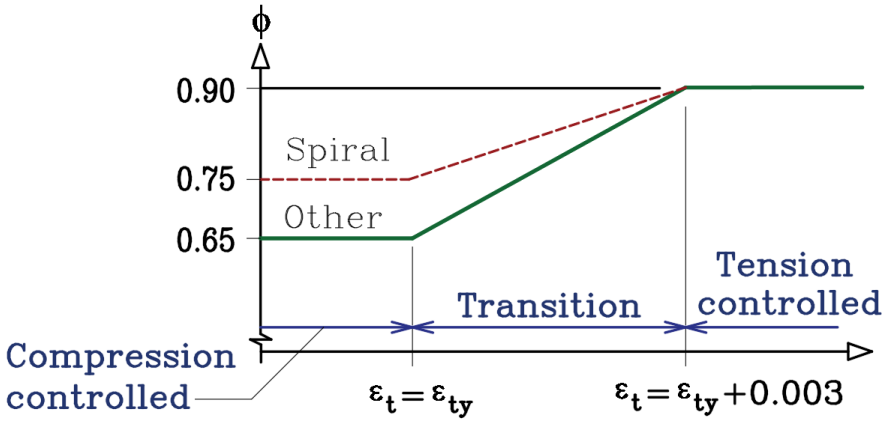

Figure 7. Variation of strength reduction factor versus tensile strength (ACI 318 & CSI)

The depth of compression, a, shall be calculated from equation 25, where c is the distance from maximum compressive strain to the neutral axis and β_1 is a factor describing the depth of rectangle compressive stress block to the depth of the neutral axis.

$$a = \beta_1 c \tag{25}$$

In the T-beam, if the moment is positive the flange is under compression and if the moment is negative the flange is under tension (ACI 22.2). If $a \leq d_s$, A_s can be calculated similar to a

rectangular section, and if a > d_s, A_s is divided into balancing the compressive force from the flange, C_f, and balancing the compressive force from the web, C_w.

F.9.3.2: Beam Shear reinforcement

For special moment frames, the shear design of beams is established on the highest probable and nominal moment strengths plus the factored design of the members. Figure 8 represents the design shear force, V_e, for beams and columns, it is assumed probable flexural strength, M_{pr}, has the opposite indication moments at the joint faces and the beam has vertical earthquake effects, $0.2S_{DS}$, and gravity loads. Concrete shear capacity, as well as shear reinforcement, shall be in accordance with ACI 318 section 22.5.

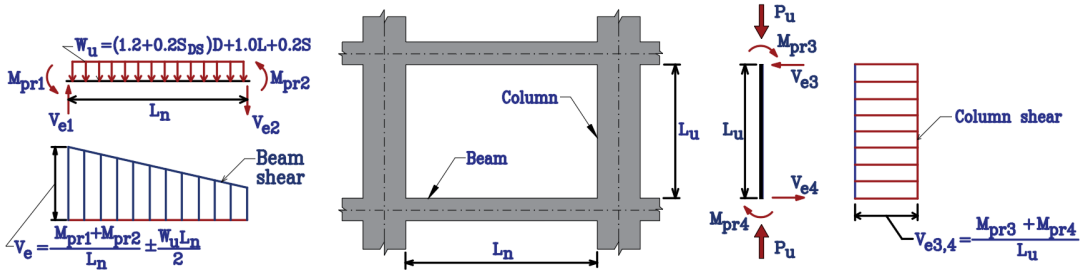

Figure 8. Shear design for beams and columns (ACI 318-19)

F.9.3.3: Beam Torsion reinforcement

The torsion reinforcement is designed based on each load combination. In Figure 9 the shear flow is constant due to torsion, therefore half of the Ni is resisted by top and bottom Chords.

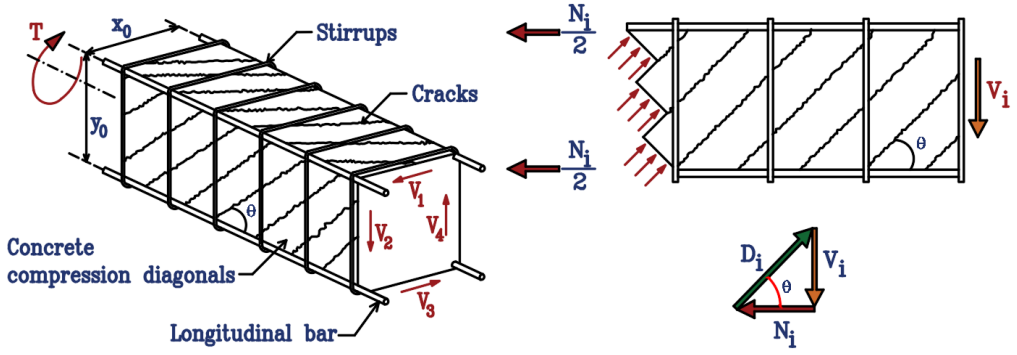

Figure 9. Resolution of shear force, V_i (based on ACI 318-19)

When factored torsion $T_u \geq \phi T_{cr}$ in the statically indeterminate structure T_u can be reduced to ϕT_{cr} (ACI 22.7.3.2). T_{cr} is cracking torsion, that for non-prestressed members with no axial load, shall be calculated with equation 26. Torsion strength reduction factor "ϕ" is equal to 0.75 (ACI 21.2).

$$T_{cr} = 4\lambda\sqrt{f_c'}\left(\frac{A_{cp}^2}{p_{cp}}\right) \tag{26}$$

Herein, A_{cp} is the enclosed area by concrete cross section's outside perimeter, p_{cp}. Section dimensions of rectangular ($A_{cp}=bh$, $p_{cp}= 2b+2h$) and T-beam ($A_{cp}=b_wh+(b_f-b_w)d_s$, $p_{cp}=2b_f+2h$) are presented in Figure 10.

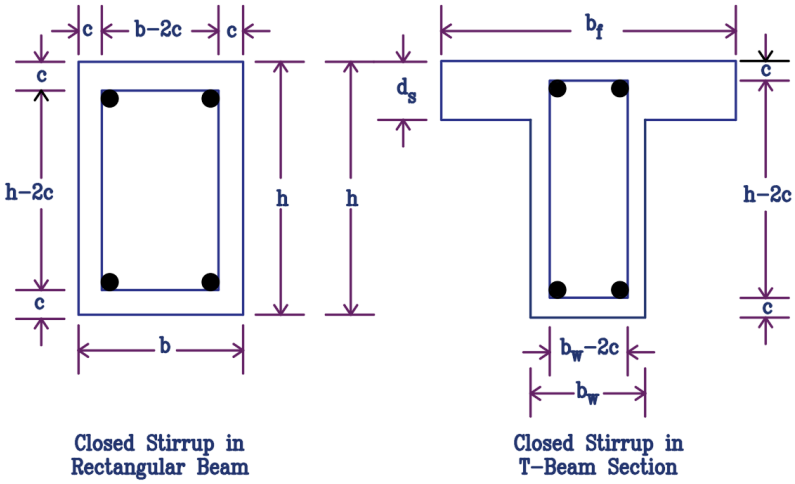

Figure 10. Closed stirrup for torsion design (based on ACI 318 & CSI)

Solid cross-section shall be limited to an upper limit of the combination V_u, and T_u, to minimize unnecessary cracking and to limit the surface concrete crushing caused by compressive stresses and shall satisfy equation 27.

$$\sqrt{\left(\frac{V_u}{b_w d}\right)^2 + \left(\frac{T_u p_h}{1.7A_{oh}^2}\right)^2} \leq \emptyset\left(\frac{V_c}{b_w d} + 8\sqrt{f_c'}\right) \tag{27}$$

Where V_u is the factored shear force, T_u is the factored torsional moment, p_h is the perimeter of the "centerline of outermost closed transverse torsional reinforcement", and A_{oh} is the area enclosed by the "centerline of the outermost closed transverse reinforcement".

F.9.4: Diaphragms

The major function of horizontal elements such as the floor, roof slabs, or a ramp is to transfer lateral forces to vertical components of the lateral force-resisting system. These elements support gravity loads and may consist of chords and collectors. Figure 11 shows a diaphragm which can be considered as a beam spanning horizontally when subjected to lateral loads, therefore it develops in-plane bending moment, shear, and other actions. A collector is a diaphragm area that may be required to transfer diaphragm shear to the vertical element, where the vertical element does not extend along with the full depth of diaphragms. The distributer is a collector when transferring the force to the lateral load resisting system.

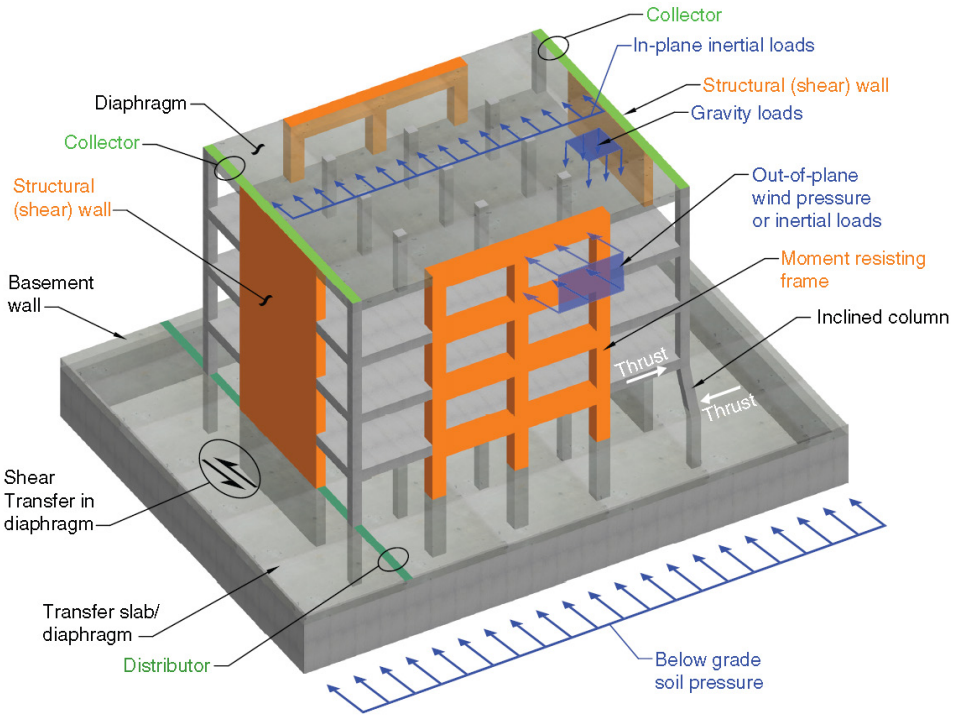

Figure 11. Typical shear wall, moment-resisting frame, and diaphragm actions (ACI 318-19)

Apart from shear strength, a diaphragm should be reinforced to transfer shear to collectors and vertical components of the lateral load-resisting system through shear friction. In cold joints additional reinforcement is required to transfer shear friction into vertical components of the lateral load resisting system, Figure 12 presents this additional reinforcement of dowels.

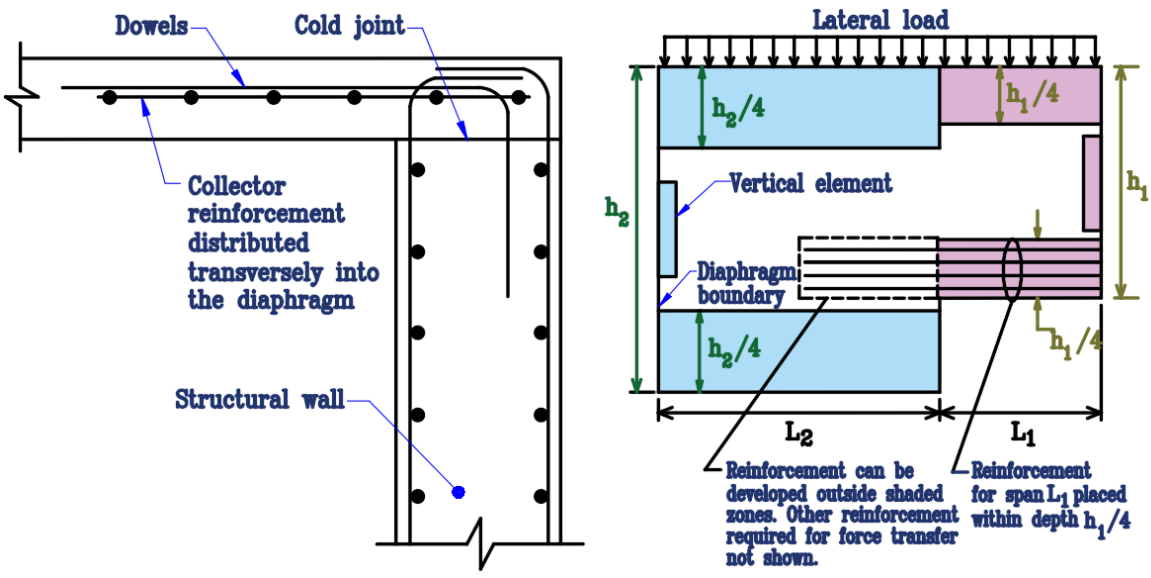

Figure 12. A common detail of dowels on the left and placement of reinforcement on the right (ACI 318-19)

Nominal shear strength can be calculated from equation 28, in this equation A_{vf} is the area of shear reinforcement, and μ id the friction coefficient from Table 22.9.42 of ACI 318-19. A_{vf} can be determined from equation 29, where φ is the strength reduction factor (ACI 318-19).

$$V_n = \mu A_{vf} f_y \tag{28}$$

$$A_{vf} = \frac{V_u}{\emptyset \mu f_y} \tag{29}$$

For a cast-in-place diaphragm, V_n can be calculated from equation 30. Herein, A_{cv} refers to the concrete total area surrounded by diaphragm web thickness and depth, ρ_t is the distributed reinforcement parallel to the in-plane shear.

$$V_n = A_{cv}(2\lambda\sqrt{f_c'} + \rho_t f_y) \tag{30}$$

$$V_u \leq \emptyset 0.66 A_{cv}\sqrt{f_c'} \tag{31}$$

$$V_n \leq 100 \quad psi \tag{32}$$

F.9.5: Beam-column joint

To ensure the adequate shear strength of the special moment-resisting frames' joint, the weak beam strong column criteria shall be satisfied at all beam to column joints of a structural frame in order to avoid column plastic hinges. This design procedure involves the panel zone design shear force, determining the effective area of joint and control panel zone shear stress. Figure 13 shows the free-body stress form of a beam-column joint.

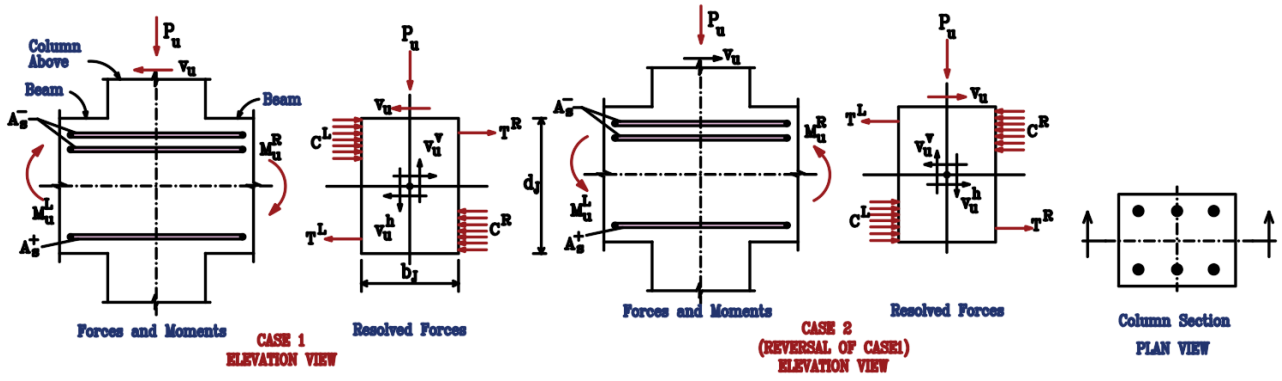

Figure 13. Beam-Column joint (ACI 318 & CSI)

The Shear force, Vu, can be determined using equation 33 by adding the moment capacities of the panel zone, as illustrated in Figure 14.

$$V_u = \frac{M_u^L + M_u^R}{H} \tag{33}$$

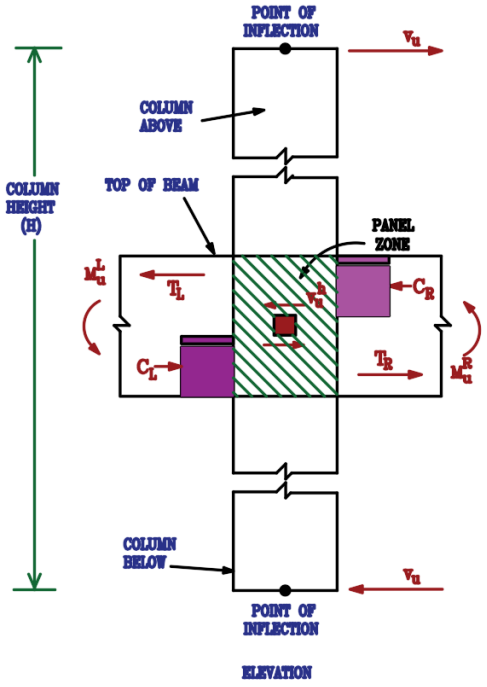

Figure 14. Column shear force (ACI 318, CSI)

The Sum of nominal flexural strengths of the columns, M_{nc}, over the sum of nominal flexural strengths of the beams, M_{nb}, shall be equal to or greater than 1.2 from equation 34.

$$\frac{\sum M_{nc}}{\sum M_{nb}} \geq 1.2 \tag{34}$$

The lateral stiffness and strength of the column framing into the joint shall be neglected, when equation 34 in not satisfied.

F.9.6: Accidental Torsion

Torsional irregularity occurs when $\delta_{max}/\delta_{ave}$ >1.2, and extreme torsional irregularity occurs when $\delta_{max}/\delta_{ave}$ >1.4, where δ_{max} and δ_{ave} are the maximum displacement at level x and the average displacement at level x, assuming torsional amplification factor A_x (Equation 35) is equal to one as presented in Figure 15. The expected 5% displacement of the center of mass shall be applied in the direction that has more effect, where earthquake forces are applied in two orthogonal directions (ASCE 7-22).

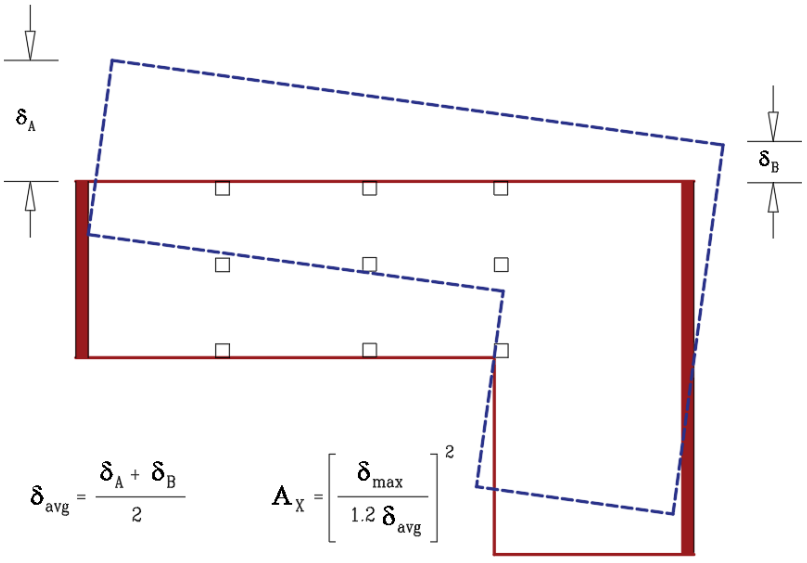

Figure 15. Torsional Amplification Factor (ASCE 7-22)

$$A_x = \left(\frac{\delta_{max}}{1.2\delta_{ave}}\right)^2 \qquad 1 \leq A_x \leq 3 \tag{35}$$

F.9.7: Stability against Overturning

The structure shall be designed to withstand the overturning effects of the lateral forces.

F.9.8: Drift and Deflection

The design story drift, Δ, shall be calculated from the difference between the centers of the mass deflections at the top and the bottom of the story. The story drift ratio can be determined by dividing the story drift over the height of the level under consideration. Figure 16 presents the story drift determination, herein F_1 and F_2 are the strength level design earthquake forces, δ_{1e} and δ_{2e} are the elastic displacements as a result of design earthquake forces, δ_1 and δ_2 are the amplified displacement which can be calculated with equation 36 in which C_d is the deflection amplification factor and I_e is the importance factor.

$$\delta_x = \frac{C_d \delta_{xe}}{I_e} \tag{36}$$

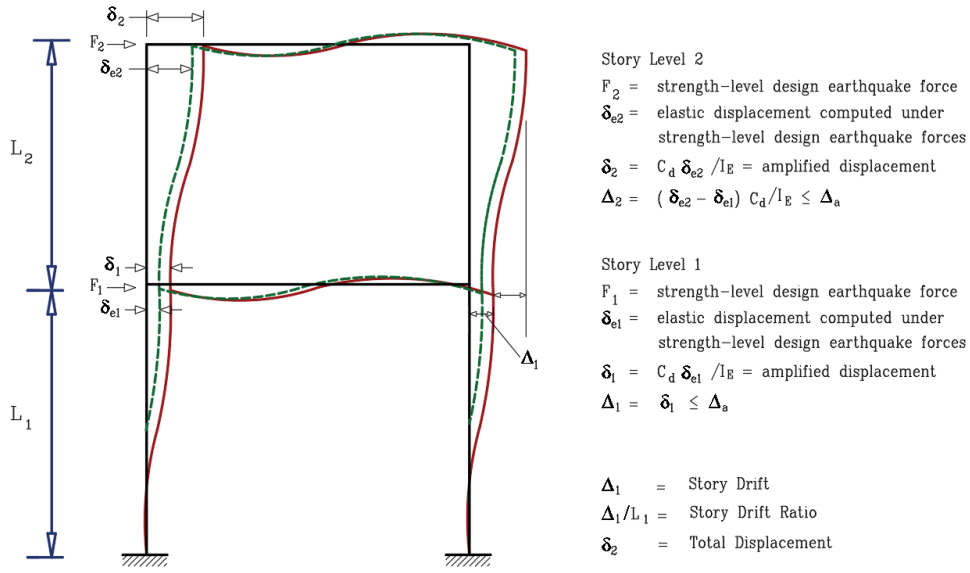

Figure 16. Story drift (based on ASCE 7)

The design story drift shall be limited to the allowable story drift presented in Table 12. Herein h_{sx} is the story height below level x.

Table 12. Allowable story drift (ASCE 7-22)

	Risk Category		
Structural types	**I or II**	**III**	**IV**
Non-masonry with a maximum of four stories	$0.025h_{sx}$	$0.020h_{sx}$	$0.015h_{sx}$
Masonry cantilever shear wall structures	$0.010h_{sx}$	$0.010h_{sx}$	$0.010h_{sx}$
Other masonry shear wall structures	$0.007h_{sx}$	$0.007h_{sx}$	$0.007h_{sx}$
All other structures	$0.020h_{sx}$	$0.015h_{sx}$	$0.010h_{sx}$

For SFRFs related to seismic design categories D, E, F the design story drift, Δ, shall be less than the allowable drift to redundancy factor, Δ_a/ρ, (ASCE 7-22).

F.9.9: Second-Order P-Delta Effects

The P-Delta effects for elastic with and without large displacement and its total effects on a frame element caused by both Δ and δ are presented in Figure 17.

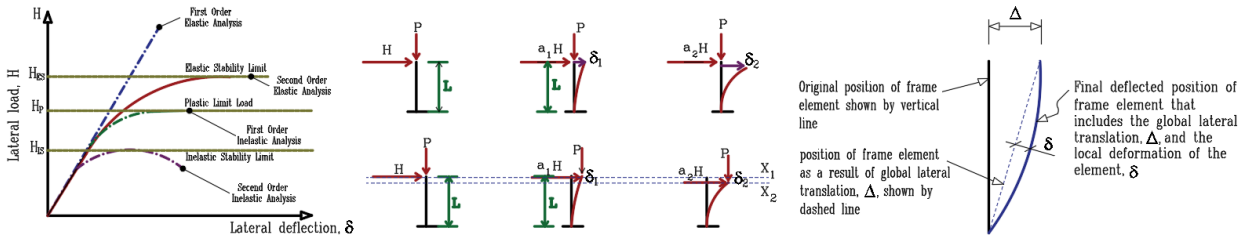

Figure 17. The second-order P-delta effects (Lignos, 2014, ACI 318, CSI)

The program is capable of calculating the P-Delta effect due to the Δ deformation, to capture the δ deformation the frame shall be broken into multiple elements over its length.

F.9.10: Stability Coefficient

Stability coefficient, θ, can be determined from equation 37, where P_x is the vertical design load at level x and above, Δ is the story drift, I_x is an important factor, V_x is the seismic shear force, h_{sx} is the story height, and C_d is the deflection amplification factor.

$$\theta = \frac{P_x \Delta I_e}{V_x h_{sx} C_d} \tag{37}$$

If the stability coefficient is equal to or less than 0.10, the P-delta effects are not required to be considered, the maximum stability coefficient can be calculated from equation 38. In this equation β is the ratio of shear demand to shear capacity.

$$\theta_{max} = \frac{0.5}{\beta C_d} \leq 0.25 \tag{38}$$

F.9.11: Modal Analysis

In this study Ritz value analysis was used to identify the natural periods of the buckling restrained brace frame, for further details, please refer to section 4.2.3.

F.9.12: Overturning

Overturning effects caused by earthquake forces shall be withstand by the structure.

F.9.13: Balancing of Base Shear Results of Static and Dynamic Analysis

A base shear shall be calculated in both orthogonal horizontal directions. If $T > C_uT_a$ then $T= C_uT_a$, where C_u is the coefficient for the upper limit on the computed period, T is the fundamental period and T_a is the approximate fundamental period (ASCE 7-22 chapters 12 and 16).

- Scaling of forces: If $V_t < V$ the forces shall be multiplied by 100% of V/V_t, where V_t is the modal base shear's combined response.
- Scaling of drifts: If $V_t < C_sW$ then drifts shall be multiplied by C_sW/V_t.

Note: When sections change during dynamic design analysis, balancing of base shear results shall be repeated. The sum of modal participating mass ratio (Sum RX and RY), as well as the torsion (Sum RZ), shall be at least 90%.